DESIGN,DEVELOPMENT AND EXPERIMENTAL STUDIES ON MICRO HYDRO PELTON TURBINE.

A Thesis submitted to Gujarat Technological University

for the Award of

Doctor of Philosophy

in

Mechanical Engineering

by

Chaudhari Anupkumar Hasmukhlal
Enrollment No 189999919008

under supervision of

Dr.Gaurangkumar C. Chaudhari

GUJARAT TECHNOLOGICAL UNIVERSITY

AHMEDABAD

August 2026

© [CHAUDHARI ANUPKUMAR HASMUKHLAL]

DECLARATION

I declare that the thesis entitled **"Design,Development and Experimental Studies on Micro Hydro Pelton Turbine."**submitted by me for the degree of Doctor of Philosophy is the record of research work carried out by me during the period from **June 2019** to **August 2026** under the supervision of **Dr.Gaurangkumar C. Chaudhari** and this has not formed the basis for the award of any degree, diploma, associateship, fellowship, titles in this or any other University or other institution of higher learning.

I further declare that the material obtained from other sources has been duly acknowledged in the thesis. I shall be solely responsible for any plagiarism or other irregularities, if noticed in the thesis.

Signature of the Research Scholar: .....Chaudhari..... Date: 06-08-2026

Name of Research Scholar: **Chaudhari Anupkumar Hasmukhlal (Enrollment.No.189999919008)**

Place: **Gujarat Technological University, Ahmedabad**

CERTIFICATE

I certify that the work incorporated in the thesis "**Design,Development and Experimental Studies on Micro Hydro Pelton Turbine.**" submitted by **Chaudhari Anupkumar Hasmukhlal (Enrollment.No.189999919008)** was carried out by the candidate under my supervision/guidance. To the best of my knowledge: (i) the candidate has not submitted the same research work to any other institution for any degree/diploma, Associate ship, Fellowship or other similar titles (ii) the thesis submitted is a record of original research work done by the Research Scholar during the period of study under my supervision, and (iii) the thesis represents independent research work on the part of the Research Scholar.

Signature of the Research Supervisor: ..... Date: 06-08-2026

Name of Supervisor: **Dr.Gaurangkumar C. Chaudhari**

Place: **Gujarat Technological University, Ahmedabad**

Course-work Completion Certificate

This is to certify that **Chaudhari Anupkumar Hasmukhlal Enrollment No.189999919008_** is enrolled for PhD program in the faculty Mechanical Engineering of Gujarat Technological University, Ahmedabad.

(Please tick the relevant option(s)

☐ He/She has been exempted from the course-work (successfully completed during M.Phil Course)

☐ He/She has been exempted from Research Methodology Course only (successfully completedduring M.Phil Course)

☑ He/She has successfully completed the PhD course work for the partial requirement for the award of PhD Degree. His/ Her performance in the course work is as follows-

Grade Obtained in Research Methodology [PH001]	Grade Obtained in Self Study Course/ Contact Program [PH002]
BB	**AB**

Supervisor's Sign: Chaudhari g.c.

Name of the Research Supervisor: : **Dr.Gaurangkumar C. Chaudhari**

Originality Report Certificate

It is certified that PhD Thesis titled "**Design,Development and Experimental Studies on Micro Hydro Pelton Turbine.**" By **Chaudhari Anupkumar Hasmukhlal Enrollment No.189999919008** has been examined by us. We undertake the following:

a. Thesis has significant new work / knowledge as compared already published or are under consideration to be published elsewhere. No sentence, equation, diagram, table, paragraph or section has been copied verbatim from previous work unless itis placed under quotation marks and duly referenced.

b. The work presented is original and own work of the author (i.e. there is no plagiarism). No ideas, processes, results or words of others have been presented as Author own work.

c. There is no fabrication of data or results which have been compiled / analyzed.

d. There is no falsification by manipulating research materials, equipment or processes, or changing or omitting data or results such that the research is not accurately represented in the research record.

e. The thesis has been checked using **turnitin** (copy of originality report attached) and found within limits as per GTU Plagiarism Policy and instructions issued from time to time (i.e. permitted similarity index <=10%).

Signature of the Research Scholar: ..... Date: 06-08-2026

Name of the Research Scholar: **Chaudhari Anupkumar Hasmukhlal**

Signature of the Research Supervisor: ..... Date: 06-08-2026

Name of the Research Supervisor: **Dr.Gaurangkumar C. Chaudhari**

Place: Gujarat Technological University, Ahmedabad

Chaudhari Anupkumar Hasmukhlal

DESIGN,DEVELOPMENT AND EXPERIMENTAL STUDIES ON MICRO HYDRO PELTON TURBINE.

DESIGN, DEVELOPMENT AND EXPERIMENTAL STUDIES ON MICRO HYDRO PELTON TURBINE

Nilesh Patel

SVNIT

Document Details

Submission ID

trn:oid:::1:3585008373

Submission Date

Jun 2, 2026, 1:11 PM GMT+5:30

Download Date

Jun 2, 2026, 1:16 PM GMT+5:30

File Name

DESIGN,_DEVELOPMENT_AND_EXPERIMENTAL_Final.pdf

File Size

6.5 MB

215 Pages

66,488 Words

403,902 Characters

6% Overall Similarity

The combined total of all matches, including overlapping sources, for each database.

Filtered from the Report

- Bibliography

Match Groups

- 382 Not Cited or Quoted 6%
  Matches with neither in-text citation nor quotation marks
- 0 Missing Quotations 0%
  Matches that are still very similar to source material
- 0 Missing Citation 0%
  Matches that have quotation marks, but no in-text citation
- 0 Cited and Quoted 0%
  Matches with in-text citation present, but no quotation marks

Top Sources

4% Internet sources
6% Publications
0% Submitted works (Student Papers)

Integrity Flags

0 Integrity Flags for Review

No suspicious text manipulations found.

Our system's algorithms look deeply at a document for any inconsistencies that would set it apart from a normal submission. If we notice something strange, we flag it for you to review.

A Flag is not necessarily an indicator of a problem. However, we'd recommend you focus your attention there for further review.

Ph.D. Thesis Non-Exclusive License to

GUJARAT TECHNOLOGICAL UNIVERSITY

In consideration of being a Research Scholar at Gujarat Technological University, and in the interests of the facilitation of research at the University and elsewhere, **I, Chaudhari Anupkumar Hasmukhlal Enrollment No.189999919008** hereby grant a non- exclusive, royalty free and perpetual license to the University on the following terms:

a. The University is permitted to archive, reproduce and distribute my thesis, in whole or in part, and/or my abstract, in whole or in part (referred to collectively as the "Work") anywhere in the world, for non-commercial purposes, in all forms of media;

b. The University is permitted to authorize, sub-lease, sub-contract or procure any of the acts mentioned in paragraph (a);

c. The University is authorized to submit the Work at any National / International Library, under the authority of their "Thesis Non-Exclusive License";

d. The Universal Copyright Notice (©) shall appear on all copies made under the authority of this license;

e. I undertake to submit my thesis, through my University, to any Library and Archives. Any abstract submitted with the thesis will be considered to form part of the thesis.

f. I represent that my thesis is my original work, does not infringe any rights of others, including privacy rights, and that I have the right to make the grant conferred by this non-exclusive license.

g. If third party copyrighted material was included in my thesis for which, under the terms of the Copyright Act, written permission from the copyright owners is required, I have obtained such permission from the copyright owners to do the acts mentioned in paragraph (a) above for the full term of copyright protection.

h. I understand that the responsibility for the matter as mentioned in the paragraph (g) rests with the authors / me solely. In no case shall GTU have any liability for any acts / omissions / errors / copyright infringement from the publication of the said thesis or otherwise.

i. I retain copyright ownership and moral rights in my thesis, and may deal with the copyright in my thesis, in any way consistent with rights granted by me to my University in this non-exclusive license.

j. GTU logo shall not be used /printed in the book (in any manner whatsoever) being published or any promotional or marketing materials or any such similar documents.

k. The following statement shall be included appropriately and displayed prominently in the book or any material being published anywhere: "The content of the published work

is part of the thesis submitted in partial fulfilment for the award of the degree of Ph.D. in Mechanical engineering of the Gujarat Technological University".

l. I further promise to inform any person to whom I may hereafter assign or license my copyright in my thesis of the rights granted by me to my University in this nonexclusive license. I shall keep GTU indemnified from any and all claims from the Publisher(s) or any third parties at all times resulting or arising from the publishing or use or intended use of the book / such similar document or its contents.

m. I am aware of and agree to accept the conditions and regulations of Ph.D. including all policy matters related to authorship and plagiarism.

Date: 06-08-2026

Place: GTU, Ahmedabad

Signature of the Research Scholar

Recommendation of the Research Supervisor: **Recommended**

Signature of the Research Supervisor

Thesis Approval Form

The viva-voce of the PhD Thesis submitted by **Chaudhari Anupkumar Hasmukhlal (Enrollment No.189999919008)** entitled **"Design,Development and Experimental Studies on Micro Hydro Pelton Turbine." was conducted on** Thursday,6th August 2026 at Gujarat Technological University.

(Please tick any one of the following option)

☑ The performance of the candidate was satisfactory. We recommend that he/she be awarded the PhD degree.

☐ Any further modifications in research work recommended by the panel after 3 months from the date of first viva-voce upon request of the Supervisor or request of Independent Research Scholar after which viva-voce can be re-conducted by the same panel again.

(briefly specify the modifications suggested by the panel)

☐ The performance of the candidate was unsatisfactory. We recommend that he/she should not be awarded the PhD degree.

(The panel must give justifications for rejecting the research work)

Dr.Gaurangkumar C.Chaudhari
Name and Signature of Supervisor with Seal

Dr.Nilesh Pitambarrao saulnke
1)(External Examiner)Name and Signature

Dr.P.L .Ramkumar
2)(External Examiner)Name and Signature

ABSTRACT

Pelton impulse turbines are the preferred prime movers for micro-hydroelectric sites characterised by high hydraulic head (up to 1,800 m) and low discharge, owing to their historically superior hydraulic efficiency and structural reliability relative to other turbine classes. The hydraulic performance of a Pelton turbine is governed almost entirely by the runner bucket geometry specifically, the speed ratio , the bucket exit angle , and the three-dimensional bucket profile. Since the turbine designer and manufacturer bear sole responsibility for optimising these parameters, a rigorous and systematic design methodology is essential to realise maximum hydraulic output in service.

This research employs an integrated multi-physics framework structured across five phases: (i) analytical hydraulic parametric design; (ii) structural static and modal finite element analysis (FEA) using ANSYS Mechanical APDL; (iii) steady-state and transient computational fluid dynamics (CFD) simulation using ANSYS Fluent; (iv) physical fabrication of the optimised runner by sand-casting; and (v) controlled experimental performance testing. Each phase informs and validates the next, ensuring that theoretical predictions are computationally verified, structurally confirmed, and experimentally substantiated on a physical prototype.

The parametric analysis, the full feasible ranges of φ and β_2 to generate a continuous efficiency surface. A peak theoretical hydraulic efficiency of 94.29% was validated at the optimum speed ratio of $\varphi \approx 0.46$ and the corresponding optimal exit angle, consistent with classical theory. FEA evaluated four candidate materials carbon steel, cast iron, stainless steel 304, and stainless steel 314 under six combined loading conditions encompassing centrifugal, hydraulic impingement, gravitational, thermal, and full peak-power loads. All twenty-four material-loading combinations satisfied the structural safety criterion, with peak Von Mises stresses concentrated at the bucket root and splitter ridge. Modal analysis confirmed no resonant coincidence at operating speed. Stainless steel 314 was selected as the material of choice on the basis of its superior yield strength, corrosion resistance in high-velocity aerated flows, and erosive wear resistance.

CFD simulation using a Volume of Fluid two-phase free-surface model resolved the pressure distribution, velocity field topology, and turbulent kinetic energy (TKE) within the bucket passage under both steady-state and transient conditions. A well-defined high-pressure stagnation zone was captured at the splitter ridge apex, with progressive pressure decay toward the lateral discharge edges. TKE concentrations were identified at the bucket cutout entry and discharge lip, consistent with jet-edge shear layer formation. All simulated trends demonstrated close quantitative agreement with published experimental benchmark data, validating the simulation fidelity.

The optimized runner was fabricated in stainless steel 314, machined to the specified dimensional tolerances, dynamically balanced, and subsequently evaluated on a controlled hydraulic test rig. Experimental assessment of the fabricated runner yielded a maximum hydraulic efficiency of 90.92% and a maximum thrust power of 2,018.97 W, representing improvements of 2.05 percentage points in hydraulic efficiency and 4.37% in thrust power relative to the conventional baseline runner.

Acknowledgement

I would like to begin by expressing my heartfelt gratitude to Lord Ganesha for blessing me with the wisdom, strength, and perseverance to undertake and complete this journey successfully.

I am sincerely thankful to my esteemed guide, ***Dr. Gaurangkumar C. Chaudhari****, Assistant Professor at CKPCET, Surat, for his invaluable insights, unwavering support, and continuous guidance throughout my research work. His profound knowledge, keen intellect, and exceptional mentorship have played a pivotal role in shaping my academic and research pursuits. I feel truly honoured and privileged to have had the opportunity to learn under his guidance.*

*It is my proud privilege to express my sincere gratitude and deep appreciation to my Doctoral Progress Committee (DPC) members****, Dr. Vimal K. Patel****, DPC Member, SVNIT, and* ***Dr. Ashish V. Doshi****, DPC Member, SVNIT. Their valuable guidance, insightful suggestions, and constructive observations during the doctoral progress presentations have greatly strengthened the quality, depth, and direction of my research work.*

Special thanks to my beloved wife, ***Divya Chaudhari****, for her unconditional love, endless patience, unwavering support, and encouragement throughout this doctoral journey. Her faith in me has been my greatest strength during every challenge and achievement. I also extend my heartfelt affection to my daughter,* ***Swara Chaudh****ari, and my son,* ***Hridyansh,*** *whose innocence, joy, and love have continuously inspired and motivated me every single day.*

I would like to offer a heartfelt and special dedication to my respected ***father-in-law, Shri Vinodbhai Chaudhari, and my mother-in-law,*** *Smt. Savitaben Chaudhari, whose blessings, wisdom, encouragement, and moral support have always been a constant source of strength and motivation. Their trust, guidance, and belief in me have played a truly significant role in this journey, and I remain deeply grateful for their presence in my life.*

I am also profoundly grateful to my beloved father, ***Shri Hasmukhlal Chaudhari****, and my dear mother,* ***Smt. Kuntaben Chaudhari****, for their unconditional love, lifelong sacrifices,*

endless blessings, and unwavering faith in me. Their values, support, and encouragement have been the strongest foundation behind every achievement in my life.

I am equally thankful to my entire family for their constant encouragement, understanding, and unwavering moral support, which have always motivated me to move forward with confidence and determination throughout this journey.

Finally, I express my sincere gratitude to everyone who directly or indirectly contributed to the successful completion of my Ph.D. work. Your encouragement, support, and faith in me have been invaluable and will always remain deeply appreciated.

Chaudhari Anupkumar Hasmukhlal

Table of Contents

Abstract **I**

Acknowledgement **III**

List of Abbreviations **XIV**

List of Symbols **XVI**

List of Figures **XIX**

List of Tables **XXV**

1. Introduction **1**

1.1 Global Energy Scenario and the Role of Hydropower 1

1.1.1 The Global Energy Transition 1

1.1.2 Current Global Electricity Generation Mix 1

1.1.3 Hydropower as Dispatchable Clean Energy 2

1.1.4 Pumped Storage Hydropower and Grid Integration 3

1.1.5 Regional Variations in Hydropower Deployment 3

1.1.6 Environmental and Social Considerations 4

1.1.7 Future Projections and the Role of Optimization 5

1.2 Hydropower Scenario in India 6

1.3 Micro-Hydropower: Definition and Significance 10

1.4 The Pelton Turbine: Principles of Operation 11

1.5 Suitability of Pelton Turbines for Micro-Hydro Applications 13

1.6 Research Motivation and Rationale 15

2. Literature Review **17**

2.1 Introduction 17

2.2 Literature Survey of Fundamentals and Design of Pelton Turbine Operation 19

2.2.1 Hydraulic Design Parameters Affecting Pelton Turbine Efficiency 22

2.2.2 Speed Ratio Optimization 22

2.2.3 Bucket Exit Angle Optimization 23

2.2.4 Bucket Geometry Optimization 24

2.2.5 Nozzle Geometry and Jet Characteristics 25

2.3 Literature review on Stress Analysis of Pelton Turbine 26

2.3.1 Stress Distribution Due to Jet Impingement 26

2.3.2 Deformation Characteristics of Pelton Buckets 27

2.3.3 Material Selection for Structural Reliability 28

2.3.4 Finite Element Analysis in Pelton Turbine Design 28

2.4 Literature Survey on Modal and Dynamic Behaviour of Pelton Turbine Runners 29

2.4.1 Sources of Dynamic Excitation in Pelton Turbines 30

2.4.2 Modal Analysis of Pelton Turbine Buckets 30

2.4.3 Influence of Material Properties on Dynamic Behaviour 31

2.4.4 Dynamic Stability and Resonance Prevention 32

2.5 Literature Survey on Computational Fluid Dynamics Analysis of Pelton Turbines 32

2.5.1 Evolution of CFD Modelling in Pelton Turbine Research 33

2.5.2 Free-Surface Flow and Jet Dynamics 34

2.5.3 Steady-State CFD Analysis 35

2.5.4 Transient CFD and Sliding Mesh Techniques 35

2.5.5 Limitations of Existing CFD Studies 36

2.6 Literature Survey on Materials Used in Pelton Turbine Buckets 37

2.6.1 Mechanical Requirements of Pelton Bucket Materials 37

2.6.2 Stainless Steel Materials 38

2.6.3 Aluminum Alloys and Lightweight Materials 39

2.6.4 Composite Materials and Advanced Material Research 39

2.6.5 Erosion and Corrosion Behaviour 40

2.6.6 Limitations of Existing Material Studies 40

2.7 Literature Survey on Experimental Investigations on Pelton Turbines 41

2.7.1 Experimental Performance Evaluation of Pelton Turbines 41

2.7.2 Influence of Bucket Geometry and Runner Parameters 42

2.7.3 Experimental Validation of Numerical Models 43

2.7.4 Dynamic Balancing and Operational Stability 43

2.7.5 Experimental Uncertainty Analysis 44

2.7.6 Limitations of Existing Experimental Studies 44

2.8 Literature Review on Multi-Physics Approaches on Pelton Turbines 45

2.8.1 Integration of Hydraulic Optimization and CFD Analysis 46

2.8.2 Coupling of Hydraulic and Structural Analysis 47

2.8.3 Integration of Modal Analysis and Dynamic Stability 47

2.8.4 Integration of Numerical and Experimental Approaches 48

2.8.5 Emerging Trends in Integrated Pelton Turbine Research 49

2.8.6 Research Limitations and Need for Integrated Frameworks 50

2.9 Research Gaps Identified from Literature 51

2.9.1 Limited Integrated Multi-Physics Design Methodologies 51

2.9.2 Insufficient Coupling Between CFD and Structural Analysis 52

2.9.3 Limited Research on Combined Static and Modal Analysis 53

2.9.4 Limited Experimental Validation of Numerical Models 53

2.9.5 Limited Studies on Micro-Hydropower-Specific Optimization 54

2.9.6 Insufficient Investigation of Transient Operating Conditions 54

2.9.7 Limited Studies on Fabrication and Practical Implementation 55

2.10 Summary of Literature Review 55

2.11 Objectives of the present work 58

3. Theoretical Background and Design Methodology 59

3.1 Fundamentals of Pelton Turbine Operation 59

3.2 Hydraulic Energy Conversion 61

3.2.1 Hydraulic Power Available in Water 62

3.2.2 Conversion of Hydraulic Energy into Jet Kinetic Energy 62

3.2.3 Momentum Transfer Between Jet and Bucket 63

3.2.4 Mechanical Power Developed by the Runner 63

3.2.5 Hydraulic Efficiency of Pelton Turbine 64

3.2.6 Factors Affecting Hydraulic Energy Conversion 64

3.3 Velocity Triangles 65

3.3.1 Inlet Velocity Triangle 66

3.3.2 Outlet Velocity Triangle 67

3.3.3 Force Developed on the Runner 67

3.3.4 Hydraulic Efficiency from Velocity Triangle Analysis 68

3.4 Governing Equations 68

3.4.1 Hydraulic Power Equation 69

3.4.2 Jet Velocity Equation 69

3.4.3 Bucket Peripheral Velocity 69

3.4.4 Speed Ratio Equation 69

3.4.5 Hydraulic Efficiency Equation 70

3.4.6 Force Developed on the Runner 70

3.4.7 Shaft Torque Equation 71

3.4.8 Shaft Power Equation 71

3.4.9 Bucket Passing Frequency Equation 71

3.4.10 Jet Ratio Equation 71

3.4.11 Number of Buckets Equation 72

3.4.12 Importance of Governing Equations in Design Methodology 72

3.5 Parametric Optimization Strategy 72

3.6 Material Selection Criteria 77

3.6.1 Functional Requirements of Pelton Turbine Materials 78

3.6.2 Mechanical Strength and Structural Stiffness 79

3.6.3 Fatigue Resistance 79

3.6.4 Erosion and Corrosion Resistance 80

3.6.5 Stainless Steel as Preferred Material 80

3.6.6 Comparison with Alternative Materials 81

3.6.7 Material Selection for Present Research 83

3.6.8 Importance of Material Selection in Integrated Design 84

3.7 Closure 85

4. Finite Element Structural and Modal Analysis of Pelton Turbine Bucket 87

4.1 Introduction 87

4.2 CAD Geometry Development 90

4.3 Material Selection 92

4.3.1 Basis for Selection of Candidate Materials 92

4.4 Mesh Generation and Grid Independence Study 98

4.5 Static Structural Analysis Methodology 101

4.5.1 Governing Equations of Static Structural Analysis 101

4.5.2 Assumptions Considered During Structural Analysis 102

4.5.3 Structural Deformation Analysis 102

4.5.4 Equivalent Stress Distribution Analysis 105

4.5.5 Effect of Incidence Angle on Structural Behaviour 108

4.6 Modal Analysis of Pelton Turbine Bucket 109

4.7 Structural Integrity and Dynamic Stability Assessment 115

4.8 Results and Discussion 118

4.8.1 Modal Analysis Results and Detailed Resonance Discussion 122

4.9 Colusre 125

5. Computational Fluid Dynamics Analysis of Pelton Turbine Bucket 126

5.1 Introduction 126

5.2 Computational Geometry Development 128

5.2.1 Governing Equations for CFD Analysis 129

5.3 Mesh Generation and Grid Independence Study 131

5.4 Boundary Conditions and Solver Setup 134

5.5 Steady-State CFD Analysis 138

5.5.1 Velocity Distribution Analysis 138

5.6 Transient CFD Analysis 143

5.7 Turbulence and Flow Behaviour Analysis 147

5.8 Hydraulic Performance Assessment 149

5.9 Validation and Discussion 152

5.10 Results and Discussion 154

5.11 Closure 159

6. Development and Experimental Investigation of Pelton Turbine 161

6.1 Introduction 161

6.2 Fabrication of Buckets and Runner 162

6.3 Parametric Comparison of Conventional and Enhanced Bucket 166

6.4 Fabrication of Enhanced Bucket and Runner Assembly 169

6.5 Balancing of Runner 173

6.6 Experimental Setup and Instrumentation 175

6.7 Experimental Procedure 178

6.8 Performance Evaluation Parameters 180

6.9 Result and Discussion 181

6.10 Closure 188

7. Conclusions and Future Scope 190

7.1 Comparative Discussion of Numerical and Experimental Results 190

7.2 Conclusion 195

7.2.1 Outcomes of Design Optimization 196

7.2.2 Outcomes of Structural Finite Element Analysis 196

7.2.3 Outcomes of Computational Fluid Dynamics Analysis 197

7.2.4 Outcomes of Fabrication and Experimental Validation 198

7.3 Limitations 199

7.4 Future Scope 200

REFERENCES 202

List of Publications 210

APPENDIX A 211

Uncertainty Analysis 211

Instruments and Calibration 211

Physical Constants 211

Error Definitions 211

Pressure Gauge 211

Spring Balance 212

Dynamic Balancing 212

Hydraulic Efficiency 212

APPENDIX B **214**

Dynamic balancing certificate 214

Calibration certificate of pressure gauge 215

Calibration certificate of Spring balance 216

APPENDIX C **217**

Experimental Result of Conventional and Enhanced Pelton Runners 217

List of Abbreviations

AHEC	:	Alternate Hydro Energy Centre
AI	:	Artificial Intelligence
ANN	:	Artificial Neural Network
ANSYS	:	Analysis System (commercial FEA/CFD software)
APDL	:	ANSYS Parametric Design Language
ASME	:	American Society of Mechanical Engineers
ASTM	:	American Society for Testing and Materials
BC	:	Boundary Condition
CAD	:	Computer-Aided Design
CEA	:	Central Electricity Authority
CFD	:	Computational Fluid Dynamics
CFX	:	ANSYS CFX (commercial CFD solver)
CNC	:	Computer Numerical Control
CO_2	:	Carbon Dioxide
DNS	:	Direct Numerical Simulation
FEA	:	Finite Element Analysis
FSI	:	Fluid–Structure Interaction
GHG	:	Greenhouse Gas
GUI	:	Graphical User Interface
GUM	:	Guide to the Expression of Uncertainty in Measurement (ISO)
GW	:	Gigawatt
IEA	:	International Energy Agency
IEC	:	International Electrotechnical Commission
ISO	:	International Organization for Standardization
kW	:	Kilowatt
LES	:	Large Eddy Simulation
MNRE	:	Ministry of New and Renewable Energy

MW	:	Megawatt
NABL	:	National Accreditation Board for Testing and Calibration Laboratories
OD	:	Outer Diameter
PSH	:	Pumped Storage Hydropower
PSP	:	Pumped Storage Project
PTC	:	Performance Test Code (ASME)
RANS	:	Reynolds-Averaged Navier–Stokes
REN21	:	Renewable Energy Policy Network for the 21st Century
RNG	:	Re-Normalisation Group (turbulence model variant)
RPM	:	Revolutions Per Minute
RSM	:	Reynolds Stress Model
SDS	:	Sustainable Development Scenario (IEA)
SHP	:	Small Hydro Power
SS	:	Stainless Steel
SST	:	Shear Stress Transport (turbulence model)
SS314	:	Stainless Steel 314
TKE	:	Turbulent Kinetic Energy
VOF	:	Volume of Fluid (CFD multiphase method)
ZN60	:	Zinc alloy grade 60 (material designation)

List of Symbols

Greek Symbols

η_h : Hydraulic efficiency

ϕ : Speed ratio

β : Bucket outlet angle

β_1 : Bucket tip (splitter) inlet angle

β_2 : Bucket middle exit angle

β_3 : Front outlet angle

β_4 : Back outlet angle

ρ : Density of water (kg/m³)

μ : Dynamic viscosity (Pa·s)

α : Bucket inclination angle

ε : Strain; Turbulent dissipation rate

σ : Stress (Pa)

σ_v : Equivalent von Mises stress (Pa)

σ_1 **to** σ_3 : Principal stresses (Pa)

Roman / Latin Symbols

B : Bucket width (mm)

C_1 : Absolute jet velocity at nozzle exit (m/s)

D : Runner pitch diameter (m)

d : Jet diameter (m); Cut-out depth (mm)

E : Young's modulus (Pa)

F : Tangential force on bucket / runner (N)

$\{F\}$: Applied force vector

Fb : Bucket-passing frequency (Hz)

g : Acceleration due to gravity (m/s²)

$\vec{g}$: Gravitational acceleration vector (m/s²)

H : Net hydraulic head (m)

k : Relative (blade) velocity coefficient; Turbulent kinetic energy (m^2/s^2)

K_v : Coefficient of velocity

[K] : Global stiffness matrix

L : Bucket length – inner (mm)

L_s : Splitter length (mm)

m : Jet ratio (D/d)

N : Rotational speed (rpm)

N_s : Specific speed

P : Shaft power output (W); Fluid pressure (Pa)

P_h : Hydraulic power available (W)

P_s : Shaft power (W)

Q : Discharge rate (m^3/s)

R : Main cup radius (mm); Runner radius (m)

R_i : Inner cup radius (mm)

T : Torque developed on shaft (N·m); Bucket depth (mm)

t : Bucket thickness (mm)

t_s : Splitter thickness (mm)

u : Bucket peripheral velocity (m/s)

{u} : Nodal displacement vector

$\vec{V}$: Velocity vector (m/s)

Vr1 : Relative velocity at bucket inlet (m /s)

Vr2 : Relative velocity at bucket outlet (m /s)

Vw1 : Whirl velocity component at inlet (m /s)

Vw2 : Whirl velocity component at outlet (m /s)

---

w : Cut-out width (mm)

Z : Number of buckets

Ø : Mounting hole diameter (mm)

Subscripts and Abbreviations

1 : Inlet condition

2 : Outlet condition

h : Hydraulic

s : Shaft

r : Relative

w : Whirl component

v : Velocity coefficient / von-Mises

b : Bucket

i : Inner

List of Figures

Figure No.	Title	Page No.
1.1	Schematic Layout of a Typical Micro-Hydropower System Showing Water Intake, Desilting Basin, Penstock, Powerhouse with Turbine and Generator, and Tailrace Channel [17]	10
1.2	Comparative Bar Chart of Capacity Ranges for Pico-Hydro (<5 kW), Micro-Hydro (5–100 kW), and Mini-Hydro (100 kW–2 MW) with Typical Applications Indicated [87]	11
1.3	A Detailed Isometric View of a Single Pelton Bucket	13
1.4	Interdisciplinary flowchart illustrating the multi-physics design methodology for Pelton turbine runners, connecting hydraulic optimization, structural analysis, CFD simulation, material selection, and experimental validation.	16
3.1	Velocity Triangle of Pelton Turbine [88]	66
3.2	Speed Ratio Versus Hydraulic Efficiency	75
3.3	Bucket Outlet Angle Versus Hydraulic Efficiency	76
4.1	Geometry of Pelton Turbine with Dimension	90
4.2	Orientation of Pelton Turbine for: (A) Vertical, and (B) Horizontal	92
4.3	Grid Independence Test for the Bucket Structure of Pelton Wheel	99

Turbine

4.4 Mesh Generation for the Bucket Structure of: (A) Vertical Orientation, and (B) Horizontal Orientation 100

4.5 Structural Deformation of a Horizontally Oriented Bucket for Different Impact Forces: (A) F = 349 N and (B) F = 153.864 kN 103

4.6 Structural Deformation of a Vertically Oriented Bucket for Different Impact Forces: (A) F = 349 N and (B) F = 153.864 kN 104

4.7 Equivalent Stress (Left) and Strain (Right) Distribution for a Horizontally Oriented Bucket for Different Impact Forces: (A,B) F = 349 N and (C,D) F = 153.864 kN, and Regions of the Pelton Bucket Influenced by Hydraulic Loading 107

4.8 Equivalent Stress (Left) and Strain (Right) Distribution for a Vertically Oriented Bucket for Different Impact Forces: (A,B) F = 349 N and (C,D) F = 153.864 kN 107

4.9 Effect of Incidence Angle on (A) Maximum Deformation and (B) Maximum Stress for F_1 = 349 N and F_2 = 153.864 kN 109

4.10 Modal Analysis Results for Horizontal Bucket Using Uniform Pressure and F = 349 N (A) & (B), and Bucket Using Uniform Pressure and F = 153.864 kN (C) & (D), and Effect of Material Stiffness on Natural Frequency 112

4.11 Structural Deformation Contours of Horizontal Bucket Under (A) F_1 = 349 N and (B) F_2 = 153.864 kN 119

4.12 Von Mises Equivalent Stress Distribution Under Combined 121

Hydraulic Loading

4.13 First Six Modal Deformation Shapes of Pelton Turbine Bucket 124

5.1 Geometry of Pelton Turbine with Dimension 129

5.2 Computational Mesh Generated for Pelton Turbine Bucket 132

5.3 Top View of Computational Mesh Distribution 133

5.4 Boundary Condition Setup in ANSYS Fluent 136

5.5 CFD Solver Setup in ANSYS Fluent 137

5.6 Convergence Plot 137

5.7 2D Velocity and Pressure Vector 139

5.8 3D Velocity and Pressure Vector 140

5.9 2D Velocity and Pressure Vector 140

5.10 3D Velocity and Pressure Vector 141

5.11 2D Velocity and Pressure Vector 141

5.12 3D Velocity and Pressure Vector 142

5.13 2D Velocity and Pressure Vector 142

5.14 3D Velocity and Pressure Vector 143

5.15	Velocity Vector	143
5.16	Transient Velocity Contours During Jet Interaction	144
5.17	Transient Pressure Distribution Inside Pelton Bucket	145
5.18	Transient Streamline Development During Bucket Rotation	146
5.19	Volume Fraction Distribution During Transient Jet Interaction	147
5.20	Residual Convergence Plot for Transient CFD Analysis	148
5.21	Turbulence Intensity Distribution Inside Pelton Bucket	149
5.22	Comparative Hydraulic Performance for Different Inlet Velocities	152
5.23	Velocity Contours Inside Optimized Pelton Turbine Bucket	156
5.24	Streamline Distribution During Water Jet Interaction with Bucket Surface	157
5.25	Turbulent Kinetic Energy Distribution Inside Pelton Bucket	158
5.26	Transient Velocity Distribution During Jet Interaction	159
6.1	Fabrication Drawing of Pelton Turbine Bucket	163
6.2	Fabrication Drawing of Enhanced Pelton Turbine Bucket	164
6.3	Fabricated Bucket Geometry Drawing	165

6.4	Fabricated Runner with Mounted Buckets	166
6.5	Conventional (A) and Enhanced Pelton (B) Bucket Geometry Comparison	167
6.6	Top View	170
6.7	Front View	171
6.8	Runner Fabrication Stages	172
6.9	Bucket Mounting Arrangement	173
6.10	Dynamic Balancing Setup of Pelton Turbine Runner	174
6.11	Front View (A) and Side View (B) of Experimental Setup of Pelton Turbine	176
6.12	Enhanced Pelton Runner Fitted in the Casing	177
6.13	Specific Speed Versus Turbine Efficiency for Conventional and Enhanced Runner at Different Nozzle Openings: (A) Hydraulic Efficiency at 20% Opening, (B) Hydraulic Efficiency at 40% Opening, (C) Hydraulic Efficiency at 60% Opening, (D) Hydraulic Efficiency at 80% Opening, and (E) Hydraulic Efficiency at 100% Opening	185
6.14	Specific Speed Versus Shaft Power for Conventional and Enhanced Runner at Different Nozzle Openings: (A) Shaft Power at 20% Opening, (B) Shaft Power at 40% Opening, (C) Shaft Power at 60% Opening, (D) Shaft Power at 80% Opening, and (E) Shaft Power at 100% Opening	186

Chapter 1 Introduction

1.1 Global Energy Scenario and the Role of Hydropower

1.1.1 The Global Energy Transition

The global energy landscape has undergone a profound structural transformation throughout the 21st century, driven by the *convergen*ce of three critical imperatives: the urgent mitigation of anthropogenic climate change, the macroeconomic volatility inherent in fossil fuel markets, and the exponentially rising energy demands of rapidly industrializing economies. Faced with the accelerating consequences of carbon-intensive energy systems including rising mean surface temperatures, extreme weather events, and the degradation of critical ecosystems nations across the geopolitical spectrum have enacted ambitious policy frameworks and large-scale capital reallocations to displace hydrocarbon-based energy infrastructure in favour of renewable and low-emission alternatives. This systemic transition, spanning solar photovoltaics, wind energy, green hydrogen, and advanced nuclear technologies, represents not merely a technological substitution, but a fundamental re-engineering of how energy is generated, distributed, stored, and consumed at a civilizational scale. The Paris agreement from 2015 set up an international way to keep temperature increases under 2 degrees centigrade above pre industrial levels. It also had goals for staying below 1.5 degrees. the energy industries need to change since they are behind about three quarters of carbon dioxide and other gas emissions right now. That part stands out as the main issue but it seems like there could be other factors too that are not always clear. [1].

The International Energy Agency (IEA) has provided a full road map for achieving climate neutral by 2050 including calling for the worldwide triple increasing of investments in clean energy by 2030 with an expectation that nearly 90 percent of all electricity produced by 2050 will come from renewable energy sources [1]. For each type of renewable energy technology (including solar, wind, geothermal, biomass, hydropower) there needs to be an unprecedented scale of deployment (in terms of technology) to reach the above-mentioned targets.

1.1.2 Current Global Electricity Generation Mix

Globally, electricity production for 2022 hit around28294 TWh, with a wide array of different types of energy sources making up those numbers, signifying progress as well as continued struggle- particularly when it comes to using alternative-sourced electricity. Of the 2022 total, 27.3 percent was made from renewable energy; however, coal was still the largest

single energy source providing approximately 35.4 percent of all power; natural gas was next at 22.7%; and nuclear was third at 9.2%.

Hydropower was still the most significant source of renewable energy, making up 15.9 percent of total global electricity generation. When compared to other renewables (wind generating ~7.3 percent, solar PV generating ~4.5 percent, and all other renewables (biomass/geothermal/tide) generating the rest combined); hydropower produced greater than 4600 TWh of power in 2022 - generating more than all wind and solar combined worldwide.

Three reasons account for why hydropower continues to be a leader in electricity generation. First, hydropower technologies are mature and understood; many hydropower facilities have operated successfully for more than 100 years. Second, many hydropower plants have long life expectancies (often between 50-100 years) which provide decades of low-cost electricity after recovery of the initial capital investment. Third, levelized cost for electricity (LCOE) from existing hydropower plants is among the lowest levelized costs of any other type of energy generation; typically less than 2 cents per kWh.. Fourth, unlike solar and wind, hydropower output is not inherently variable and can be dispatched on demand to meet load requirements [1].

1.1.3 Hydropower as Dispatchable Clean Energy

A major factor to consider when classifying renewable sources of energy is whether the source of energy is variable or dispatchable. For example, both wind and solar energy are variable sources because their generation is subject to variability in weather, time of day, and season. While battery energy storage can assist in mitigating short-term variations in output, long-term variations in output caused by lengthy periods of low sun or low wind will need to find a different solution.

The opposite situation occurs with hydropower, which is a dispatchable source of energy. Hydropower plants that have storage reservoirs have the capability to store water and release it through turbines at the precise time that electricity demand requires. This unique ability allows hydropower to provide three important functions to the electric grid: (1) follow load—moderate output to meet the fluctuations in electricity demand; (2) frequency regulation—respond quickly, within seconds, to achieve stability in the electric grid; and (3) provide reserve capacity—provide back-up power when other forms of generation or variable sources fail or experience an unanticipated decline in output. [1]

According to the IEA's projections for climate neutral by 2050, hydropower will be the largest dispatchable source of clean energy by 2050. Under these projections, hydropower will provide more than 40 percent of the electricity generated by dispatchable clean sources of energy, which is more than the combined total of nuclear, geothermal, and battery storage electricity generation sources. Hydropower's status as the leading dispatchable source of energy will not arise from the development of new technological advancements, but rather through the strategic importance of hydropower to the future of the combination of variable renewable sources of drive into the electric grid.

1.1.4 Pumped Storage Hydropower and Grid Integration

An increasingly important kind of hydropower is pumped storage. As water batteries, pumped storage hydropower (PSH) plants Water is conveyed from the lower reservoir to the upper reservoir through a pumping mechanism. during period the power is cheap and there's little demand for electricity; then during periods when there is lots of demand for electricity, PSH plants will release water through turbines to create electricity. PSH represents over 90% of the total worldwide energy storage capacity, and PHS exceeds all other battery systems combined in terms of capacity [2].

With the rapid increases in wind and solar resources, the value of PSH continues to grow. Recognizing the strategic importance, in April 2023, the government issued comprehensive Guidelines for Pumped Storage Hydropower Projects, creating a consistent regulatory environment for developers across India [2]. This set of guidelines aims to facilitate the development of India's pumped storage hydropower (PSH) resource, which has a potential capacity of approximately 100 GW, that will provide critical grid flexibility to enable the country to achieve its goal of 500 GW of capacity from non-fossil fuel resources by 2030.

1.1.5 Regional Variations in Hydropower Deployment

The regional variation in hydropower deployment is largely due to critical factors such as geographic characteristics, availability of infrastructure, and policy guidelines.

China is the leading global producer of hydropower, with more than 400 gigawatts (GW) of generation capacity. The hydroelectric resources of China are being aggressively developed; major projects being completed include China's Three Gorges Dam (22.5 GW) and many additional large hydropower projects are still being undertaken. Approximately 16% of electricity produced in China is generated by hydropower, and new project construction continues in southwestern China, increasing generation capacity in those regions [3].

Many of the countries in South America receive very high percentages (i.e., more than 60%) of their total electricity consumption from hydroelectric sources; among those countries who utilize hydropower in their energy mix are Brazil, Paraguay, and Venezuela. Among the largest operational hydropower facilities Globally, Itaipu Dam (14 GW), is located on the border between Brazil and Paraguay.

Hydropower is also used extensively in North America, which has substantial hydropower infrastructure; Canada generates more than 60% of its electricity from hydropower and the United States generates approximately 6% of its electricity from hydropower. A majority of the premier potential hydropower sites in North America have already been developed, and thus most of the investment in hydropower is for the rehabilitation and upgrade of existing facilities.

In Africa, there is a large amount of untapped hydroelectricity that could be produced from rivers such as the Congo. One of the biggest new hydroelectric facilities in the world is the Grand Ethiopian Renaissance Dam (6.45 GW) located on the Nile River. Hydropower is estimated to play a significant role in facilitating grid connectivity for nearly 600 million people who currently lack reliable access to electricity [3].

In Europe, countries like Norway (where over 90% of total electrical production comes from hydroelectricity), Switzerland, Austria, and Sweden all have developed hydropower industries. The European Union has adopted a Renewable Energy Directive to promote the use of hydropower and other forms of renewable energy according to environmental sustainability guidelines.

India, which we discussed earlier in Section 1.2, has about 52 GW of existing hydroelectric capacity from large dams, as well as smaller generation facilities; however, it also has a very large amount of potential future hydroelectric generation capacity that is not currently being utilized, especially in the Himalayas and the Western Ghats.

1.1.6 Environmental and Social Considerations

While hydropower offers clear climate benefits compared to fossil fuel generation, it is not without environmental and social impacts. Large reservoir projects can inundate forests, agricultural land, and human settlements, leading to displacement of communities and loss of terrestrial ecosystems. Reservoir creation can alter river flow regimes, affect fish migration patterns, and change downstream sediment transport—potentially impacting agriculture and coastal ecosystems [4].

These considerations have shifted attention toward small-scale, low-impact hydropower, including micro-hydro and pico-hydro systems. Such systems typically operate as run-of-river installations, requiring no large reservoir and causing minimal environmental disruption. They are particularly suited for remote, off-grid locations where the alternative would be diesel generators or no electricity at all. The Pelton turbine, which is the focus of this thesis, is the technology of choice for many such installations due to its high efficiency, mechanical simplicity, and adaptability to varying flow conditions [5, 4].

1.1.7 Future Projections and the Role of Optimization

The IEA's Stated Policies Scenario (STEPS) and Sustainable Development Scenario (SDS) provide contrasting projections for hydropower's future. Under STEPS, which reflects existing and announced policies, global hydropower capacity grows from approximately 1,400 GW in 2022 to about 1,800 GW by 2050—a modest but steady increase. Under the SDS, which aligns with the Paris Agreement goals, capacity reaches approximately 2,000 GW by 2050, with significant expansion in developing countries [1].

Achieving these projections requires not only new construction but also optimization of existing facilities. Many hydropower turbines currently in operation operate below their theoretical maximum efficiency due to suboptimal design, wear and tear, or mismatch between original design conditions and actual operating conditions. Systematic parametric optimization, informed by computational fluid dynamics and validated by experimental testing, offers a pathway to improve the performance of both new and existing installations without additional civil works or environmental impact.

This is particularly true for Pelton turbines used in micro-hydro applications. As noted in the introduction to this chapter, many micro-hydro Pelton turbines currently in service are scaled-down versions of larger commercial designs, fabricated without site-specific parametric optimization. Consequently, these turbines often achieve hydraulic efficiencies of only 70-85%, leaving substantial room for improvement. The research presented in this thesis directly addresses this gap by developing and validating an integrated optimization methodology applicable to micro-hydro Pelton turbines.

1.2 Hydropower Scenario in India

India has emerged as a global leader in renewable energy deployment, driven by a combination of energy security concerns, climate commitments, and rapid economic growth. As of fiscal year 2024-25, The nation's total installed power generation capacity attained approximately 450 GW.

Table 1.1 presents the distribution of this capacity across various sources.

Table 1.1 Installed Power Generation Capacity in India as of FY 2024-25 [6]

Source	Installed Capacity (GW)	Share (%)
Thermal (Coal, Gas, Oil)	~239	~53
Renewable (Solar, Wind, Small Hydro, Bio)	~159	~35
Large Hydropower	~52	~12
Nuclear	~7.5	~1.7
Total	**~450**	**100**

While thermal power still constitutes the majority of India's energy mix, the share of renewable sources has grown substantially over the past decade. Within the renewable portfolio, large hydropower remains a critical baseload component, offering both energy storage and grid stability benefits that variable sources like solar and wind cannot provide on their own. India ranks among the top five countries globally in terms of hydroelectric generating capacity [6]. However, despite this standing, the country's hydropower potential has been far from fully exploited.

According to comprehensive estimates prepared by the Alternate Hydro Energy Centre at the Indian Institute of Technology Roorkee, India possesses approximately 148 GW of total hydropower potential (including large and small schemes). Yet the majority of this remains commercially undeveloped due to a combination of factors, including geological challenges, land acquisition issues, environmental clearances, and infrastructure constraints [7]. More specifically, the small hydro sector—defined as plants with an installed capacity of up to 25 MW and administered by the Ministry of New and Renewable Energy (MNRE)—has been assessed across 7,133 potential development sites nationwide. These sites represent a total estimated potential of 21,133 MW. Of this, only about 25 percent (approximately 5,280 MW)

has been developed to date [7], highlighting a significant gap between potential and exploitation. Table 1.2 shows hydropower projects in India with more than 25MW of capacity.

Table 1.2 Hydro Power projects with more than 25MW capacity[85].

S. No.	Name of the Projects	Capacity (MW)	District
1	Balimela	510	Malkangiri
2	Hirakud (Burla)	287.8	Sambalpur
3	Hirakud (Chiplima)	72	Sambalpur
4	Rengali	250	Angul
5	**Upper Indravati**	**600**	**Kalahandi**
6	Upper Kolab	320	Koraput
7	Machkund	114.75	Koraput
8	Bhimkund	30	Keonjhar
9	Baljori	230	Keonjhar
10	Lodani	64	Sundergarh
11	Tikkarpara	220	Angul
12	Salki	70	Boudh
13	Kharag	63	Kandhmal
Total		**2831.55**	

Recognizing this untapped potential and the need for flexible, dispatchable renewable energy, the Government of India has initiated several policy measures to accelerate hydropower development. In April 2023, the Ministry of Power issued comprehensive Guidelines for Pumped Storage Hydropower Projects, establishing a consistent regulatory framework for hydropower construction nationwide [2]. These guidelines address critical issues such as

tariff determination, water usage charges, and environmental compliance, which have historically hindered project viability.

Furthermore, the Small Hydro Power Development Scheme (2026-31) has been allocated Rs. 2,584.60 crore (approximately USD 310 million) as central financial assistance. This outlay is designed to facilitate an estimated total investment of approximately Rs. 15,000 crore (about USD 1.8 billion) in small hydroelectric projects across the country, leveraging public funds to attract private sector participation [6]. Based on projections from the Central Electricity Authority, which take into account projects under construction, approved, and planned, India's installed hydropower generation capacity (including both large and small hydro) is expected to reach 61.6 GW by the fiscal year ending March 2030 [8]. Table 1.3 shows the chronological evolution of Hydropower Policies in India.

Table 1.3 Chronological Evolution of Hydropower Policies in India [8]

Year	Policy / Initiative	Key Features and Impact
2008	National Action Plan on Climate Change (NAPCC)	Recognized hydropower as a critical renewable energy source for reducing carbon emissions and improving grid stability.
2014	Revised Small Hydro Power (SHP) Programme	Enhanced Central Financial Assistance (CFA) for projects up to 25 MW to encourage private participation and electrification in remote regions.
2016	Hydro Power Policy Reforms	Introduced policy measures addressing categorization and incentives for both large and small hydro projects, emphasizing renewable energy integration, viability gap support, and faster environmental clearances. (Wikipedia)
2019	Large Hydro Declared Renewable Energy	Hydropower projects above 25 MW were officially categorized as renewable energy projects, enabling Renewable Purchase Obligation (RPO) benefits and budgetary support for flood moderation and enabling infrastructure. (Wikipedia)

2023	Pumped Storage Project (PSP) Guidelines	Ministry of Power issued guidelines promoting rapid development of pumped storage projects through simplified approvals, private sector participation, concessional land allocation, and streamlined DPR procedures. The policy recognized PSPs as key long-duration energy storage systems supporting solar and wind integration. (Ministry of Power)
2025	CEA Pumped Storage Expansion Roadmap	Central Electricity Authority projected aggressive pumped storage expansion to support India's renewable energy targets. The roadmap estimated national pumped storage potential exceeding 100 GW and outlined phased capacity addition plans up to 2035–36. (Central Electricity Authority)
2026	Small Hydro Power (SHP) Development Scheme (FY 2026–31)	Union Cabinet approved a ₹2584.60 crore scheme targeting approximately 1500 MW additional SHP capacity. The scheme prioritizes hilly and northeastern states with enhanced financial assistance for border and remote regions. (Press Information Bureau)
2030 (Projected)	CEA Renewable Integration and Hydro Capacity Targets	CEA forecasts indicate hydropower and pumped storage will play a central role in achieving India's 500 GW non-fossil energy target by 2030, with rapid expansion of PSPs for grid balancing and renewable integration. (S&P Global)

Despite these positive trends, challenges remain. Hydropower projects in India often face long gestation periods, cost overruns, and local opposition related to displacement and ecological impacts. Nevertheless, with renewed policy support and the increasing value of energy storage in a renewable-heavy grid, the sector is poised for moderate but significant growth over the coming decade.

1.3 Micro-Hydropower: Definition and Significance

Within the broader hydropower sector, micro-hydropower occupies a distinct and important niche. Unlike large-scale hydropower projects that require massive dams and reservoirs, micro-hydro systems are decentralized, low-impact energy solutions. Typically, micro-hydro refers to plants with an installed capacity ranging from a few kilowatts up to 100 kW, though definitions vary by country. For context, pico-hydro (under 5 kW) serves single households, while mini-hydro (100 kW to 1–2 MW) approaches small commercial scales. These systems are particularly well-suited for remote, off-grid locations in hilly and mountainous terrains where grid extension is economically unviable due to high transmission costs and challenging geography. Figure 1.1 shows a schematic layout of a typical micro-hydropower system with all components.

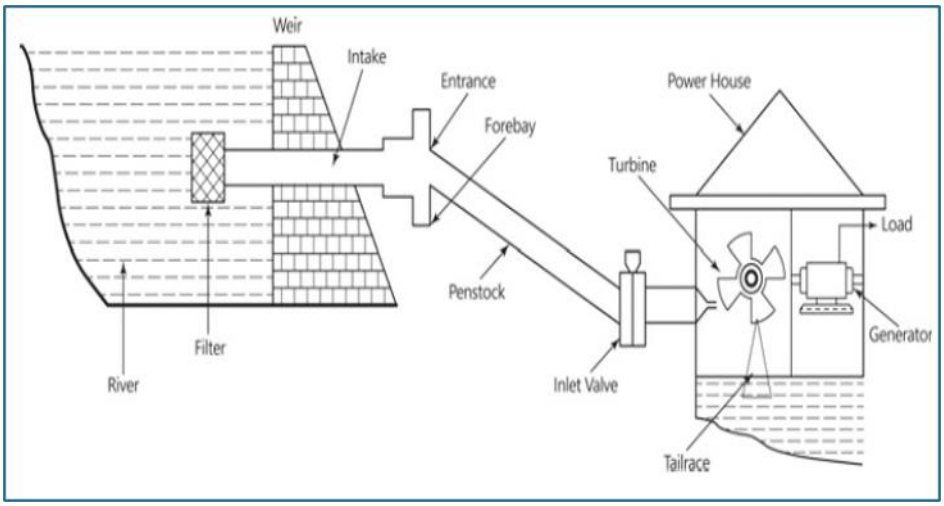

Figure 1.1 Schematic layout of a typical micro-hydropower system showing water intake, desilting basin, penstock, powerhouse with turbine and generator, and tailrace channel [17]

The advantages of micro-hydropower are manifold. First, these systems can operate with minimal environmental impact, as they often require no large reservoirs or dams; instead, they divert a portion of stream flow through a pipeline (penstock) and return it downstream. Second, unlike solar or wind systems, micro-hydro provides continuous, predictable power output unaffected by diurnal or weather variations—assuming a perennial water source. This makes it a baseload renewable option. Third, the technology is mature, reliable, and can be maintained with locally available skills after basic training. Fourth, micro-hydro plants have exceptionally long operational lives, often exceeding 40 years with regular maintenance, and their components (e.g., nozzles, buckets) are often repairable or replaceable locally.

Figure 1.2 shows a comparative bar chart of the capacity of different ranges. In the Indian context, micro-hydropower holds particular promise for the Himalayan and Western Ghats regions, where numerous perennial streams with high hydraulic head (vertical drop) and low discharge rates remain unexploited. These sites are ideally suited for impulse turbines, among which the Pelton turbine has historically demonstrated superior operational efficiency and structural integrity compared to other turbine types [4]. The Himalayan states such as Uttarakhand, Himachal Pradesh, and Jammu & Kashmir, as well as the Western Ghats in Kerala, Karnataka, and Maharashtra, contain thousands of potential sites below 100 kW capacity that could serve village electrification, small enterprises, and community loads.

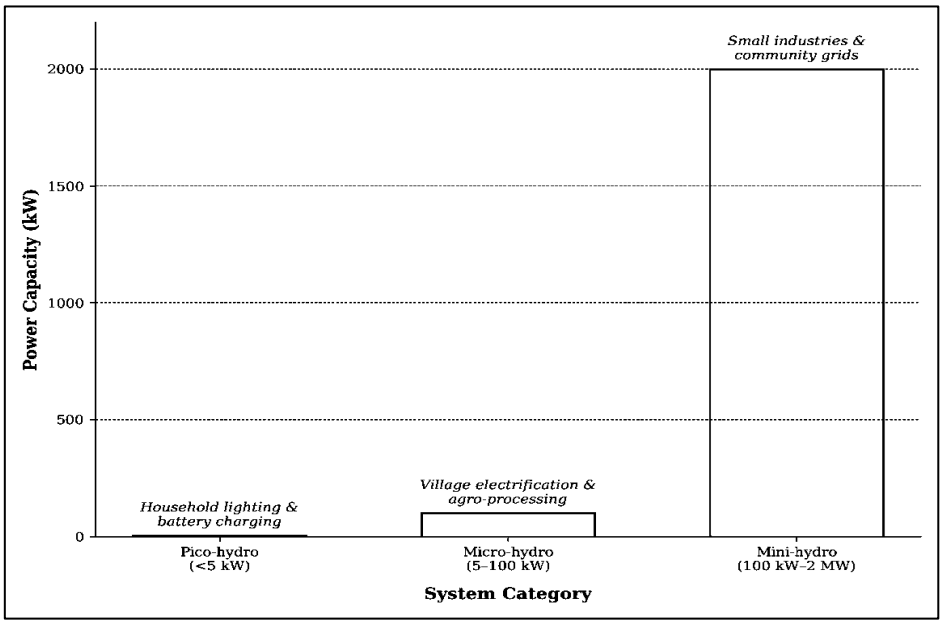

Figure 1.2 Comparative bar chart of capacity ranges for pico-hydro (<5 kW), micro-hydro (5–100 kW), and mini-hydro (100 kW–2 MW) with typical applications indicated [87]

1.4 The Pelton Turbine: Principles of Operation

The Pelton wheel is an impulse-type hydraulic turbine invented by the American engineer Lester Allan Pelton in the 1870s. Pelton's original patent, titled "Water Wheel," was granted in 1880 [9]. Prior designs used simple flat or cup-shaped buckets, which wasted significant energy. Pelton’s insight was to shape the bucket as a double-dish geometry that splits the jet and turns it smoothly. The turbine transforms the kinetic energy of high-velocity water jets into mechanical work through a rotating shaft, making it ideal for high-head, low-flow conditions common in micro-hydro sites.

The operating principle of the Pelton turbine fundamentally differs from reaction turbines such as Francis and Kaplan machines. In reaction turbines, the runner operates while fully submerged, and pressure energy is continuously converted as water flows through the blade passages; the runner is surrounded by water at above-atmospheric pressure. In contrast, the Pelton turbine operates at atmospheric pressure; all pressure energy supplied by the water is converted into kinetic energy within the nozzle before the water jet contacts the runner buckets. The high-velocity jet strikes the buckets tangentially, and only kinetic energy is transferred to the shaft [10]. This design eliminates the need for a sealed turbine casing, reducing manufacturing complexity and maintenance. Figure 1.3 shows detailed isometric view of a single Pelton bucket showing the splitter ridge, elliptical cavity shape, and the path of water jet entry and exit.

Pelton's innovative contribution was the double-dish bucket design. This geometry allows the incoming jet to be split at the splitter ridge (also called the splitter or knife edge), turned smoothly within the bucket's elliptical cavities, and discharged with minimal residual velocity. The splitter ridge ensures even division of the jet, preventing lateral thrust that could damage bearings. When the bucket tip speed is approximately half the jet velocity a condition defined by the speed ratio $\varphi = 0.47$ to 0.52, ideally $\varphi = 0.5$the exiting water possesses near-zero absolute velocity, indicating near-complete transfer of available kinetic energy to the shaft. This characteristic makes the Pelton turbine one of the most volume-efficient hydraulic machines ever devised. Efficiency can exceed 90% under optimal conditions, with losses occurring only due to windage, bearing friction, and minor residual jet energy.

Among all design parameters, the bucket geometry is the most influential factor governing the hydraulic performance of a Pelton turbine because it directly determines the efficiency of momentum transfer between the high-velocity water jet and the runner. The splitter geometry, bucket curvature, bucket depth, outlet angle, cut-out profile, and surface contour collectively control jet bifurcation, pressure distribution, flow attachment, turbulence generation, splash losses, and residual outlet velocity. Properly designed bucket geometry ensures smooth flow guidance with minimum hydraulic losses, thereby maximizing hydraulic efficiency and shaft power. Conversely, poorly designed bucket geometry leads to flow separation, excessive turbulence, increased residual kinetic energy, uneven loading, and lower turbine efficiency. In addition to hydraulic performance, bucket geometry also affects structural stress distribution, vibration behaviour, erosion characteristics, and manufacturability. Therefore, bucket geometry forms the fundamental basis of the present research, and its optimization

serves as the foundation for the integrated analytical, CFD, FEA, and experimental investigations presented work.

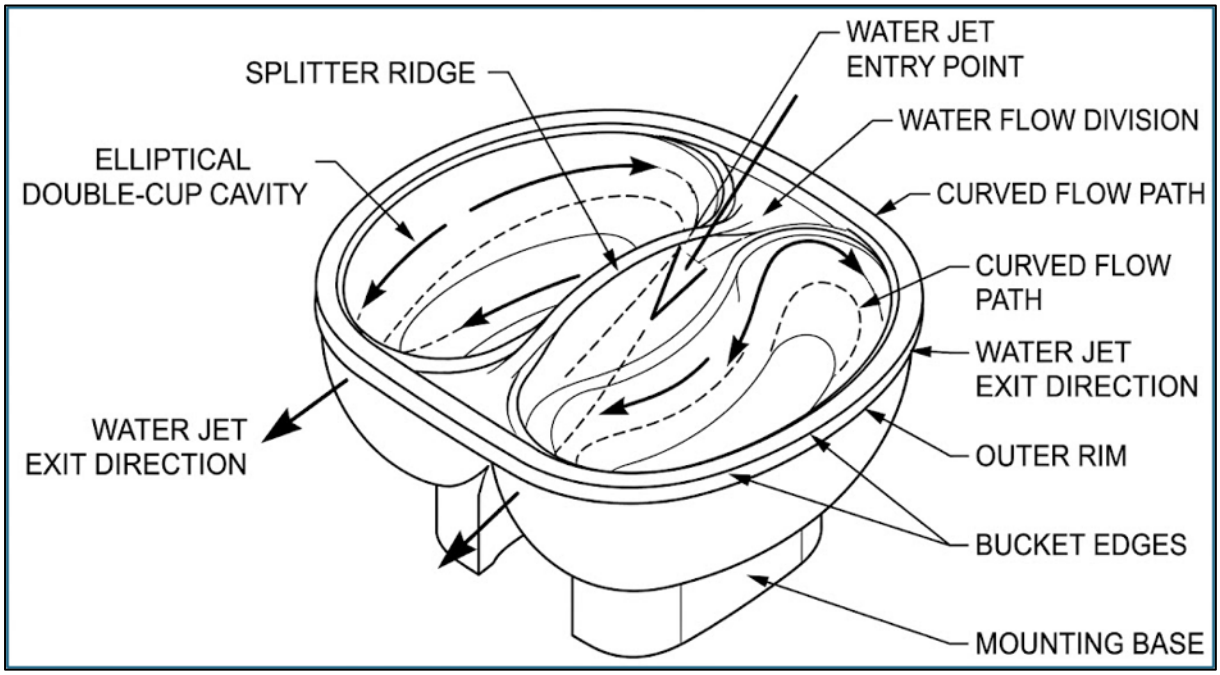

Figure 1.3 A detailed isometric view of a single Pelton bucket

1.5 Suitability of Pelton Turbines for Micro-Hydro Applications

The Pelton turbine is uniquely suited for micro-hydro applications characterized by high hydraulic head and low discharge rates—conditions commonly encountered in mountainous regions [4]. Heads ranging from 50 meters to over 1,800 meters can be effectively utilized, with corresponding jet velocities reaching 58.7 m/s or higher at the largest heads. This operational flexibility makes the Pelton turbine the default choice for off-grid and remote power generation in terrains where alternative turbine types, such as Francis or Kaplan, would be economically or technically infeasible.

The absence of submergence requirements simplifies civil works, as the turbine can be positioned above the tailwater level. Unlike reaction turbines that must be housed within a draft tube submerged below the tailwater, the Pelton runner operates in air. This eliminates draft tube losses, reduces maintenance complexity, and significantly lowers the cost of the powerhouse foundation. Furthermore, the modular nature of Pelton turbines—with multiple nozzles arranged around the runner—allows capacity expansion without complete system redesign. For instance, a single-nozzle configuration can be upgraded to a twin- or four-nozzle arrangement to accommodate seasonal flow variations or increased community

demand, simply by adding spear valves and nozzles while retaining the existing runner and housing.

However, the performance of Pelton turbines in micro-hydro applications is highly sensitive to geometric design parameters. Unlike large commercial Pelton turbines that have benefited from decades of evolutionary refinement through full-scale model testing and empirical corrections, many micro-hydro Pelton turbines currently in service are scaled-down versions of larger designs. These scaled geometries are often produced without systematic parametric optimization for the specific hydraulic and operating conditions (e.g., jet diameter-to-bucket width ratio, number of buckets, cutout geometry) of the installation site. Consequently, these turbines frequently operate below their theoretical maximum hydraulic efficiency, with reported field efficiencies between 65% and 75%, compared to potential laboratory efficiencies exceeding 85% [11, 12]. Table 1.4 Comparative Analysis of Operational Head and Flow Ranges for Various Turbine Types.

Table 1.4 Comparison of operational head and flow ranges for different turbine types

Turbine Type	**Operating Head Range (m)**	**Flow Range**	**Suitable Flow Condition**	**Typical Application Domain**
Pelton Turbine	50 – 1800	Low	Low discharge, high velocity jet	High-head mountainous regions
Francis Turbine	20 – 300	Medium	Moderate discharge and head	Medium-head hydropower plants
Kaplan Turbine	2 – 40	High	Large discharge, low head	Run-of-river and low-head plants
Cross-flow Turbine	5 – 200	Low to Medium	Variable flow conditions	Small and micro hydropower systems

1.6 Research Motivation and Rationale

The literature review (presented comprehensively in Chapter 2) reveals a significant research gap. While numerous studies have examined individual aspects of Pelton turbine design—hydraulic parametric optimization [5, 11, 13, 14], structural finite element analysis [12, 15, 16], material selection for erosion resistance [15, 16, 17, 18], computational fluid dynamics (CFD) modeling [19, 20, 21, 22, 23, 24], and experimental performance testing [5, 25, 26]—no single investigation has integrated all these dimensions into a unified research framework for micro-hydro applications. Most existing studies remain siloed within their respective disciplines: hydraulic optimizers rarely consult structural constraints, while CFD specialists often employ idealized geometries that ignore manufacturing realities.

This fragmentation creates a knowledge deficit. Designers and practitioners lack confidence when developing new Pelton runners because the interdependencies between hydraulic geometry, structural integrity, material behavior, and actual flow phenomena are not simultaneously addressed in existing literature. A bucket geometry that maximizes theoretical hydraulic efficiency may exhibit unacceptable stress concentrations under jet impact; a structurally robust material (e.g., hardened stainless steel) may perform poorly in CFD simulations due to surface finish limitations from casting defects; a design that excels in numerical models may prove difficult to fabricate with the required dimensional accuracy using locally available manufacturing methods such as CNC machining or 3D printing. Figure 1.4 shows Interdisciplinary Flowchart Representing the Multi-Physics Design Methodology for Pelton Turbine Runners Incorporating Hydraulic Optimization, Structural Analysis, CFD Simulation, Material Selection, and Experimental Validation.

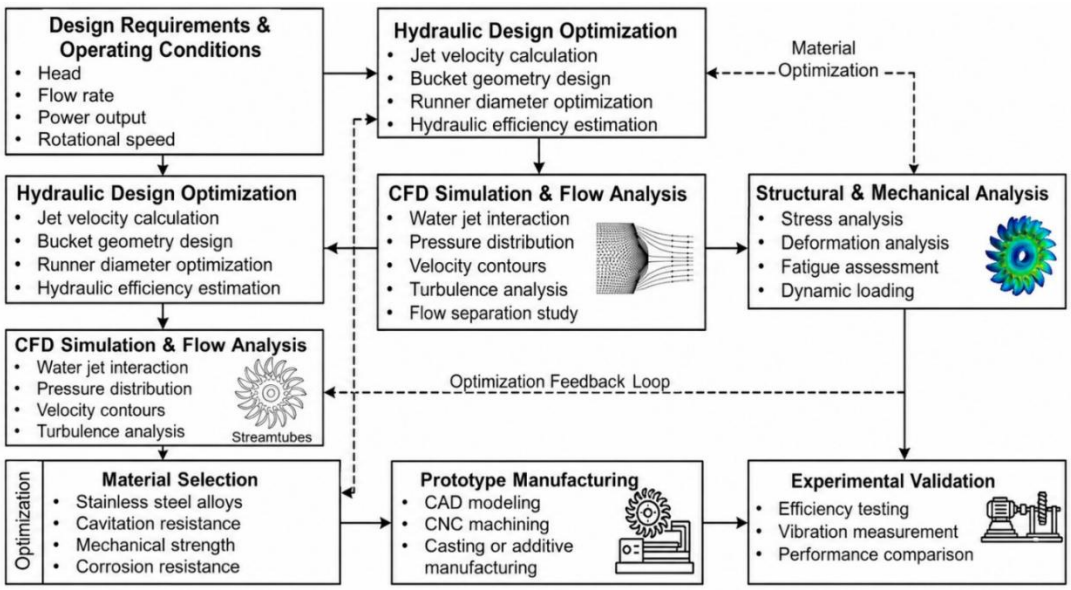

Figure 1.4 Interdisciplinary flowchart illustrating the multi-physics design methodology for Pelton turbine runners, connecting hydraulic optimization, structural analysis, CFD simulation, material selection, and experimental validation.

Furthermore, the micro-hydro context imposes additional constraints. Cost sensitivity demands judicious material selection and fabrication methods—exotic alloys or five-axis machining may be unaffordable, whereas cast iron or additively manufactured polymers may offer acceptable trade-offs. Remote installation locations necessitate corrosion resistance and wear tolerance, particularly in sediment-laden Himalayan streams where quartz particles accelerate bucket erosion [16]. The absence of grid connectivity requires consistent efficiency across varying loads, meaning that the turbine must maintain acceptable performance during partial flow conditions (e.g., single-nozzle operation) without excessive jet interference or back splashing.

These considerations motivated the present research. The central premise is that a truly optimal Pelton turbine runner for micro-hydro applications can only be realized through an integrated multi-physics methodology that encompasses: (1) systematic parametric hydraulic optimization using design of experiments and response surface methods; (2) rigorous static structural and pre-stress modal finite element analysis to verify mechanical integrity and avoid resonance; (3) comprehensive steady-state and transient computational fluid dynamics simulation using volume of fluid (VOF) multiphase models to resolve jet-bucket interaction; (4) informed material selection and fabrication using appropriate manufacturing techniques (e.g., CNC machining from billet, investment casting, or fused deposition modeling); and (5) controlled experimental validation supported by formal uncertainty analysis in accordance with established standards [14].

Chapter 2 Literature Review

2.1 Introduction

The continuously increasing global demand for electrical energy, combined with rapid depletion of fossil fuel reserves and growing environmental concerns associated with greenhouse gas emissions, has accelerated the worldwide transition toward renewable and sustainable energy systems. Among the various renewable energy resources currently available, hydropower remains one of the most mature, reliable, and efficient methods of electricity generation due to its high energy conversion efficiency, long operational life, stable output characteristics, and relatively low operating cost [1,2]. In comparison with intermittent renewable sources such as solar and wind energy, hydropower offers superior controllability and can provide continuous base-load power generation under suitable hydrological conditions.

According to recent global energy assessments, hydropower contributes the largest share among renewable electricity generation technologies and is expected to continue playing a major role in achieving future carbon-neutral energy targets [1,2]. The International Energy Agency (IEA) has projected that hydropower will remain a critical component of future clean-energy infrastructure due to its operational flexibility and grid-stabilization capability [1]. Similarly, the Renewable Energy Policy Network for the 21st Century (REN21) identified hydropower as one of the most dependable renewable technologies for supporting long-term sustainable development goals [2].

India possesses substantial untapped hydropower potential due to its favorable geographical and hydrological conditions, particularly within mountainous regions such as the Himalayas, Western Ghats, and northeastern states. Recent reports published by the Ministry of New and Renewable Energy (MNRE) and the Central Electricity Authority (CEA) indicate that although significant large-scale hydropower infrastructure has already been developed, a considerable portion of small and micro-hydropower potential still remains unexploited [3,4]. The Alternate Hydro Energy Centre (AHEC), IIT Roorkee, identified thousands of potential small-hydropower sites throughout India capable of supporting decentralized electricity generation for remote and rural communities [5]. To further accelerate hydropower deployment, the Government of India has introduced several policy initiatives and financial support schemes aimed at encouraging investment in small and micro-hydropower projects [6].

Micro-hydropower systems generally operate within the power range of a few kilowatts to several hundred kilowatts and are particularly suitable for isolated rural regions where extension of the conventional electrical grid is economically impractical. Such systems provide multiple advantages, including reduced transmission losses, improved rural electrification, low environmental impact, and enhanced energy sustainability. The selection of an appropriate hydraulic turbine plays a crucial role in determining the efficiency and reliability of a micro-hydropower system, and turbine selection is primarily governed by the available hydraulic head and discharge conditions at the installation site.

Among the different classes of hydraulic turbines, the Pelton turbine is widely recognized as the most suitable turbine for high-head and low-discharge applications. The Pelton turbine, originally developed by Lester Allan Pelton during the late nineteenth century, operates on the principle of impulse momentum transfer, where the entire hydraulic head is first converted into kinetic energy in the form of a high-velocity water jet before interacting with the turbine runner buckets [7]. Unlike reaction turbines such as Francis or Kaplan turbines, the Pelton turbine operates under atmospheric pressure conditions, thereby simplifying its construction and reducing cavitation-related complications under many operating conditions.

The characteristic double-cup bucket geometry of the Pelton runner enables efficient redirection of the incoming water jet, allowing maximum transfer of kinetic energy to the rotating runner. The hydraulic efficiency of a Pelton turbine depends strongly upon several interrelated design parameters, including speed ratio, bucket geometry, splitter shape, bucket exit angle, nozzle configuration, runner dimensions, and number of buckets [8–12]. Even small variations in these parameters can significantly influence jet interaction, momentum transfer, flow separation, splash losses, and overall turbine performance.

With advancements in computational modelling and numerical simulation techniques, modern Pelton turbine research has increasingly focused on improving hydraulic performance through Computational Fluid Dynamics (CFD), Finite Element Analysis (FEA), transient flow simulations, parametric optimization, and experimental validation studies. Researchers have investigated free-surface flow behavior, bucket stress distribution, resonance characteristics, erosion mechanisms, cavitation phenomena, and multi-nozzle interactions using advanced software platforms such as ANSYS Fluent, ANSYS CFX, and ANSYS Mechanical APDL [13–18]. These developments have significantly improved the

understanding of complex fluid–structure interactions occurring within Pelton turbine systems.

Despite substantial progress in Pelton turbine research, existing literature reveals that many studies focus primarily on isolated aspects such as hydraulic optimization, CFD flow analysis, structural analysis, or experimental investigations independently. Very few investigations integrate hydraulic design optimization, structural static analysis, modal analysis, transient CFD simulations, fabrication methodology, experimental validation, and uncertainty analysis within a unified multi-physics framework specifically tailored for micro-hydropower applications. Consequently, a comprehensive integrated design methodology for micro-hydro Pelton turbines remains insufficiently explored.

The present research aims to address this gap by developing an integrated framework for the design, development, analysis, fabrication, and experimental evaluation of an optimized micro-hydro Pelton turbine runner. The study combines analytical hydraulic optimization, structural and modal finite element analysis, steady-state and transient CFD simulations, fabrication using advanced manufacturing techniques, and experimentally validated performance testing under controlled operating conditions. The literature reviewed in this chapter establishes the theoretical and technical foundation necessary for the development of the proposed research methodology.

2.2 Literature Survey of Fundamentals and Design of Pelton Turbine Operation

Hydraulic turbines are broadly classified into impulse turbines and reaction turbines based on the mechanism through which hydraulic energy is converted into mechanical energy. In reaction turbines, pressure energy conversion occurs continuously throughout the runner passage, whereas in impulse turbines the entire hydraulic head is first converted into kinetic energy before interacting with the runner blades. Among impulse turbines, the Pelton turbine represents one of the most efficient and widely used configurations for high-head and low-discharge hydropower applications [7,8].

The Pelton turbine operates according to the principle of impulse momentum transfer. Water available at high elevation possesses significant potential energy due to the hydraulic head. This hydraulic head is converted into kinetic energy through a specially designed nozzle that produces a high-velocity free jet directed tangentially onto the turbine runner buckets. The water jet strikes the splitter located at the center of each bucket and divides symmetrically into two streams that flow over the curved inner surfaces of the bucket before exiting at the

outlet edge [9,10]. The change in momentum of the water jet during this deflection process generates an impulsive force on the runner, causing rotation of the turbine shaft.

Unlike reaction turbines, the Pelton turbine runner operates under atmospheric pressure conditions because pressure conversion occurs entirely within the nozzle before jet impact. Consequently, Pelton turbines are free from many of the pressure-related operational complexities associated with reaction turbines, such as draft-tube requirements and severe cavitation under normal operating conditions [8]. This operational simplicity contributes significantly to the high reliability and durability of Pelton turbines in remote micro-hydropower installations.

The fundamental performance characteristics of a Pelton turbine are governed by velocity-triangle relationships developed from Euler's turbine equation. The hydraulic efficiency of a Pelton turbine depends primarily upon the relationship between the peripheral speed of the runner buckets and the velocity of the incoming water jet. This relationship is commonly expressed using the speed ratio, defined as:

$$\phi = \frac{u}{V_1} \text{----------[1]}$$

where $u$represents the bucket peripheral velocity and V_1represents the jet velocity at nozzle exit. Extensive theoretical and experimental investigations have demonstrated that maximum hydraulic efficiency is obtained when the runner speed approaches approximately one-half of the jet velocity [9–12]. Under ideal conditions, the optimum speed ratio generally lies between 0.46 and 0.49, allowing maximum transfer of kinetic energy from the water jet to the rotating runner.

The theoretical hydraulic efficiency of a Pelton turbine may be expressed as:

$$\eta_h = 2\phi(1-\phi)(1+k\cos\beta \text{ ----------[2]}$$

This relationship indicates that hydraulic efficiency depends strongly on both speed ratio and bucket outlet angle. Lower outlet angles generally reduce residual exit velocity and improve momentum transfer, thereby increasing turbine efficiency [13–16]. Consequently, optimization of bucket geometry and outlet angle represents one of the most important aspects of Pelton turbine design.

The geometry of the Pelton bucket plays a critical role in controlling jet bifurcation, water-sheet formation, flow attachment, and energy transfer efficiency. The splitter, which divides

the incoming jet into two equal streams, must be carefully designed to minimize impact losses and ensure smooth flow distribution across the bucket surfaces [15]. Similarly, bucket depth, width, curvature, and outlet geometry influence the degree of jet deflection and the magnitude of residual kinetic energy remaining in the discharged water. Improper bucket geometry may lead to flow separation, turbulence, splash losses, and reduction in hydraulic efficiency [14,15].

The number of buckets mounted on the runner also significantly affects turbine performance. If too few buckets are used, portions of the water jet may pass through the runner without effective interaction, reducing energy extraction efficiency. Conversely, excessive bucket numbers may create interference between successive buckets and increase hydraulic losses [11,18]. Kim et al. [11] developed a theoretical methodology for selecting the optimum number of buckets based on runner diameter and jet dimensions, while Zidonis and Aggidis [18] employed Computational Fluid Dynamics (CFD) techniques to determine bucket-number configurations that maximize hydraulic performance.

Another important design parameter is nozzle configuration. The nozzle converts pressure energy into kinetic energy and controls jet quality, velocity distribution, and jet coherence. Uniform jet formation is essential to ensure stable interaction between the water jet and the runner buckets. Poor nozzle geometry or jet misalignment can result in asymmetric loading, increased vibration, splash losses, and reduced efficiency [13,17].

Modern Pelton turbine research increasingly incorporates advanced numerical simulation techniques to study free-surface flow behavior and fluid–structure interaction within the turbine runner. CFD investigations have enabled detailed visualization of jet bifurcation, pressure distribution, turbulent kinetic energy, and transient flow behavior inside rotating buckets [13–18]. These studies have significantly enhanced the understanding of Pelton turbine hydrodynamics and established the foundation for modern optimization methodologies.

Overall, the operational characteristics of Pelton turbines depend on the combined interaction of hydraulic design parameters including speed ratio, bucket geometry, splitter shape, outlet angle, nozzle configuration, and bucket number. Proper optimization of these parameters is essential for achieving high hydraulic efficiency, stable operation, and long-term reliability in micro-hydropower applications. The following sections discuss in detail the various design

parameters, numerical analyses, structural considerations, and experimental investigations associated with Pelton turbine performance enhancement.

2.2.1 Hydraulic Design Parameters Affecting Pelton Turbine Efficiency

The hydraulic performance of a Pelton turbine is governed primarily by the interaction between the high-velocity water jet and the rotating runner buckets. Since the Pelton turbine operates entirely through impulse momentum transfer, even small variations in hydraulic design parameters can significantly influence jet deflection characteristics, energy transfer efficiency, flow stability, splash losses, and overall turbine performance. Consequently, optimization of hydraulic parameters has remained one of the most extensively investigated areas in Pelton turbine research [13–15].

Researchers have identified several important hydraulic design parameters affecting Pelton turbine efficiency, including speed ratio, bucket outlet angle, splitter geometry, nozzle configuration, runner dimensions, and number of buckets [13–20]. These parameters are highly interdependent, and improper selection of one parameter may adversely influence the effectiveness of others. Modern optimization studies therefore increasingly focus on integrated parametric investigations rather than isolated parameter analysis.

2.2.2 Speed Ratio Optimization

Among all Pelton turbine design parameters, the speed ratio is considered one of the most influential factors governing hydraulic efficiency. The speed ratio represents the ratio between bucket peripheral velocity and incoming jet velocity and directly controls the momentum transfer process occurring between the water jet and the runner buckets. Theoretically, maximum energy transfer occurs when the runner speed approaches approximately half of the jet velocity [9,10].

Several researchers have experimentally and analytically demonstrated that optimum Pelton turbine performance generally occurs within a speed-ratio range of approximately 0.46 to 0.49 [9,10,13]. Nasir [9] established analytical design procedures for micro-hydropower Pelton turbines and reported that maximum efficiency is obtained when the bucket velocity is nearly half of the jet velocity. Similar conclusions were reported by Cobb and Sharp [10] during experimental investigations on pico-hydropower impulse turbines.

Shah et al. [13] conducted a detailed parametric optimization study of Pelton turbine runners and observed that hydraulic efficiency increases progressively with speed ratio up to an

optimum value near 0.485, beyond which efficiency begins to decline due to insufficient relative jet velocity. Their study demonstrated that optimized speed-ratio selection can substantially improve turbine performance under micro-hydropower operating conditions.

The influence of speed ratio on hydraulic efficiency may also be explained physically through jet interaction behavior. At low speed ratios, the runner buckets move too slowly relative to the incoming jet, causing incomplete energy extraction and increased residual velocity at bucket exit. Conversely, excessively high speed ratios reduce the relative velocity between the jet and the bucket surfaces, thereby decreasing impulsive force generation and reducing shaft power output [13,16]. Therefore, precise optimization of runner speed relative to jet velocity is essential for maximizing energy transfer efficiency.

Recent investigations have additionally examined the combined interaction between speed ratio and other geometric parameters such as bucket outlet angle, splitter curvature, and bucket dimensions. Suryaningrat and Permatasari [16] demonstrated that hydraulic efficiency optimization cannot be achieved through isolated speed-ratio selection alone and must instead consider combined parametric interactions involving bucket geometry and flow behavior.

2.2.3 Bucket Exit Angle Optimization

The bucket outlet angle plays a major role in controlling the direction and residual velocity of water leaving the runner bucket after momentum transfer. The primary objective of bucket outlet-angle optimization is to maximize jet deflection while minimizing residual kinetic energy losses at bucket exit [14–17].

Rossetti et al. [15] investigated the influence of bucket geometry on Pelton turbine performance and observed that smaller outlet angles generally improve hydraulic efficiency by reducing splash losses and promoting smoother jet redirection. Their study showed that optimized bucket curvature significantly enhances jet attachment along the bucket surface and reduces flow separation.

Similarly, Cordebela et al. [17] experimentally evaluated the effect of outlet-angle variation on Pelton turbine performance and concluded that outlet angles within the range of approximately 10° to 15° provide superior hydraulic efficiency for most practical operating conditions. Suryaningrat and Permatasari [16] performed CFD-based optimization of Pelton bucket deflection angles and reported that decreasing outlet angle improves momentum transfer by reducing residual exit velocity.

Theoretical hydraulic efficiency relationships also demonstrate strong dependence upon outlet angle:

$$\eta_h = 2\phi(1-\phi)(1+k\cos\beta) \text{ ----------[3]}$$

This equation indicates that lower outlet angles increase the cosine component and thereby improve theoretical hydraulic efficiency. However, excessively small outlet angles may introduce manufacturing difficulties and increase the likelihood of jet interference between adjacent buckets [14–17]. Consequently, outlet-angle optimization requires careful balancing between hydraulic performance and practical design constraints.

2.2.4 Bucket Geometry Optimization

The Pelton bucket geometry strongly influences jet bifurcation, water-sheet development, flow attachment, and momentum transfer efficiency. The splitter geometry located at the center of the bucket is particularly important because it directly controls the initial division of the incoming water jet into two symmetrical streams [14,15].

Erazo et al. [14] performed geometrical optimization studies on Pelton turbine buckets and demonstrated that modifications in bucket width, depth, and curvature can substantially improve overall turbine efficiency. Their results indicated that wider buckets with optimized internal cavity profiles promote smoother flow development and improved jet capture capability.

Rossetti et al. [15] further observed that bucket geometry strongly affects pressure distribution and free-surface flow behavior within the runner. Improper bucket curvature may produce flow separation zones, turbulence generation, and splash losses that reduce hydraulic efficiency.

The number of buckets mounted on the runner also represents a significant hydraulic design parameter. Kim et al. [11] developed theoretical procedures for determining optimum bucket number based on runner dimensions and jet diameter. Zidonis and Aggidis [18] later employed CFD techniques to identify bucket configurations producing maximum hydraulic performance while minimizing jet interference between successive buckets.

Additional studies by Chen et al. [19] and Xiao et al. [20] demonstrated that runner dimensions and bucket spacing influence flow stability and energy extraction efficiency, particularly under transient operating conditions. These investigations confirmed that

hydraulic optimization requires simultaneous consideration of multiple geometric parameters rather than isolated design-variable selection.

2.2.5 Nozzle Geometry and Jet Characteristics

The nozzle is responsible for converting hydraulic pressure energy into kinetic energy and producing a coherent high-velocity water jet directed toward the runner buckets. The quality of the jet generated by the nozzle strongly influences Pelton turbine performance because unstable or non-uniform jets reduce momentum-transfer efficiency and increase hydraulic losses [21–27].

Jo et al. [21] experimentally investigated the effect of nozzle diameter variation on micro-hydropower Pelton turbine performance and reported that nozzle diameter significantly affects jet velocity distribution and turbine efficiency. Larger nozzle diameters increase discharge flow rate but may reduce jet coherence if improperly designed.

Nedelcu et al. [22] performed numerical simulations of nozzle flow behavior and demonstrated that nozzle geometry strongly influences velocity uniformity and jet stability. Their CFD analysis showed that optimized nozzle contours improve jet coherence and reduce turbulence formation at nozzle exit.

Petley et al. [23] investigated injector geometry using transient CFD simulations and experimental validation techniques. Their results indicated that injector shape and internal flow characteristics substantially influence pressure distribution and jet quality. Similar findings were reported by Zhang et al. [24], who demonstrated that optimized nozzle geometry improves hydraulic efficiency through enhanced jet formation and reduced energy dissipation.

Jet alignment is another important factor affecting turbine performance. Deng et al. [25] observed that jet misalignment produces asymmetric bucket loading, increased vibration, and reduced efficiency due to uneven momentum transfer. Experimental investigations by Lesmana et al. [26] and Saputra et al. [27] further confirmed that nozzle angle and jet orientation strongly influence turbine output power and operating stability.

Overall, existing literature demonstrates that hydraulic efficiency in Pelton turbines depends on the combined interaction of speed ratio, bucket outlet angle, bucket geometry, nozzle configuration, and jet characteristics. Although substantial progress has been achieved in parametric optimization studies, many existing investigations focus on isolated parameters

independently. Comprehensive integrated optimization frameworks incorporating hydraulic analysis, structural considerations, CFD simulations, and experimental validation remain relatively limited in current Pelton turbine research.

2.3 Literature review on Stress Analysis of Pelton Turbine

The Pelton turbine bucket is continuously subjected to highly dynamic hydraulic loading conditions resulting from repeated high-velocity jet impingement during turbine operation. Unlike reaction turbines, where loading is distributed more uniformly across runner blades, Pelton turbine buckets experience localized impulsive forces concentrated primarily near the splitter region and bucket inner surfaces. These repeated impact loads generate complex stress distributions, cyclic deformation, vibration, and potential fatigue damage that can significantly influence the structural integrity and operational reliability of the turbine runner [28–31].

As micro-hydropower systems increasingly operate under higher rotational speeds and optimized hydraulic conditions, structural analysis of Pelton turbine buckets has become an essential component of turbine design methodology. Modern structural investigations primarily focus on stress concentration behavior, deformation characteristics, fatigue resistance, material selection, and resonance safety using Finite Element Analysis (FEA) techniques [28–34].

2.3.1 Stress Distribution Due to Jet Impingement

The impact of the high-velocity water jet on the bucket splitter produces complex localized stress fields that vary continuously during runner rotation. The splitter region experiences the highest hydraulic loading because it is the first point of contact between the incoming jet and the bucket surface. Consequently, stress concentration zones are commonly observed near the splitter root and bucket-arm junction [28,29].

Sharma and Dhama [28] conducted structural stress analysis of Pelton turbine buckets subjected to jet impingement loading using finite element modelling techniques. Their results demonstrated that the maximum Von Mises stress occurs near the splitter-root junction due to geometric discontinuity and concentrated impulsive loading. The study also showed that stress magnitude decreases gradually from the splitter region toward the bucket lip.

Similar findings were reported by Li and Saw [29], who investigated fatigue behavior and reinforcement effects in Pelton turbine buckets under cyclic hydraulic loading. Their analysis

revealed that repeated jet impacts generate fluctuating stress fields capable of initiating fatigue cracks at regions of stress concentration. The researchers concluded that proper geometric reinforcement near the splitter-root region significantly improves fatigue life and structural durability.

The hydraulic force generated by jet impingement depends strongly upon jet velocity, discharge rate, bucket geometry, and flow deflection characteristics. Under transient operating conditions, additional stress fluctuations may arise due to unstable flow attachment, asymmetric jet loading, and pressure oscillations [28–31]. Therefore, accurate prediction of stress distribution requires detailed consideration of hydraulic loading conditions and realistic boundary constraints.

2.3.2 Deformation Characteristics of Pelton Buckets

In addition to stress concentration, deformation behavior represents another critical consideration in Pelton turbine structural design. Excessive deformation may alter bucket geometry, affect jet interaction characteristics, and reduce hydraulic efficiency. Deformation analysis therefore plays an important role in evaluating structural stiffness and operational stability [30].

Mbiu et al. [30] compared deformation behavior of Pelton turbine buckets manufactured using different materials including aluminum alloys and steel-based materials. Their finite element analysis showed that aluminum buckets exhibit significantly larger deformation compared with steel buckets due to lower elastic modulus and reduced structural stiffness. The study concluded that material selection strongly influences both deformation characteristics and long-term structural reliability.

Structural deformation is influenced not only by material properties but also by bucket geometry, loading orientation, and hydraulic operating conditions. Under high-head operating conditions, impulsive hydraulic forces can generate substantial localized deformation near the splitter tip and bucket sidewalls [28–30]. Consequently, optimization of bucket geometry must consider both hydraulic efficiency and structural stiffness simultaneously.

Recent studies increasingly employ mesh-independent finite element models containing large numbers of nodes and elements to accurately capture stress gradients and localized deformation regions [33,34]. These advanced numerical approaches improve prediction accuracy and provide detailed understanding of stress propagation within complex bucket geometries.

2.3.3 Material Selection for Structural Reliability

Material selection plays a major role in determining the structural safety, fatigue resistance, corrosion behavior, and wear durability of Pelton turbine runners. Since Pelton buckets operate continuously under repeated impact loading and exposure to water containing suspended sediments, materials must possess adequate strength, toughness, corrosion resistance, and erosion resistance [29–31].

Traditionally, stainless steels and martensitic steels have been widely used in Pelton turbine applications due to their high yield strength and superior corrosion resistance. Mbiu et al. [30] demonstrated that steel-based materials provide significantly better structural performance than lightweight aluminum alloys under identical hydraulic loading conditions.

Li and Saw [29] further reported that fatigue resistance can be substantially improved through proper material selection and geometric reinforcement. Their study highlighted the importance of balancing structural strength with manufacturing feasibility and cost considerations.

Rai et al. [31] investigated particle-induced loading and erosive behavior in Pelton turbine buckets and observed that suspended sediment particles create additional impact stresses capable of accelerating material degradation. The splitter region was identified as one of the most vulnerable locations for erosion-induced structural damage due to direct jet interaction and high particle concentration.

Modern Pelton turbine research increasingly explores advanced materials and surface-treatment techniques aimed at improving wear resistance and operational lifespan. However, many existing studies remain limited to isolated material comparisons without integrating hydraulic optimization, structural analysis, and experimental validation within a unified framework [29–31].

2.3.4 Finite Element Analysis in Pelton Turbine Design

Finite Element Analysis has become one of the most widely used numerical techniques for evaluating structural behavior of Pelton turbine components under complex loading conditions. FEA enables detailed prediction of stress distribution, deformation, strain concentration, fatigue behavior, and structural safety prior to physical fabrication [28–34].

Modern structural investigations typically employ three-dimensional finite element models with refined meshing techniques and realistic loading conditions to simulate actual hydraulic

operating environments. Static structural analysis is commonly used to evaluate maximum stress and deformation under steady hydraulic loading, while transient structural analysis enables investigation of dynamic loading behavior during bucket rotation and jet interaction [33,34].

Recent work by Chaudhari et al. [33,34] employed ANSYS Mechanical APDL to perform detailed static and modal analysis of Pelton turbine buckets subjected to multiple hydraulic loading conditions. Their studies demonstrated that proper finite element modelling can accurately identify critical stress regions, evaluate resonance safety, and verify structural adequacy under severe operating conditions.

Despite substantial progress in numerical structural analysis, existing literature indicates that many studies focus primarily on isolated static loading conditions without incorporating coupled hydraulic–structural interaction effects. Furthermore, relatively few investigations integrate structural analysis with hydraulic optimization, CFD simulations, modal analysis, fabrication, and experimental validation within a unified design framework.

Overall, structural stress analysis remains an essential aspect of Pelton turbine design because hydraulic efficiency improvements achieved through geometric optimization must also satisfy long-term structural safety requirements. Advanced finite element methodologies continue to improve the understanding of stress behavior and deformation characteristics in Pelton turbine buckets, thereby contributing toward the development of more reliable and efficient micro-hydropower systems.

2.4 Literature Survey on Modal and Dynamic Behaviour of Pelton Turbine Runners

In addition to static hydraulic loading, Pelton turbine runners are subjected to dynamic excitation caused by repeated jet impacts, rotational motion, pressure fluctuations, asymmetric flow behavior, and transient hydraulic disturbances during operation. These dynamic effects can induce vibration, resonance, cyclic stress accumulation, and fatigue damage within the runner assembly, thereby influencing turbine reliability, structural safety, and operational lifespan [32–34]. Consequently, modal and dynamic analysis has become an increasingly important aspect of modern Pelton turbine design methodology, particularly for high-speed micro-hydropower applications.

The dynamic response of a Pelton runner depends primarily on the interaction between excitation frequencies generated during operation and the natural frequencies of the turbine structure. If the operating excitation frequency approaches one of the natural frequencies of

the runner system, resonance may occur, resulting in excessive vibration amplitudes, structural instability, and possible mechanical failure [32]. Therefore, accurate determination of modal characteristics and resonance safety margins is essential for ensuring stable turbine operation.

2.4.1 Sources of Dynamic Excitation in Pelton Turbines

The dominant source of excitation in a Pelton turbine arises from periodic jet impact on successive runner buckets. As the runner rotates, each bucket intercepts the high-velocity water jet, generating repeated impulsive loading at regular intervals. This produces a characteristic excitation frequency commonly referred to as the bucket-passing frequency [32–34].

The bucket-passing frequency is expressed as:

$$f_b = \frac{ZN}{60} \text{----------} [4]$$

This excitation frequency acts continuously on the runner structure and may induce resonance if it coincides with the natural frequencies of the turbine system. Additional dynamic excitation sources include pressure pulsations, jet instability, asymmetric flow attachment, nozzle misalignment, cavitation-induced oscillations, and shaft imbalance [30,32].

Kramer et al. [51] reported that air entrainment and unstable jet interaction may produce fluctuating hydraulic loading capable of increasing vibration intensity and reducing operational stability. Similarly, Deng et al. [25] demonstrated that jet deviation and flow asymmetry generate non-uniform impulsive forces that contribute to vibration and dynamic stress fluctuations within the runner assembly.

2.4.2 Modal Analysis of Pelton Turbine Buckets

Modal analysis is a numerical technique used to determine the natural frequencies, mode shapes, and vibration characteristics of mechanical structures. In Pelton turbine research, modal analysis is commonly performed using finite element methods to evaluate resonance safety and identify dynamically sensitive regions of the runner [32–34].

Pesatori [32] conducted one of the early investigations into the dynamic behavior of Pelton turbine runner systems and demonstrated that resonance safety depends strongly upon bucket geometry, material properties, runner stiffness, and operating speed. The study showed that

the lowest natural frequencies generally occur in bucket bending modes and splitter deformation modes.

Modern investigations increasingly employ three-dimensional finite element models combined with pre-stressed modal analysis techniques to simulate realistic hydraulic operating conditions. In pre-stressed modal analysis, static hydraulic loading is first applied to the runner structure before extraction of modal characteristics, thereby improving prediction accuracy under actual operating environments [33,34].

Chaudhari et al. [33] performed modal analysis of Pelton turbine buckets using ANSYS Mechanical APDL and reported that the natural frequencies of the runner were significantly higher than the bucket-passing frequency, thereby ensuring resonance-free operation. Their analysis demonstrated that proper geometric design and material selection can provide substantial safety margins against dynamic instability.

Further investigations by Chaudhari et al. [34] integrated static structural analysis with modal analysis to evaluate both stress behavior and dynamic safety simultaneously. Their results indicated that all investigated bucket materials possessed natural frequencies well above operational excitation frequencies, confirming adequate resonance safety under severe loading conditions.

2.4.3 Influence of Material Properties on Dynamic Behaviour

Material properties strongly influence the modal characteristics and vibration response of Pelton turbine runners. Parameters such as density, Young’s modulus, damping capacity, and structural stiffness directly affect natural frequencies and mode shapes [30,32–34].

Materials with higher stiffness generally exhibit higher natural frequencies and improved resistance to deformation under dynamic loading conditions. However, increased stiffness may also reduce damping capability and influence vibration transmission behavior. Therefore, optimal material selection requires balancing structural rigidity, fatigue resistance, corrosion resistance, and dynamic stability [30].

Mbiu et al. [30] observed that lightweight aluminum-based buckets exhibit lower structural stiffness and larger deformation compared with steel-based materials. Such deformation behavior may alter modal characteristics and reduce dynamic stability during long-term operation. Stainless steel materials, on the other hand, provide superior stiffness and fatigue resistance, making them more suitable for high-head Pelton turbine applications [33,34].

2.4.4 Dynamic Stability and Resonance Prevention

The primary objective of modal analysis in Pelton turbine design is to ensure that operational excitation frequencies remain sufficiently separated from structural natural frequencies. This separation is commonly expressed in terms of resonance safety factor [32–34].

A sufficiently large resonance safety factor minimizes the likelihood of dynamic amplification and ensures stable long-term operation under varying hydraulic conditions. Modern Pelton turbine studies typically aim to maintain natural frequencies several times higher than the bucket-passing frequency in order to prevent resonance-related structural damage.

Dynamic instability may also arise due to manufacturing imperfections, runner imbalance, asymmetric bucket geometry, or unstable jet interaction. Consequently, dynamic balancing of the complete runner assembly represents an important practical requirement prior to experimental testing and field operation [33].

Although substantial progress has been achieved in finite element-based modal analysis, existing literature indicates that relatively few investigations incorporate fully coupled fluid–structure interaction effects during dynamic simulations. Most available studies analyze structural vibration independently without directly coupling transient hydraulic loading obtained from CFD simulations [32–34]. Furthermore, comprehensive integrated investigations combining hydraulic optimization, structural analysis, modal analysis, transient CFD, fabrication, and experimental validation remain limited in current Pelton turbine research.

Overall, modal and dynamic analysis plays a critical role in ensuring the operational reliability and structural safety of Pelton turbine runners. Advanced finite element techniques continue to improve the understanding of vibration behavior, resonance characteristics, and dynamic stability under realistic hydraulic operating conditions, thereby contributing toward the development of safer and more efficient micro-hydropower systems.

2.5 Literature Survey on Computational Fluid Dynamics Analysis of Pelton Turbines

The flow behavior within a Pelton turbine is highly complex due to the interaction of high-velocity free-surface water jets with continuously rotating runner buckets. During operation, the incoming jet undergoes rapid bifurcation, strong curvature-induced acceleration, turbulent

mixing, pressure fluctuations, and transient free-surface deformation while interacting with the bucket geometry. Accurate prediction of these phenomena is essential for understanding hydraulic performance, energy-transfer mechanisms, pressure distribution, flow separation, splash losses, and transient flow stability [35–48].

Traditional analytical approaches and experimental investigations provide useful insight into Pelton turbine operation; however, they often face limitations in visualizing internal flow structures and transient free-surface phenomena occurring within rotating runner systems. The development of Computational Fluid Dynamics (CFD) techniques has therefore significantly advanced Pelton turbine research by enabling detailed numerical simulation of fluid flow behavior under realistic operating conditions [35,36].

Modern CFD analysis of Pelton turbines commonly involves numerical modelling of multiphase free-surface flow, turbulent jet interaction, transient runner rotation, and moving mesh interfaces using advanced software platforms such as ANSYS Fluent, ANSYS CFX, and OpenFOAM [35–47]. These techniques provide detailed information regarding velocity distribution, pressure variation, turbulence generation, jet bifurcation, and energy conversion mechanisms inside the runner buckets.

2.5.1 Evolution of CFD Modelling in Pelton Turbine Research

The application of CFD techniques in Pelton turbine analysis has evolved considerably over the past two decades. Early numerical investigations primarily focused on simplified steady-state simulations with relatively coarse computational meshes and limited turbulence modelling capability [35–37]. Although these early studies provided valuable qualitative understanding of jet interaction behavior, they were unable to accurately capture transient free-surface dynamics and rotating runner effects.

Patel et al. [37] conducted one of the early numerical simulation studies on Pelton turbine flow behavior and demonstrated the usefulness of CFD for predicting velocity and pressure distribution within turbine buckets. However, computational limitations at that time restricted the accuracy of transient flow representation and free-surface modelling.

Subsequent advancements in numerical algorithms, turbulence models, and computational power enabled increasingly sophisticated simulations involving rotating runner systems, transient jet interaction, and moving mesh techniques [35,36]. Zidonis and Aggidis [35] presented a comprehensive review of numerical modelling developments in Pelton turbine

research and highlighted the transition from simplified steady-state models toward advanced transient multiphase simulations.

Bhattarai et al. [36] further reviewed modern Pelton turbine modelling techniques and emphasized the growing importance of CFD in hydraulic optimization, transient flow analysis, and design validation. Their study concluded that modern numerical methods significantly improve prediction accuracy compared with conventional analytical approaches, particularly for free-surface flow behavior and transient jet interaction.

2.5.2 Free-Surface Flow and Jet Dynamics

One of the most challenging aspects of Pelton turbine CFD analysis is accurate modelling of free-surface jet interaction within rotating buckets. As the high-velocity water jet strikes the splitter, the flow divides into two symmetrical streams that spread over the curved bucket surfaces before exiting the runner. During this process, the water undergoes rapid acceleration, deceleration, pressure variation, and turbulence generation [39–42].

Perrig [40] conducted one of the most influential investigations on free-surface hydrodynamics within Pelton turbine buckets. Through combined theoretical and experimental analysis, the study explained the mechanisms of jet bifurcation, water-sheet formation, and pressure development along the bucket surface. The research demonstrated that smooth flow attachment and controlled jet deflection are essential for maximizing hydraulic efficiency.

Similarly, Klemensten [39] investigated free-surface flow behavior in Pelton turbines and reported that optimized bucket curvature minimizes turbulence generation and flow separation. The study also showed that pressure gradients developed along the bucket surface strongly influence energy-transfer efficiency.

Han et al. [41] performed unsteady numerical simulations of jet interaction with rotating Pelton buckets and demonstrated that the bucket cut-out geometry significantly affects jet branch separation behavior. Their transient simulations revealed complex free-surface deformation patterns occurring during bucket rotation.

Anagnostopoulos [42] numerically investigated flow behavior inside Pelton turbine runners and demonstrated that CFD simulations can accurately predict jet deflection patterns, pressure distribution, and internal flow characteristics when appropriate turbulence models and boundary conditions are applied.

2.5.3 Steady-State CFD Analysis

Steady-state CFD analysis is widely used to evaluate pressure contours, velocity fields, turbulence intensity, and hydraulic loading within Pelton turbine buckets under constant operating conditions. Although steady-state simulations cannot fully capture transient jet interaction, they provide valuable insight into overall flow behavior and hydraulic performance trends [38,43].

Panthee et al. [38] performed CFD analysis of Pelton turbine flow using ANSYS Fluent and observed that pressure reaches maximum values near the splitter stagnation region, while velocity gradually decreases along the bucket contour due to momentum transfer. Their study confirmed that properly designed bucket geometry promotes smooth flow attachment and minimizes turbulence-related losses.

Wang et al. [43] further demonstrated that accurate three-dimensional bucket modelling significantly improves CFD prediction accuracy for velocity distribution and pressure variation. Their work highlighted the importance of refined mesh generation and geometric precision in numerical Pelton turbine simulations.

Steady-state CFD investigations commonly employ turbulence models such as the standard $k-\varepsilon$, realizable $k-\varepsilon$, SST $k-\omega$, and Reynolds Stress Models (RSM) to simulate turbulent flow behavior [35–43]. Among these models, the standard $k-\varepsilon$model remains widely used due to its computational efficiency and satisfactory prediction capability for many engineering applications.

Turbulent kinetic energy (TKE) distribution is another important parameter commonly evaluated in steady-state simulations because it indicates regions of strong turbulence generation and energy dissipation. High TKE values are typically observed near the splitter edge and jet–bucket interaction region where rapid conversion of kinetic energy into pressure energy occurs [38].

2.5.4 Transient CFD and Sliding Mesh Techniques

Although steady-state simulations provide useful hydraulic information, accurate representation of Pelton turbine operation requires transient analysis because bucket interaction with the water jet is inherently time-dependent. Transient CFD analysis enables detailed simulation of rotating runner motion, jet evolution, free-surface deformation, and dynamic pressure fluctuation during operation [44–48].

Modern transient simulations commonly employ sliding mesh or moving mesh techniques to represent runner rotation relative to the stationary nozzle and casing domains. These methods allow accurate modelling of periodic jet impact and transient momentum transfer between the water jet and rotating buckets [44–47].

Petley and Aggidis [44] combined transient CFD simulations with experimental validation to investigate Pelton turbine casing designs. Their results demonstrated that transient numerical modelling accurately predicts jet interaction behavior and pressure fluctuations within rotating systems.

Sun et al. [45] investigated startup flow characteristics in Pelton turbines using transient CFD and reported that significant energy dissipation and unstable flow structures occur during transient operating conditions. Their study emphasized the importance of transient analysis for evaluating operational stability.

Zeng et al. [46] conducted full-flow-path simulations of four-nozzle Pelton turbines and observed complex jet interaction patterns between adjacent buckets during runner rotation. Their simulations demonstrated that multi-nozzle configurations require detailed transient modelling to accurately capture hydraulic interaction effects.

Decaix and Münch-Alligné [47] investigated the influence of mesh quality and numerical discretization schemes on transient Pelton turbine simulations using OpenFOAM. Their study highlighted the importance of refined mesh resolution and stable numerical algorithms for achieving accurate free-surface flow prediction.

Similarly, Gupta et al. [48] numerically simulated six-jet Pelton turbine systems and demonstrated that multi-jet interactions significantly affect pressure distribution and flow stability within the runner domain.

2.5.5 Limitations of Existing CFD Studies

Despite major advancements in numerical modelling capability, several limitations remain within existing Pelton turbine CFD research. Many studies focus primarily on isolated hydraulic flow analysis without integrating structural stress analysis, modal analysis, material behaviour, and experimental validation within a unified design framework [35–48].

Additionally, fully coupled fluid–structure interaction (FSI) simulations remain relatively limited due to their high computational cost and modelling complexity. Most available

investigations analyze fluid flow independently from structural deformation effects, thereby neglecting potential interaction between hydraulic loading and structural response.

Transient free-surface simulations involving rotating runners also require extremely fine computational meshes and substantial computational resources, particularly for multi-nozzle systems and high-resolution turbulence modelling [44–47]. Consequently, many researchers continue to employ simplified assumptions that may reduce simulation accuracy under certain operating conditions.

Nevertheless, CFD analysis remains one of the most powerful tools for modern Pelton turbine design and optimization because it enables detailed understanding of hydraulic flow mechanisms that are difficult to observe experimentally. Continuous improvements in computational capability, numerical algorithms, and multiphase modelling techniques are expected to further enhance the accuracy and applicability of CFD in future Pelton turbine research.

2.6 Literature Survey on Materials Used in Pelton Turbine Buckets

Material selection is one of the most important considerations in Pelton turbine design because the runner buckets operate continuously under severe hydraulic loading, high-velocity jet impingement, cyclic stress fluctuations, erosive particle interaction, and corrosive environmental conditions. The selected material must therefore possess adequate mechanical strength, fatigue resistance, toughness, hardness, corrosion resistance, and erosion resistance to ensure long-term structural reliability and stable turbine operation [29–31,49–51].

Unlike many conventional rotating components, Pelton turbine buckets are exposed directly to high-energy water jets that generate repeated impulsive loading at localized regions, particularly near the splitter and inner bucket surfaces. In addition, micro-hydropower installations often operate using natural water sources containing suspended sediment particles, dissolved minerals, and abrasive contaminants that accelerate material degradation over time [31,50]. Consequently, inappropriate material selection may result in excessive deformation, fatigue cracking, erosion damage, corrosion, and significant reduction in turbine efficiency and service life.

2.6.1 Mechanical Requirements of Pelton Bucket Materials

The primary mechanical requirement for Pelton bucket materials is the ability to withstand repeated impact loading without experiencing excessive deformation or structural failure.

High yield strength and adequate stiffness are essential for maintaining bucket geometry and ensuring efficient momentum transfer during operation [29,30].

Mbiu et al. [30] performed finite element structural analysis of Pelton turbine buckets manufactured using different materials and reported that materials possessing higher elastic modulus and yield strength exhibit significantly lower deformation under hydraulic loading conditions. Their study demonstrated that aluminum-based materials experience substantially larger deformation compared with steel-based materials due to lower stiffness characteristics.

Similarly, Li and Saw [29] investigated fatigue behavior in Pelton turbine buckets subjected to repeated cyclic loading and concluded that material fatigue resistance is critical for preventing crack initiation near stress concentration regions. The splitter-root junction was identified as one of the most vulnerable locations for fatigue damage because of repeated jet impact and fluctuating stress distribution.

The material must additionally possess sufficient toughness to resist sudden impact loading generated by high-velocity water jets. Brittle materials may fail prematurely under impulsive loading conditions, particularly in high-head Pelton turbine applications where jet velocity becomes extremely large [29–31].

2.6.2 Stainless Steel Materials

Stainless steels are among the most widely used materials for Pelton turbine runners due to their excellent combination of mechanical strength, corrosion resistance, fatigue resistance, and wear durability [30,34]. Austenitic and martensitic stainless steels are particularly preferred for high-performance Pelton turbine applications operating under aggressive hydraulic conditions.

The high chromium content present in stainless steels provides excellent corrosion resistance against continuous water exposure and dissolved chemical contaminants. In addition, stainless steels exhibit relatively high yield strength and superior resistance to impact loading compared with lightweight metallic materials [30].

Recent investigations by Chaudhari et al. [34] demonstrated that stainless steel materials provide superior structural safety and resonance stability under combined hydraulic loading conditions. Their finite element analysis indicated that stainless steel buckets exhibit lower deformation and improved dynamic behavior compared with alternative material options.

Stainless steel materials also possess relatively good fatigue strength and erosion resistance under long-term operational conditions. Consequently, they are widely used in commercial Pelton turbine manufacturing despite higher material and fabrication costs [29,30,34].

2.6.3 Aluminum Alloys and Lightweight Materials

Aluminum alloys are sometimes considered for small-scale Pelton turbine applications due to their low density, ease of machining, and reduced manufacturing cost. Lightweight runners may additionally reduce rotational inertia and simplify transportation and installation for remote micro-hydropower systems [30].

However, aluminum-based materials generally possess lower stiffness and lower fatigue resistance compared with steel materials. Mbiu et al. [30] reported that aluminum buckets experience substantially larger deformation under hydraulic loading conditions because of their relatively low Young's modulus. Excessive deformation may alter bucket geometry, reduce hydraulic efficiency, and increase the likelihood of fatigue-related damage during long-term operation.

In addition, aluminum alloys generally possess lower erosion resistance under sediment-laden water conditions. High-velocity abrasive particles may progressively remove material from the splitter and bucket surfaces, thereby reducing operational lifespan [31,50].

Consequently, although aluminum alloys offer certain economic and manufacturing advantages, their application in high-head Pelton turbines remains limited where severe hydraulic loading and erosion conditions exist.

2.6.4 Composite Materials and Advanced Material Research

Recent research has increasingly explored the use of composite materials and advanced surface-treatment techniques for Pelton turbine applications. Composite materials offer advantages such as reduced weight, improved corrosion resistance, and potentially lower manufacturing cost [49].

Islam et al. [49] investigated the application of composite materials for Pelton turbine runners and reported that composite buckets provide good corrosion resistance and reduced structural weight. However, the study also observed that composite materials generally exhibit lower erosion resistance compared with stainless steel materials under sediment-rich operating conditions.

Advanced coatings and surface hardening techniques are also being investigated to improve erosion resistance and fatigue durability in Pelton turbine runners [50]. Such approaches aim to extend operational lifespan while maintaining hydraulic efficiency and structural reliability.

Despite these developments, widespread industrial adoption of composite materials in high-head Pelton turbines remains limited due to concerns regarding long-term fatigue behavior, manufacturing complexity, and resistance to severe hydraulic impact loading [49–51].

2.6.5 Erosion and Corrosion Behaviour

Erosion and corrosion represent major operational challenges for Pelton turbine materials, particularly in mountainous micro-hydropower installations where water frequently contains suspended sediment particles and dissolved minerals [31,50].

Padhy and Saini [50] investigated the mechanisms of silt erosion in Pelton turbine buckets and reported that erosion damage occurs predominantly near the splitter region and bucket cut-out surfaces where particle impact intensity becomes highest. Their study demonstrated that sediment concentration, particle size, and jet velocity strongly influence erosion rate and material degradation behavior.

Similarly, Rai et al. [31] analyzed particle-force interaction within Pelton buckets and observed that erosive stresses generated by suspended particles significantly accelerate surface wear under high-head operating conditions. The splitter region was again identified as one of the most critical zones for material degradation.

Corrosion effects may additionally reduce material strength and fatigue resistance during long-term operation. Materials with poor corrosion resistance may experience surface pitting, crack initiation, and progressive structural weakening under continuous water exposure [49–51]. Consequently, corrosion-resistant materials such as stainless steels remain highly preferred for micro-hydropower Pelton turbine applications.

2.6.6 Limitations of Existing Material Studies

Although numerous investigations have evaluated material behavior in Pelton turbine runners, many existing studies remain limited to isolated structural or erosion analysis without integrating hydraulic optimization, CFD analysis, modal analysis, fabrication constraints, and experimental validation within a unified design framework [29–31,49–51].

Furthermore, relatively few studies evaluate the combined influence of hydraulic loading, dynamic vibration, sediment erosion, and fatigue behavior simultaneously under realistic operating conditions. Most available investigations also focus on conventional materials, while advanced composite and hybrid-material approaches remain insufficiently explored for high-head micro-hydropower applications.

Overall, material selection continues to play a critical role in determining the structural reliability, hydraulic performance, and operational durability of Pelton turbine systems. Future research integrating advanced material science with hydraulic and structural optimization methodologies may further improve the efficiency and lifespan of micro-hydropower Pelton turbines.

2.7 Literature Survey on Experimental Investigations on Pelton Turbines

Experimental investigations play a crucial role in validating analytical models, Computational Fluid Dynamics (CFD) simulations, structural analyses, and hydraulic optimization methodologies associated with Pelton turbine research. Although modern numerical simulation techniques provide extensive insight into internal flow behavior and structural response, experimental studies remain essential for verifying turbine performance under realistic operating conditions and establishing the practical reliability of proposed design improvements [21,26,27,52–56].

Experimental testing enables direct measurement of important performance parameters such as hydraulic efficiency, shaft power, rotational speed, discharge rate, pressure variation, flow stability, and vibration behavior. In addition, experimental investigations provide valuable information regarding manufacturing feasibility, operational stability, dynamic balancing, and uncertainty associated with measured data [52–56].

Over the past two decades, numerous researchers have developed laboratory-scale and prototype-scale experimental rigs for evaluating Pelton turbine performance under varying hydraulic and geometric conditions. These investigations have focused on nozzle geometry, speed ratio optimization, bucket shape modification, nozzle angle variation, multi-jet operation, and flow-control mechanisms [21,26,27,52–56].

2.7.1 Experimental Performance Evaluation of Pelton Turbines

The primary objective of experimental investigation in Pelton turbine research is to determine turbine efficiency and power output under controlled operating conditions. Experimental

setups generally consist of a closed-loop hydraulic circuit incorporating a water reservoir, centrifugal pump, nozzle assembly, pressure measurement devices, flow-control valves, tachometer, brake dynamometer, and instrumentation for discharge and power measurement [21,26,27].

Jo et al. [21] experimentally investigated the effect of nozzle diameter variation on micro-hydropower Pelton turbine performance and reported that turbine efficiency increases with improved jet coherence and optimized nozzle geometry. Their study demonstrated that nozzle diameter strongly affects jet velocity distribution and momentum transfer efficiency.

Lesmana et al. [26] evaluated the influence of nozzle angle variation on Pelton turbine performance and observed that proper nozzle orientation significantly improves hydraulic efficiency by enhancing jet alignment with the runner buckets. Their results indicated that nozzle angles within a specific range provide superior performance due to reduced splash losses and smoother jet attachment.

Similarly, Saputra et al. [27] experimentally investigated the combined influence of water pressure and nozzle angle on turbine performance. The study concluded that increasing inlet pressure increases shaft power generation, while optimized nozzle geometry improves momentum-transfer efficiency and operational stability.

These investigations collectively demonstrate that even relatively small geometric variations in nozzle configuration and flow-control parameters can significantly influence Pelton turbine performance.

2.7.2 Influence of Bucket Geometry and Runner Parameters

Several experimental studies have investigated the effect of bucket geometry, runner dimensions, and bucket number on Pelton turbine performance [52–54]. Since bucket geometry directly controls jet bifurcation and momentum transfer behavior, optimization of runner configuration remains essential for maximizing hydraulic efficiency.

Dhakan and Chalil [52] experimentally studied multi-jet Pelton turbine configurations and reported that symmetric jet distribution is necessary to maintain stable runner operation and minimize vibration effects. Their investigation demonstrated that improper jet alignment produces asymmetric loading and reduced turbine efficiency.

Kholifah et al. [53] performed performance testing under varying runner design parameters and observed that hydraulic efficiency depends strongly upon bucket geometry and operating

conditions. Their work confirmed that optimized bucket curvature and runner dimensions significantly improve energy-transfer effectiveness.

Similarly, Sumita et al. [54] investigated the influence of nozzle and runner variation on Pelton turbine output characteristics and reported that optimized geometric design improves shaft power generation and overall hydraulic efficiency.

Experimental investigations additionally show that the number of buckets mounted on the runner influences both jet interaction frequency and flow stability. Excessive bucket numbers may increase interference between adjacent buckets, while insufficient bucket numbers reduce effective utilization of the incoming jet [18,52–54].

2.7.3 Experimental Validation of Numerical Models

One of the most important functions of experimental investigations is validation of analytical and CFD-based numerical models. Since Pelton turbine flow behavior involves highly transient free-surface interaction and multiphase turbulence, numerical predictions must be experimentally verified to establish reliability and practical applicability [35–48].

Experimental pressure measurements, flow visualization techniques, and performance curves are commonly compared with CFD simulation results to evaluate prediction accuracy. Petley and Aggidis [44] combined transient CFD analysis with experimental testing and demonstrated strong agreement between numerical predictions and measured hydraulic performance.

Similarly, Chaudhari [56] performed numerical, experimental, and flow-visualization studies on conventional and modified Pelton turbine runners. The investigation successfully validated CFD-predicted flow behavior through experimental performance measurements and visualization techniques. The study demonstrated that integrated numerical and experimental methodologies significantly improve understanding of hydraulic flow mechanisms within Pelton turbines.

Experimental validation is particularly important for transient CFD simulations involving moving mesh techniques because such numerical models require accurate representation of rotating runner interaction with the incoming jet [44–48].

2.7.4 Dynamic Balancing and Operational Stability

Dynamic balancing of the runner assembly represents another critical aspect of experimental Pelton turbine investigation. Since the turbine operates at relatively high rotational speeds,

improper mass distribution may generate excessive vibration, shaft instability, and structural loading during operation [33,34].

Experimental studies frequently include balancing procedures to ensure stable operation prior to performance testing. Proper dynamic balancing improves measurement accuracy, reduces vibration-induced error, and enhances operational reliability during experimental evaluation [56].

Operational stability additionally depends upon:

- jet alignment,
- nozzle symmetry,
- rotational speed consistency,
- and hydraulic flow stability.

Experimental investigations commonly evaluate these factors through repeated performance measurements under varying operating conditions [21,26,27,52–56].

2.7.5 Experimental Uncertainty Analysis

Measurement uncertainty represents an important consideration in experimental turbine testing because observed performance variations may arise from instrumentation limitations, flow fluctuations, calibration error, and operational instability. Consequently, formal uncertainty analysis is necessary to determine the reliability and statistical significance of measured results.

Despite its importance, relatively few Pelton turbine studies perform detailed uncertainty analysis in accordance with international standards such as ASME PTC 22 or ISO GUM methodologies. Most available investigations report performance improvements without quantifying measurement uncertainty or statistical confidence levels [52–56].

Recent research increasingly emphasizes the importance of uncertainty analysis for validating experimental observations and comparing enhanced runner designs with conventional configurations. Proper uncertainty evaluation improves scientific reliability and enables objective interpretation of performance improvements under experimental conditions.

2.7.6 Limitations of Existing Experimental Studies

Although numerous experimental investigations have contributed significantly to Pelton turbine research, several important limitations remain within the available literature. Many

experimental studies focus primarily on isolated hydraulic parameters such as nozzle angle or bucket geometry without integrating structural analysis, modal analysis, CFD simulation, and material behavior within a unified framework [21,26,27,52–56].

Additionally, most laboratory-scale investigations operate under simplified hydraulic conditions that may not fully represent actual field environments involving sediment-laden water, transient loading, and long-term operational wear. Experimental studies involving coupled hydraulic–structural interaction and real-time vibration monitoring also remain relatively limited.

Furthermore, detailed uncertainty analysis and statistical validation are absent from many existing investigations, reducing confidence in reported performance improvements. Consequently, comprehensive integrated experimental methodologies combining optimization, CFD, structural analysis, fabrication, dynamic balancing, and uncertainty evaluation remain insufficiently explored in current Pelton turbine research.

Overall, experimental investigations continue to play a fundamental role in validating theoretical and numerical Pelton turbine research. Continued advancement of experimental methodologies, instrumentation systems, and integrated validation techniques is expected to further improve the reliability and efficiency of future micro-hydropower Pelton turbine systems.

2.8 Literature Review on Multi-Physics Approaches on Pelton Turbines

Modern Pelton turbine research has increasingly recognized that turbine performance cannot be accurately evaluated through isolated hydraulic or structural investigations alone. The interaction between fluid flow behavior, structural response, dynamic vibration, material characteristics, and experimental operating conditions creates a highly coupled multi-physics environment within the turbine system. Consequently, recent research trends increasingly focus on integrated methodologies combining hydraulic optimization, Computational Fluid Dynamics (CFD), Finite Element Analysis (FEA), modal analysis, fabrication, and experimental validation within unified design frameworks [57–60].

Traditional Pelton turbine studies generally investigate individual aspects such as hydraulic efficiency, bucket geometry, stress distribution, or transient flow behavior independently. Although such investigations have significantly improved understanding of individual physical phenomena, isolated analysis approaches often fail to capture the coupled interaction

between hydraulic loading, structural deformation, dynamic vibration, and operational performance [35–56].

Integrated multi-physics research methodologies therefore represent an important advancement in Pelton turbine design because they enable simultaneous consideration of multiple engineering domains affecting turbine efficiency, reliability, and long-term operational stability.

2.8.1 Integration of Hydraulic Optimization and CFD Analysis

Hydraulic optimization is commonly the first stage in integrated Pelton turbine design methodology because geometric parameters directly influence flow behavior and energy-transfer efficiency. Modern optimization studies increasingly employ CFD simulations to evaluate pressure distribution, jet interaction, turbulence generation, and free-surface flow characteristics under varying geometric configurations [57,58].

Barragan et al. [57] combined CFD analysis with optimization techniques to improve Pelton turbine hydraulic efficiency through systematic geometric modification of bucket parameters. Their investigation demonstrated that integrated optimization frameworks significantly improve prediction capability compared with conventional trial-and-error design approaches.

Similarly, Ibarra et al. [58] incorporated Artificial Neural Networks (ANN), CFD simulations, and statistical optimization methods to reconstruct and optimize Pelton turbine bucket geometry. Their study reported substantial improvement in turbine performance through AI-assisted optimization methodology.

These investigations highlight the increasing importance of combining numerical optimization algorithms with advanced CFD techniques for improving Pelton turbine hydraulic design. Integrated CFD-based optimization frameworks enable simultaneous evaluation of:

- jet coherence,
- pressure distribution,
- turbulence intensity,
- splash losses,
- and momentum-transfer efficiency.

However, many available studies remain limited to hydraulic performance analysis without considering structural safety and dynamic behaviour simultaneously [57,58].

2.8.2 Coupling of Hydraulic and Structural Analysis

Hydraulic loading generated during Pelton turbine operation directly influences structural stress distribution and deformation behavior within the runner buckets. Consequently, integration of CFD analysis with structural FEA has become increasingly important for evaluating the combined influence of hydraulic flow and mechanical response [28–34].

Integrated hydraulic–structural analysis generally involves:

1. CFD simulation of fluid flow and pressure distribution,
2. transfer of hydraulic loading data to structural finite element models,
3. evaluation of stress, deformation, and fatigue behavior.

Such coupled methodologies improve prediction accuracy by incorporating realistic hydraulic loading conditions rather than simplified static assumptions.

Nigussie et al. [59] developed a site-specific integrated design methodology for Pelton turbines combining hydraulic optimization and numerical analysis techniques. Their work demonstrated that integrated modelling improves turbine efficiency and enables more accurate adaptation to practical operating conditions.

Recent investigations by Chaudhari et al. [34] further integrated static structural analysis with hydraulic optimization to evaluate both efficiency enhancement and structural safety simultaneously. Their results demonstrated that optimized runner configurations can achieve improved hydraulic performance while maintaining acceptable stress and deformation limits.

Despite these developments, fully coupled fluid–structure interaction (FSI) simulations remain relatively limited in Pelton turbine research because of their high computational complexity and numerical instability associated with transient free-surface flow [35–48].

2.8.3 Integration of Modal Analysis and Dynamic Stability

Dynamic stability and resonance safety represent critical considerations for high-speed Pelton turbine operation. Therefore, recent integrated studies increasingly incorporate modal analysis within the overall design optimization framework [32–34].

Integrated modal investigations generally involve:

- hydraulic optimization,
- structural stress analysis,
- extraction of natural frequencies,
- resonance evaluation,
- and vibration safety assessment.

Chaudhari et al. [33] performed modal analysis using ANSYS Mechanical APDL to evaluate the natural frequencies and resonance characteristics of Pelton turbine runners under practical operating conditions. Their study demonstrated that integrated structural and modal evaluation significantly improves design reliability and operational safety.

Further work by Chaudhari et al. [34] combined static structural analysis and modal analysis within a unified finite element framework. Their results confirmed that optimized bucket geometries maintain sufficient resonance safety margins while simultaneously satisfying structural strength requirements.

The integration of modal analysis with hydraulic and structural optimization is particularly important because geometric modifications intended to improve hydraulic efficiency may unintentionally alter dynamic characteristics and vibration behaviour [32–34]. Consequently, simultaneous evaluation of hydraulic and dynamic performance is necessary for reliable turbine design.

2.8.4 Integration of Numerical and Experimental Approaches

The integration of Computational Fluid Dynamics (CFD), Finite Element Analysis (FEA), and experimental validation provides a comprehensive methodology for Pelton turbine design and performance evaluation. CFD enables prediction of pressure distribution, velocity fields, turbulence intensity, and hydraulic efficiency, while FEA evaluates structural stresses, deformation, and dynamic characteristics under realistic hydraulic loading. Experimental validation confirms the accuracy of numerical predictions under actual operating conditions and identifies practical factors such as manufacturing tolerances, mechanical losses, and measurement uncertainties that cannot be completely represented in numerical models. Therefore, the combined application of CFD, FEA, and experimental testing significantly improves design reliability, reduces development cost, enhances structural safety, and provides greater confidence in the practical implementation of optimized Pelton turbine runners.

Experimental validation remains an essential component of integrated multi-physics Pelton turbine research because numerical simulations alone cannot fully represent all physical operating conditions [44,56].

Modern integrated methodologies increasingly combine:

- analytical design,
- CFD simulation,
- structural analysis,
- modal analysis,
- fabrication,
- Experimental performance testing within a single research framework.

Petley and Aggidis [44] combined transient CFD analysis with experimental testing to validate pressure distribution and hydraulic performance predictions for Pelton turbine systems. Their investigation demonstrated strong agreement between numerical and experimental results.

Similarly, Chaudhari [56] conducted integrated numerical, experimental, and flow-visualization studies on Pelton turbine runners and successfully validated CFD-based flow predictions through laboratory testing and visualization techniques.

Integrated experimental validation provides several advantages:

- verification of numerical accuracy,
- assessment of practical feasibility,
- evaluation of operational stability,
- and identification of real-world performance limitations.

Such methodologies significantly improve confidence in proposed optimization strategies and provide stronger scientific justification for turbine design modifications.

2.8.5 Emerging Trends in Integrated Pelton Turbine Research

Recent research trends indicate growing interest in advanced integrated methodologies involving:

- Artificial Intelligence (AI),

- machine learning,
- optimization algorithms,
- digital twin systems,
- and real-time condition monitoring [57,58].

Artificial Neural Networks and surrogate modelling techniques are increasingly being used to reduce computational cost associated with repeated CFD simulations during optimization studies. Similarly, advanced sensor systems and vibration-monitoring techniques are being investigated for predictive maintenance and operational diagnostics in micro-hydropower systems.

Researchers are additionally exploring:

- additive manufacturing techniques,
- advanced composite materials,
- hybrid optimization frameworks, and multiphase transient CFD simulations to further improve Pelton turbine efficiency and operational reliability.

However, despite substantial progress, comprehensive integrated frameworks combining hydraulic optimization, CFD, structural analysis, modal analysis, fabrication, uncertainty analysis, and long-term experimental validation remain relatively limited within current literature [57–60].

2.8.6 Research Limitations and Need for Integrated Frameworks

The literature survey indicates that most existing Pelton turbine investigations focus on isolated engineering domains independently. Hydraulic optimization studies frequently neglect structural and dynamic effects, while structural investigations often employ simplified loading assumptions without realistic CFD-derived pressure distribution [28–60].

Similarly, many CFD investigations lack experimental validation, and relatively few studies perform detailed uncertainty analysis during performance testing. Fully coupled transient fluid–structure interaction simulations also remain computationally challenging and insufficiently explored.

Therefore, there exists a clear need for comprehensive integrated research methodologies capable of simultaneously addressing:

- hydraulic optimization,
- structural safety,
- dynamic stability,
- CFD flow analysis,
- Fabrication feasibility, and experimental validation within a unified micro-hydropower Pelton turbine framework.

The present research aims to contribute toward this requirement by developing an integrated methodology combining analytical design optimization, CFD simulation, static and modal finite element analysis, fabrication, and experimentally validated performance evaluation for micro-hydropower Pelton turbine applications.

2.9 Research Gaps Identified from Literature

A comprehensive review of the available literature indicates that substantial research has been conducted on various aspects of Pelton turbine design, hydraulic optimization, Computational Fluid Dynamics (CFD), structural analysis, modal analysis, material behaviour, and experimental performance evaluation. Researchers have investigated the influence of speed ratio, bucket geometry, nozzle configuration, runner dimensions, free-surface flow characteristics, stress distribution, vibration behaviour, and erosion mechanisms using both numerical and experimental methodologies [13–60].

Although these investigations have significantly improved the understanding of Pelton turbine operation and performance enhancement strategies, several important technical and research limitations remain insufficiently addressed within existing literature. The present section summarizes the major research gaps identified from the reviewed studies and establishes the motivation for the proposed research work.

2.9.1 Limited Integrated Multi-Physics Design Methodologies

One of the most significant observations from the literature survey is that most existing investigations focus primarily on isolated engineering domains rather than comprehensive integrated design methodologies. Many studies investigate hydraulic optimization independently using CFD techniques [13–27,35–48], while structural investigations separately evaluate stress distribution and deformation behaviour using finite element analysis [28–34].

Similarly, modal and vibration analyses are frequently conducted independently without direct coupling with hydraulic flow behaviour or transient loading conditions [32–34]. Experimental investigations also commonly evaluate isolated geometric parameters such as nozzle angle, bucket number, or pressure variation without integrating CFD analysis, structural safety evaluation, and dynamic stability assessment [21,26,27,52–56].

Consequently, relatively few studies combine:

- hydraulic optimization,
- transient CFD analysis,
- structural finite element analysis,
- modal analysis,
- fabrication methodology,
- experimental validation, and uncertainty analysis within a unified multi-physics framework specifically intended for micro-hydropower Pelton turbine applications [57–60].

2.9.2 Insufficient Coupling Between CFD and Structural Analysis

The literature review indicates that most CFD investigations evaluate hydraulic flow behaviour independently without considering the influence of hydraulic loading on structural deformation and stress distribution [35–48]. Similarly, many structural analyses employ simplified static loading assumptions instead of realistic pressure distributions obtained directly from CFD simulations [28–34].

Although several studies have attempted partial integration of hydraulic and structural analyses, fully coupled fluid–structure interaction (FSI) investigations remain relatively limited due to computational complexity and modelling challenges associated with transient free-surface flow [35–48].

As a result, the interaction between:

- hydraulic pressure fluctuation,
- transient jet impact,
- structural deformation, and dynamic stress behaviour remains insufficiently explored within current Pelton turbine research.

2.9.3 Limited Research on Combined Static and Modal Analysis

Structural stress analysis and modal analysis are both essential for ensuring reliable Pelton turbine operation; however, most available investigations address these aspects separately [28–34].

Numerous studies evaluate static stress concentration and deformation under hydraulic loading [28–31], while relatively fewer investigations analyse resonance behaviour and dynamic stability [32–34]. Even fewer studies perform integrated static and modal evaluation to simultaneously verify:

- structural strength,
- deformation behaviour,
- natural frequencies,
- resonance safety,
- operational vibration characteristics.

This limitation becomes particularly important for high-speed micro-hydropower turbines where optimized hydraulic geometry may significantly influence vibration behaviour and dynamic stability.

2.9.4 Limited Experimental Validation of Numerical Models

Modern Pelton turbine research increasingly relies on advanced CFD simulations and finite element modelling techniques; however, many numerical investigations lack detailed experimental validation [35–48].

Several CFD studies successfully predict pressure contours, velocity distribution, turbulence intensity, and free-surface flow behaviour, but relatively few compare numerical predictions directly with experimentally measured turbine performance [44,56].

Similarly, many structural and modal analyses remain purely numerical without validation through vibration measurements or physical prototype testing [28–34]. The absence of comprehensive experimental validation reduces confidence in numerical predictions and limits the practical applicability of proposed optimization methodologies.

Furthermore, detailed uncertainty analysis and statistical validation procedures are absent from many experimental investigations [52–56]. Consequently, there remains a strong need

for experimentally validated integrated research frameworks supported by formal uncertainty evaluation.

2.9.5 Limited Studies on Micro-Hydropower-Specific Optimization

A significant portion of existing Pelton turbine research focuses on large-scale commercial hydropower applications. Comparatively fewer investigations specifically address optimization methodologies tailored for micro-hydropower systems operating under low discharge and moderate power conditions [13–27].

Micro-hydropower turbines often operate under unique practical constraints including:

- compact runner dimensions,
- limited manufacturing capability,
- cost restrictions,
- simplified maintenance requirements,
- variable operating conditions.

Consequently, optimization methodologies developed for large-scale systems may not always be directly applicable to small-scale decentralized micro-hydropower applications.

The literature indicates limited research specifically integrating:

- micro-hydropower design constraints,
- fabrication feasibility,
- compact runner optimization, experimentally validated performance evaluation within a single framework.

2.9.6 Insufficient Investigation of Transient Operating Conditions

Many existing CFD and structural investigations focus primarily on steady-state operating conditions [35–43]. However, actual Pelton turbine operation involves transient phenomena such as:

- startup and shutdown conditions,
- fluctuating jet interaction,
- rotating bucket engagement,
- transient pressure fluctuation,

- and dynamic flow separation.

Although some researchers have performed transient CFD simulations using sliding mesh techniques [44–48], comprehensive transient studies coupled with structural and modal response analysis remain relatively limited.

Additionally, transient hydraulic loading effects on fatigue behaviour, vibration characteristics, and long-term structural reliability are insufficiently explored within current literature.

2.9.7 Limited Studies on Fabrication and Practical Implementation

While numerous studies focus on theoretical optimization and numerical simulation, comparatively fewer investigations address practical fabrication methodology, manufacturing constraints, and prototype implementation [52–56].

Practical considerations such as:

- manufacturability of optimized bucket geometry,
- fabrication tolerances,
- dynamic balancing, assembly accuracy,
- experimental rig development are often insufficiently discussed in available literature.

This creates a gap between theoretical optimization studies and practical implementation of improved Pelton turbine designs for real micro-hydropower applications.

2.10 Summary of Literature Review

The literature review presented in this chapter provides a comprehensive understanding of the current state of research related to Pelton turbine design, hydraulic optimization, Computational Fluid Dynamics (CFD), structural analysis, modal analysis, material behaviour, erosion mechanisms, and experimental performance evaluation for micro-hydropower applications.

The review initially established the growing importance of renewable energy systems and highlighted the significant role of hydropower in sustainable electricity generation. It was observed that Pelton turbines remain one of the most suitable hydraulic turbines for high-head and low-discharge conditions commonly encountered in micro-hydropower installations [1–8]. The fundamental operational principles of Pelton turbines, including impulse

momentum transfer, speed ratio, jet interaction, and bucket geometry characteristics, were also discussed in detail [9–12].

Extensive literature on hydraulic optimization demonstrated that turbine efficiency is strongly influenced by several interrelated parameters including speed ratio, bucket outlet angle, splitter geometry, nozzle configuration, runner dimensions, and bucket number [13–27]. Researchers have reported that optimum speed ratio generally lies within the range of approximately 0.46–0.49 for maximum energy transfer efficiency [9,10,13]. Similarly, optimization of bucket geometry and outlet angle has been shown to significantly influence jet bifurcation, flow attachment, splash losses, and residual kinetic energy [14–20].

The review further revealed that Computational Fluid Dynamics has become one of the most powerful tools for analysing Pelton turbine flow behaviour and hydraulic performance [35–48]. Modern CFD investigations successfully predict pressure distribution, velocity fields, turbulence generation, transient jet interaction, and free-surface flow dynamics using advanced numerical techniques such as moving mesh and multiphase flow modelling. However, many existing CFD studies remain limited to isolated hydraulic analysis without coupling with structural and dynamic investigations.

Structural analysis studies indicated that Pelton turbine buckets experience severe localized stress concentration near the splitter-root region due to repeated high-velocity jet impact [28–31]. Finite Element Analysis has been widely employed to evaluate stress distribution, deformation behaviour, and fatigue resistance under hydraulic loading conditions. Modal analysis investigations additionally demonstrated the importance of evaluating natural frequencies and resonance safety to ensure stable turbine operation under dynamic loading conditions [32–34].

The literature also showed that material selection significantly influences the structural reliability, erosion resistance, and operational durability of Pelton turbine systems [29–31,49–51]. Stainless steels remain widely preferred because of their superior mechanical strength and corrosion resistance, while advanced composite materials and surface treatment techniques are increasingly being explored for future turbine applications.

Studies related to erosion and cavitation highlighted that sediment-laden water and unstable free-surface flow can progressively degrade bucket surfaces and reduce turbine efficiency during long-term operation [31,39,40,50,51]. The splitter region was consistently identified as one of the most vulnerable locations for erosive wear and hydraulic instability.

Experimental investigations conducted by various researchers confirmed the importance of validating analytical and numerical models using laboratory-scale and prototype-scale testing methodologies [21,26,27,52–56]. Experimental studies have successfully evaluated nozzle variation, bucket geometry optimization, pressure effects, and turbine performance characteristics under controlled operating conditions. Nevertheless, detailed uncertainty analysis and comprehensive integrated validation frameworks remain relatively limited in current literature.

The review further demonstrated that recent Pelton turbine research increasingly emphasizes integrated multi-physics methodologies involving CFD analysis, hydraulic optimization, structural analysis, modal analysis, and experimental validation [57–60]. However, despite substantial progress, most available studies still investigate hydraulic, structural, and dynamic aspects independently rather than within a unified framework.

Based on the reviewed literature, several major research gaps were identified:

- limited integration of CFD and structural analysis,
- insufficient coupled static and modal investigations,
- lack of experimentally validated multi-physics frameworks,
- inadequate uncertainty analysis,
- limited studies focused specifically on micro-hydropower applications,
- and insufficient consideration of fabrication feasibility and transient operating conditions.

These identified gaps establish the motivation for the present research work. The current study aims to develop an integrated methodology for micro-hydropower Pelton turbine optimization by combining:

- analytical hydraulic design,
- Computational Fluid Dynamics,
- static structural analysis,
- modal analysis,
- fabrication, and experimentally validated performance evaluation within a unified research framework.

The outcomes of the present work are expected to contribute toward improved hydraulic efficiency, structural reliability, dynamic stability, and practical applicability of Pelton turbine systems for decentralized renewable energy generation.

2.11 Objectives of the present work

To fulfil the research gap, the objectives of the present work are as follows:

- To carry out systematic hydraulic design and parametric optimisation of the Pelton turbine bucket geometry.
- To perform static structural analysis and pre-stress modal analysis of the Pelton turbine bucket in ANSYS Mechanical APDL.
- To conduct steady-state and transient computational fluid dynamics analysis of the Pelton turbine bucket in ANSYS Fluent,
- To fabricate the optimized Pelton runner and dynamically balance the complete assembly to ensure accurate and reliable experimental testing.
- To carry out a comparative assessment between conventional and enhanced Pelton turbines under identical operating conditions to evaluate their performance levels.

Chapter 3 Theoretical Background and Design Methodology

3.1 Fundamentals of Pelton Turbine Operation

The Pelton turbine is an impulse-type hydraulic turbine widely used for high-head and low-discharge hydropower applications. Unlike reaction turbines, where pressure energy conversion occurs gradually within the runner passages, the Pelton turbine converts the entire available hydraulic head into kinetic energy before the water interacts with the turbine runner. This kinetic energy is transferred to the runner through impulse momentum exchange between the high-velocity water jet and specially designed Pelton buckets [7–12].

The fundamental operating principle of the Pelton turbine is based on Newton's second law of motion and conservation of momentum. Water stored at a higher elevation possesses hydraulic potential energy due to the available head. This pressure energy is converted into kinetic energy by passing water through a nozzle, which generates a high-velocity free jet directed tangentially onto the runner buckets [8,9].

The runner consists of a series of double hemispherical buckets mounted around the periphery of a circular wheel. Each bucket contains a central splitter that divides the incoming jet into two symmetrical streams. The water flows over the curved bucket surfaces and undergoes significant momentum change before exiting the bucket at the outlet edge. The force generated due to this momentum change produces torque on the runner shaft, thereby converting hydraulic energy into mechanical rotational energy [7–10].

The operational principle of the Pelton turbine is fundamentally characterised by the hydrodynamic interaction between a high-velocity water jet and the rotating runner buckets, wherein the mechanics of momentum transfer dictate the overall energy conversion performance of the machine. As the incoming jet impinges upon the central splitter ridge of each bucket, the flow is symmetrically bifurcated and progressively redirected along the curved interior surfaces of the bucket through a deflection angle that generally ranges between 160° and 170°, a geometric constraint imposed to prevent the deflected flow from interfering with the advancing jet stream. The effectiveness of this momentum exchange process is critically contingent upon several hydrodynamic conditions that must be simultaneously satisfied to minimise energy dissipation throughout the interaction zone. Specifically, smooth jet bifurcation is required to ensure that the incoming flow is divided

symmetrically and without abrupt directional discontinuities that would otherwise induce localised pressure fluctuations and kinetic energy degradation. Minimal flow separation along the bucket surface is equally imperative, as boundary layer detachment introduces regions of recirculating flow that reduce the effective wetted area available for momentum transfer and promote turbulent energy dissipation. Controlled free-surface flow behaviour within the bucket interior must furthermore be maintained to preserve the coherent hydraulic film necessary for sustained and uniform force application across the bucket geometry. Finally, low residual exit velocity at the point of flow discharge from the bucket is essential, since any kinetic energy retained by the departing water represents a direct and irrecoverable loss from the energy conversion cycle, thereby reducing the overall hydraulic efficiency of the turbine.

Consequently, bucket geometry plays a major role in determining turbine efficiency and hydraulic performance [13–16].The hydraulic efficiency of a Pelton turbine depends primarily on the relationship between jet velocity and runner peripheral speed. The runner speed must be carefully optimized to ensure maximum extraction of kinetic energy from the water jet. If the runner rotates too slowly, a significant portion of jet kinetic energy leaves the bucket unused. Conversely, excessively high runner speed reduces the relative velocity between the jet and bucket surfaces, thereby decreasing impulsive force generation [9,10,13].

The ideal hydraulic efficiency of a Pelton turbine is governed by the following relationship:

$$\eta_h = 2\left(\frac{u}{C_1}\right)(1 + k\cos\beta)\left(1-\frac{u}{C_1}\right) \text{----------} [5]$$

This equation indicates that turbine efficiency depends strongly upon speed ratio and outlet angle. Maximum hydraulic efficiency is generally obtained when the bucket speed is approximately one-half of the jet velocity [9–13].

The Pelton turbine operates entirely under atmospheric pressure conditions because pressure conversion occurs within the nozzle before jet interaction. Therefore, cavitation effects are significantly lower compared with reaction turbines operating under submerged pressure conditions [8]. However, free-surface instability, air entrainment, and localized pressure fluctuation may still influence hydraulic performance and long-term operational stability under certain conditions [39,40,51].

Modern Pelton turbine systems may employ single-nozzle or multi-nozzle arrangements depending upon discharge requirements and power output. Multi-nozzle configurations

improve power capacity while maintaining high hydraulic head operation; however, they also introduce complex transient flow interaction and dynamic loading behaviour [46,48,52].

The governing operational characteristics of a Pelton turbine are influenced by several important design parameters, namely speed ratio, jet ratio, bucket geometry, bucket outlet angle, nozzle configuration, runner diameter, and number of buckets. Proper optimization of these parameters is essential for achieving maximum hydraulic efficiency, stable operation, structural reliability, and long-term durability in micro-hydropower applications.

In recent years, advancements in Computational Fluid Dynamics (CFD), Finite Element Analysis (FEA), and transient numerical simulation techniques have significantly improved understanding of Pelton turbine hydrodynamics and structural behaviour [35–48]. Modern research increasingly focuses on integrated optimization methodologies combining hydraulic design, structural analysis, modal evaluation, and experimental validation to improve turbine performance and operational reliability.

The present research utilizes these theoretical principles as the foundation for analytical design optimization, numerical simulation, structural evaluation, and experimental validation of a micro-hydropower Pelton turbine runner.

3.2 Hydraulic Energy Conversion

The primary function of a Pelton turbine is the conversion of hydraulic energy available in water into useful mechanical energy at the turbine shaft. This conversion process occurs through a sequence of energy transformations involving pressure energy, kinetic energy, and rotational mechanical energy. Since the Pelton turbine is an impulse turbine, the entire hydraulic head is converted into kinetic energy before interaction with the turbine runner [8–10].

In a hydropower system, water stored at an elevated location possesses potential energy due to the available hydraulic head. When water flows through the penstock toward the turbine nozzle, this potential energy is converted into pressure energy and subsequently transformed into kinetic energy at the nozzle exit. The high-velocity jet produced by the nozzle strikes the Pelton bucket surfaces and transfers momentum to the runner, thereby generating rotational motion and mechanical power at the shaft [7–10].

The complete energy conversion process in a Pelton turbine may therefore be summarized as:

Hydraulic Potential Energy → Pressure Energy → Kinetic Energy → Mechanical Energy

The efficiency of this conversion process depends strongly on the effectiveness of momentum transfer between the water jet and the rotating buckets. Losses occurring during jet formation, flow separation, turbulence generation, splash losses, friction, and residual exit velocity reduce the overall hydraulic efficiency of the turbine [13–16].

3.2.1 Hydraulic Power Available in Water

The total hydraulic power available at the turbine inlet depends upon the hydraulic head and discharge rate of water flowing through the system. The theoretical hydraulic power available is expressed as:

$$P_h = \rho g Q H \text{----------[6]}$$

This equation indicates that available hydraulic power increases directly with both discharge and hydraulic head. Pelton turbines are particularly suitable for applications involving high hydraulic head and comparatively low discharge [8,9].

The net head available at the turbine is generally lower than the gross head because of hydraulic losses occurring in the penstock, bends, valves, and fittings. Therefore, accurate estimation of head losses is important for realistic turbine design and performance evaluation.

3.2.2 Conversion of Hydraulic Energy into Jet Kinetic Energy

The nozzle plays a crucial role in Pelton turbine operation because it converts pressure energy into kinetic energy by accelerating water through a converging passage. The velocity of the water jet emerging from the nozzle is determined using Bernoulli's principle and may be expressed as:

$$C_1 = K_v \sqrt{2gH} \text{----------[7]}$$

The coefficient of velocity accounts for hydraulic losses occurring inside the nozzle due to friction and turbulence. In practical Pelton turbine systems, the coefficient of velocity generally ranges between 0.97 and 0.99 depending upon nozzle design quality [8–10].

Efficient nozzle design is essential to ensure uniform velocity distribution, stable jet formation, minimum turbulence, and high jet coherence.

Improper nozzle geometry may result in flow separation, jet instability, and reduced hydraulic efficiency [21–24].

3.2.3 Momentum Transfer Between Jet and Bucket

The Pelton turbine extracts energy from the water jet through impulse momentum transfer. When the high-velocity jet strikes the splitter, the water is redirected over the bucket surface and exits at a significantly reduced velocity. The force exerted on the bucket is governed by Newton's second law and depends upon the rate of change of momentum of the water jet [8–10].

The tangential force acting on the runner may be expressed as:

$$F = \rho Q (V_{w1} - V_{w2}) \text{----------} [8]$$

The generated force produces torque on the runner shaft, causing rotational motion and mechanical power generation.

Maximum momentum transfer occurs when:

- jet interaction is smooth,
- flow separation is minimized,
- residual outlet velocity remains low,
- and bucket speed is properly optimized relative to jet velocity [13–17].

3.2.4 Mechanical Power Developed by the Runner

The mechanical power produced by the Pelton turbine runner is obtained from the torque generated on the turbine shaft. The shaft power developed by the turbine is expressed as:

$$P = \frac{2\pi NT}{60} \text{----------} [9]$$

This equation indicates that shaft power depends directly on both torque and rotational speed. Therefore, optimization of runner geometry and hydraulic interaction is essential for maximizing shaft power generation.

In practical systems, the actual shaft power is invariably lower than the theoretical hydraulic power due to the cumulative influence of several energy dissipation mechanisms, including hydraulic losses arising from flow resistance and imperfect energy transfer within the buckets, mechanical friction generated at rotating components and sealing interfaces, windage losses resulting from aerodynamic drag on the rotating runner, and bearing losses attributed to frictional resistance at the support bearings.

The ratio between actual shaft power and available hydraulic power determines the overall turbine efficiency.

3.2.5 Hydraulic Efficiency of Pelton Turbine

Hydraulic efficiency represents the effectiveness of converting jet kinetic energy into mechanical rotational energy. It is one of the most important performance indicators for Pelton turbine operation [9–16].

The hydraulic efficiency relationship is expressed as:

$$\eta_h = 2\left(\frac{u}{C_1}\right)(1 + k\cos\beta)\left(1 - \frac{u}{C_1}\right) \text{----------} [10]$$

This equation demonstrates that hydraulic efficiency depends strongly upon:

- speed ratio,
- outlet angle,
- and relative flow velocity.

The efficiency becomes maximum when the speed ratio approaches approximately 0.5 under ideal conditions [9,10,13].

3.2.6 Factors Affecting Hydraulic Energy Conversion

The efficiency of hydraulic energy conversion in a Pelton turbine is governed by a set of interrelated factors that collectively determine the extent to which the available hydraulic energy is successfully transformed into useful mechanical output. These factors encompass nozzle efficiency, which dictates the quality and velocity uniformity of the impinging jet, jet coherence, which reflects the degree to which the jet maintains its structural integrity prior to bucket impact, speed ratio, which defines the kinematic relationship between jet velocity and runner peripheral speed, and bucket geometry, which fundamentally shapes the hydrodynamic interaction between the jet and the rotating runner. Further influencing this conversion process are the bucket outlet angle, which controls the direction of flow discharge and thereby affects residual kinetic energy losses, flow separation phenomena occurring along bucket surfaces, turbulence generation arising from internal flow irregularities, and the magnitude of residual outlet velocity, which represents energy that remains unconverted at the point of flow exit from the runner.

Additional factors such as erosion, cavitation, air entrainment, and transient flow instability may further reduce energy-transfer efficiency during long-term operation [39,40,50,51].

Modern research increasingly utilizes CFD analysis and experimental validation to improve understanding of hydraulic energy conversion mechanisms and optimize Pelton turbine performance under realistic operating conditions [35–48].

The theoretical principles discussed in this section provide the fundamental basis for the analytical design equations and optimization methodology presented in the subsequent sections of this chapter.

3.3 Velocity Triangles

Velocity triangles represent one of the fundamental analytical tools used in Pelton turbine design and performance evaluation. They provide a graphical and mathematical representation of the relationship between jet velocity, bucket velocity, and relative flow velocity during interaction between the water jet and the rotating runner buckets. Proper understanding of velocity triangles is essential for determining hydraulic efficiency, momentum transfer, shaft power generation, and optimum operating conditions of the turbine [8–13].

In a Pelton turbine, energy transfer occurs through impulse momentum exchange between the high-velocity water jet and the moving bucket surfaces. The velocity components at inlet and outlet determine the magnitude of force acting on the runner and consequently influence turbine efficiency and power output [8–10].

The velocity triangle analysis of a Pelton turbine is generally divided into:

1. Inlet velocity triangle
2. Outlet velocity triangle

These velocity relationships form the basis for deriving hydraulic efficiency equations and design parameters such as speed ratio and outlet angle. Figure 3.1 shows a schematic of the velocity triangle of a Pelton Turbine.

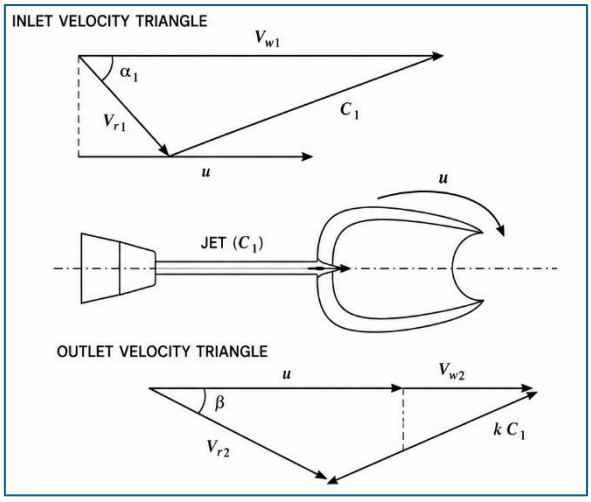

Figure 3.1 Velocity triangle of Pelton Turbine[88]

3.3.1 Inlet Velocity Triangle

At the inlet, water emerges from the nozzle with absolute velocity $C_1$and strikes the bucket moving with peripheral velocity u. Since the jet enters tangentially to the runner, the inlet jet angle is generally considered equal to zero under ideal conditions [8–10].

The inlet velocity triangle is governed by the relationship between:

- jet velocity,
- bucket speed,
- and relative velocity of water with respect to the moving bucket.

The relative velocity at inlet is expressed as:

$$V_{r1} = C_1 - u \text{----------[11]}$$

Since the jet enters tangentially, the whirl component of velocity at inlet becomes:

$$V_{w1} = C_1 \text{----------[12]}$$

The flow velocity component at inlet is negligible under ideal conditions because the jet is directed tangentially onto the bucket surface.

The inlet velocity triangle illustrates that the effective momentum transfer depends strongly on the relative difference between jet velocity and bucket speed. If the runner speed approaches the jet velocity, the relative velocity decreases and insufficient impulsive force is generated. Conversely, excessively low runner speed produces large residual exit velocity and reduced hydraulic efficiency [9–13].

3.3.2 Outlet Velocity Triangle

After striking the splitter, the water jet divides into two streams and flows over the curved bucket surfaces before leaving the runner at the outlet edge. During this process, the relative velocity decreases slightly because of frictional and hydraulic losses occurring along the bucket surface [14–16].

The relative velocity at outlet is expressed as:

$$V_{r2} = kV_{r1} \text{----------[13]}$$

The coefficient $k$accounts for frictional losses occurring during flow over the bucket surface. In practical Pelton turbines, the value of $k$generally ranges between 0.85 and 0.95 depending upon bucket surface finish and hydraulic conditions [8–10].

The outlet velocity triangle additionally depends upon the bucket outlet angle β, which determines the direction of exiting water flow. The whirl component of outlet velocity is expressed as:

$$V_{w2} = V_{r2}\cos\beta - u \text{----------[14]}$$

The outlet angle significantly influences residual kinetic energy and hydraulic efficiency. Smaller outlet angles generally improve energy transfer by reducing residual exit velocity; however, excessively small outlet angles may increase flow interference and manufacturing difficulty [14–17].

3.3.3 Force Developed on the Runner

The force acting on the Pelton runner is obtained from the rate of change of whirl momentum of the water jet. According to Newton's second law, the tangential force acting on the runner is given by:

$$F = \rho Q(V_{w1} - V_{w2}) \text{ ----------[15]}$$

This force produces torque on the runner shaft and converts hydraulic energy into rotational mechanical energy.

The magnitude of force generated depends directly upon:

- discharge rate,
- jet velocity,
- bucket speed,

- and outlet velocity characteristics.

Efficient Pelton turbine operation therefore requires minimizing the outlet whirl velocity component to maximize momentum transfer [9–17].

3.3.4 Hydraulic Efficiency from Velocity Triangle Analysis

Using the inlet and outlet velocity relationships, the hydraulic efficiency equation of the Pelton turbine may be derived analytically [8–13].

The hydraulic efficiency is expressed as:

$$\eta_h = 2\left(\frac{u}{C_1}\right)(1 + k\cos\beta)\left(1 - \frac{u}{C_1}\right) \text{----------[16]}$$

This equation indicates that hydraulic efficiency depends upon:

- speed ratio,
- blade velocity coefficient,
- and bucket outlet angle.

The speed ratio is defined as:

$$\phi = \frac{u}{C_1} \text{----------[17]}$$

Substituting the speed ratio into the efficiency equation enables analytical optimization of runner speed for maximum hydraulic performance.

the hydraulic efficiency becomes maximum when:

$$\frac{u}{C_1} = 0.5 \text{----------[18]}$$

Thus, the optimum bucket speed is theoretically equal to one-half of the jet velocity.

3.4 Governing Equations

The hydraulic design and performance evaluation of a Pelton turbine are based on several governing equations derived from principles of fluid mechanics, conservation of momentum, and rotational dynamics. These equations establish the theoretical relationship between hydraulic head, jet velocity, runner speed, torque generation, and turbine efficiency. The governing equations additionally form the analytical basis for optimization of runner geometry, speed ratio, bucket configuration, and operating parameters [8–13].

The present research utilizes these governing equations for analytical design calculations, numerical modelling, and performance evaluation of the micro-hydropower Pelton turbine system.

3.4.1 Hydraulic Power Equation

The total hydraulic power available at the turbine inlet depends upon the net head and discharge rate of water flowing through the system. The theoretical hydraulic power is expressed as:

$$P_h = \rho g Q H \text{----------[19]}$$

This equation represents the total energy available in the flowing water before conversion into mechanical energy.

3.4.2 Jet Velocity Equation

The nozzle converts hydraulic pressure energy into kinetic energy by accelerating water to high velocity before interaction with the turbine runner. The jet velocity at nozzle exit is determined using Bernoulli's principle and is expressed as:

$$C_1 = K_v\sqrt{2gH} \text{----------[20]}$$

The coefficient of velocity accounts for hydraulic losses occurring within the nozzle passage. Efficient nozzle design aims to maximize the coefficient of velocity and ensure stable jet formation [21–24].

3.4.3 Bucket Peripheral Velocity

The peripheral velocity of the runner bucket is directly related to the runner diameter and rotational speed. It is expressed as:

$$u = \frac{\pi D N}{60} \text{----------[21]}$$

The bucket speed is one of the most critical parameters affecting hydraulic efficiency and momentum transfer characteristics.

3.4.4 Speed Ratio Equation

The speed ratio represents the ratio between bucket speed and jet velocity. It is one of the most important non-dimensional design parameters governing Pelton turbine efficiency [9–13].

The speed ratio is defined as:

$$\phi = \frac{u}{C_1} \text{----------[22]}$$

For maximum hydraulic efficiency, the speed ratio generally lies between 0.46 and 0.49 under practical operating conditions [9,10,13].

3.4.5 Hydraulic Efficiency Equation

The hydraulic efficiency of a Pelton turbine represents the effectiveness of converting jet kinetic energy into mechanical energy at the runner shaft. Using velocity triangle relationships and momentum analysis, hydraulic efficiency is expressed as:

$$\eta_h = 2\left(\frac{u}{C_1}\right)(1 + k\cos\beta)\left(1 - \frac{u}{C_1}\right) \text{----------[23]}$$

This equation indicates that efficiency depends strongly upon:

- speed ratio,
- bucket outlet angle,
- and frictional losses over the bucket surface.

Maximum hydraulic efficiency occurs when the bucket speed approaches approximately one-half of the jet velocity.

$$\eta_h = V_{122u}(V_{w1} - V_{w2})$$

Since the outlet whirl velocity ($Vw2V_\{w2\}Vw2$) depends on the bucket exit angle, variation in the exit angle directly affects the change in whirl velocity and consequently the hydraulic efficiency.

3.4.6 Force Developed on the Runner

The force acting on the turbine runner is obtained from the rate of change of momentum of the water jet. The tangential force developed on the runner is expressed as:

$$F = \rho Q(V_{w1} - V_{w2}) \text{ ----------[24]}$$

This force generates torque and rotational motion of the turbine shaft.

3.4.7 Shaft Torque Equation

The torque developed by the Pelton turbine runner is related to the tangential force and runner radius. The shaft torque is expressed as:

$$T = FR \text{----------[25]}$$

Higher torque generation improves mechanical power output and overall turbine performance.

3.4.8 Shaft Power Equation

The mechanical power generated at the turbine shaft is expressed as:

$$P = \frac{2\pi NT}{60} \text{----------[26]}$$

This equation relates the rotational speed and developed torque to the mechanical power output of the turbine.

3.4.9 Bucket Passing Frequency Equation

During turbine operation, successive buckets periodically interact with the incoming water jet, generating cyclic hydraulic loading and dynamic excitation. The bucket-passing frequency is an important parameter in modal and vibration analysis and is expressed as:

$$f_b = \frac{ZN}{60} \text{----------[27]}$$

This excitation frequency is used to evaluate resonance safety and dynamic stability of the turbine runner [32–34].

3.4.10 Jet Ratio Equation

The jet ratio is defined as the ratio of runner pitch diameter to jet diameter and represents an important geometric design parameter for Pelton turbines [9–13].

The jet ratio is expressed as:

$$m = \frac{D}{d} \text{----------[28]}$$

Proper selection of jet ratio ensures efficient jet interaction and smooth runner operation.

3.4.11 Number of Buckets Equation

The number of buckets mounted on the runner influences flow continuity, jet interaction frequency, and hydraulic efficiency. An empirical relationship commonly used for determining the number of buckets is given by:

$$Z = 15 + \frac{D}{2d} \text{----------[29]}$$

This relationship provides sufficient bucket spacing for effective jet interception while minimizing interference between adjacent buckets [11,18].

3.4.12 Importance of Governing Equations in Design Methodology

The governing equations discussed in this section form the theoretical foundation for:

- hydraulic design calculations,
- runner geometry optimization,
- efficiency prediction,
- structural loading estimation,
- and experimental performance evaluation.

These equations are further utilized in:

- CFD boundary condition development,
- finite element loading calculations,
- modal analysis,
- and optimization methodology adopted in the present research work.

The subsequent sections of this chapter discuss the practical design parameters and optimization strategies developed using these governing theoretical relationships.

3.5 Parametric Optimization Strategy

The hydraulic performance and operational stability of a Pelton turbine are significantly influenced by several interdependent design parameters such as speed ratio, bucket outlet angle, jet ratio, runner geometry, and bucket configuration. These parameters directly affect momentum transfer, pressure distribution, flow separation, turbulence generation, residual outlet velocity, and shaft power output during turbine operation. Therefore, systematic

optimization of the governing design variables is essential for achieving maximum hydraulic efficiency and stable operating behaviour in micro-hydropower applications.

Since bucket geometry directly governs momentum transfer, hydraulic efficiency, and structural loading, optimization of the bucket profile was considered the primary design objective in the present research. The analytical optimization performed in this work therefore focuses on identifying the optimum bucket exit angle and speed ratio capable of maximizing hydraulic performance while maintaining structural integrity.

Conventional Pelton turbine design methods are generally based on empirical relationships and trial-and-error procedures. Although such approaches provide satisfactory preliminary designs, they are often unable to identify optimum operating conditions because the design variables are highly interconnected. Consequently, modern turbine-development methodologies increasingly combine analytical calculations, Computational Fluid Dynamics (CFD), structural analysis, and experimental validation to improve prediction accuracy and hydraulic performance [60].

The present research adopts an integrated parametric optimization strategy primarily focused on optimization of bucket outlet angle and speed ratio because these parameters strongly influence energy-transfer efficiency and hydraulic behaviour of the Pelton runner. Previous investigations reported in literature demonstrated that careful selection of outlet angle and speed ratio can significantly improve turbine efficiency and operational stability [60].

In the optimization methodology adopted for the present work, the bucket outlet angle is varied within the range of 10° to 15°, while the speed ratio is investigated between 0.445 and 0.485. The influence of these parameters on hydraulic efficiency is evaluated using analytical relationships derived from Pelton turbine theory and empirical performance equations. The optimization procedure additionally incorporates design calculations associated with net head, turbine speed, runner diameter, nozzle diameter, bucket dimensions, and output power evaluation [60].

The speed ratio represents the ratio between bucket peripheral velocity and jet velocity and plays a major role in determining momentum-transfer efficiency between the water jet and the rotating runner buckets. If the runner speed is excessively low, a large portion of jet kinetic energy leaves the bucket unused, resulting in higher residual outlet velocity and reduced efficiency. Conversely, excessively high runner speed reduces the relative velocity between the jet and bucket surfaces, thereby decreasing impulsive force generation.

Literature investigations indicate that maximum hydraulic efficiency is generally achieved when the speed ratio lies within a narrow optimum range [60].

Similarly, the bucket outlet angle significantly affects outlet flow direction, residual kinetic energy, and flow-separation characteristics. Smaller outlet angles improve momentum transfer by reducing residual exit velocity and increasing energy extraction from the water jet. However, excessively small outlet angles may create undesirable backflow conditions and unstable hydraulic interaction near the bucket exit region. Therefore, optimization of outlet angle is necessary to achieve a balance between efficient momentum transfer and stable flow behaviour [60].

The analytical results obtained from the optimization study indicate that turbine efficiency varies considerably with changes in both speed ratio and bucket outlet angle. The maximum hydraulic efficiency was observed near a speed ratio of 0.480 with bucket outlet angles in the range of approximately 10° to 11°. The study further reported that speed ratios between 0.475 and 0.485 provide comparatively better hydraulic performance under micro-hydropower operating conditions [60].

Table 3.1 Results Bucket angle and Speed ratio

Bucket Angle(β)	**10**	**11**	**12**	**13**	**14**	**15**
Speed Ratio (φ)	Th	Th	Th	Th	Th	Th
0.445	96.0269	95.8827	95.7179	94.605	94.4214	95.1411
0.450	96.2329	96.0887	95.9136	95.7385	94.6152	95.3368
0.455	95.4822	95.3292	95.166	94.9926	95.7282	95.5222
0.460	95.6454	95.4924	95.3292	95.1558	95.893	94.758
0.465	95.7882	95.6454	95.472	95.2986	96.0372	94.9008
0.470	95.9208	96.7067	95.6046	96.3565	96.1608	95.9548
0.475	96.0228	96.8097	96.6449	95.523	96.2741	96.0578

0.480	97.0466	95.9616	95.7882	96.5522	95.421	96.1505
0.485	96.1248	95.9718	96.7479	95.625	95.4312	95.2272

The relationship between speed ratio and hydraulic efficiency is illustrated in Figure 3.1. The graph demonstrates that efficiency increases progressively with increasing speed ratio until an optimum condition is achieved near a speed ratio of 0.480. Beyond this operating range, the efficiency variation becomes unstable because of changes in outlet-flow characteristics and residual kinetic energy losses.

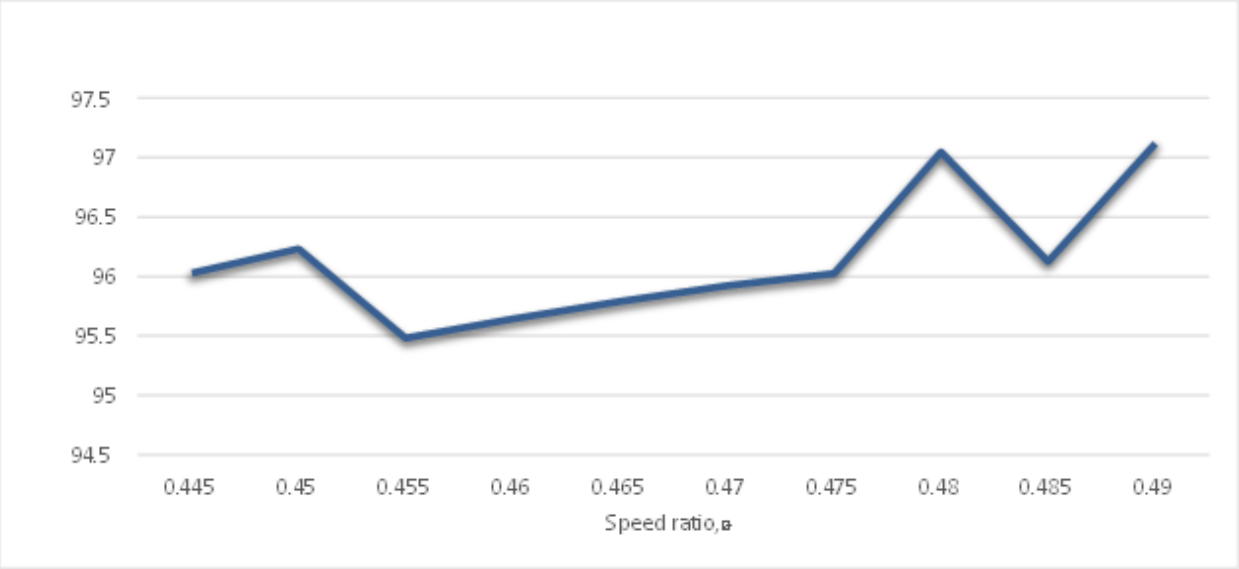

Figure 3.2 Speed Ratio versus Hydraulic Efficiency

The influence of bucket outlet angle on turbine efficiency is similarly presented in Figure 3.2. The graph indicates that outlet angles between 10° and 11° produce comparatively higher efficiency because of improved momentum transfer and reduced residual outlet velocity. However, further reduction in outlet angle may increase flow interference and backflow tendency near the bucket exit region [60].

The bucket exit angle (β_2) plays a decisive role in determining the hydraulic efficiency of a Pelton turbine because it governs the direction and velocity of water leaving the bucket after momentum transfer. Based on the impulse-momentum principle, the useful work developed by the runner depends on the reduction in the whirl component of the jet velocity. An appropriately selected exit angle allows the water jet to undergo maximum deflection while maintaining smooth flow attachment along the bucket surface. Consequently, the residual outlet velocity is minimized, resulting in maximum energy extraction and higher hydraulic

efficiency. Conversely, a smaller exit angle increases frictional losses due to prolonged flow contact, whereas a larger exit angle causes premature flow separation, increased splash losses, and higher residual kinetic energy. Therefore, optimization of the bucket exit angle is essential for achieving efficient momentum transfer, reducing hydraulic losses, and maximizing turbine performance. In the present study, the exit angle was systematically varied between **10° and 15°**, and its influence on hydraulic efficiency was evaluated analytically. The optimum exit angle, together with the optimum speed ratio, yielded the highest theoretical hydraulic efficiency of **94.29%**, which was subsequently validated through CFD simulations and experimental investigations.

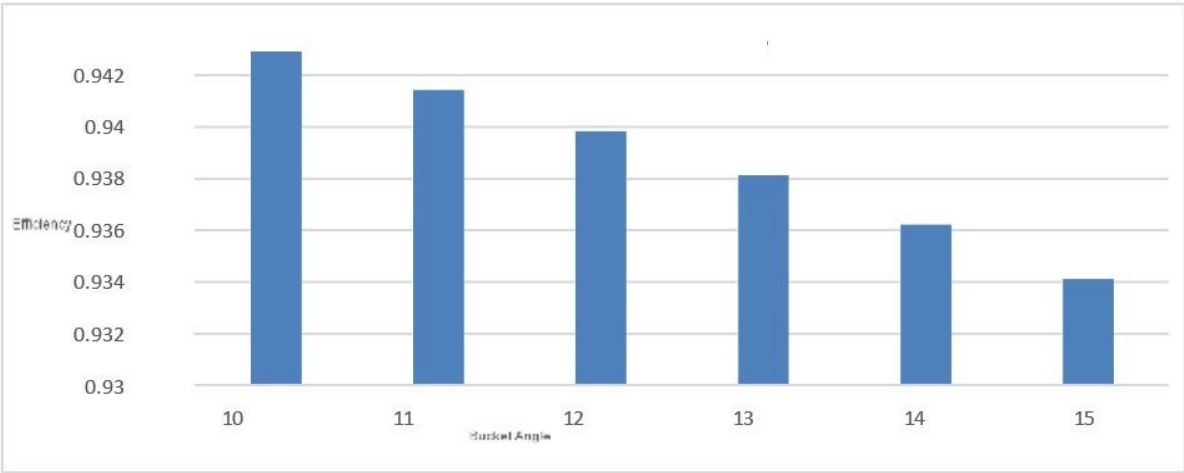

Figure 3.3 Bucket Outlet Angle versus Hydraulic Efficiency

Figure 3.3 illustrates the relationship between bucket exit angle and hydraulic efficiency. It is evident that hydraulic efficiency initially increases with increasing exit angle because the water jet undergoes more effective momentum transfer with reduced residual outlet velocity. However, beyond the optimum value, hydraulic efficiency decreases due to increased flow separation and splash losses. This behaviour demonstrates that bucket exit angle must be optimized together with speed ratio to achieve maximum turbine efficiency.

The speed ratio is a critical hydraulic design parameter because it governs the relative velocity between the water jet and the moving bucket, thereby controlling momentum transfer and energy conversion efficiency. At lower speed ratios, the bucket rotates too slowly, causing a significant portion of the jet kinetic energy to leave the bucket without effective utilization. Conversely, at higher speed ratios, the relative velocity between the jet and the bucket decreases, reducing the impulse force generated on the runner. Consequently, both extremely low and extremely high speed ratios lead to reduced hydraulic efficiency. An

optimum speed ratio provides maximum change in whirl velocity, minimum residual outlet velocity, and maximum energy extraction from the water jet. In the present study, analytical optimization identified a speed ratio of approximately **0.485** as the optimum value, corresponding to a maximum theoretical hydraulic efficiency of **94.29%**, which was subsequently validated through CFD simulations and experimental investigations.

The present research utilizes the findings of the above optimization study as the theoretical basis for further hydraulic and structural evaluation of the Pelton turbine runner. The optimized design parameters obtained from analytical investigation are subsequently incorporated into CFD simulation, structural analysis, modal analysis, and experimental validation to develop an efficient and operationally reliable micro-hydropower Pelton turbine system.

3.6 Material Selection Criteria

Material selection is a critical aspect of Pelton turbine design because the runner buckets are continuously subjected to high-velocity jet impingement, cyclic hydraulic loading, vibration, erosive particle interaction, and environmental exposure during operation. The selected material must therefore provide adequate mechanical strength, structural stiffness, fatigue resistance, corrosion resistance, and erosion durability while maintaining acceptable manufacturability and economic feasibility [29–31,49–51].

In a Pelton turbine, the bucket splitter and inner bucket surfaces are subjected to severe and highly localised hydraulic loading conditions arising from the repetitive impingement of high-velocity water jets, a phenomenon that imposes substantial cyclic mechanical stresses upon the structural components of the runner assembly. The intensity and concentration of these hydrodynamic forces are particularly pronounced at the splitter ridge, where the incoming jet first makes contact with the bucket surface, generating peak impact pressures that are considerably higher than those experienced across the remaining wetted interior geometry. Under such demanding operational conditions, the selection of an inappropriate or structurally inadequate material may precipitate a range of deleterious mechanical consequences that progressively compromise the integrity and serviceability of the turbine. Excessive plastic deformation may occur in regions of stress concentration, permanently altering the carefully optimised bucket geometry and thereby degrading the hydraulic performance of the runner. Fatigue crack initiation is a further manifestation of prolonged cyclic loading, wherein microscopic surface or subsurface discontinuities progressively

propagate under repeated stress fluctuations until critical fracture conditions are reached. Surface erosion, driven by the combined action of high-velocity impingement and the abrasive character of entrained particulate matter within the flow, gradually degrades the hydro dynamically refined bucket profile, introducing surface irregularities that promote flow separation and energy dissipation. Vibration instability may additionally arise from asymmetric material degradation or geometric distortion, inducing dynamic imbalance within the rotating assembly and generating resonant excitation that further accelerates structural deterioration. In the most severe cases, the cumulative progression of these damage mechanisms may culminate in premature structural failure, resulting in unplanned operational downtime and significant economic consequences. It is therefore imperative that a rigorous and systematic evaluation of candidate material properties be undertaken during the design phase, with particular consideration given to yield strength, fatigue endurance limit, hardness, and corrosion resistance, so as to ensure long-term operational reliability, structural safety under sustained dynamic loading, and the preservation of stable hydraulic performance throughout the intended service life of the turbine.

The present research considers material selection as an important component of the overall design methodology and evaluates material suitability based on both hydraulic and structural operating requirements.

3.6.1 Functional Requirements of Pelton Turbine Materials

The selection of an appropriate runner material for a Pelton turbine must simultaneously address a comprehensive set of functional requirements arising from the hydraulic, structural, and operational conditions to which the runner assembly is continuously subjected during service. The material must exhibit high yield strength and adequate stiffness to resist permanent deformation and preserve the optimised bucket geometry under intense impulsive jet loading, alongside good fatigue resistance and high impact toughness to withstand the millions of stress cycles accumulated over the operational lifetime of the turbine without crack initiation or brittle fracture. Corrosion resistance and erosion resistance are equally essential, as prolonged exposure to water and suspended sediment particles promotes electrochemical surface degradation and abrasive material loss that progressively distort the hydraulic profile and undermine structural integrity [28–31]. Good machinability and dimensional stability under cyclic loading are further required to ensure precise fabrication and sustained geometric accuracy throughout the service life of the runner.

The runner buckets experience repeated impulsive loading from high-velocity water jets and must therefore withstand prolonged fluctuating stresses without excessive deformation or fatigue damage [28–31]. Since micro-hydropower installations frequently utilise natural water sources containing suspended sediment, the material must additionally resist abrasive wear, surface erosion, and corrosion-related degradation [31, 50].

3.6.2 Mechanical Strength and Structural Stiffness

Mechanical strength represents one of the primary material requirements for Pelton turbine runners, owing to the large impulsive hydraulic forces generated during repeated jet impingement events. The selected material must possess sufficiently high yield strength, tensile strength, and elastic modulus to prevent excessive deformation and structural failure under sustained hydraulic loading conditions [28–30]. Finite element analysis investigations reported in the literature consistently indicate that maximum stress concentration occurs in the vicinity of the splitter-root region, whilst maximum deformation is typically localised near the bucket lip and sidewall areas [28–31]. Materials exhibiting inadequate stiffness are susceptible to excessive elastic deformation that progressively alters the optimised bucket geometry, resulting in reduced hydraulic efficiency and heightened vibration levels within the rotating assembly.

High structural rigidity is therefore essential for maintaining dimensional stability and ensuring consistent hydraulic performance throughout the operational lifespan of the turbine.

3.6.3 Fatigue Resistance

Pelton turbine buckets are subjected to continuous cyclic loading as successive buckets repeatedly interact with the high-velocity water jet during runner rotation, imposing fluctuating stress conditions that progressively accumulate fatigue damage within the material microstructure over the operational lifetime of the turbine. This cyclic hydraulic loading may gradually initiate fatigue cracks at regions of geometric stress concentration, most notably at the splitter root, bucket-arm junction, and cut-out regions, where localised stress amplitudes are considerably elevated relative to the nominal stress state of the surrounding material [29].

The selected material must therefore possess good fatigue resistance characterised by a high endurance limit and slow crack propagation rate, so as to ensure sustained structural integrity under prolonged fluctuating stress conditions. The criticality of fatigue behaviour is

particularly pronounced in high-speed micro-hydropower turbines, multi-nozzle configurations, and installations involving long-duration continuous operation, where the frequency and cumulative number of stress cycles are substantially higher than in conventional low-speed applications. Materials exhibiting inadequate fatigue resistance may develop progressive crack propagation and ultimately suffer catastrophic structural failure even when their static strength properties appear nominally sufficient, underscoring the necessity of evaluating dynamic fatigue performance as an independent and indispensable criterion in the material selection process.

3.6.4 Erosion and Corrosion Resistance

In practical hydropower applications, the water flowing through a Pelton turbine often contains suspended abrasive particles such as sand, silt, quartz, and various mineral impurities. During turbine operation, these particles strike the bucket surfaces at very high velocity along with the water jet, gradually causing erosive wear on the runner material. The splitter region of the bucket is particularly susceptible to erosion because it directly receives the incoming jet and experiences the highest impact intensity. Continuous exposure to such abrasive action can progressively damage the bucket surface, alter the original geometry, and reduce hydraulic efficiency over time. Therefore, the selected runner material must possess high surface hardness and good wear resistance to withstand erosive particle interaction under long-term operating conditions.Apart from erosion, prolonged exposure to water and atmospheric conditions may also lead to corrosion-related deterioration of the runner material. Oxidation, surface pitting, and chemical degradation can gradually weaken the bucket surfaces and reduce the fatigue strength of the material. Corrosion damage becomes more critical in micro-hydropower systems operating continuously under varying environmental conditions.

Since erosion and corrosion often act simultaneously, the combined effect may accelerate material degradation and reduce the operational life of the turbine runner. Consequently, corrosion resistance is considered an essential criterion in the material-selection process for Pelton turbine applications.[49–51].

3.6.5 Stainless Steel as Preferred Material

Based on extensive literature review and established engineering practice, stainless steel is widely recognized as one of the most suitable materials for Pelton turbine runners because it offers an excellent combination of mechanical strength, structural stiffness, corrosion

resistance, fatigue durability, and erosion resistance. The operating conditions of Pelton turbines involve continuous exposure to high-velocity water jets, cyclic hydraulic loading, vibration, and abrasive particle interaction. Under such demanding conditions, the runner material must maintain both structural integrity and hydraulic performance over long periods of operation. Stainless steel satisfies these requirements effectively and therefore has become the preferred material in most modern Pelton turbine applications.

One of the major advantages of stainless steel is its high chromium content, which forms a protective oxide layer on the material surface and significantly improves resistance against oxidation, water-induced corrosion, and surface degradation. This protective characteristic is particularly important in hydropower installations operating under continuous moisture exposure and fluctuating environmental conditions. In addition to corrosion resistance, stainless steel also possesses high yield strength, adequate toughness, and good fatigue performance, enabling the runner buckets to withstand repeated impulsive hydraulic loading without excessive deformation or crack initiation[30,34].

Previous investigations reported in the literature further support the suitability of stainless steel for Pelton turbine applications. Finite Element Analysis studies conducted by Mbiu et al. demonstrated that stainless steel buckets exhibit lower deformation, improved structural rigidity, and better operational stability when compared with lightweight materials such as aluminum alloys. Similarly, modal-analysis investigations performed by Chaudhari et al. showed that stainless steel runners provide higher natural frequencies and improved resonance safety, thereby enhancing the overall structural reliability of the turbine system. These characteristics are particularly important in micro-hydropower turbines where cyclic excitation and vibration behaviour strongly influence long-term operational stability.

Considering its superior mechanical and hydraulic characteristics, stainless steel is selected as the preferred runner material for the present research work. The material selection supports the objective of achieving improved structural safety, stable hydraulic performance, enhanced durability, and reliable long-term operation of the micro-hydropower Pelton turbine system.

3.6.6 Comparison with Alternative Materials

Several alternative materials have been investigated for Pelton turbine applications in an effort to reduce structural weight, improve manufacturability, and enhance corrosion resistance. Among the commonly studied alternatives are aluminum alloys, composite materials, and coated metallic materials. Although these materials provide certain advantages

under specific operating conditions, their overall suitability for high-head Pelton turbine applications remains limited when compared with stainless steel. Material selection for turbine runners must consider not only weight reduction and manufacturability but also long-term structural reliability, fatigue resistance, erosion durability, and hydraulic loading capability.

Aluminum alloys are frequently considered because of their low density, reduced structural weight, and ease of machining. The lightweight nature of aluminum can reduce rotational inertia and simplify manufacturing processes. However, literature studies indicate that aluminum alloys generally possess lower stiffness and reduced fatigue resistance compared with stainless steel. Under high-velocity jet impact and cyclic hydraulic loading, aluminum runners may experience larger deformation and reduced dimensional stability. In addition, aluminum materials exhibit comparatively poor erosion resistance when exposed to abrasive particles present in natural water sources. These limitations make aluminum alloys less suitable for high-head Pelton turbine applications where severe hydraulic loading and long-term operational durability are critical requirements.

Composite materials have also attracted research interest because they offer advantages such as low structural weight, good corrosion resistance, and flexibility in geometric design. Advanced composite structures can potentially reduce overall runner mass while maintaining acceptable strength-to-weight ratios. However, the practical implementation of composite materials in Pelton turbines remains limited due to several engineering challenges. Concerns related to impact resistance, fatigue behaviour, erosion durability, and manufacturing complexity continue to restrict their widespread use in practical hydropower systems. Repeated high-velocity jet interaction may produce localized damage and progressive material degradation in composite structures, particularly in the splitter and bucket-surface regions where hydraulic loading is most severe [30].

Coated metallic materials and surface-treated runners have also been explored to improve erosion and corrosion resistance. Although protective coatings may enhance surface durability to some extent, long-term coating stability under continuous hydraulic impact remains an important concern. Coating delamination, surface cracking, and maintenance requirements may reduce operational reliability during prolonged turbine operation [49].

Considering the combined requirements of mechanical strength, structural rigidity, fatigue resistance, erosion durability, corrosion resistance, and long-term operational stability,

stainless steel continues to remain the most reliable and widely accepted material for practical micro-hydropower Pelton turbine applications.

3.6.7 Material Selection for Present Research

Based on the detailed literature review, hydraulic operating conditions, structural loading requirements, and practical manufacturing considerations, stainless steel is selected as the runner material for the present research work. The selection of material is an important component of the overall turbine design methodology because the runner is continuously subjected to high-velocity jet impact, cyclic hydraulic loading, vibration, and erosive particle interaction during operation. Therefore, the selected material must ensure both hydraulic reliability and structural safety under long-term operating conditions.

The choice of stainless steel is primarily justified by its superior mechanical and operational characteristics. Stainless steel possesses high structural strength and adequate stiffness, which help maintain dimensional stability and reduce excessive deformation under impulsive hydraulic loading. The material also provides good fatigue resistance, enabling the runner buckets to withstand repeated cyclic stresses generated during continuous turbine operation. In addition, its excellent corrosion resistance protects the runner surfaces from oxidation, pitting, and moisture-related degradation, thereby improving operational durability in practical hydropower environments.

Another important advantage of stainless steel is its improved erosion resistance against abrasive particles present in natural water sources. Since Pelton turbine buckets are frequently exposed to suspended sand, silt, and mineral impurities, resistance to erosive wear becomes essential for maintaining bucket geometry and hydraulic efficiency over prolonged service periods. Stainless steel additionally offers good weldability and machinability, which simplifies fabrication and manufacturing of the runner assembly while ensuring reliable structural performance.

The selected material is considered particularly suitable for micro-hydropower applications involving fluctuating hydraulic loading and continuous operation. Consequently, stainless steel is adopted in the present study to achieve improved structural integrity, enhanced fatigue life, stable hydraulic behaviour, and reliable long-term performance of the Pelton turbine runner.

To further verify the suitability of the selected material, the stainless steel runner is subsequently evaluated using static structural analysis, modal analysis, and experimental

testing. These investigations assist in assessing stress distribution, deformation characteristics, vibration behaviour, and overall structural reliability under realistic operating conditions.

3.6.8 Importance of Material Selection in Integrated Design

Material selection plays a highly significant role in the overall design and performance of a Pelton turbine because the mechanical behaviour of the runner is directly influenced by the physical and structural properties of the selected material. The runner buckets are continuously exposed to hydraulic loading, cyclic stresses, vibration, and erosive flow conditions during operation. Consequently, the selected material affects not only the structural integrity of the runner but also the hydraulic efficiency, fatigue life, deformation characteristics, and operational stability of the turbine system.

The influence of material properties extends to several important performance aspects including stress distribution, deformation behaviour, vibration response, fatigue resistance, and long-term reliability. Materials with insufficient stiffness may undergo excessive deformation under hydraulic loading, resulting in alteration of bucket geometry and reduction in hydraulic efficiency. Similarly, materials with poor fatigue resistance may experience crack initiation and propagation under repeated cyclic loading conditions, eventually leading to structural failure. Therefore, proper material selection is essential for ensuring safe and stable turbine operation over prolonged service life.

Material characteristics also influence the dynamic behaviour of the runner assembly. The natural frequencies and vibration response of the turbine depend strongly upon material stiffness and mass distribution. Inadequate material selection may increase the possibility of resonance under cyclic hydraulic excitation, thereby affecting operational stability and structural safety. Additionally, erosion and corrosion resistance directly determine the durability of bucket surfaces exposed to abrasive particle interaction and continuous water contact.

Because of these interrelated effects, material selection cannot be considered independently from hydraulic optimization and structural analysis. Modern Pelton turbine development increasingly adopts an integrated design methodology in which hydraulic performance evaluation, Computational Fluid Dynamics (CFD) simulation, structural analysis, modal analysis, and material selection are combined within a unified optimization framework. Such

an integrated approach enables simultaneous improvement of hydraulic efficiency, structural reliability, vibration stability, and operational safety.

The present research follows this integrated methodology by combining hydraulic analysis, numerical simulation, structural evaluation, modal investigation, and material-selection considerations to develop an optimized micro-hydropower Pelton turbine system with improved efficiency, durability, and long-term operational reliability.

3.7 Closure

This chapter presented the theoretical background and design methodology adopted for the hydraulic and structural development of the micro-hydropower Pelton turbine runner. The fundamental operating principle of the Pelton turbine was discussed, emphasising its impulse-type energy conversion mechanism in which the entire available hydraulic head is first converted into kinetic energy within the nozzle before interacting with the runner buckets. The governing energy conversion sequence, from hydraulic potential energy through pressure energy and kinetic energy to mechanical rotational energy, was outlined along with the role of Newton's second law and conservation of momentum in describing the impulsive force developed on the runner.

A systematic parametric optimization study was conducted to evaluate the influence of speed ratio and bucket outlet angle on hydraulic efficiency. The speed ratio was varied between 0.445 and 0.485, while the bucket outlet angle was investigated over the range of 10° to 15°. The analytical results indicated that the maximum theoretical hydraulic efficiency of 97.05 % was achieved at a speed ratio of 0.480 and a bucket outlet angle of 10°. Speed ratios between 0.475 and 0.485 consistently produced higher hydraulic performance under micro-hydropower operating conditions. These optimised values of speed ratio and outlet angle were adopted as the primary design parameters for the Pelton turbine runner developed in the present research.

Material selection was discussed as an important component of the overall design methodology. The functional requirements for runner materials were identified, encompassing high yield strength, adequate stiffness, fatigue resistance, impact toughness, corrosion resistance, erosion resistance, and dimensional stability under cyclic hydraulic loading. Stainless steel was selected as the preferred runner material based on its superior combination of mechanical strength, structural stiffness, fatigue performance, corrosion resistance, and erosion durability. Alternative materials including aluminum alloys and

composite materials were evaluated and found to exhibit limitations related to stiffness, fatigue life, and erosion resistance under the severe hydraulic loading conditions characteristic of Pelton turbine operation. The selection of stainless steel was further supported by findings reported in published Finite Element Analysis and modal analysis investigations.

The theoretical principles, governing equations, optimised design parameters, and material selection criteria developed in this chapter collectively provide the foundation for the subsequent stages of the research. The hydraulic design values derived analytically are directly utilised in CFD simulation boundary conditions, finite element loading calculations, modal analysis, and experimental test conditions. The integrated design methodology combining hydraulic analysis, numerical simulation, structural evaluation, and material selection ensures that the micro-hydropower Pelton turbine runner developed in the present work achieves improved hydraulic efficiency, structural reliability, stable vibration behaviour, and reliable long-term operational performance.

Chapter 4 Finite Element Structural and Modal Analysis of Pelton Turbine Bucket

4.1 Introduction

Due to their high hydraulic efficiency, easy-to-use and appropriate for application in decentralized micro-hydro systems, Pelton turbines have become popular for generating electricity through high-head hydropower and low-discharge hydropower. Whereas reaction turbines operate on the basis of impulse momentum transfer principle, utilizing the entire hydraulic head will first be converted into kinetic energy by the nozzle prior to acting on the turbine runner bucket through the use of a jet of high-velocity water [1-3]. Therefore, due to their ability to operate under high-head conditions, Pelton turbines are widely used for electricity generation in mountainous areas and smaller-scale hydropower installations where the requirement for dependable and sustainable electricity exists. There are numerous operational advantages to the use of Pelton turbines; however, the turbine runners and bucket assemblies are continually exposed to severe hydraulic and dynamic loading environment throughout their operation. The water jet generated at the nozzle impacts the splitter region of the bucket producing a large impulsive load, resulting in localized stress concentrations, pressure fluctuation and dynamic deformation of the bucket assembly [4-6]. As a result of the constant impact of the water jet on the rotating surface of the bucket under cyclic operating conditions, the runner will experience multiple load reversals, which could have a significant impact on the durability and fatigue life of the turbine components.

The Pelton turbine runner's structural reliability ranks among the top issues affecting long-term operational reliability or maintenance of the micro hydro system. Improper bucket shape, material selection, stress concentrations at the split region, and dynamic loads can lead to a variety of issues including cracking, permanent deformation, erosion damage, vibration failure, and eventually structural failure of the runner [7–9]. Under actual operating conditions there are many additional variables that make the bucket's structural behaviour more difficult to analyse such as hydraulic load variations, non-uniform jet interaction, temporal instability of flow, cavitation, silt erosion, and etc. Researchers have determined that although maximum stress generally occurs at the Pelton runner's maximum bucket area (jet impact area) near the jet impact, the cyclic impact created, while turbine operation itself is expected to result in fatigue stress and dynamic vibration in the runner's material causing

reduction of operational life and increasing frequency of maintenance. Therefore, accurately predicting the bucket's stress distribution, deformation characteristics, and dynamic performance is vital for the development of structurally and hydraulically efficient turbine systems. In addition to static structural loading due to Pelton turbine runners being continually exposed to vibrations, they are particularly prone to vibrations from resonance effects. During normal operation, runners will also experience periodic excitation from cyclic jet impacts, rotation, hydraulic fluctuations, and adjacent bucket interactions [13-15]. When the excitation frequency produced by the turbine operation matches the natural frequency of one of the buckets in the runner assembly, resonance occurs resulting in high vibration amplitudes, unsafe/unstable structure, noise, and possible catastrophic failure of the turbine runner assembly. Therefore, it is important to conduct modal analyses on the bucket assembly in order to determine the natural frequencies and modes of the bucket structure in order to ensure that the turbine will operate safely and that there will not be any failures related to resonance.

The use of advanced computational analysis techniques (like Finite Element Analysis) has allowed for more accurate evaluation of complicated behaviour of hydraulic turbines. For example, the use of FEA provides the ability to predict how much stress will be distributed throughout, displaced, or vibrated on a structure for a given load without extensive physical prototyping. Finite element software is available from several commercial companies (such as ANSYS Mechanical APDL) and has advanced analysis capabilities for performing static structural analyses, static/vibrational modal analyses, pre-stressed structural vibrational analyses, and multi-physics simulations. Static structural analyses provide the ability to evaluate deformation, equivalent von-Mises stresses, and elastic strains for the bucky structure caused by the hydraulic loads. These static analyses can also be used to determine where the maximum stress will occur, what is the safety limit for the structure, and allow for a determination of what material should be used for the bucket under operational service loading. On the other hand, vibrational modal analyses are used to identify the natural frequencies and vibrational mode shapes of the bu based on configuration, so that the possibility of resonance and stability can be determined. Together, using both static and vibrational modal analyses on the buckets provides thorough knowledge regarding the overall performance of Pelton power turbines in realistic operating environments.

Improvement of hydraulic efficiency and structural strength through optimization of Pelton turbine bucket geometry is a focus of much current research. The computational methods

used to study the effects of various bucket geometries (e.g., splitter configuration, outlet angle, runner dimensions and material properties) on stress and vibrational behavior were documented in [25–27]. In addition to optimizing geometry, researchers have also evaluated the best materials available for use on Pelton turbines by conducting evaluation tests based on geometric parameters including mean minimum/maximum yield tensile strength, tensile strength, fatigue strength, erosion resistance and machinability with respect to corrosion-resistant materials (stainless steel, structural steel, cast aluminum alloys) and advanced composite materials; examples of these studies are outlined in [28–30]. Overall, regardless of whether a Pelton turbine construction material is made of stainless steel or another material, researchers agree that stainless steel is one of the best available for producing high-performance Pelton buckets because of its superior corrosion resistance, strength, and wear-resistance ability to withstand highly-charged hydraulic operating environments [30].

In this study, an optimized Pelton turbine bucket for micro-hydropower applications was evaluated structurally and dynamically by finite element analyses. The finite element analyses were conducted using ANSYS Mechanical APDL (ANSYS Inc., 2100 W. 21st St., Suite 136, Plano, TX 75074, USA) to quantify the structural response of the bucket to various loads. The structure of the Pelton bucket was investigated through the performance of Static Structural Analysis for the following loading types: Force; Pressure; and Combined loading. The Static Structural performance of the bucket was evaluated in terms of Deformation; Equivalent Stress; and Strain characteristics for each loading condition. Modal analysis was performed to assess the natural frequency and vibration mode shape of the bucket for a variety of loading and orientation conditions. A variety of materials, including CA6NM steel; Structural Steel; A390 Cast Al; and Stainless 314, were evaluated for their structural suitability in the design of the Pelton bucket. Finite element analyses were performed for both Vertical and Horizontal Bucket orientations to evaluate the impact of the buck's geometric interface on its structural performance and dynamic response. Mesh generation; grid independence; loading assumptions; boundary-condition implementation; and resonance evaluations were the included numerical components of this study, using pre-stressed modal-analysis methodologies.

Therefore, the goals of this chapter are to develop a thorough finite element model that will allow for assessments of the structural integrity of the optimized Pelton turbine bucket as well as its dynamic stability under operational conditions that reflect actual service. The results of the present analysis provide critical information about stress concentration areas, deformation

characteristics, vibration performance, and the safe operation limits of the turbine runner. The results of this research will also assist in the creation of structurally sound, dynamically stable, and hydraulically effective Pelton turbine systems for sustainable micro-hydropower systems.

4.2 CAD Geometry Development

Using the design dimensions of the micro hydropower turbine system, an example of the Pelton turbine bucket was created using Solid Works CAD Software for the geometry of the turbine bucket. After developing the above noted bucket geometry, it was imported into ANSYS Mechanical APDL for Finite Element Analysis. The bucket profile was modeled ellipses in long and cross sections to enable smooth guidance of the hydraulic flow and to efficiently transfer momentum from the water jet through the jet and runner assembly of the turbine.

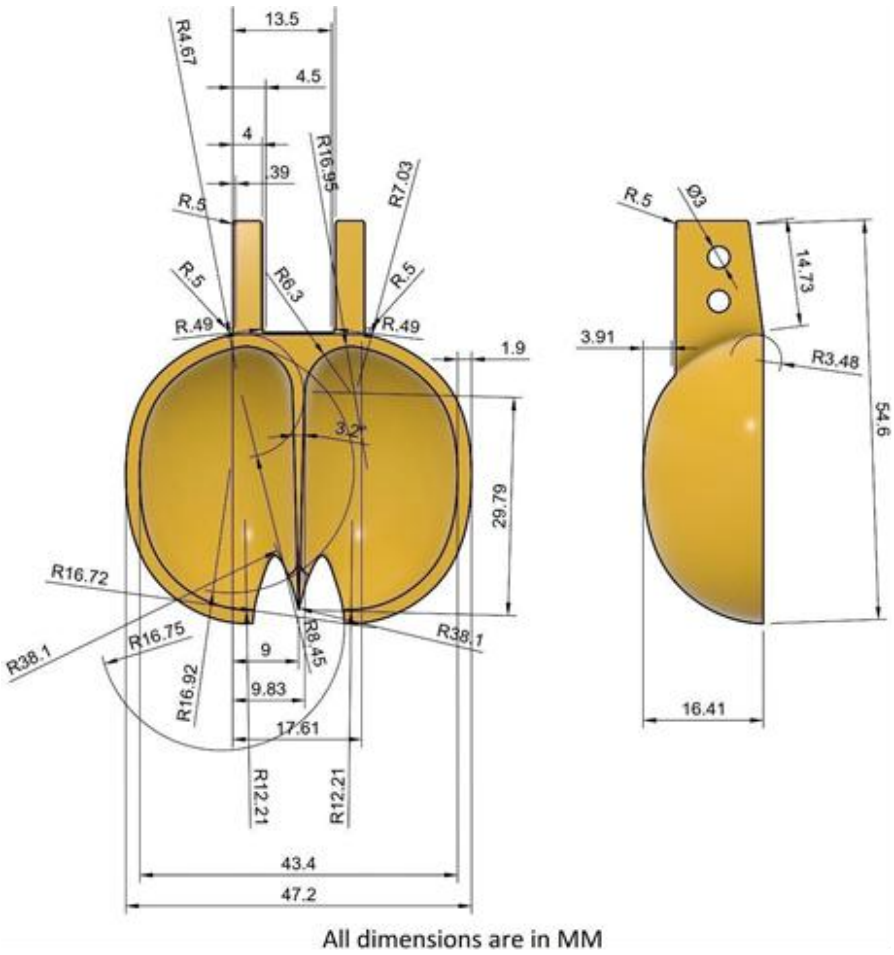

Figure 4.1 Geometry of Pelton turbine with dimension

The bucket geometry, which is shown in Figure 4.1 consisted of:

- splitter region,
- bucket curvature,
- outlet edge,
- cut-out region,
- and mounting arm interface.

The splitter area was designed with care because it is the initial area that the incoming water jets strike the bucket and then split into two different flows. It is essential to have a properly designed splitter geometry because improper design can produce:

- Severe hydraulic shock
- Splash loss
- Uneven pressure distribution
- Concentration of local stress

The Pelton bucket was analyzed in two different ways, vertical (90°) and horizontal (180°) orientation. The reason to use two different orientations is that the direction of load transfer and the contribution of structural stiffness is significantly different based on bucket orientation during hydraulic loading. Figure 4.2 shows the vertical and horizontal orientation of pelton turbine bucket.

A vertical bucket orientation (the bucket oriented perpendicular) to the down shoes of each runner is used for comparison against a horizontal or parallel bucket orientation to the runner rotating plane to evaluate deformation behaviour, stress distribution and vibrations under varying load conditions.

In addition to providing the curvature transition between the splitter and outlet sides of the bucket which would reduce hydraulic losses and increase the ability of the structure to dissipate load, the optimized bucket shape would further serve (from a structural and modal perspective) as the basis for the remaining structural or modal evaluation

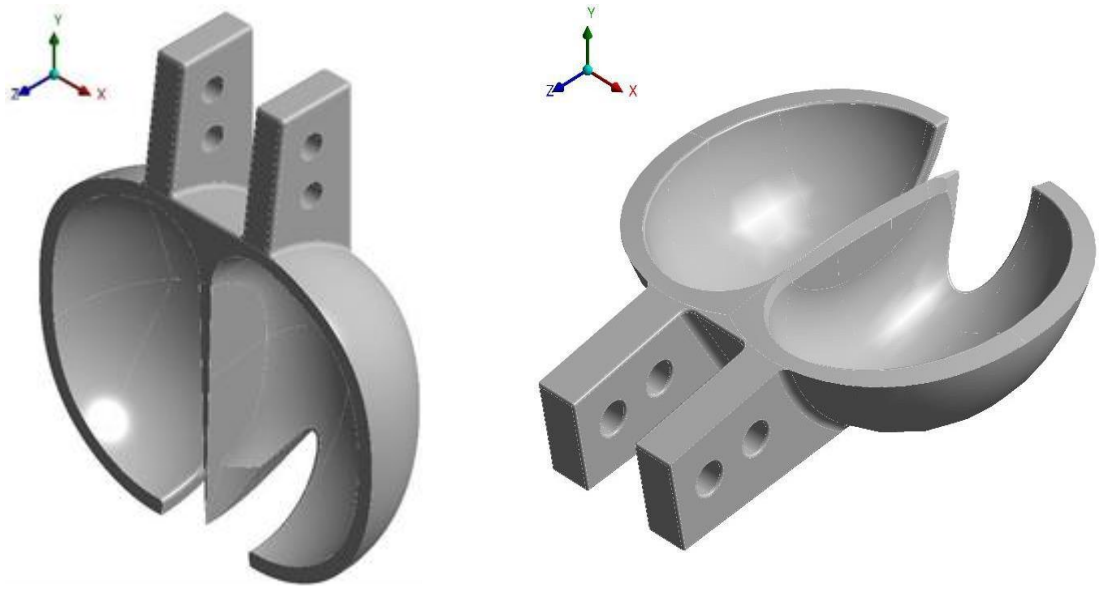

(a) (b)

Figure 4.2 Orientation of Pelton turbine for: (a) Vertical, and (b) Horizontal

4.3 Material Selection

4.3.1 Basis for Selection of Candidate Materials

The candidate materials considered in the present investigation were selected based on their engineering applicability in hydraulic turbines, mechanical properties, corrosion resistance, erosion resistance, manufacturability, and availability. Rather than evaluating only one material, four representative engineering materials were selected to investigate the influence of material properties on structural behaviour and dynamic performance under identical hydraulic loading conditions.

Structural Steel was selected as the reference material because of its widespread industrial use, good mechanical strength, low manufacturing cost, and ease of fabrication. However, its comparatively lower corrosion and erosion resistance make it less suitable for prolonged hydraulic service.

A390 Cast Aluminum Alloy was included because of its low density and excellent casting characteristics, which reduce runner weight and rotational inertia. However, its relatively lower modulus of elasticity and wear resistance may limit its structural performance under repeated jet impact loading.

CA6NM Stainless Steel is extensively used in hydroelectric turbine runners owing to its high strength, excellent toughness, and superior resistance to corrosion, cavitation, and erosion. Therefore, it represents an established benchmark material for comparison.

Stainless Steel 314 was selected because of its high mechanical strength, greater structural stiffness, excellent corrosion resistance, and good resistance to high-temperature oxidation. These characteristics make it a suitable candidate for evaluating structural integrity and dynamic stability under severe hydraulic loading conditions.

The selected materials therefore represent four different engineering material classes with distinct mechanical and physical properties, enabling a comprehensive comparison of structural behaviour, modal characteristics, and suitability for micro-hydropower Pelton turbine applications.

Choosing the right material for Pelton turbine buckets is crucial due to the extreme hydraulic and dynamic loading conditions encountered during operation of the runner. When the turbine operates, the bucket surface receives multiple high-velocity water jet impacts, large variations in hydraulic pressure, loads applied in a cyclic manner, vibrations, cavitation, erosion caused by suspended particles, and corrosion from the environment [1-3]. The selected material must have sufficient strength, fatigue resistance, chemical resistance (to corrosion), and resistance to wear to allow for dependable and long-lasting operation of the turbine system. Pelton turbine buckets are commonly submerged in variable quality water (e.g., containing silt or other impurities) in micro-hydropower applications. Water quality affects the lifetime of the bucket, as it can create a deterioration of the materials (loss of mechanical properties), leading to surface erosion, (lack of) mechanical performance, large deformations, cracks, fatigued failures, cavitation failures, etc., and result in lower turbine efficiencies [4-6]. Therefore, it is critical to conduct an extensive investigation of potential materials in order to ensure the structural integrity and hydraulic performance of the turbine runner.

Many researchers have explored how materials affect how Pelton turbine buckets work and how they perform during operation. For example, Li Ji-Qing and others [7] completed a fatigue analysis of Pelton turbine buckets made from various materials and found that stainless steel provided greater structural safety than cast iron or aluminium alloys. Ishola et al. [8] have also performed a comparative analysis of micro-Pelton turbine wheels using steel, aluminium alloy, and plastic materials and reported that material density and material

strength had a significant impact on the dynamics of the runner and on stability during operation. In addition, Gudukeya et al. [9] have shown that the surface finish of the bucket and the hardness of the material used in the bucket have a direct influence on the hydraulic efficiency and erosion resistance of the turbine bucket. Four different candidate materials have been selected for this study based on the literature review and the operational requirements of micro-hydropower systems to compare the structural properties of Pelton turbine buckets made from these materials. These materials include:

- CA6NM Steel
- Structural Steel
- A390 Cast Aluminum Alloy
- Stainless Steel 314 (SS314)

The selected materials represent a combination of high-strength ferrous materials and lightweight non-ferrous alloys commonly considered for hydraulic turbine applications. The selection was performed considering important parameters such as density, Young's modulus, yield strength, corrosion resistance, machinability, wear resistance, and operational durability under hydraulic loading conditions [10–12]. The material properties incorporated in the ANSYS Mechanical APDL simulations were obtained from standard engineering material databases, ASM handbooks, ASTM standards, and published literature [13–16]. The primary criteria considered during material selection for the Pelton turbine bucket are summarized below:

- High tensile and yield strength
- Resistance to hydraulic impact loading
- Good fatigue strength under cyclic operation
- Corrosion resistance in water environments
- Resistance to cavitation and erosion
- Dimensional stability under loading
- Ease of manufacturing and machining
- Long operational life with minimum maintenance
- Economic feasibility for micro-hydropower systems

Among these criteria, resistance to corrosion and erosion is particularly important because the turbine bucket continuously interacts with high-speed water jets during operation. Similarly, sufficient stiffness and structural strength are essential for minimizing deformation and

vibration-related instability in the runner assembly. The material properties used during finite element analysis are summarized in Table 4.2 to Table 4.5.

Table 4.1 Mechanical Properties of CA6NM Steel[15]

Property	**Value**
Density	1695 kg/m^3
Young's Modulus	1.9995×10^5 MPa
Poisson's Ratio	0.27
Bulk Modulus	1.4489×10^{10} Pa
Shear Modulus	7.872×10^{10} Pa
Yield Strength	689.43 MPa
Ultimate Strength	827.37 MPa

Table 4.2 Mechanical Properties of Structural Steel[17]

Property	**Value**
Density	7850 kg/m^3
Young's Modulus	2×10^{11} Pa
Poisson's Ratio	0.30
Bulk Modulus	1.6667×10^{11} Pa
Shear Modulus	7.692×10^{10} Pa
Yield Strength	250×10^6 Pa
Ultimate Strength	460×10^6 Pa

Table 4.3 Mechanical Properties of A390 Cast Aluminum Alloy[18,19]

Property	**Value**
Density	2700 kg/m³
Young's Modulus	75 × 10³ MPa
Poisson's Ratio	0.33
Bulk Modulus	73529.4 MPa
Shear Modulus	28195.5 MPa
Yield Strength	180 MPa
Ultimate Strength	180 MPa

Table 4.4 Mechanical Properties of Stainless Steel 314 (SS314)[21]

Property	**Value**
Density	7750 kg/m³
Young's Modulus	1.93 × 10⁵ MPa
Poisson's Ratio	0.31
Bulk Modulus	1.693 × 10⁵ MPa
Shear Modulus	7.3664 × 10⁴ MPa
Yield Strength	586 MPa
Ultimate Strength	207 MPa

The results of the comparison between the materials examined suggest that the various materials considered here have unique benefits and limitations in terms of their use in Pelton

turbine applications. Structural steel offers excellent stiffness, as well as low cost of production. However, under a continuous water environment, it has poor corrosion resistance properties. Copper alloy A390 has a lower density than structural steel as well as a much lighter weight then can help improve the performance of the turbine by providing better rotational response; however, its lower strength and resistance to erosion limit its use under high hydraulic loads.

CA6NM steel has demonstrated high strength, fatigue resistance and is therefore applicable to high-load applications of turbines; however, the best overall balance of corrosion resistance, wear resistance, structural strength and operational durability from the examined materials is exhibited by stainless steel (SS) 314. The presence of a high percentage of chromium and nickel in SS314 improves its oxidation resistance while preventing corrosion and/or erosion from occurring at the surface of the bucket over extended periods of time in a water environment. Additionally, SS314 has excellent thermal shock resistance and high impact resistance, which will help it resist the effects of transient hydraulic loads on the turbine bucket. The mechanical performance characteristics exhibited by SS314 also assist in reducing the likelihood of developing excessive deformation and/or fatigue cracks in the bucket. Therefore, SS314 is particularly well suited to Pelton turbine applications, which involve high speed water jet impacts onto the turbine bucket combined with continuous cyclic loading conditions.

A comparative study presented during the research investigation also demonstrated that stainless steel 314 provides superior performance in terms of corrosion resistance, hardness, wear resistance, and structural stability compared with mild steel and gun metal materials commonly used in conventional turbine systems. The comparative characteristics of these materials are summarized in Table 4.5.

Table 4.5 Comparative Characteristics of Materials for Pelton Turbine Bucket

Material	Reason for Selection	Expected Advantages	Expected Limitations
Structural Steel	Reference engineering material	Low cost, easy fabrication	Lower corrosion resistance
A390 Cast Aluminium Alloy	Lightweight casting alloy	Low density, reduced inertia	Lower stiffness and wear resistance
CA6NM Stainless Steel	Widely used in hydro turbines	High strength, cavitation and corrosion resistance	Higher cost
Stainless Steel 314	High-strength stainless steel	High stiffness, corrosion resistance, structural	Higher material cost

		stability	

From the comparative evaluation of structure and function, Stainless Steel 314 (SS314) has been found to be the best material for use in fabricating and assessing the Pelton turbine bucket. This material has the best combination of corrosion resistance, extreme fatigue resistance, high-strength, and erosion resistance required for long-term micro-hydropower applications. Therefore, SS314 was used for finite element analyses (FEA), computational fluid dynamics (CFD) analyses, prototypes of the Pelton turbine buckets, and experimental validation pieces of research conducted in this study. The material properties were then applied to the ANSYS Mechanical APDL environment in order to conduct static (structural) and dynamic (modal) analyses of the optimized Pelton turbine bucket under various applied loads.

4.4 Mesh Generation and Grid Independence Study

The accuracy of results found through finite element analysis relies on the quality of the mesh, the discretization of the elements, and the numerical stability of the computational model. For structural and modal studies of parts with complex shapes including Pelton turbine buckets, generating an accurate mesh is critical to achieving reliable predictions about the deformation, stress, strain, and vibrations that occur during the analysis. Due to the curvature of the bucket's shape, there are areas where the surface changes from highly curved to heavily split to having a gradual transition to an interface for mounting. For this reason, it was necessary to use the appropriate meshing techniques to accurately model any local stresses and deformations that occur due to hydraulic loading conditions. Based upon this requirement, detailed studies of mesh generation and grid independence were completed prior to performing structural and modal analyses on the bucket. The first step in determining an appropriate mesh for the analysis was to conduct an investigation of various mesh densities to determine the optimal configuration, which will produce numerically stable and converging solutions while maintaining sufficient computation time. The principal goal of the grid independence investigations was to validate that the deformation and stress results obtained are independent of the level of refinement of the mesh, thus producing representative results of the bucket's true structural response.

The grid independence study involved increasing the number of nodes and elements and closely observing the change in equivalent stress and deformation. At lower levels of mesh density, the results for stress prediction had irregular fluctuations due to the coarse nature of

the discretization and thus not capturing localized stress concentrations at both the splitter and bucket curvature of the bucket. As the mesh density increased, the fluctuation in numerical predictions slowly stabilized because the finer mesh improved the representation of the bucket geometry and load distribution. Figure 4.3 shows Grid independence test for the bucket structure of Pelton wheel turbine

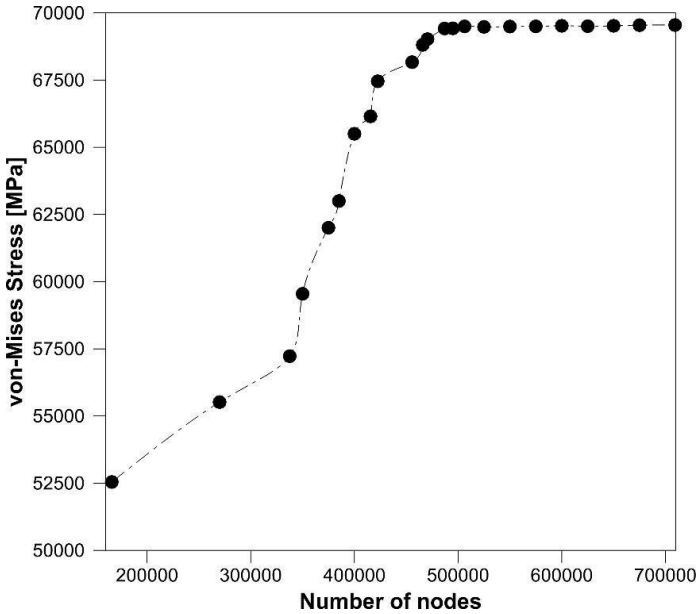

Figure 4.3 Grid independence test for the bucket structure of Pelton wheel turbine

The results from grid independence illustrated that increasing mesh densities resulted in deformation and equivalent stress values approaching convergence. After approximately 500,000 mesh nodes, the numerical results became nearly constant thereby indicating numerical convergence and mesh independence of the finite element solution. Continuing beyond this point resulted in negligible improvements in predicting stress and deformation, but significantly higher computing costs, memory requirements, and simulation time per run. Hence, this mesh density was optimal for all future structural and modal analysis performed throughout the study. Following the grid independence study, tetrahedral finite elements were generated for the entire bucket geometry. Tetrahedral meshing was chosen because it provides superior adaptability for geometrically complex areas such as areas with curved surfaces, splitter contouring, bucket curvature, mount arm interface, etc. The finite element mesh created accurately captured the geometric characteristics of Pelton turbine bucket, with a smooth transition between fine and coarse mesh areas. Figure 4.4 shows Mesh generation for the bucket structure

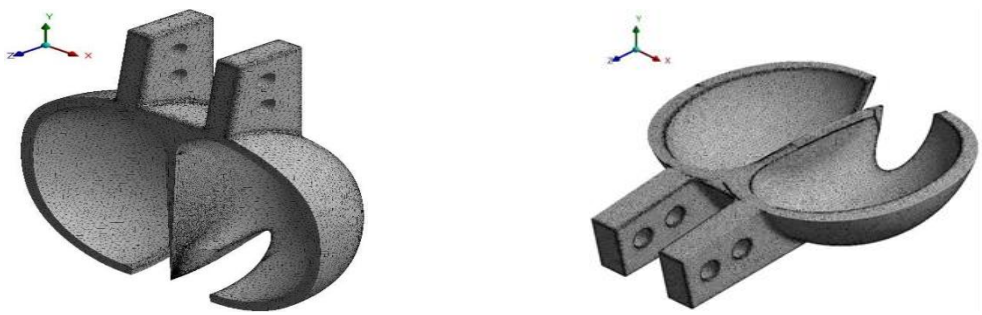

(a) (b)

Figure 4.4 Mesh generation for the bucket structure of: (a) vertical orientation, and (b) horizontal orientation

Results regarding mesh generation revealed that the areas near the splitter region, bucket curvature, outlet edges, and mounting arm interfaces are well-refined (i.e., highly refined) due to hydraulic interactions, stress concentrations, and deformations occurring during turbine operation in those areas. The splitter region, in particular, was provided with a very fine density of mesh because incoming water jet strikes the surface of the splitter while turbine operates to produce highly-localized hydraulic loading and bending stresses. Similarly, refined meshing near the mounting arms allowed accurate prediction of load transfer behaviour and support reaction forces developed in the bucket structure.

For the horizontally oriented bucket, the meshing generated a total of 709,309 nodes and 465,288 elements, while the vertically oriented bucket produced 1,410,071 nodes and 921,522 elements. The greater number of nodes and elements in the vertical orientation makes sense due to the need for greater refinement to correctly model stress variation and deformation gradients along the vertical direction of load application. The generated mesh also ensures smooth transitions from one element to another and minimizes discontinuity of the numerical result through the entire computational model. The mesh quality was within acceptable limits for engineering and no elements were excessively distorted during the finite element simulations. Thus, the use of a refined mesh allowed for an accurate prediction of localised stress amplification, deformation gradients and vibratory response of the entire bucket structure under the various hydraulically applied loads.

Ultimately, both the mesh generation and the grid independence investigation established a sound numerical basis for all the subsequent structural and modal analyses conducted in this research.

4.5 Static Structural Analysis Methodology

Static analysis is a fundamental numerical method for evaluating how something behaves mechanically when subjected to a force that may change over time. A Pelton turbine has a hydraulic load placed on the bucket due to being impacted continuously by water launched through an impact nozzle at high velocity. This interaction creates impulsive loads resulting in localized stress concentrations, elastic deformation, bending stresses, and strains in the bucket structure [1–3]. Therefore, for the safe operation, stability of the structure, and durability of the Pelton turbine bucket, it is critical that the bucket be properly analyzed for structural strength using static structural analysis methods.

In this research, an optimized Pelton turbine bucket was analyzed for deformation, equivalent von-Mises stress distribution, and strain under varying hydraulic conditions using ANSYS Mechanical APDL software. The analysis was completed using finite element analysis (FEA) techniques based on the ability of FEA to provide accurate forecasting of the location of localized stress concentration areas as well as providing predicted responses of complex geometries when subjected to normal operating loads [4–6].

The structural analysis was performed in two major stages:

- Static Structural Analysis
- Modal Analysis

The present section focuses on the methodology adopted for static structural analysis, whereas modal analysis is discussed separately in the subsequent section.

4.5.1 Governing Equations of Static Structural Analysis

The finite element formulation used in static structural analysis is based on equilibrium conditions between externally applied forces and internally developed stresses within the structure. The general equilibrium equation governing static structural analysis is expressed as:

$$[K]\{u\} = \{F\} \text{----------} [30]$$

The stress-strain relationship for isotropic linear elastic materials is governed by Hooke's law:

$$\sigma = E\varepsilon$$

For evaluating yielding behaviour under complex multi-axial loading conditions, equivalent von-Mises stress was used as the primary failure criterion. The equivalent stress is expressed as:

$$\sigma_v = \sqrt{\frac{1}{2}[(\sigma_1 - \sigma_2)^2 + (\sigma_2 - \sigma_3)^2 + (\sigma_3 - \sigma_1)^2]} \text{----------[31]}$$

The von-Mises criterion is widely used for ductile metallic materials because it accurately predicts yielding behaviour under combined stress states [7–9].

4.5.2 Assumptions Considered During Structural Analysis

Several simplifying assumptions were considered during the static structural analysis in order to reduce computational complexity while maintaining acceptable numerical accuracy. The assumptions considered are listed below:

- The material was assumed to be homogeneous and isotropic.
- Linear elastic behaviour was considered for all materials.
- The bucket geometry was assumed to be free from manufacturing defects.
- The bucket was considered rigidly fixed at the mounting region.
- The water jet was assumed to strike exactly at the splitter region.
- Thermal loading effects were neglected.
- Dynamic fluid-structure interaction effects were not considered during static analysis.
- External aerodynamic and environmental effects were neglected.

These assumptions simplified the finite element implementation and enabled effective comparison of structural behaviour under different loading conditions.

4.5.3 Structural Deformation Analysis

The deformation behaviour obtained for the horizontally oriented bucket under different hydraulic impact forces is presented in Figure 4.5.

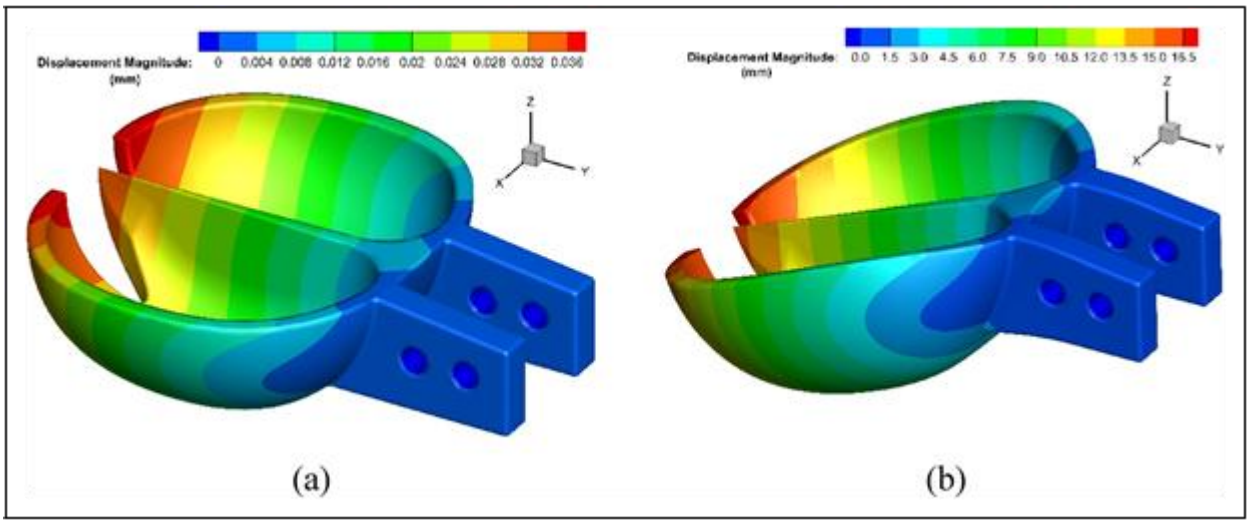

Figure 4.5 Structural deformation of a horizontally oriented bucket for different impact forces: (a) F=349 N and (b) F=153.864 KN.

The deformation contours indicated that maximum displacement occurs mainly in the areas of the splitter tip, bucket lip, and outlet curvature regions, where there is maximum hydraulic interaction and lower local structural stiffness (the maximum displacement would also correspond to the locations along the bucket structure where there are direct hydraulic interactions before dividing into 2 streams). The splitter region especially exhibited large amounts of deformation, because the incoming water jet impacts the splitter surface before it separates into 2 streams. There was extreme bending deformation and localized large amounts of displacement near the splitter-root junction due to hydraulic loading conditions.

With a hydraulic loading of F_1=349 N, deformation was relatively low across the bucket structure, since the hydraulic loading conditions were low enough so that the applied loading from the hydraulic force was within a low extension range for the material. The distribution of deformation showed a progressively varying amount of smooth displacement across the bucket structure from the splitter region to outlet curvature, indicating a stable structural response and gradual distribution of the load. The increase in deformation, however, was substantial when comparing the hydraulic loading condition of F_2=153.864 kN to the prior loading condition; this was because of the extremely high degree of impulsive hydraulic interactions generated by the incoming water jet. The increased degree of deformation produced an increased amount of bending deformation along the bucket curvature, which then produced a greater amount of displacement near the outer edge of the bucket.

Additionally, the deformation results indicated that there was a greater displacement in the horizontally positioned bucket compared to other orientations due to increased bending

deformation caused by the loading direction of the hydraulic forces acting on the bucket's curvature. As a result, the horizontally oriented bucket exhibited less structural stiffness participation in the direction of load application, yielding greater elastic deformation under hydraulic impact loads. Deformation along the length of the bucket diminished as the location of the fixtures got closer together due to fixed support conditions near the attachment points, which aided in efficient load transfer to the runner assembly.

The deformation behaviour obtained for the vertically oriented bucket under different loading conditions is presented in Figure 4.6.

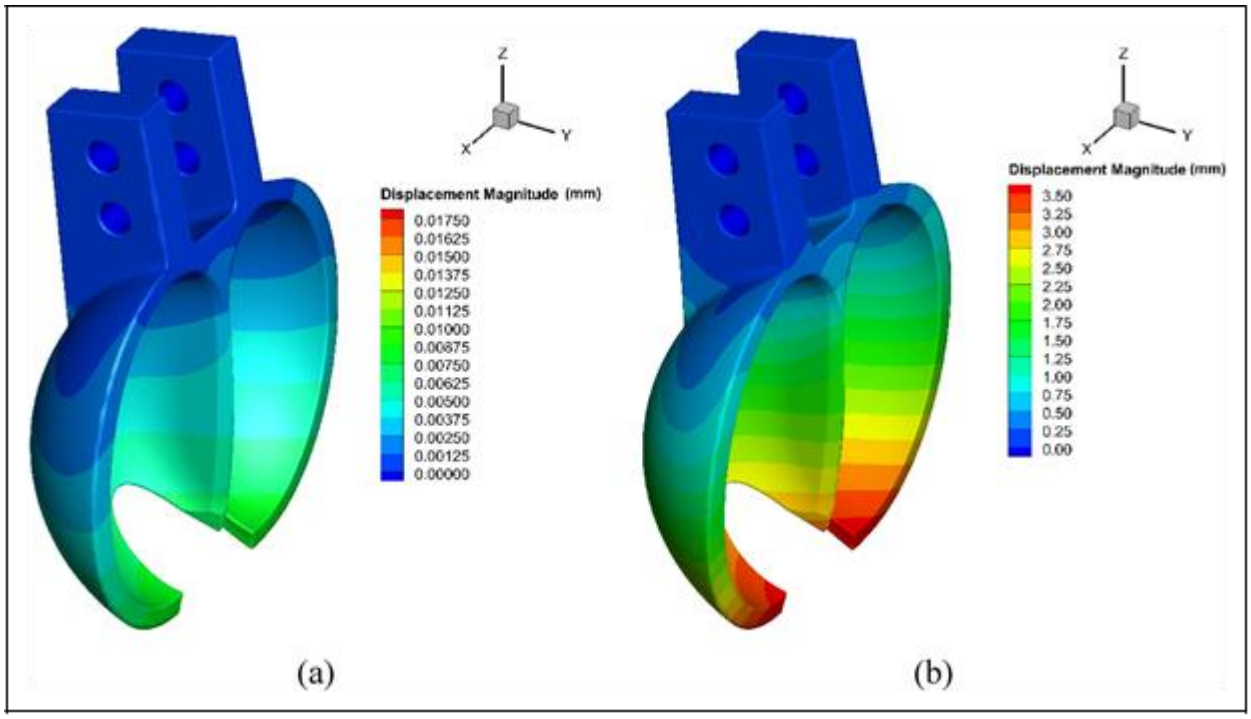

Figure 4.6 Structural deformation of a vertically oriented bucket for different impact forces: (a) F=349 N and (b) F=153.864 KN.

Vertical buckets showed an increase in structural deformation than horizontal buckets because of the greater uniform distribution of the hydraulic load transfer through the mounting arms of the bucket in addition to providing more structural stiffness to the bucket's geometry along the loading axis to help control and reduce bending deformations and provide greater load sharing on each of the surfaces of the bucket with improvements in the structural performance of the vertical bucket compared to a horizontal bucket configuration.

The results of this comparative study showed that bucket orientation strongly affects deformation behaviour and structural stability of the Pelton turbine bucket. Vertical buckets exhibited improvement from better load transfer characteristics and lower bending

deformations during the hydraulic working of the buckets than horizontal bucket configurations.

Investigating the comparative materials has highlighted how influential stiffness is on deformational behaviour. A390 cast aluminium has deformed the greatest amount of all the materials studied. This was due to its relatively lower Young's modulus and if you look at the material's structural stiffness it again has the lowest value of any material. Therefore, there is more elastic deformation when subjected to hydraulic loading conditions with alluminium alloy materials than with any other material. Conversely, stainless steel 314 & CA6NM have deformed less than any other material because their stiffness characteristics are "greater" than those of the alluminium alloy; they also have much greater resistance when bending than any of the materials (similar with structural steel). Therefore, the behaviour of structural steel is more in line with both stainless steel than that of aluminium.

4.5.4 Equivalent Stress Distribution Analysis

Through the hydraulic load arrangement, the von-Mises stress distribution provided a comprehensive overview of the safety and behaviour of these structure(s) due to stress concentrations within the bucket geometry. Maximum and Minimum Stress Concentrations were located around the junction of the splitter and bucket's root, the mounts for the arms near their junction with the bucket and transitions between the bucket and the Splitters, as these areas are geometrically discontinuous areas and the shape of the bucket and splitter does not provide for a smooth transition, nor does the in-bound payload-flow provide a smooth transition across its surfaces during rippling of the water as it encounters the splitter face.

The largest concentration of stress occurred around the junction at the splitter and bucket's root location as this is where the in-bound stream of water strikes the splitter's surface as it divides into two separate and opposing flows after hitting the splitter's surface at high velocity (Hydraulics). The In-Bound Mechanical Transfer (Hydraulically) creates multiple stress-areas in various types of load paths, which create significant stresses in their mechanical and hydraulic peace throughout the entire assembly at the rear of the assembly adjacent to (on) the main arm mount points, which creates one of the two main transfer path loads to the upper (runner) assembly of the vehicle support assembly.

The stress contours illustrated that, as hydraulic energy is progressively dissipated downstream in the direction of water flow, the magnitude of stress decreases gradually

through the stress contour lines until reaching a point of lower-stressed outlet regions. The gradual decrease in stress magnitude is evidence of the effective dissipation of loads and stable performance characteristics within the optimized bucket geometry. Lower-stressed outlet regions are due to the transfer of significant momentum between the water jet and the bucket surface prior to reaching the outermost curvature of the bucket. The maximum equivalent induced stress, even at maximum hydraulic loading, for the bucket structure did not exceed material yield strength limits of all materials investigated. Consequently, the bucket structure did not yield, exhibit plastic deformation or fail and functioned completely in an elastic regime with no failure or yielding. The data supports the conclusion that the optimized bucket geometry provides sufficient load-carrying capacity and long-term structural reliability to be operated under conditions of high hydraulic loading. Figure 4.7 and Figure 4.8 show Equivalent stresses in different conditions.

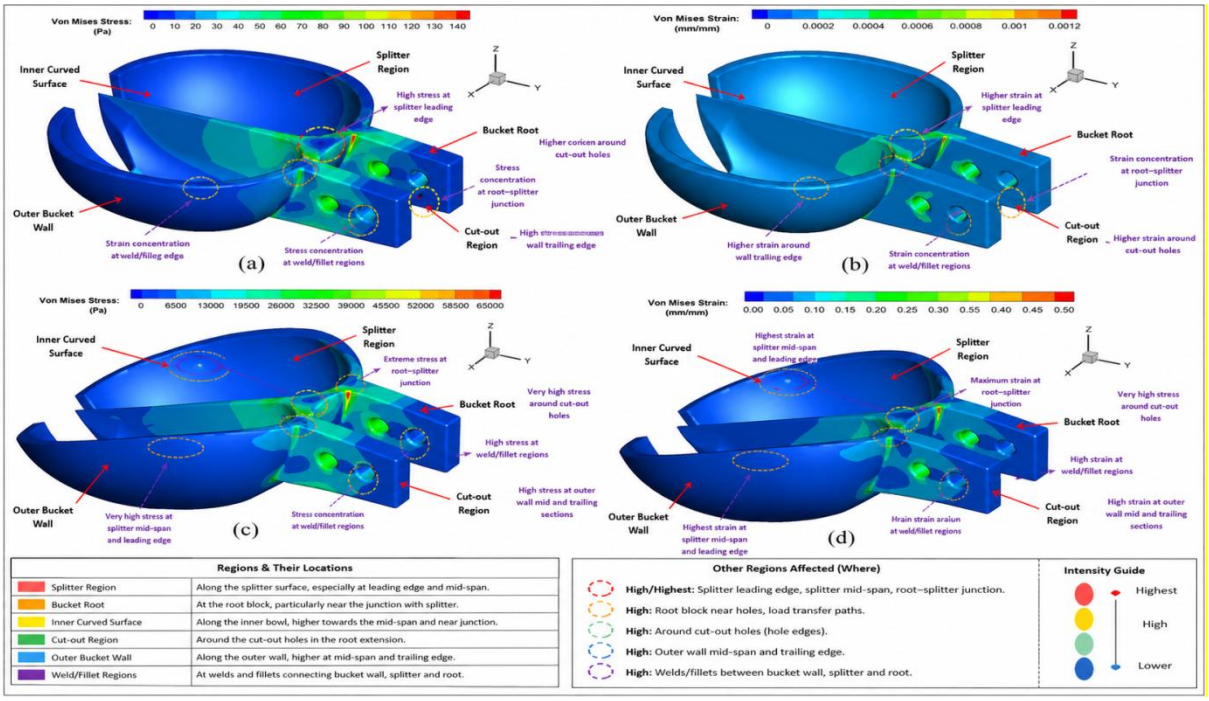

Figure 4.7 Equivalent stress (left) and strain (right) distribution for a horizontally oriented bucket for different impact forces: (a,b) F =349 N and (c,d) F = 153.864 KN.and Regions of the Pelton Bucket Influenced by Hydraulic Loading

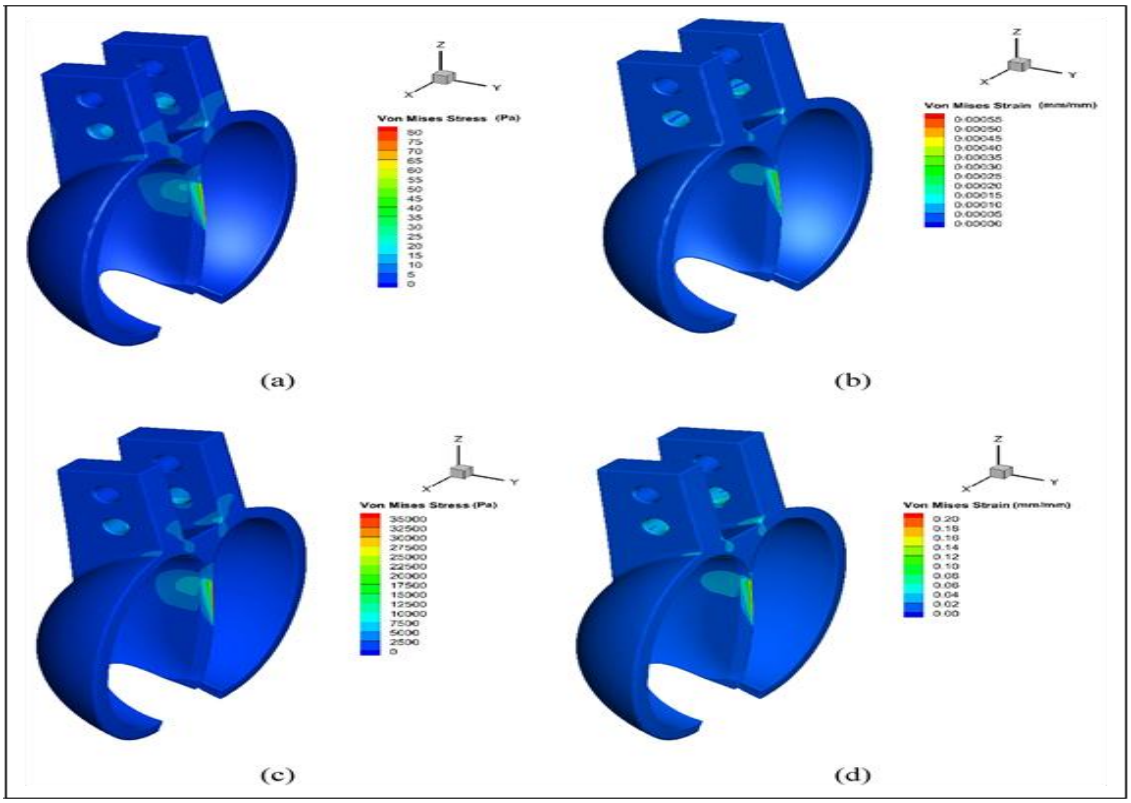

Figure 4.8 Equivalent stress (left) and strain (right) distribution for a vertically oriented bucket for different impact forces: (a,b) F =349 N and (c,d) F = 153.864 KN.

Although the maximum equivalent stress is observed near the splitter-root region due to direct jet impact and geometric discontinuity, hydraulic loading influences the entire bucket

surface. As the water jet travels along the inner bucket profile, hydraulic pressure is continuously distributed over the curved surface, producing moderate stresses throughout the bucket body. The bucket root region experiences bending stresses because it transfers hydraulic forces from the bucket to the runner. Localized stress concentrations are also observed near the bucket cut-out due to changes in flow direction and pressure distribution. In contrast, the outer bucket wall is subjected to relatively lower stress levels and primarily contributes to maintaining the structural stiffness of the bucket. Thus, the stress distribution within the bucket results from the combined effects of hydraulic loading, momentum transfer, structural constraints, and geometric features rather than geometric discontinuities alone.

Furthermore, the stress evaluation proved that the superior mechanical and structural performance of Stainless Steel 314 was enhanced by its high yield strength, great corrosion resistance, great fatigue durability, and increased carrying capacity of loads due to its significant Alloying Component's (i.e., chromium & nickel) contribution to cavitation, erosion, and corrosion that occurs under constant contact with high-velocity water streams. This confirmed that Stainless Steel 314 had been identified as the best possible material for real-world use in Pelton turbine buckets.

4.5.5 Effect of Incidence Angle on Structural Behaviour

The influence of jet incidence angle on deformation and stress behaviour was additionally investigated in order to understand the effect of hydraulic loading direction on structural response of the bucket geometry. Figure 4.9 shows effect of incidence angle.

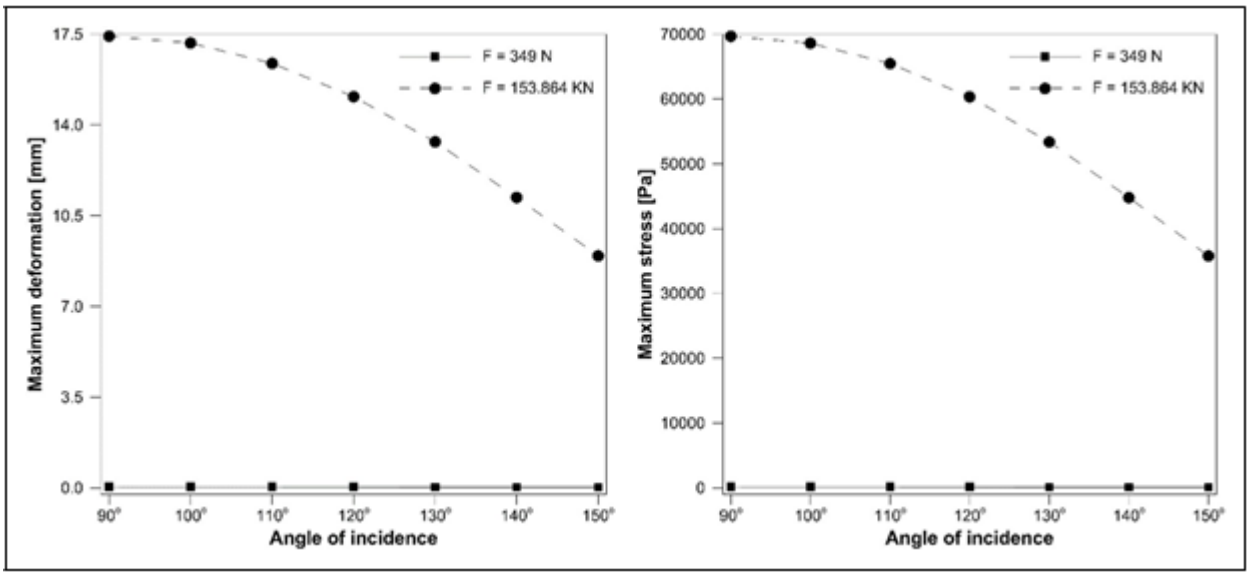

Figure 4.9 Effect of incidence angle on (a) maximum deformation and (b) maximum stress for F1=349 N and F2=153.864 KN.

The research showed that changing the angle of the jet stream had an effect on both how the bucket supports a load and how the stress spread through the bucket changed. The change in angle of the jet stream caused a change in how the hydraulic forces spread along the surface of the bucket, resulting in different local stress concentration and deformation. The lower angles created a more uniform distribution of force all along the curve of the bucket, while the higher angles created greater localized forces at the splitter and transition regions. The change in angle created more localized deformation and stress concentration, since as the angle of the jet increased, the impact of the hydraulic force became more concentrated on a smaller area of the bucket surface. It was also shown that the effect of angle increases as the load on the bucket increases, because the larger hydraulic impact results in greater bending deformation and higher stress. Therefore, the shape of the bucket affects how the load is spread, and how the stress is concentrated, depending on the loading conditions.

4.6 Modal Analysis of Pelton Turbine Bucket

Modal analysis is a method that can be used to determine dynamic behaviours of engineering structures under UV and cyclical loading. For example, Pelton turbine systems experience dynamic loading from various sources, which include fluctuating hydraulic excitations due to periodic jet impacts, the rotational motion of the runner, pressure pulsation, and interaction with adjacent buckets. This dynamic loading can cause vibration in the bucket structure and may ultimately lead to a resonance, fatigue failure, excessive noise, and structural instability in the event that the operating excitation frequency approaches the natural frequency of the

bucket assembly.

The natural frequency of a structure is fundamentally governed by its stiffness-to-mass ratio. According to classical vibration theory, the natural frequency is directly proportional to the square root of structural stiffness and inversely proportional to the square root of mass. Consequently, materials possessing a higher modulus of elasticity exhibit greater structural stiffness, resulting in higher natural frequencies under identical geometric and loading conditions. Since Stainless Steel 314 and CA6NM Steel possess significantly higher elastic moduli than Structural Steel and A390 Cast Aluminium Alloy, they offer greater resistance to elastic deformation and consequently demonstrate improved dynamic stability. The higher natural frequencies obtained for these materials indicate that their vibration modes remain sufficiently separated from the operating excitation frequency of the Pelton runner, thereby minimizing resonance risk and enhancing structural reliability.

The modal analysis as a prediction tool has been recognised to play a crucially important role in helping to identify the safe and reliable operating parameters of the Pelton turbine runner through accurate assessment of its natural frequencies and vibrational mode shapes. Modal analysis also assists in the prediction of the structure's dynamic response characteristics and assists with the identification of resonant operating parameters. This study documented the use of the finite element modal analysis method to assess the vibrational behaviour of the optimally designed Pelton turbine bucket under various loading conditions and orientations.

Modal analysis was performed to evaluate the dynamic characteristics of the Pelton turbine bucket and to ensure safe operation under cyclic hydraulic loading. During turbine operation, each bucket is repeatedly impacted by the water jet, producing periodic excitation forces known as the bucket-passing frequency. If the natural frequency of the runner approaches the excitation frequency, resonance may occur, resulting in excessive vibration, fatigue damage, structural instability, and premature failure. Therefore, determining the natural frequencies and mode shapes of the runner is essential to verify adequate resonance safety. In the present investigation, modal analysis was carried out after the static structural analysis to evaluate the dynamic stability of the optimized runner. The results were used to compare candidate materials and to select the material providing the highest resonance safety and structural reliability.

The relationship between material stiffness and vibration behaviour is well established in structural dynamics. Materials possessing a higher modulus of elasticity provide greater

resistance to elastic deformation under dynamic loading because structural stiffness is directly proportional to Young's modulus. According to classical vibration theory, the natural frequency of a structure increases with increasing stiffness and decreases with increasing mass. Consequently, materials with higher stiffness generally exhibit higher natural frequencies, lower vibration amplitudes, and improved resistance to resonance. In the present investigation, Stainless Steel 314 and CA6NM Steel demonstrated higher natural frequencies than Structural Steel and A390 Cast Aluminium Alloy because of their greater elastic modulus and structural stiffness. Similar observations have been reported in the vibration literature, where increased stiffness has been shown to enhance dynamic stability and reduce the likelihood of resonance in rotating mechanical systems.

An ANSYS Mechanical APDL modal analysis evaluated the natural frequencies, mode shape and resonance characteristics of the Pelton turbine bucket. Given that periodic hydraulic excitation causes dynamic vibration in the bucket during turbine operation, the modal analysis is important. If the excitation frequency coincides with the natural frequency of the bucket, resonance will occur, leading to excessive vibration and structural instability. The Block Lanczos eigenvalue extraction method was used for the modal analysis because it is a highly efficient computational method for solving large and complex finite element structures. Figure 4.11 shows modal analysis in various orientations.

The analysis of both horizontal and vertical orientations of buckets yielded significant insight into both the vibration characteristics and the dynamic stability of the Pelton turbine under hydraulic conditions, as represented by the modal analysis results. The natural frequencies progressively increased with increasing mode number for the finite element modal simulation because of the greater relative stiffness participation and more complex deformation behaviour of the components that define the higher vibration modes versus the lower vibration modes. For the lower vibration modes of the horizontal bucket, the primary representation of the complete bucket's global bending behaviour occurred in this mode. Displacement of the vibrating bucket occurred predominantly in the vicinity of the splitter edge region, bucket lip region, and curvature of the outlet due to these locations having relatively lower local stiffness and being directly associated with hydraulic interaction during operation of the turbine. Due to being fixed to the support structure at the mounting arm interfaces, the amount of dynamic motion in the attachment areas was limited compared to the rest of the bucket, resulting in relatively low vibration displacement.

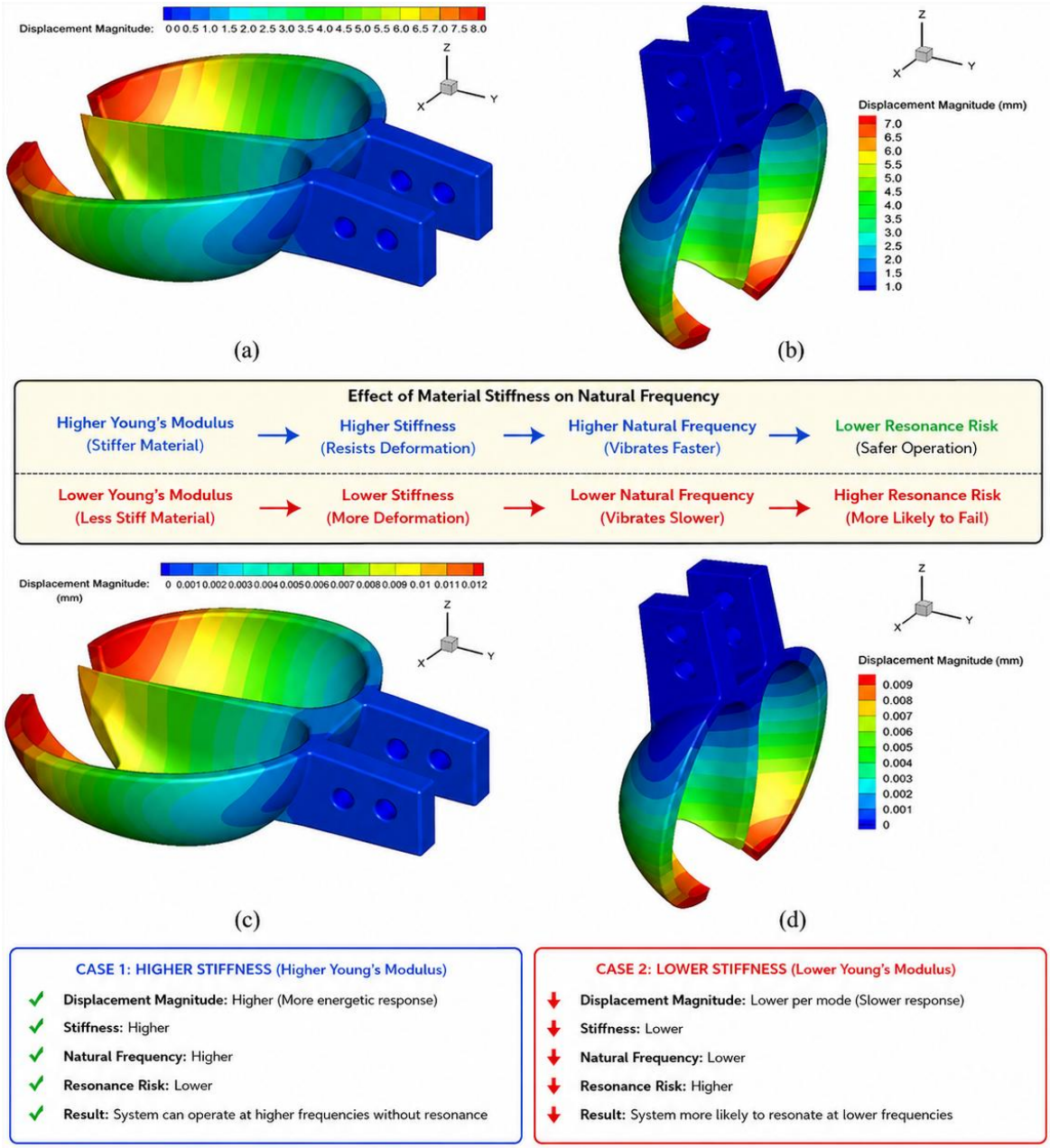

Figure 4.10 Modal analysis results for horizontal bucket using uniform pressure and F = 349 N (a) & (b) and bucket using uniform pressure and F = 153.864 KN (c) & (d) and Effect of Material Stiffness on Natural Frequency

.The first natural frequency for the bucket mounted horizontally was much higher than the operational excitation frequency due to rotating turbines. This relatively large frequency difference indicates that resonance conditions are very unlikely to be present in normal operating conditions. Also, with increasing vibration mode numbers, the complexity of the mode shapes and localized deformations in the splitter-root junction and outlet regions significantly increased. Higher-order vibration modes also exhibited increased twisting and curvature localized deformation because of the complex stiffness interaction within the bucket geometry. The vertically mounted bucket, compared to a horizontally mounted bucket,

developed comparatively higher natural frequencies because of increased stiffness participation along the loading direction due to the vertical orientation of the bucket. The vertical bucket provided a more uniform distribution of load to the bucket mounting arm resulting in greater overall buckling resistance, thus reducing the potential for operational vibration-related damage. Overall, the vertical bucket provided a higher degree of dynamic stability and a lower degree of operational vibration deformation during modal excitation compared with a horizontal bucket.

The vibration mode shapes measured in the case of vertical orientation had the most uniform deformation distribution across the surface of the bucket, relative to the case of horizontal orientation. The reduced bending displacement at the splitter and outlet curvature areas suggests that the bucket in a vertical orientation has greater ability to resist dynamic vibration produced by hydraulic turnings.

The modal testing has also shown that the vibration modes studied had no closely spaced natural frequencies. This is significant as closely spaced natural frequencies could contribute to modal coupling, resulting in dynamic amplification under varying levels of hydraulic excitation. Therefore, the lack of closely spaced modes confirms stable vibration characteristics, with less chance for instability caused by resonance.

The operational excitation frequency generated during turbine operation, commonly referred to as the bucket passing frequency, was calculated using:

$$f_b = \frac{ZN}{60} \text{----------[32]}$$

For the present investigation:

- $Z = 19$,
- and $N = 1000\ rpm$.

Therefore, the bucket passing frequency becomes:

$$f_b = 316.67\ Hz \text{----------[33]}$$

The minimum natural frequency obtained from the modal analysis was significantly higher than the calculated excitation frequency. Therefore, resonance conditions could not develop during turbine operation. The resonance safety factor calculated from the ratio of natural

frequency to excitation frequency confirmed excellent dynamic stability of the bucket structure.

$$Safety\ Factor = \frac{4231.8}{316.67} = 13.37 \text{----------} [34]$$

According to the FEA modal analysis, the resonance safety factor of 13.37 indicates that the bucket is well outside of resonance conditions, thus providing excellent vibration stability at practical operational conditions. This large frequency separation indicates that the hydraulic excitation produced by the turbine will not cause any excessive vibration amplification within the bucket structure.

The modal analysis also showed that vibration characteristics and natural frequencies of the bucket structure are affected significantly by the material properties. Higher stiffness materials, such as Stainless Steel 314 and CA6NM steel, showed higher natural frequencies than lower stiffness materials, such as A390 cast aluminum alloy. More specifically, higher stiffness material (higher modulus of elasticity) has better resistance to vibrating deformation; therefore, it would show higher natural frequencies than lower stiffness material (lower modulus of elasticity).

Overall, in comparing all of the materials tested, Stainless Steel 314 offered the greatest overall dynamic performance due to the following benefits:

- Higher Natural Frequencies;
- Improved Stiffness;
- Stable Vibration Characteristics, and
- Greater Resistance to Dynamic Deformation.

Additionally, since Stainless Steel 314 has a high stiffness-to-strength ratio, it is expected that its use will enhance the vibration stability of the bucket and will reduce the possibility of resonance-induced fatigue failure for the turbine during long-term operation.

The modal analysis confirmed that all candidate materials exhibited natural frequencies significantly higher than the bucket-passing frequency generated during turbine operation. This indicates that resonance is unlikely under normal operating conditions. Among the evaluated materials, Stainless Steel 314 demonstrated the highest natural frequencies and consequently the greatest dynamic stability. These findings confirm that modal analysis is an essential design tool for improving the operational reliability, fatigue resistance, and service life of Pelton turbine runners.

The overall results of the modal analyses demonstrate that the optimised Pelton turbine bucket has exceptional dynamic stability, adequate resistance to vibrational forces, and safe operation for practical hydraulic loading. The modal analysis results also confirm that the bucket's geometry and material configuration are dynamically appropriate for long-term use of micro-hydropower projects where there will be continuous cycles of hydraulic forces applied to the bucket.

4.7 Structural Integrity and Dynamic Stability Assessment

The static and modal analysis conducted throughout this study provided a thorough characterization of both the loading-carrying capability and overall structural integrity, including both dynamic stability, of an optimized Pelton bucket impellor under various hydraulic operational conditions. The analytical results produced by the modelling of the bucket's geometry demonstrated that the modelled bucket is able to withstand hydraulic impacts experienced during operation of a turbine without excessive deformation or yielding, vibration-induced instability, or resonance failure.

Through performing the static and modal analysis, it was found that the use of the optimized bucket geometry refers to the distribution of hydraulic loadings and minimizes the occurrence of excessive stress in areas of interaction between the water jet and the bucket. Deformation contour plots of bucket geometries subjected to hydraulic loading provided evidence that the majority of maximum displacement occurs at three locations: at the splitter tip; at the bucket lip; and at the outlet curvature, as these regions contact incoming water jets and have a correspondingly reduced local stiffness. Under maximum hydraulic impact loading condition, deformation is within acceptable engineering tolerances for all materials studied. Therefore, the characteristics of deformation observed from the results confirms that optimized bucket geometry is able to have enough stiffness and resistance to bending from hydraulic impact on the bucket during long-term operation of the turbine to be considered structurally sound.

The equivalent von Mises stress evaluation has confirmed the bucket geometry developed as structurally safe. Stress contours indicated the highest stress concentrations were located at the splitter-root junction and at the mounting arm interface. This is due to these areas experiencing very intense hydraulic loads and abrupt changes in geometry during momentum transfer between the water jet and bucket structure. However, the stress values developed in these regions were considerably less than the yield strength limits of all materials evaluated for both low and high load cases. Therefore, the overall bucket structure was sufficiently

below the elastic limit and exhibited no plasticity or yielding behaviour of the structure. The gradual drop off in stress values from the splitter region to the curve at the outlet further supports the fact that the profile of the optimized bucket dissipates hydraulic loading across the entire surface of the bucket. The absence of excessive localised stress concentrations is also critical to enhancing structural integrity and minimising the likelihood of initiation of cracking or failure from fatigue during turbine cyclic operation. Stress distribution also shows that loads transfer from the bucket surface to the mounting arm interfaces in a stable manner, thereby confirming that structural loads are dissipated efficiently throughout the bucket geometry.

During modal analysis of the optimized Pelton Turbine Bucket, the investigation provided the assurance of dynamic stability and vibration resistance in the optimized turbine bucket. The modal simulation of finite elements indicated the natural frequency values were far above the frequency of the excitation resulting from turbine operation. This significant separation of frequencies is very beneficial to preventing resonance vibration amplification during operation.

The vibration mode shapes indicated that the primary areas of dynamic deformation were located at the splitter edges, the bucket lips, and the outlet curvature because those areas are associated with lower local stiffness and the hydraulic excitation occurring in those areas is transmitted directly to the bucket structure. However, the amplitudes of vibration were well controlled, and at no time was there any indication of excessive dynamic instability to the investigated operating range. Similarly, because the fixed support conditions would limit the displacement of the mounting arm near the attachment of the bucket, those interfaces exhibited relative stability during the investigation. Additionally, the calculated resonance safety factor confirmed the bucket structure's outstanding dynamic stability. The significant separation of the bucket's natural frequency from the excitation frequency during a bucket's pass therefore restricted the development of resonance conditions as a result of turbine operation. Similarly, the absence of closely spaced vibration modes confirmed the stable dynamic characteristics and minimized the potential for modal coupling and vibration amplification due to variable hydraulic loading conditions.

The research that compared different materials revealed that the properties of the materials were a major factor in the structural and dynamic performance of Pelton buckets, and that the more stiff a material was, the less it would deform, and the higher the bucket's natural

frequency would be, since improved structural rigidity acts to resist both hydraulic deformation and vibration displacement. After examining all of the materials, it was found that Stainless Steel 314 had by far the most favorable overall properties; it has an extremely rigid structure, is very resistant to corrosion, has high durability in fatigue, and has very stable vibration properties. The high levels of chromium and nickel in Stainless Steel 314 allow it to perform better than any other material in resisting cavitation, corrosion, erosion, and cyclical fatigue caused when continuously subjected to high-velocity water jet interaction. In addition, the stiffness and strength of Stainless Steel 314 will reduce the amount of deformation occurring and improve the vibration stability under hydraulic excitation. Therefore, Stainless Steel 314 is the ideal material for Pelton buckets that will be subjected to extreme hydraulic operating conditions.

The combined structural and modal investigations therefore confirmed that the optimized Pelton turbine bucket possesses, The FEA results indicate that the optimized Pelton runner satisfies the structural performance requirements by exhibiting sufficient structural reliability, adequate load-carrying capability, stable deformation behaviour, acceptable stress distribution, excellent vibration resistance, and safe resonance-free operation, thereby ensuring reliable performance under operating conditions for long-term micro-hydropower applications.

The obtained results additionally validated the effectiveness of the developed bucket geometry and established a reliable numerical foundation for subsequent CFD analysis and experimental investigations discussed in the later chapters of the thesis.

Table 4.6 Comparison of Candidate Materials

Parameter	Structural Steel	A390 Alloy	CA6NM Steel	SS314
Strength	Good	Moderate	High	High
Deformation	Moderate	High	Low	Lowest
Equivalent Stress	Moderate	Higher	Low	Low
Natural Frequency	Moderate	Lowest	High	Highest
Corrosion Resistance	Moderate	Good	Excellent	Excellent
Erosion Resistance	Moderate	Moderate	Excellent	Excellent
Manufacturability	Good	Good	Good	Good

The final selection of Stainless Steel 314 was based on a comprehensive comparison of the structural, dynamic, and practical performance of all four candidate materials. Structural Steel provided acceptable mechanical strength but comparatively lower corrosion resistance. A390 Cast Aluminium Alloy offered reduced weight but experienced greater deformation and lower structural stiffness because of its lower modulus of elasticity. CA6NM Steel exhibited

favourable corrosion resistance and mechanical strength; however, its overall structural stiffness and dynamic characteristics were slightly inferior to those of Stainless Steel 314 under identical loading conditions. Stainless Steel 314 demonstrated the most favourable combination of low deformation, acceptable equivalent stress, higher natural frequencies, improved resonance safety, excellent corrosion resistance, and superior erosion resistance. The successful fabrication and experimental validation of the SS314 runner further confirmed its suitability for micro-hydropower Pelton turbine applications. Therefore, Stainless Steel 314 was selected as the optimum runner material for the present investigation.

4.8 Results and Discussion

This study utilized ANSYS Mechanical APDL to perform a Finite Element Analysis (FEA) of Pelton turbine buckets for the purpose of determining their structural integrity, deformation characteristics, distribution of stresses, and ability to carry loads under realistic hydraulic load conditions. This numerical analysis was done assuming both horizontal and vertical orientations of the bucket blades when subjected to various combinations of loadings characteristic of typical operational conditions of Pelton turbines.

The finite element model consisted of highly refined mesh structures in order to increase the accuracy of stress and deformation predictions during hydraulic load conditions. The discretized model had approximately 687,557 nodes and 921,522 elements incorporated into it, which provided adequate numerical resolution to effectively capture localized stress concentrations and behaviour deformation near regions of critical importance of the bucket geometry. A grid independence check was performed on the finite element model prior to running the production simulations to confirm that all numerical equations converged as expected and that solutions were stable throughout the entire analysis process.

The analysis involved structuring loads applied to Pelton turbine buckets under a variety of different loading types such as low impact, high hydraulic impact, uniform pressure, non-uniform pressure and combined hydraulic loading conditions. The purpose of using the above loading conditions was to simulate the forces that Pelton turbine buckets continually receive. The forces Pelton turbine buckets experience are due to the high velocity water jet impacting and transferring energy to the bucket, producing localized areas of varying hydraulic pressures and also producing transient loading across the surface of the bucket especially in the splitter area and at the discharge radius. Figure 4.11 illustrates Structural Deformation Contours of Horizontal Bucket.

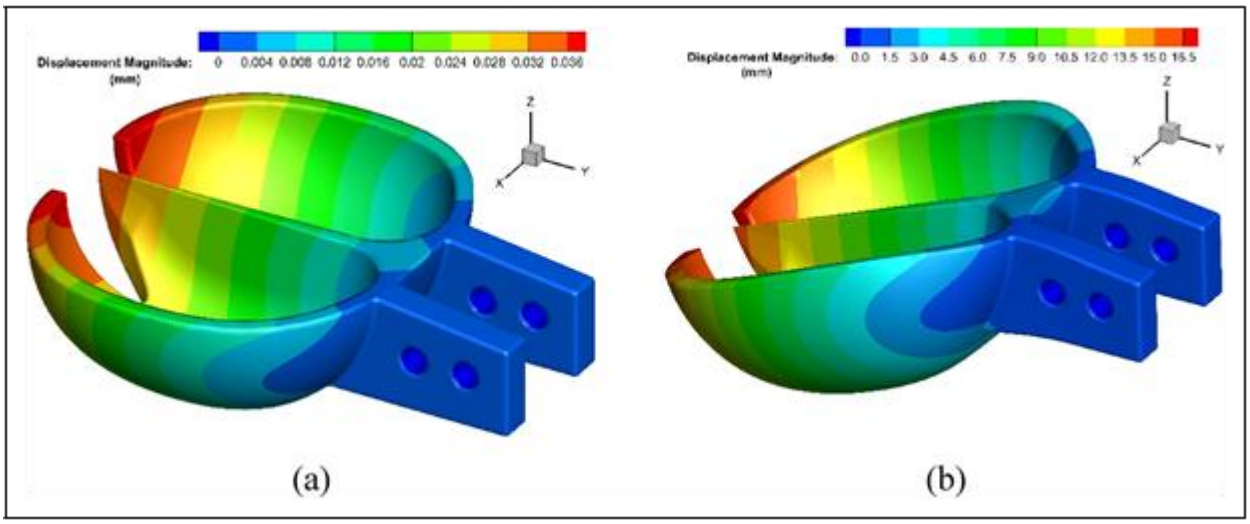

Figure 4.11 Structural Deformation Contours of Horizontal Bucket under (a) F_1 = 349 N and (b) F_2 = 153.864 kN

Representations of the deformations experienced by each of the materials were developed using the numerical simulations, demonstrating a distinct dependency on the curvature of the bucket, the amount of elastic or inelastic deformation that occurs within the bucket material when loaded and how the amount of elastic/ inelastic deformation is determined based upon the stiffness of the material, loading conditions applied to the bucket and support conditions (including the bucketing mechanism support) to which the bucket is exposed. When evaluating the structural behaviour of the materials as a result of relatively low impact loads applied (F_1=349N), the majority of the materials produced relatively small levels of deformation. Although all material suited for a functional embodiment demonstrate a relatively low level of deformation at this relatively low load level, at the time of the relatively large impact load (F_2=153.864kN), deformation can be observed on or about the tip of the splitter, on or about the front lip/ edges of the bucket and on or about the outer curvature of the bucket as a result of direct jet impact and momentum transfer.

The deformation patterns from experiments showed that the splitter and outlet curve experienced more bending than the mounting arms, because these areas were the only ones subjected to hydraulic forces, and because they experienced less structural restraint than do the mounting arms. Accordingly, the mounting interfaces have less likely to have experienced significant bending deformation, because of the fixed support used during analysis. This evidence indicates that the support configuration provides sufficient hydraulic load transfer from the bucket to the runner assembly with minimal localized deformations in the region of the mounting interface.

A390 cast aluminum alloy showed the largest amount of deformation because of the lowest relative elastic modulus and reduced stiffness. The relatively low structural rigidity of A390 alloy causes lower resistance to hydraulic impact loadings and bending deformations than the other testing materials. Conversely, SS314 and CA6NM demonstrated significantly less deformation that the aluminum alloy due to their relatively greater elastic modulus, increased structural stiffness and superior ability to carry load. The smaller deformation of SS314 indicates improved dimensional stability during turbine operation and good hydraulic interaction, while at the same time minimize instabilities of the flow within the bucket.

The numerical results further demonstrated that even under the most severe hydraulic loading conditions, the developed bucket geometry maintained deformation behaviour within the elastic operating range of the selected materials. The maximum deformation obtained during the investigation remained within acceptable engineering limits and no permanent yielding or structural instability was observed. This confirms that the optimized bucket geometry possesses sufficient structural stiffness and operational reliability for long-term micro-hydropower applications involving repetitive hydraulic loading conditions. Figure 4.12 shows Von-Mises Equivalent Stress Distribution

Finite element analysis of the equivalent von-Mises stress distribution produced by the test significantly identified a high level of stress concentration developed at three distinct regions. These areas of high stress occurred at the junction of the splitter to the root of the bucket, the interface of the bucket mounting arms and the two curvatures of the bucket and support arms. All three regions created geometric discontinuities which caused abrupt changes in the cross-sectional geometry and subsequently, localized stress amplification under hydraulic loading conditions.

The maximum level of stress concentration developed at the junction of the splitter to the bucket root as a result of the fact that the first point of contact the water from the jet makes is at the splitter region before the stream divides evenly into two symmetrical currents flowing over the surface of the bucket. Consequently, at the junction of the splitter to the root, there will be large impulsive loading and bending moment stresses at the splitter-to-root interface caused by the rapid transfer of momentum from the water jet to the bucket resulting in high levels of stress. Also, the stress contour plots indicated that there was a gradual decrease in the maximum stress value in the direction of the outlet curvature and bucket lip regions

which indicated a redistribution of load transferring smoothly across the surface of the bucket.

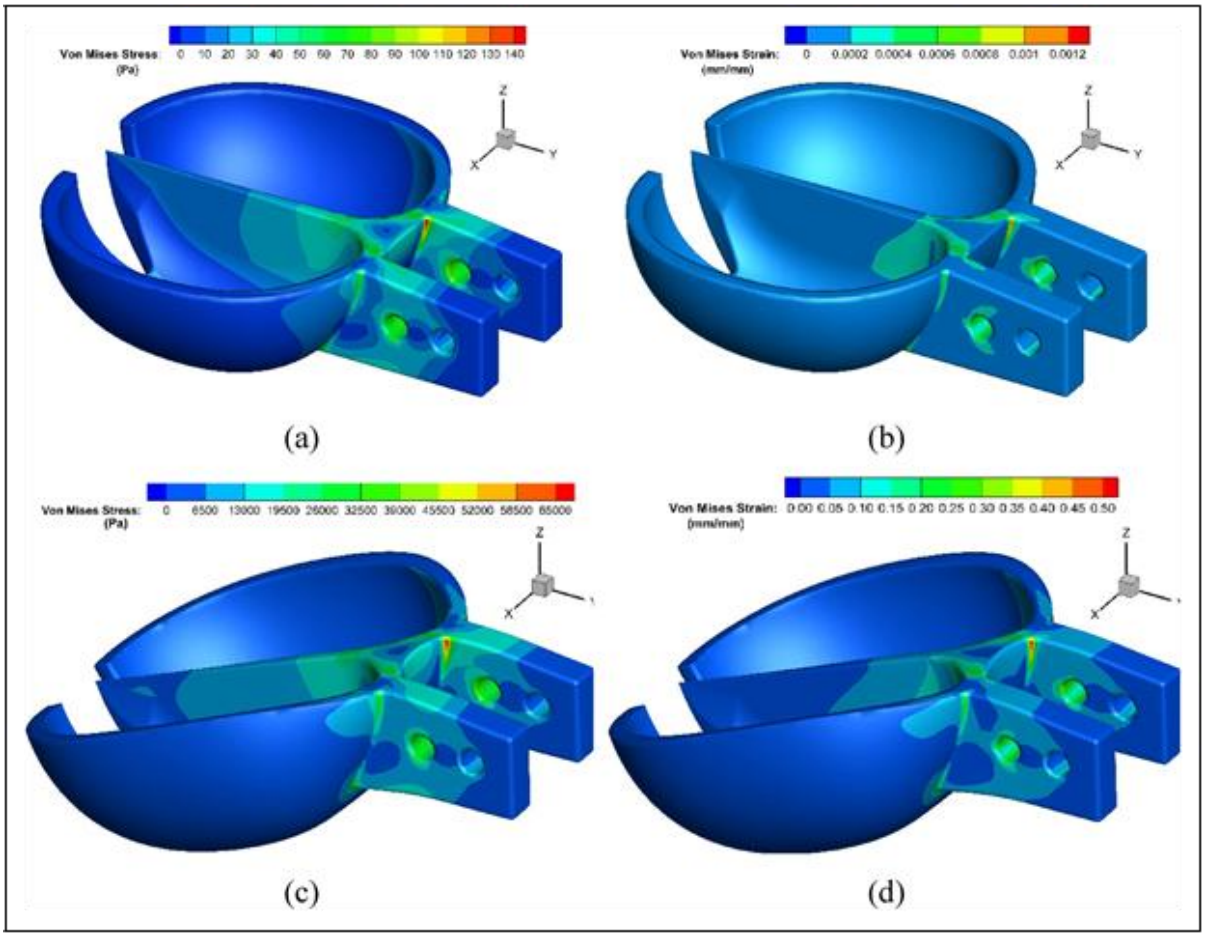

Figure 4.12 Von-Mises Equivalent Stress Distribution under Combined Hydraulic Loading

The amount of maximum equivalent von-Mises stress recorded in this study was significantly less than the yield strength limits of all of the materials in this investigation. This provides clear evidence that the entire structure of the bucket operates completely within the elastic deformation region for all of the hydraulic loading conditions investigated in these tests. No yielding behaviour or plastic deformation was observed even under maximum impact loading conditions, thereby establishing a high structural safety margin for the developed bucket geometry.

The comparative analysis of stress showed that the overall distribution of stress was comparable between each of the materials investigated. The main reason for this was because the loading path and the geometry were identical throughout each of the simulations. However, the degree of structural deformation varied between all the materials due to the fact

that the way in which the materials deformed is directly related to the stiffness and elastic modulus of the material. Therefore, it can be concluded that, taking into consideration all of the different aspects of the structures behaviour, namely deformation behaviour, stress distributions, corrosion resistance, fatigue characteristics and operational durability, stainless steel SS314 would be the most appropriate choice of material for the developed Pelton turbine bucket. The structural stiffness and strength of SS314 provide excellent resistance to hydraulic impact loads, cavitation damage, and cyclic stress from the operation of the turbine. Additionally, high levels of chromium in SS314 provide excellent resistance to corrosion, erosion, and surface deterioration due to the constant exposure to high-velocity water jets.

Ultimately, the structural finite element analysis supports the conclusion that an optimized geometry for the Pelton turbine bucket, combined with SS314 material, provides structural integrity with high load-carrying capacity, excellent deformation resistance, and dependable long-term operation for micro-hydropower.

4.8.1 Modal Analysis Results and Detailed Resonance Discussion

After completing the static analysis of the Pelton turbine bucket, pre-stressed modal analysis was performed to determine the natural frequencies, mode shapes, vibration characteristics and dynamic stability of the developed runner geometry under operating conditions. Excessive vibration in hydraulic turbine systems due to resonance-induced vibration is one of the most critical dynamic phenomena that can lead to fatigue failure, noise generation, shaft instability/structure damage, and reduced operational reliability. Therefore, accurately determining the natural frequency and resonance behaviour is essential for ensuring safe and stable turbine operation under continuous cyclic hydraulic loading conditions.

Modal analysis was conducted via the Block Lanczos eigenvalue extraction method due to its computational efficiency, as well as its suitability for large finite element models of complex 3D geometries. The pre-stressed structural condition due to hydraulic loading was used for this analysis in order to reproduce realistic operating conditions of the Pelton turbine bucket during actual use. The mode shapes and natural frequencies from this analysis were used to evaluate the dynamic response characteristics and susceptibility to resonance of the developed bucket geometry.

The excitation frequency generated during turbine operation was determined using the bucket-passing frequency relationship given by:

$$f_b = \frac{ZN}{60} \text{----------} [35]$$

where Zrepresents the number of buckets mounted on the runner and Ndenotes the rotational speed of the turbine in revolutions per minute. Considering 19 buckets operating at a rotational speed of 1000 rpm, the bucket-passing excitation frequency was calculated as approximately 316.67 Hz. This excitation frequency represents the periodic hydraulic loading frequency generated due to successive interaction of the water jet with the rotating bucket assembly.

Based on the results of modal analysis, the design of the bucket geometry has much higher first mode of vibration frequency than operation frequency at which the bucket geometry will be excited from the operation of the turbine. The highest first mode of vibration frequency in this study was calculated at 4231.8 Hz, producing a resonance safety factor of 13.37. The very large difference between frequency at which the turbine will be excited and the first mode of vibration frequency indicates that it is virtually impossible to have resonance occur in normal operation of the turbine.

The very high value of this resonance safety factor supports the design of the optimized bucket geometry exhibiting excellent dynamic stability because there is a large separation between natural and excitation frequencies that occur when operating under actual practical conditions. This large separation of frequencies greatly reduces the likelihood of vibration amplification and preventing development of dynamic instability of the bucket geometry under long-term operation of the turbines. Modal analysis shown in figure 4.13, therefore, supports that the Pelton turbine runner will operate outside of the resonance region safely and exhibit stable vibration response to cyclic hydraulic loads.

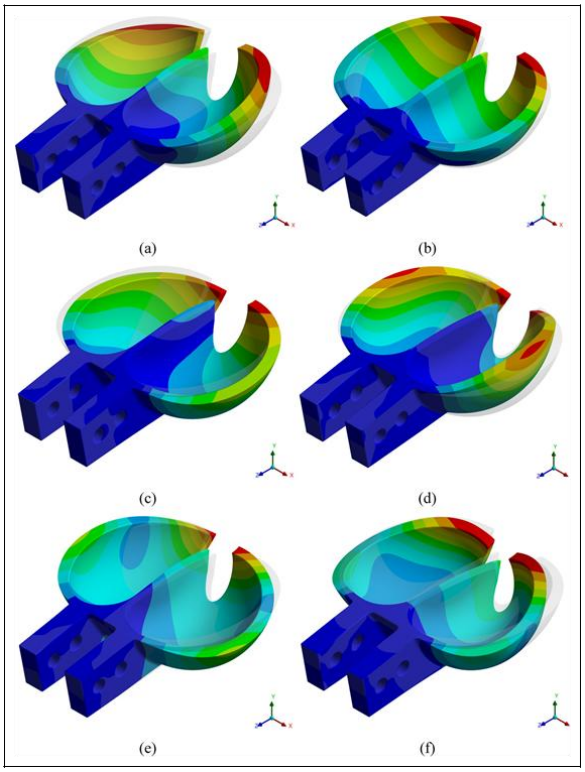

Figure 4.13 First Six Modal Deformation Shapes of Pelton Turbine Bucket

The vibration deformation modal contours showed that vibration deformations developed predominantly in the splitters edges, outlet curvature and bucket lip surfaces. Areas of the bucket with low relative stiffness compared to other areas of the bucket experienced direct interactions with hydraulic forces created from the operation of the turbines. Conversely, areas of the bucket mount arm were found to be dynamically stable due to having rigid support conditions and sufficient structure rigidity provided by the optimal bucket geometry.

The low order vibration modes of the bucket represent the bending mode patterns of the entire bucket structure, with the higher order vibration modes representing localized deformation in the regions around the splitter and the outlet of the bucket. Additionally, the deformation patterns measured during the modal analyses correspond with the results of the optimization which had occurred in the bucket geometry, indicating that the bucket assembly efficiently distributes the stiffness though the entire bucket assembly thus eliminating excessive concentration of localized vibrations.

The modal performance of the turbine was also assessed, indicating that there were large separations between the vibration modes and there was little or no significant coupling of modal frequencies. The large separation of modal frequencies is critical because modal coupling and internal resonance can cause large amplitude vibration of the turbine assembly

when subjected to variable hydraulic loading conditions. Therefore the large separation of modal frequencies contribute to the stability of the dynamic performance of the assembly and reduce the fatigue of the structure caused by vibratory loads.

The structural and modal investigations together provide confirmation regarding the optimized Pelton turbine bucket's outstanding stiffness, dynamic stability, and resonance-free operational behavior; these properties have been shown to be appropriate for practical applications of micro hydroelectricity. The design of the bucket geometry supports a high level of resistance to vibrational instability due to dynamic forces and enables safe operation over a long period of time under repeated cyclic hydraulic loads experienced in Pelton turbine operations.

4.9 Colusre

A CAD model of the optimized Pelton turbine bucket was developed in SolidWorks® based on established hydraulic design parameters and imported into ANSYS Mechanical APDL for FEA. Geometric optimizations included splitter width, bucket curve radius, outlet angles, and support arm geometry.

Material Evaluation across four candidates CA6NM steel, structural steel, A390 cast aluminum, and SS314 identified Stainless Steel 314 as optimal due to superior yield strength, corrosion resistance, and structural stability.

Static Structural Analysis under force, uniform/non-uniform pressure, and combined loading revealed peak stress concentrations and deformation at the splitter and mounting arms. A390 aluminum exhibited maximum deformation; structural steel and CA6NM demonstrated higher load-bearing capacity; SS314 showed best overall performance. All stress values remained within material yield limits.

Modal Analysis via Block Lanczos extraction of six mode shapes confirmed increasing natural frequencies per successive mode. Vertical orientation exhibited higher modal frequencies than horizontal, indicating greater dynamic rigidity. Maximum modal deformation was localized at the splitter geometry. All natural frequencies maintained adequate separation from operational excitation frequencies, minimizing resonance risk.

The optimized bucket geometry demonstrates satisfactory structural integrity, stable stress distribution, and dynamic stability under micro-hydropower operating conditions. Results provide the basis for subsequent CFD analysis of hydraulic flow and pressure distribution.

Chapter 5 Computational Fluid Dynamics Analysis of Pelton Turbine Bucket

5.1 Introduction

CFD is one of the best methods available to study the complex behaviour of fluids flowing through pipes that are producing power using a turbine and how those fluids will perform inside of a turbine. In a hydraulic turbine, CFD provides a detailed visual representation/comparison analysis of where the pressure acts on a turbine or other components (nozzles and runners), where there are differences in velocity throughout the turbine/compressors, how the fluid behaviour changes through the use of streamlines or streamline behaviour of a fluid, how much turbulence is created, where or if any flow separates from a turbine/compressor rotor blade or bucket, and how energy is transferred from one component to another in a turbine. The use of CFD for the study of Pelton turbines is of particular interest because a Pelton turbine is an impulse turbine that uses a high-velocity jet of water acting on the bucket's surface and transmitted to the runner, which creates very complex free-surface flow behaviour as well as transient hydrostatic conditions.

The Pelton turbine is a type of impulse turbine that is most-commonly used in high-head/low-discharge hydropower plants due to the fact the incoming hydraulic energy is first [3, 4, 5, 6,11,12, 15, 18, 20] converted from hydraulic energy to kinetic energy in a nozzle prior to the impact and transfer of that kinetic energy from the incoming film of water to the bucket surface (runner). The hydraulic efficiency of the turbine (system) is highly reliant upon how effective the momentum transfer occurs between the incoming jet of water and the surface of the bucket. Thus, it is critical to investigate the relationship between a jet of water, how it behaves once it contacts the bucket surface of a Pelton bucket, the pressure created by the incoming jet, how turbulence is generated, flow separation, and streamline behaviour within the bucket in order to improve the hydraulic efficiency and overall operational stability of the hydroelectric power generation system.

The hydraulic flow behavior in a Pelton turbine bucket is exceedingly intricate due to the influence of several factors such as high impact from the water jets, turbulent fluid flow characteristics, pressure fluctuations, the formation of a free-surface, as well as transient interaction caused by water jet - bucket geometry relationship. Performing experimental tests of these complex hydraulic phenomena is generally impracticable, expensive, and labour-

intensive because of the difficulties associated with measurement instrumentation and obtaining visualizations of unsteady flow behaviour. Therefore, Computational Fluid Dynamics (CFD) analysis has emerged as an effective means for predicting the hydraulic performance and flow characteristics of Pelton turbine systems across a variety of operating conditions.

The assessment of the hydraulic performance and optimization of a Pelton turbine bucket via CFD modelling has been conducted by numerous researchers. Early studies found that the following design features significantly affected hydraulic efficiency and momentum transfer through a Pelton turbine: bucket geometry, splitter arrangement, outlet angle, and development of streamlines. Additionally, the computational fluid dynamics performed for various Pelton turbine systems indicated that improper bucket geometry can result in flow separation, excessive generation of turbulence, splash loss, and incomplete momentum transfer leading to a reduction in turbine efficiency and operational stability.

The Pelton turbine's hydraulic performance is influenced by many design and operating parameters including inlet jet speed; bucket shape; splitters; the profile of the outlet curvature; nozzle diameter; speed of rotation; and pressure inside the buckets. The design of these parameters was optimised, in order to promote a smooth hydraulic interaction, the development of stable streamlines, and efficient energy conversion during operation. Therefore, the optimally sized buckets, which were developed in the first part of this study have been evaluated using Computational Fluid Dynamics (CFD) to determine hydraulic suitability, as well as flow behaviour.

In addition to steady-state flow, Pelton turbines will also experience transient hydraulic action during operation due to the continuous interaction of the water jet and the surface of the bucket. These transient interactions cause fluctuating pressure fields, turbulence, changing streamline patterns, and dynamic vortex formations within the bucket area. All of the above transient hydraulic phenomena have a pronounced effect on the hydraulic efficiency, vibration characteristics, and reliability of the turbine. Therefore, both steady and transient CFD analyses will be used in the current study to gain a total understanding of the hydraulic behaviour of the optimally sized Pelton buckets.

This chapter focuses primarily upon completing a detailed Computational Fluid Dynamics (CFD) Analysis of the optimised bucket for the Pelton turbine as created during the earlier stages of this investigation. The CFD simulations have been conducted using the ANSYS

Fluent Program to not only clarify the velocity distribution, pressure variation, streamline, turbulence characteristics, flow separation, and hydraulic interaction, but, also the CFD investigation involves the development of the computational geometry, creation of the CFD mesh generation, analysis of mesh independence, implementation of the boundary conditions, turbulence modelling, steady-state analysis, transient flow analysis and hydraulic performance assessment.

The governing equations that were used during the CFD analysis were based upon conservation of mass and momentum for the incompressible turbulent flow. The analysis used appropriate numerical discretisation techniques and turbulence modelling to accurately predict hydraulic behaviour within the Pelton bucket. The CFD analysis conducted during the present investigation provides detailed understanding of the hydraulic performance and energy transfer characteristics of an optimised Pelton bucket for micro-hydropower applications.

5.2 Computational Geometry Development

Using SolidWorks® CAD software, a computational model of the Pelton turbine bucket was created and then imported into ANSYS Fluent for computational fluid dynamics (CFD) simulations. The bucket geometry used for hydraulic investigation was obtained from prior structural and hydrodynamic design and analysis, providing consistency between structural integrity determination and fluid flow assessment. Important hydrodynamic design parameters, such as the splitter geometry, bucket depth, outlet curvature, bucket width, and flow channel configuration, were considered when designing the bucket model to ensure maximum momentum transfer from the water stream to the runner of the turbine.

In designing the splitter region, great care was taken, since the incoming high-velocity water stream directly strikes the splitter at high speed prior to splitting into two equal streams. The splitter configuration is very important in Pelton turbines because it directly impacts jet splitting, hydraulic efficiency, pressure distribution, and minimizes losses due to splashing.

Care was also taken in the design of the curvature of the bucket to guide the water stream from the inlet to the outlet in a smooth manner and reduce flow separation and hydraulic losses. Figure 5.1 shows Geometry of Pelton turbine with dimension

This dimensioned bucket configuration was selected based on the optimised Pelton turbine bucket geometry which was developed during previous structural and dynamic analysis phases of the development phase of the project. The bucket includes two identical

hemispherical cups separated by a centre splitter, as well as outlet edges which are smoothed so that the water jet can be redirected effectively to maximise the amount of hydraulic energy extracted from it.

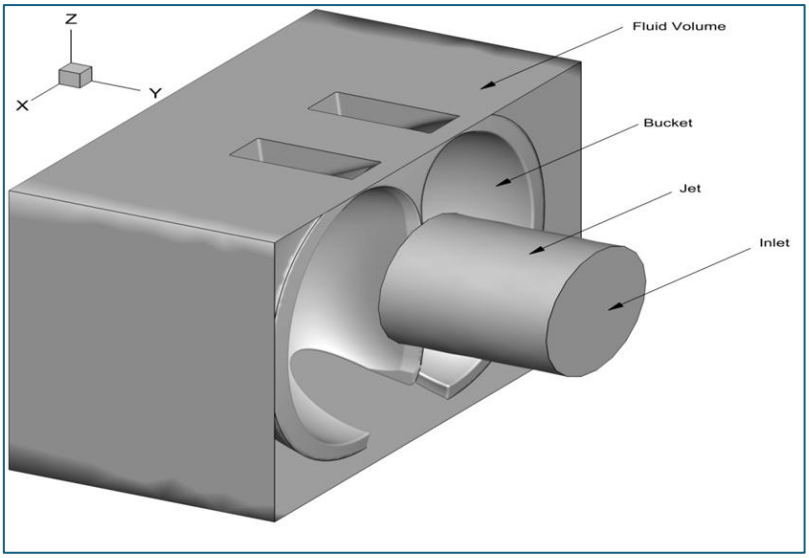

Figure 5.1 Geometry of Pelton turbine with dimension

The computational domain for the CFD analysis was created to contain all of the relevant portions of the flow, including the nozzle flow region, jet interaction zone, bucket surface, and the surrounding fluid enclosure. Proper care was taken in creating the fluid domain to ensure that the incoming jet develops to a sufficient degree to be stable when it interacts with the bucket surface and that it does not become numerically unstable near the outlet region of the domain. There was sufficient enclosure distance (enclosure distance is the distance between the boundary of the enclosed fluid domain and the bucket boundaries) around the geometry of the bucket to allow for accurate capture of pressure changes, streamline development, turbulence creation, and jet dispersion during the CFD analysis.

In addition to the initial geometry development phase, there were several phases of geometry preparation where the geometrical irregularities were simplified and critical flow areas were refined to provide maximum numerical simulation stability and convergence. In addition, the resulting computational geometry produced a high-quality mesh for predicting hydraulic flow behaviour accurately during simulated hydraulic performance evaluation.

5.2.1 Governing Equations for CFD Analysis

A CFD study of Pelton turbine bucket uses the fundamental governing equations for fluid flow based on the conservation laws of mass and momentum for fluid flow and requires

appropriate mathematical formulations. Within the computational domain, water interacts with the bucket via high-velocity water jets creating very complex turbulent flow behaviour, with large increases in the amount of pressure, changes from one streamline to the next, and large amounts of momentum transferred between the two surfaces. Because the density of water does not vary greatly compared to the density of the surrounding air, flow can be considered to be incompressible. This means that the governing equations to model CFD analysis in this study describe continuous flow and the use of the Navier-Stokes momentum equation for turbulent flow, as well as the continuity equation.

Thus, the conservation of mass of an incompressible fluid defined by CFD modelling can be expressed mathematically as follows:

$$\frac{\partial u}{\partial x} + \frac{\partial v}{\partial y} + \frac{\partial w}{\partial z} = 0 \text{----------[36]}$$

where u, v, and $w$represent the velocity components in the x, y, and $z$directions respectively.

The governing momentum conservation equations for flow in all three dimensions of the flow field are obtained from the Navier Stokes equation. The governing equations of motion of fluid as a result of hydraulic interaction with the surface of the bucket include the total force resulting from the fluid's pressure, viscous forces, inertial forces, and other external forces acting on it from the surrounding environment. The generalized momentum equation for incompressible turbulent flow is expressed as:

$$\rho\left(\frac{\partial \vec{V}}{\partial t} + \vec{V} \cdot \nabla\vec{V}\right) = -\nabla P + \mu\nabla^2\vec{V} + \rho\vec{g} \text{----------[37]}$$

where ρ represents fluid density, P denotes pressure, μ represents dynamic viscosity, $\vec{V}$indicates velocity vector, and $\vec{g}$ represents gravitational acceleration.

Due to the extremely high inlet jet velocity at which the water enters the Pelton turbine bucket, as well as the water jet's abrupt strike against the splitter region of the bucket, the resulting flow pattern inside the bucket is anticipated to be turbulent; therefore, it is essential to model turbulence in order to accurately predict several hydraulic characteristics, such as velocity fluctuations, pressure variations, vortex formation, and the distribution of turbulence intensity. For this study, the standard k–ε turbulence model was selected based on its stability numerically, computational efficiency, and its suitability for modelling turbulent flow conditions at Reynolds numbers typically associated with Pelton turbine operation [17].

The transport equation for turbulent kinetic energy (k) used in the turbulence model is expressed as:

$$\frac{\partial(\rho k)}{\partial t} + \frac{\partial(\rho k u_i)}{\partial x_i} = \frac{\partial}{\partial x_j}\left[\left(\mu + \frac{\mu_t}{\sigma_k}\right)\frac{\partial k}{\partial x_j}\right] + G_k - \rho\varepsilon \text{----------[38]}$$

The turbulent dissipation rate equation (ε) for the turbulence model is as follows:

$$\frac{\partial(\rho \varepsilon)}{\partial t} + \frac{\partial(\rho \varepsilon u_i)}{\partial x_i} = \frac{\partial}{\partial x_j}\left[\left(\mu + \frac{\mu_t}{\sigma_\varepsilon}\right)\frac{\partial \varepsilon}{\partial x_j}\right] + C_{1\varepsilon}\frac{\varepsilon}{k}G_k - C_{2\varepsilon}\rho\frac{\varepsilon^2}{k} \text{----------[39]}$$

The incoming jet flow had a sufficient Reynolds number to ensure that flow inside the computational volume would be classified as turbulent. The relationship for the hydraulic flow is expressed as the following equation:

$$Re = \frac{\rho V D}{\mu} \text{----------[40]}$$

where V represents inlet jet velocity and D denotes nozzle diameter.

A CFD analysis of the behaviour of a Pelton turbine bucket includes gravitational effects, pressure loading, and wall interactions to accurately simulate and predict the hydraulic performance of the bucket. Additional detailed solutions to the governing equations were obtained using the finite volume method in ANSYS Fluent. The pressure–velocity coupling and turbulence equations were solved iteratively until convergence criteria were achieved for all residual parameters.

The governing equations and turbulence model used for the current study allowed for good prediction of velocity profiles, pressure contours, streamline behavior, turbulence intensity, and hydraulic interactions in the optimized Pelton bucket under various operating conditions.

5.3 Mesh Generation and Grid Independence Study

The quality of mesh generation and proper discretization of computational domain have a major influence on the accuracy and reliability of the Computational Fluid Dynamics (CFD) analysis. This investigation focused on developing a mesh that would be able to accurately represent the complex hydraulic interaction of a high velocity water jet with the surface of a Pelton turbine bucket. The CFD mesh was generated using ANSYS Workbench meshing module and imported from SolidWorks® computational geometry development software.

The computational domain of a Pelton turbine bucket is made up of several geometric elements (splitter geometry) as well as jet interaction regions and the outlet curvature. All of these elements require an appropriate discretization method for numerically predicting the velocity distribution, pressure variation, turbulence development, and streamline behaviour respectively. Tetrahedral mesh elements were used in this study, as this type of mesh provides an adaptable means of discretizing very complex geometries (including irregular flow domains and curved hydraulic surfaces) when developing computed mesh models.

The mesh refinement process was performed extensively at the splitter, inner surface of the bucket, impact zone of the jet, and outlet radius, as these areas were subjected to large pressure gradients and rapid fluctuations in velocity due to hydraulic interaction. To better predict turbulence characteristics and momentum transfer, finer elements were located near the wall surfaces. Coarser elements were used in regions farther away from the critical hydraulic interaction because of the need to balance computational costs with the need to provide numerical accuracy.

Figure 5.2 illustrates the computational mesh created for the Pelton turbine bucket. This figure represents the discretized fluid domain occupying the volume of fluid surrounding the bucket geometry during the CFD simulations and shows that there are enough mesh elements around the surface of the bucket and jet interaction to accurately capture the hydraulic flow pattern.

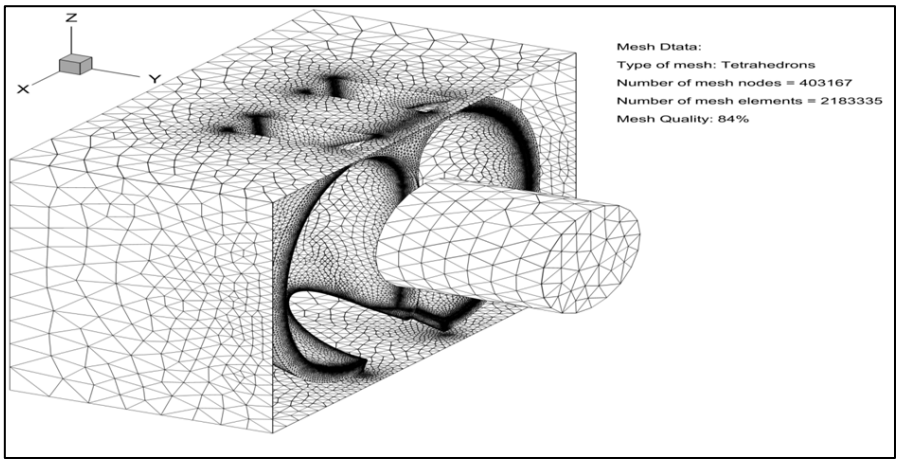

Figure 5.2 Computational Mesh Generated for Pelton Turbine Bucket

Figure 5.3 displays the top view of the computational mesh distribution created to represent the Pelton turbine bucket. The manner in which the mesh was created demonstrates the use of finer discretization in the vicinity of both the splitter and the curvature of the bucket, where

there is a significant amount of change occurring in both pressure and velocity due to jet impingement.

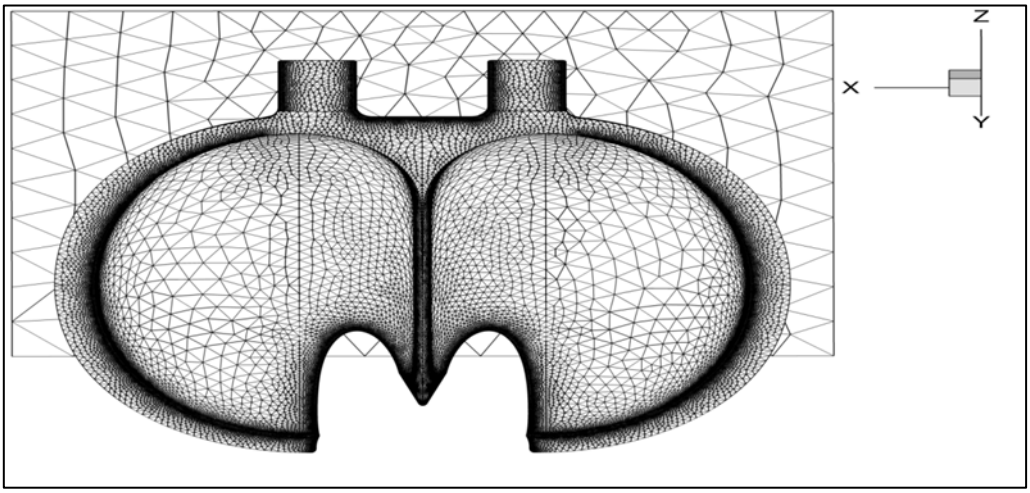

Figure 5.3 Top View of Computational Mesh Distribution

The CFD mesh parameters that were utilized in this study, as summarized in Table 5.1, have sufficient mesh density/mesh accuracy/convergence behaviour for both transient and steady state flow simulations to allow for numerical accuracy during these simulations.

Table 5.1 CFD Mesh Parameters

Sr. No.	Parameter	Value
1	Mesh Type	Tetrahedral
2	Mesh Size	0.5 mm
3	Number of Nodes	403167
4	Number of Elements	2183335
5	Type of Study	Single Phase Water Flow
6	Viscous Model	Turbulent

In addition to verifying that CFD simulations were conducted using the appropriate mesh density, a grid independence study was conducted to determine that the numerical results obtained from CFD simulations were independent of the mesh density. Variations of the

number of mesh nodes were used to develop different mesh configurations, and the predicted pressure and velocity results calculated from these configurations were compared. It was determined from this study that beyond a certain level of mesh refinement, there was very little change in predicted hydraulic parameters, which demonstrates stable numerical convergence and grid independent behaviour.

The results of a grid convergence study determined that the chosen mesh density produced sufficient output for accurately predicting velocity contour plots, pressure distribution, turbulence intensity and pasting streamlines in the Pelton turbine bucket. Therefore, the final optimized mesh configuration was selected for use in all of the Computational Fluid Dynamics (CFD) simulations carried out as part of this research.

The quality of the resulting mesh is very important in achieving numerical stability and providing reliable convergence within the CFD; accordingly, sufficient level of refinement was applied to the mesh in the vicinity of the splitter and jet interaction regions in order to accurately determine hydraulic loading, turbulence generation and momentum transfer characteristics within the Pelton turbine bucket. Hence, the resulting configuration of the mesh provides accurate numerical analysis of the hydraulic performance of the optimized bucket geometry at a variety of inlet velocity conditions.

5.4 Boundary Conditions and Solver Setup

Accurate and stable computational fluid dynamics (CFD) simulations require proper selection of boundary conditions and solver parameters. The hydraulic characteristics of the water in a Pelton turbine bucket are significantly affected by the velocity of the water jet entering the bucket, the pressure distribution in the bucket, how turbulence develops within the bucket and how the water interacts with the walls of the bucket, and the flow conditions after exiting the bucket. As a result of these effects, appropriate boundary conditions were established in ANSYS Fluent to simulate the interaction of a high velocity water jet with the bucket's surface for various operating conditions in an accurate manner.

The CFD simulations were performed by modeling water as the working fluid and using incompressible turbulent flow. The optimized Pelton bucket geometry that had been developed previously was used for all of the numerical simulations conducted during the present study. The bucket was made of SS314 stainless steel which has an excellent resistance to corrosion, relatively high strength, and is well suited to applications where hydraulic turbines operate.

The CFD analysis parameters considered during the present investigation are summarized in Table 5.2.

Table 5.2 CFD Analysis Parameters

Parameter	Value
Bucket Width	33 cm
Bucket Height	110 cm
Bucket Length	95 mm
Nozzle Diameter	10 mm
Geometry Thickness	2 mm
Inlet Velocities	15, 20, 35, 45 and 58.7 m/s
Outlet Condition	Zero Pressure Outlet
Turbulence Model	k-ε Model
Working Fluid	Water

The inlet boundary condition was decided as a velocity inlet to allow some incoming water jet into the computational domain through the nozzle zone. Different inlet velocities of 15 m/s, 20 m/s, 35 m/s, 45 m/s, and 58.7 m/s were assumed for the study concerning how the operating conditions influence velocity distribution, pressure variation, turbulence intensity, and hydraulic interaction within the Pelton turbine bucket.

The outlet boundary condition was set as zero pressure at the outlet to allow water to discharge smoothly from the computational domain without creating any artificial pressure buildup at the outlet zone. In order to save on computational time while keeping the numerical accuracy constant during the simulation process, symmetry boundary conditions were applied to the side surfaces of the computational enclosure[17].

Smooth wall no-slip boundary conditions were imposed on all bucket surfaces to delineate accurately the interaction between water flow and the solid boundary of the turbine bucket. The no-slip wall condition implies that the fluid velocity relative to the wall surface becomes

zero at the solid-fluid interface. This is an important condition for an accurate prediction of boundary layer formation, pressure loading, turbulence generation, and wall shear behavior during hydraulic interaction.

The boundary condition setup implemented in ANSYS Fluent for the present CFD investigation is illustrated in Figure 5.4.

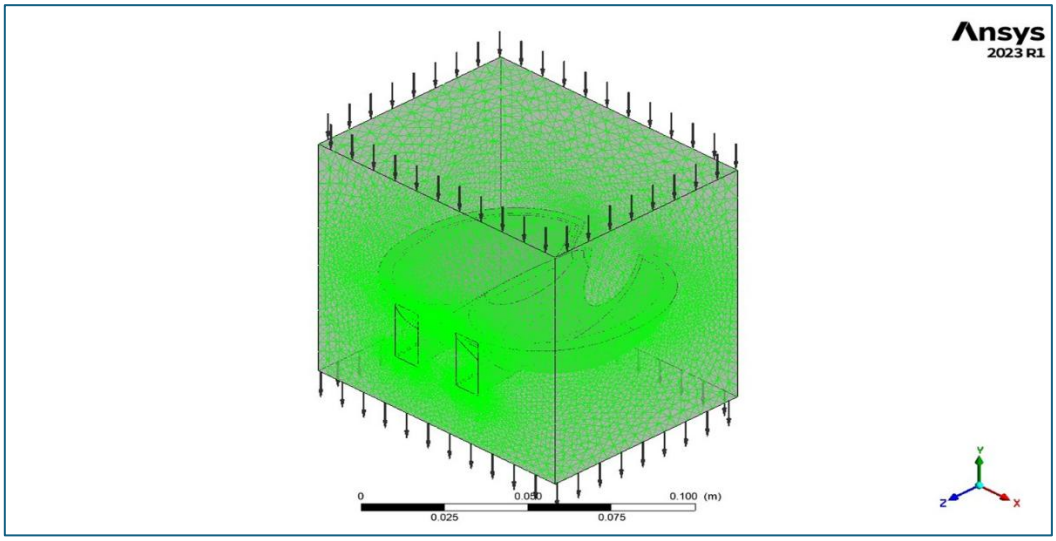

Figure 5.4 Boundary Condition Setup in ANSYS Fluent

CFD analysis was conducted with ANSYS Fluent's pressure-based solver, which used the SIMPLE algorithm for its stability and suitability for incompressible, turbulent fluid. Second order discretization for the pressure and momentum equations gave the numerical solution improved accuracy for predicting pressure and velocity fields respectively.

The present study used the standard k-epsilon turbulence model due to its predictive accuracy in producing stable convergence behaviour and good agreement with measured turbulent, high Reynolds number behaviour commonly found in Pelton turbines. The standard k-epsilon turbulence model predicts many important characteristics of turbulence, including intensity, vortex formation, streamline development and fluctuating hydraulic behaviour, in the region where water enters the buckets of a Pelton turbine.

Gravity was included in the CFD analysis to account for the effect of the gravitational force acting on the water flowing in the computational domain. The CFD investigation included both steady and transient flow computations to account for the hydraulic interaction characteristics under variable operating conditions.

The numerical simulations continued until all residual parameters had reached stable convergence behaviour. The convergence plots generated during the CFD analysis showed

that all residuals decreased progressively with increasing iteration count, demonstrating both the numerical stability of the simulation and convergence onto a reliable solution. Figure 5.5 shows CFD setup solver. The convergence behaviour obtained during CFD simulation is illustrated in Figure 5.6. The residual plots demonstrate stable numerical convergence for continuity, momentum, and turbulence equations during the iterative solution process.

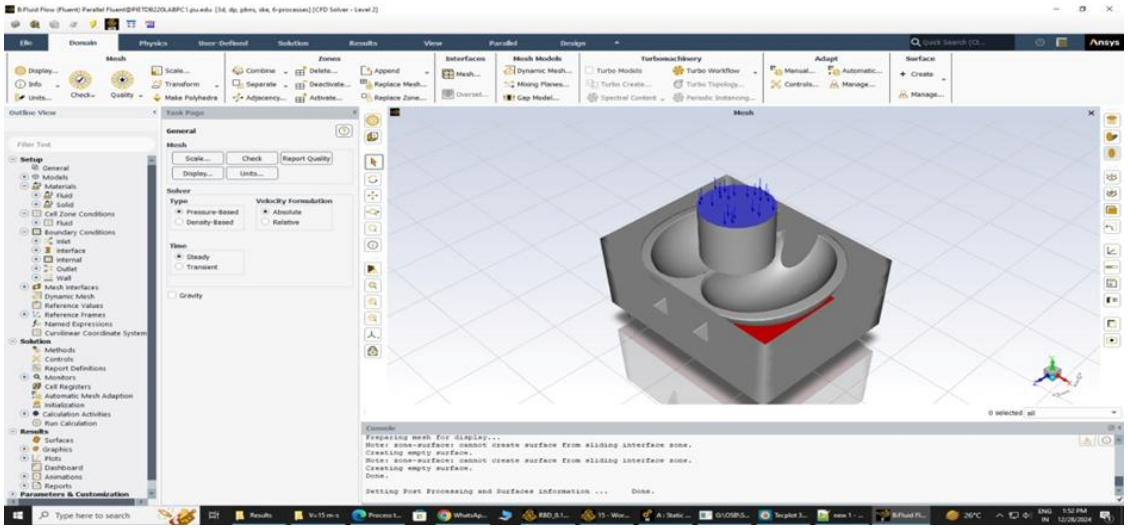

Figure 5.5 CFD Solver Setup in ANSYS Fluent

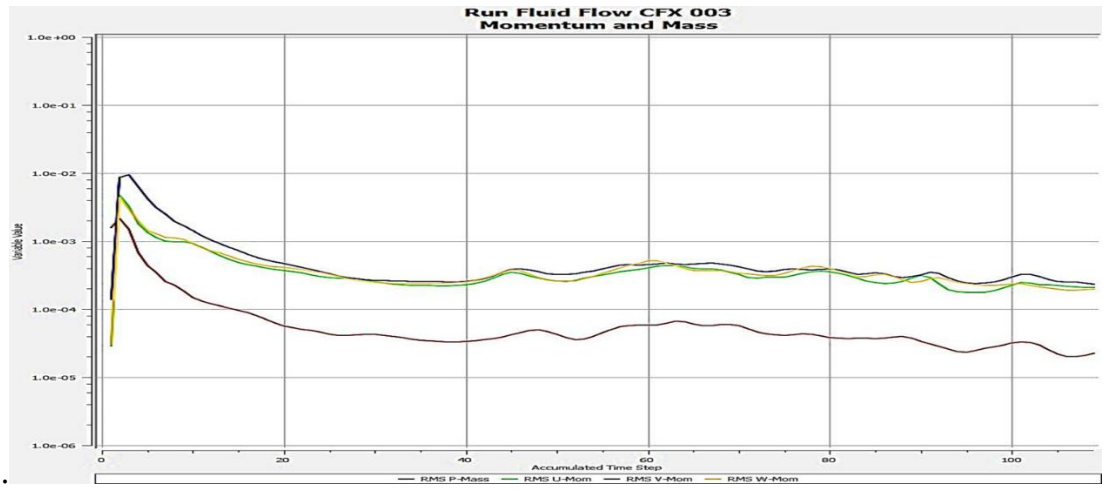

Figure 5.6 Convergence Plot

The implemented boundary conditions and solver configuration enabled accurate prediction of hydraulic characteristics including pressure distribution, velocity contours, turbulence development, streamline behaviour, and momentum transfer inside the Pelton turbine bucket under different inlet jet velocity conditions.

5.5 Steady-State CFD Analysis

Steady-state computational fluid dynamics evaluation of the hydraulic operation of the optimized pelton turbine bucket and its hydraulic interaction with the (non-optimized) high-velocity water jet was performed at multiple operating conditions. ANSYS Fluent software was used to carry out numerical simulations and, based on the simulation outputs, the velocity distributions, pressure variations, streamline characteristics, turbulence development, and hydraulic behavior within the bucket geometry were evaluated. The goal of the steady-state simulations was to further understand how momentum transfer and hydraulic performance about the optimized bucket configuration was affected by the incoming water jet (high-velocity water jet).

The simulations were performed using multiple inlet jet velocities (15 m/s, 20 m/s, 35 m/s, 45 m/s, and 58.7 m/s) in order to evaluate how increasing inlet jet velocity alters the pressure loads on the bucket, turbulence intensity, streamline characteristics, and hydraulic efficiency of the pelton turbine bucket.

The CFD simulations indicated that the incoming water jet impacts the splitter section of the bucket, and then splits into two symmetrical water jets that flow over the inner surface of the bucket. In this way, the optimized splitter geometry allows for improved splitting of the incoming water jet and reduces undesirable water splashes as a result of hydraulic action due to the water jet impacting the bucket.. The steady-state simulations additionally confirmed that the developed bucket curvature effectively guided the water flow toward the outlet region while maintaining continuous momentum transfer throughout the interaction process.

5.5.1 Velocity Distribution Analysis

In determining how efficient a Pelton turbine will operate hydraulically and how efficiently it will transfer momentum, an understanding of how fluid velocity is distributed within the turbine's buckets is vital. A computational fluid dynamics analysis was performed to analyze how the maximum fluid velocity for a Pelton turbine bucket occurs close to the nozzle exit due to jet impingement and water entering the computational domain.

Generally, when entering an inlet jet velocity of low speed, the water flows smoothly over the turbine bucket, with lower levels of turbulence and stable streamline behaviour. As entry jet velocity increased, so too did the range of velocity for the turbine bucket. Higher velocity at the inlet created greater hydraulic interaction between the turbine and water flow (high velocity stream wall) and more momentum transferred to the turbine.

In addition, the Velocity Contour Plots illustrated a gradual decrease in the velocity of the fluid as it travelled down the curved interior of the buckets. Decreased velocities were the result of the continuous conversion of the kinetic energy of the water jet to the bucket due to hydrodynamic interaction. The presence of the lower residual exit velocity at the turbine outlet indicates that the optimized bucket design (reduced residual exit velocity) is allowing for the extraction of more hydraulic energy. Figure 5.7 shows the two-dimensional velocity and pressure vectors for the inlet jet velocity of 15 m/s.

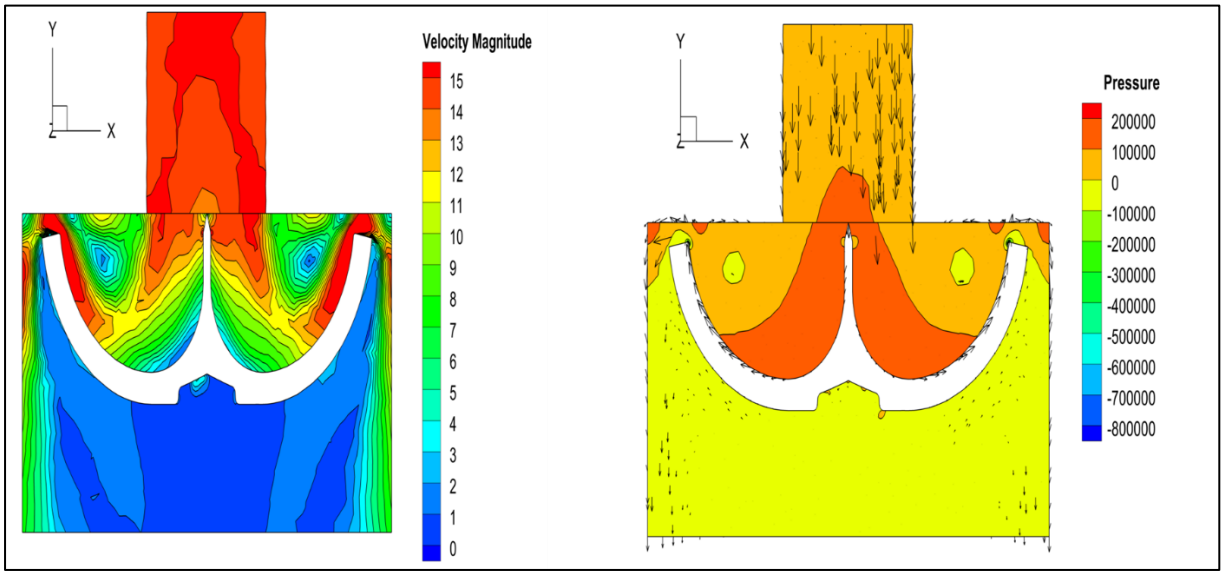

Figure 5.7 2D-velocity and pressure vector

The corresponding three-dimensional velocity and pressure vector distribution for 15 m/s inlet velocity is illustrated in Figure 5.8.

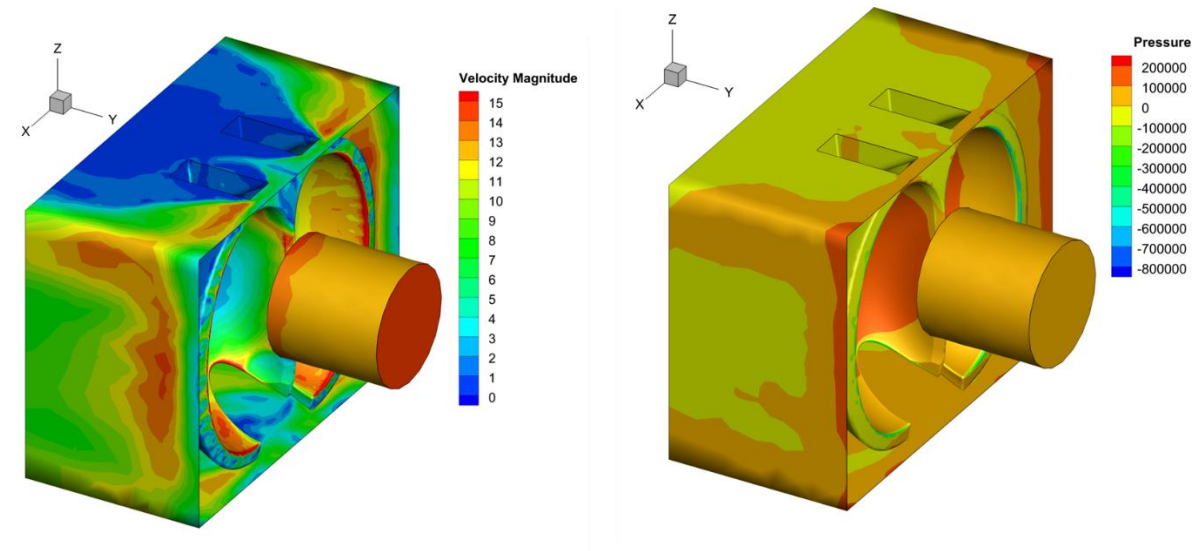

Figure 5.8 3D-velocity and pressure vector

The Computational Fluid Dynamics (CFD) investigation results are shown in figure 5.9 and figure 5.10 obtained from 20 m/s inlet velocity simulations showed an overall higher velocity magnitude and stronger hydraulic interaction in the splitter region than previously characterized. Additionally, the flow velocity distribution over the bucket surface was nearly equally distributed, which confirmed that the water jet was successfully bifurcated by both halves of the bucket.

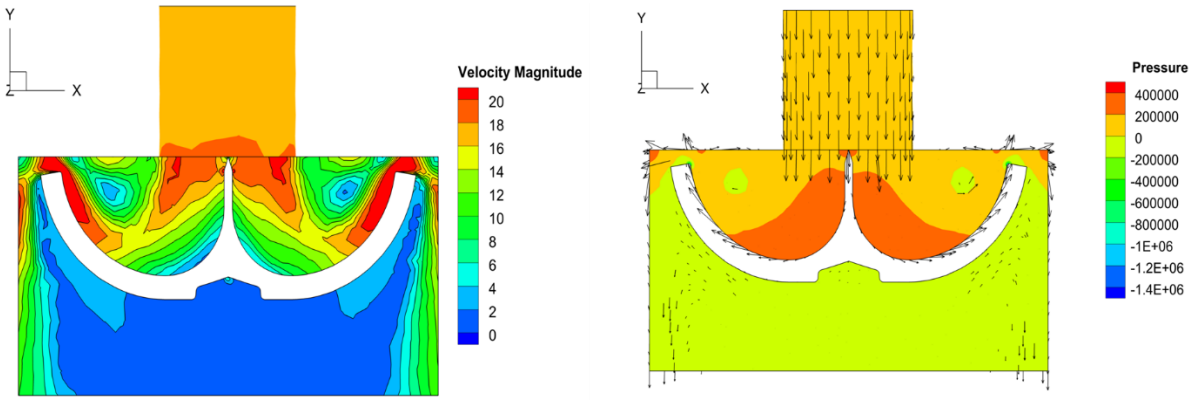

Figure 5.9 2D-velocity and pressure vector

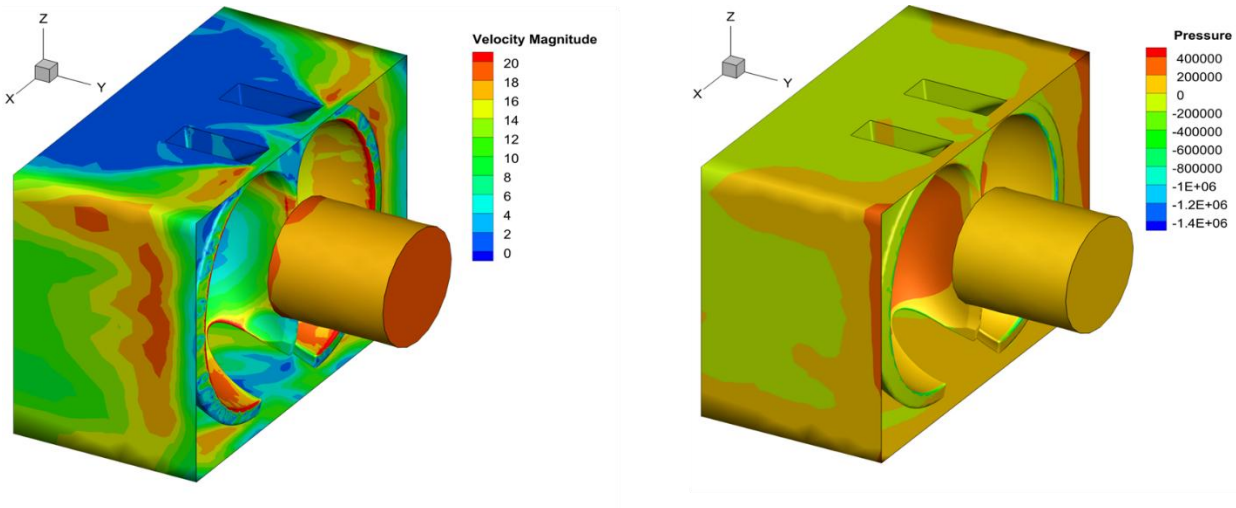

Figure 5.10 3D-velocity and pressure vector

The CFD investigation results are shown in figure 5.11 and figure 5.12 obtained from 35 m/s inlet velocity simulations showed very large increases in both the velocity magnitude and localized turbulence generation due to very large jet impact and momentum transfer characteristics near both the splitter and the outlet region.

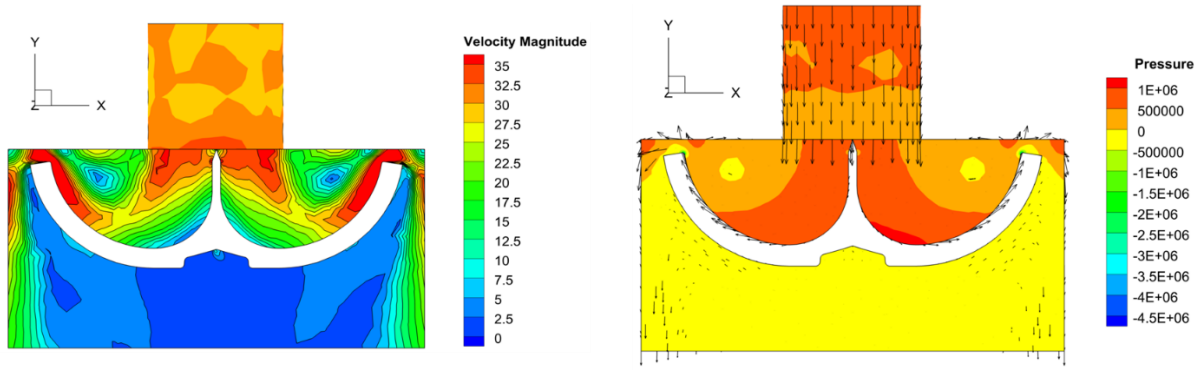

Figure 5.11 2D-velocity and pressure vector

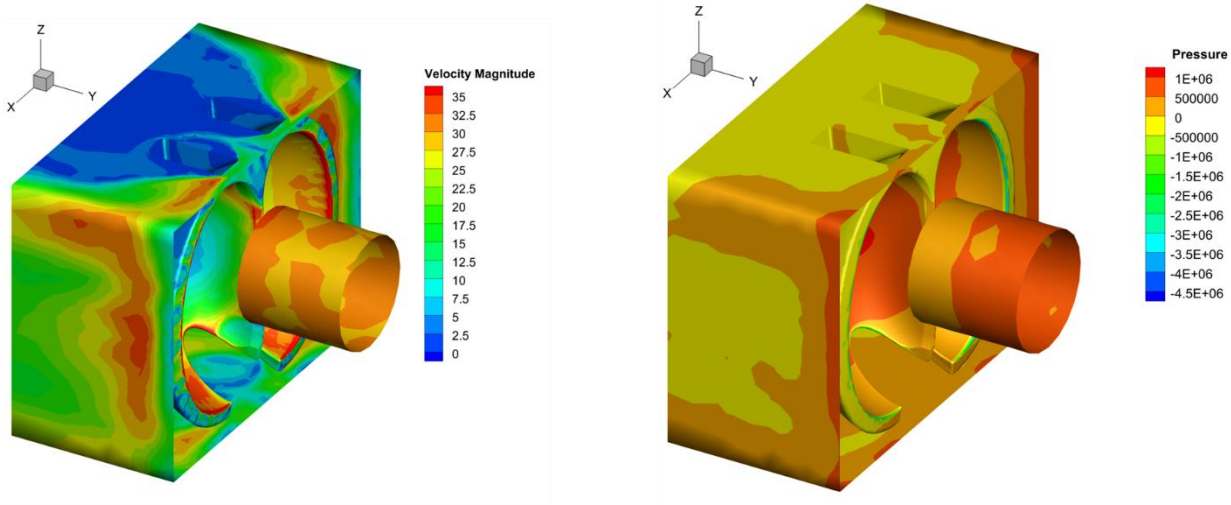

Figure 5.12 3D-velocity and pressure vector

Finally, the 45 m/s inlet velocity CFD investigation results are shown in figure 5.13 and figure 5.14 indicated a significant increase in flow disturbances and comparatively stronger turbulence development near the outlet curvature due to the increased outlet jet velocity. Nonetheless, the optimized bucket geometry demonstrated the ability to maintain stable flow guidance and minimize excessive hydraulic losses.

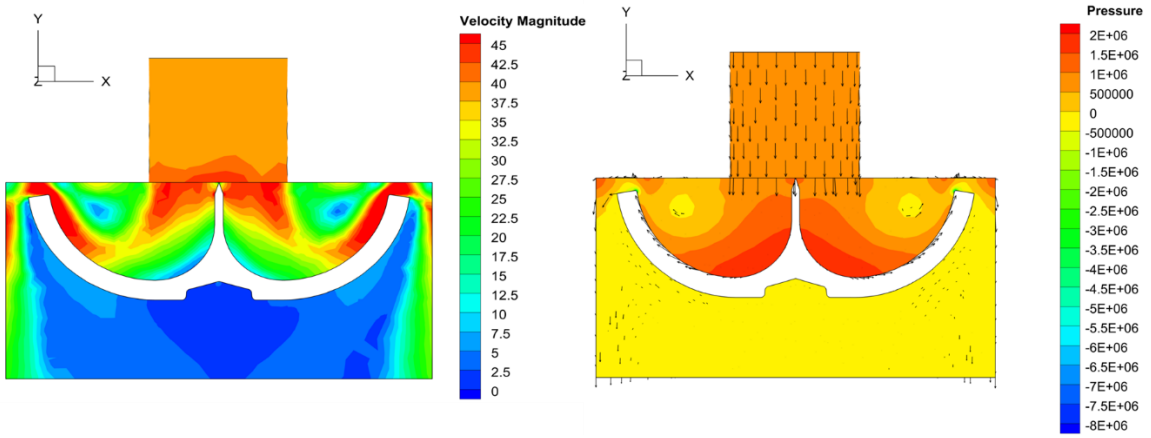

Figure 5.13 2D-velocity and pressure vector

The 58.7 m/s inlet velocity condition are shown in figure 5.15 produced the maximum hydraulic interaction and velocity magnitude within the computational domain. The simulated flow vectors illustrated the effective redirection of the incoming water jet to the outlet region while maintaining a continuous return of momentum across the entire surface of the bucket.

Therefore, from the investigation conducted, it can be concluded that the experimental data has confirmed that the optimized Pelton turbine bucket geometry has sufficiently delivered smooth hydraulic guidance, efficient jet bifurcation, stable momentum transfer, and minimal residual exit velocities. The obtained velocity distribution behaviour validated the hydraulic suitability of the optimized bucket design for micro-hydropower applications.

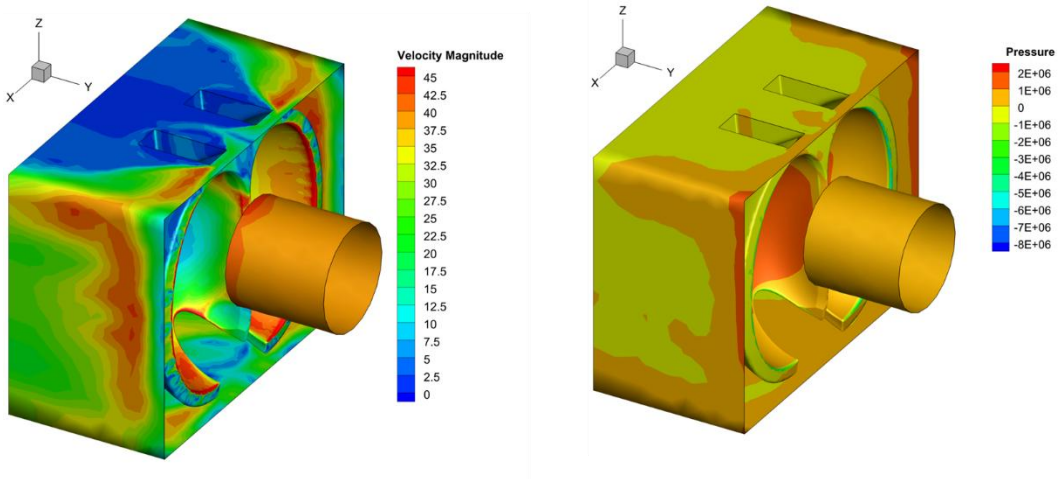

Figure 5.14 3D-velocity and pressure vector

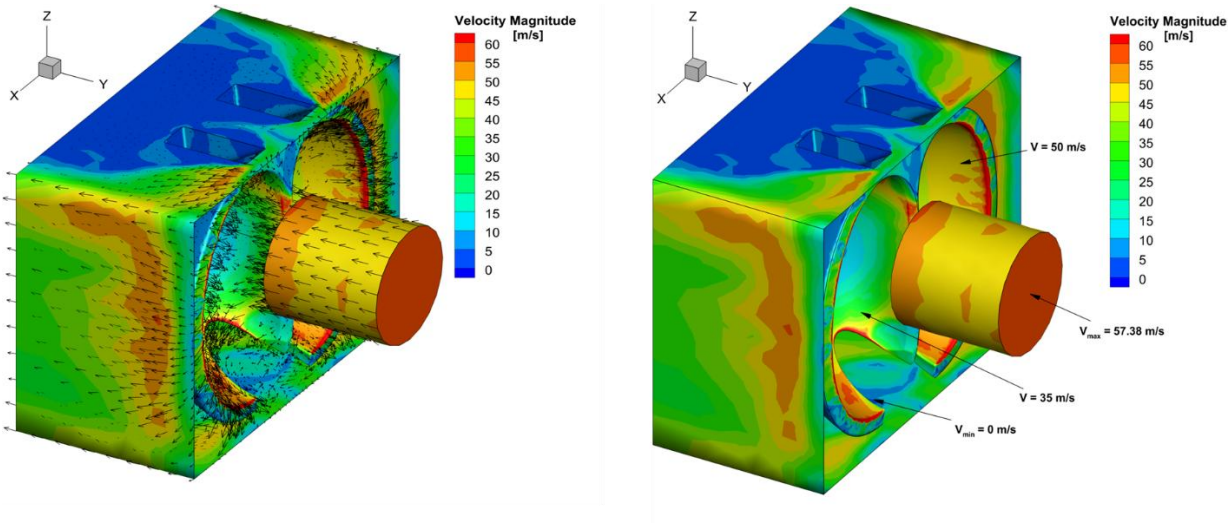

Figure 5.15 Velocity Vector

5.6 Transient CFD Analysis

The time-dependent interaction of both the high-velocity jet and the rotating bucket is being investigated using transient CFD analysis, which is different than a steadystate analysis because it captures flows that are unsteady in nature, particularly with regards to flow pattern changes due to pressure variation, dynamic turbulence and development of the water sheet from the point of turbine operation.

To evaluate the transient interaction of the jet and the bucket, transient analysis was completed using time dependent solver settings within ANSYS Fluent, with small time steps in order to adequately capture each transient hydraulic interaction that exists between the jet and the bucket's surface.

The results of the transient analyses provided detailed information regarding the following:

- The variation in dynamic pressure across the bucket surface
- The unsteady velocity distribution over the entire bucket surface
- Turbulence fluctuation in relation to jet and bucket surface interaction
- Vortex formation at and surrounding the jet as it impinges on the bucket and begins to separate from the surface.

As illustrated by the transient velocity contours, the continuous evolution of the developing water sheet occurred for each jet to bucket surface interaction. Initially, the jet impacted the splitter (wedge) section of the bucket and then separated and created two (2) symmetric jets that travelled over the bucket shape.

As shown in figure 5.16 the flow progressed from jet-to-bucket surface interaction, the resultant streamlines and velocity magnitudes varied over time, as a direct result of the "transient" fluid interaction from the jet and bucket surface interaction, creating "dynamic" redirection of the fluid's resultant path. On.

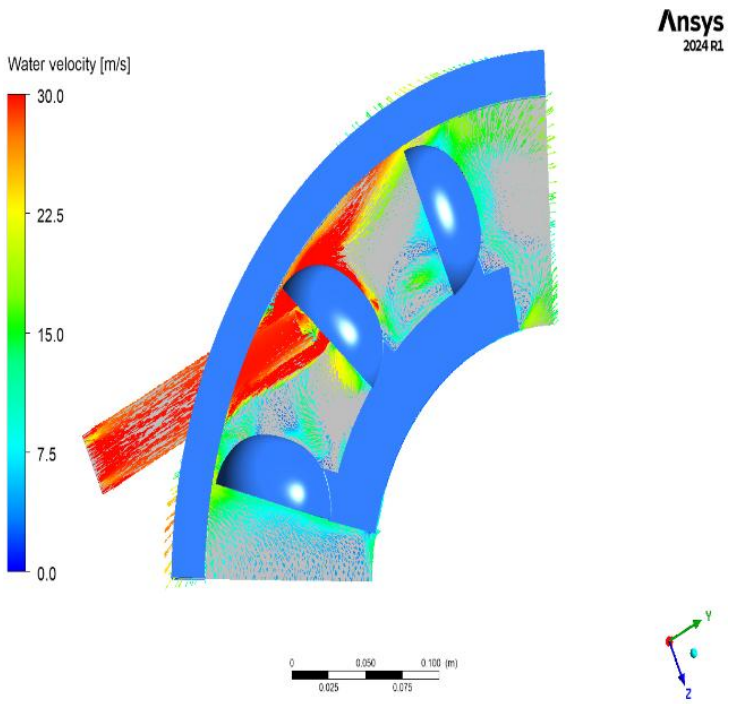

Figure 5.16 Transient Velocity Contours during Jet Interaction

Additionally, results of transient analysis indicate that high-velocity zones or regions developed around the splitter shortly after the jet hits the bucket. As water flows across the surface of the bucket, the speed is reduced due to the momentum transfer between flowing fluid and bucket surface.

In some cases, increased velocity fluctuation and localized turbulence generation occurred at the outlet curvature at higher inlet water velocities. The optimized geometry successfully maintained smooth flow attachment to most areas of the bucket surface.

Transient pressure distribution analysis as shown n figure 5.17 shows that there are fluctuation factors near the splitter and outlet sections of the bucket due to fluctuating hydraulic bottle.

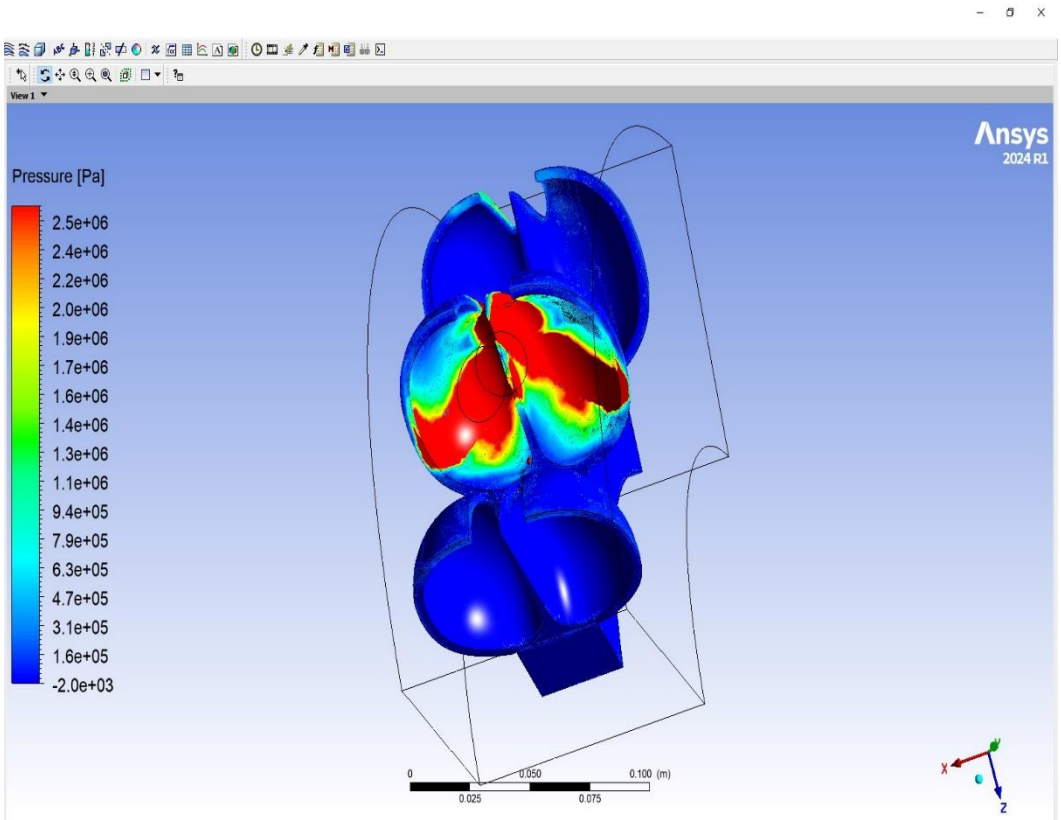

Figure 5.17 Transient Pressure Distribution inside Pelton Bucket

Maximum pressure occurred at the splitter region during jet-impact monitoring due to stagnation effects associated with very sudden deceleration of the jet. As the fluid moves around the bucket's curve, the pressure ultimately disappears at the outlet.

The pressure fluctuation results also include localized oscillation of pressure near the outlet of the bucket while operating under high-speed water flow conditions. Such oscillation is primarily caused by the formation of transient vortices and by the local separation of the fluid flowing in the bucket.

Figure 5.18 shows Streamline analyses also substantiate the dynamic development of the water-jet due to transient flow conditions.

The analysis of the streamline contours shows that the highly optimized bucket shape created a good smooth hydraulic guide and minimized water splash losses, even during transient conditions. However, there was limited vortex formation near the outlet curvature, with this occurring mostly under high velocity inlet jet flow conditions.

Transient CFD analysis also indicated that the splitter geometry is very important in preventing flow separation around the splitter and stabilizing the water sheet during dynamic jet interaction.

Finally, the volume fraction contours provided further depiction of the distribution of water flow in the bucket during the transient interaction of jet flow.

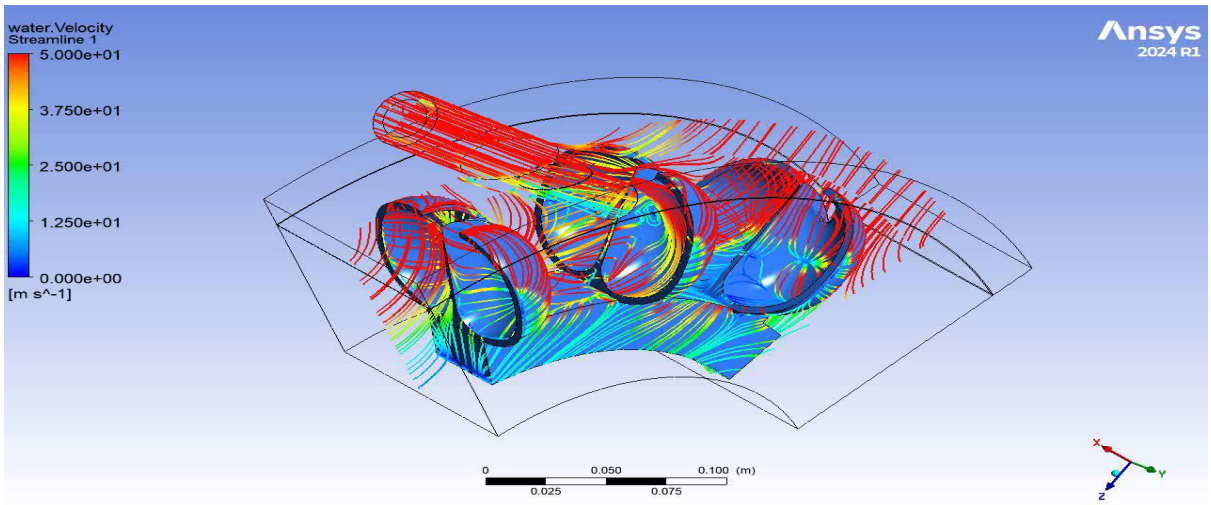

Figure 5.18 Transient Streamline Development during Bucket Rotation

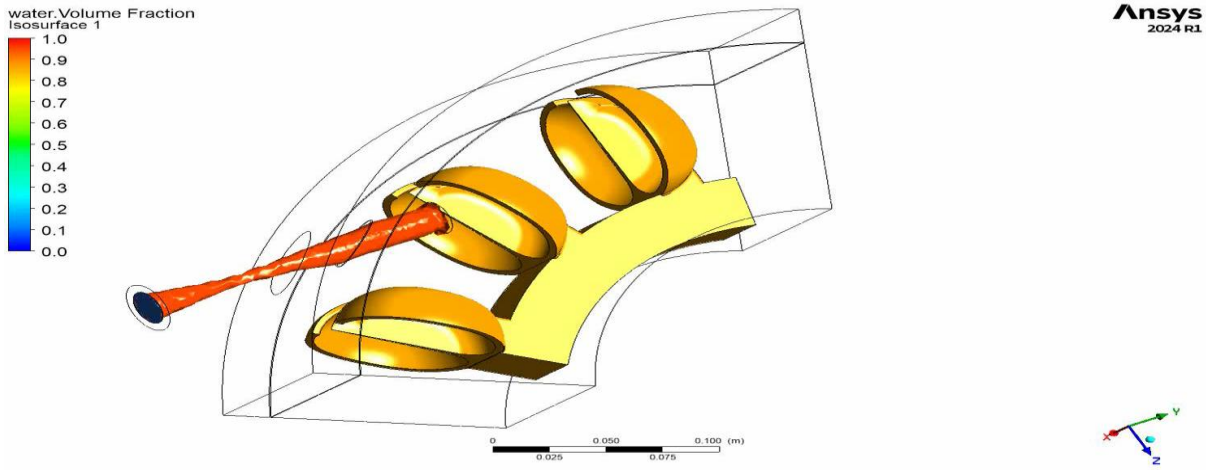

Figure 5.19 Volume Fraction Distribution during Transient Jet Interaction

The volume fractional results indicated in figure 5.19 an overall smooth filling and discharging action inside the bucket. In addition, the distribution of water on the bucket generally remained even on both sides of the bucket; thus, confirming effective jet bifurcation and balanced momentum transfer have occurred.

Residual convergence plots from the transient simulations also exhibited stable numerical convergence behavior throughout the entirety of the analysis.

Based on the convergence history shown in figure 5.20, it has been confirmed that the mesh density, turbulence model, and solver settings used in the CFD analysis were all chosen correctly and produced numerically stable and converging solutions.

The transient CFD analysis confirmed that the optimized Pelton turbine bucket geometry offered:

- stable transient hydraulic performance
- smooth redirection of water flow
- controlled development of turbulence
- reduced hydraulic losses

across the range of operating conditions typical for a micro-hydropower application.

Figure 5.20 Residual Convergence Plot for Transient CFD Analysis

5.7 Turbulence and Flow Behaviour Analysis

For the purpose of analysing the turbulence and flow behaviour within the Pelton turbine bucket that arise from the interactions between the high speed water jets and the bucket surfaces, a detailed analysis of, but not limited to, the characteristics of turbulence, streamlines, vortex generation and flow separation are required to enable an accurate determination of the performance of the turbine. In fact, the presence of excessive turbulence and unstable flow within the turbine bucket will significantly affect the efficiency of momentum transfer, resulting in increased hydraulic losses during the operation of the turbine.

The Computational Fluid Dynamics (CFD) analysis conducted as part of this research has provided a collaborative view of a number of parameters that influence the generation of

turbulence within the Pelton turbine bucket, including but not limited to, inlet jet velocity, splitter geometry, outlet curvature and flow redirection behaviour. Initial impacts of the water jet onto the splitter surfaces create a rapid change in velocity and pressure within that region resulting in localized turbulence in the vicinity of the impact zone. As the flow moves on to the inner circumference of the bucket surfaces, due to the smooth hydraulic guidance provided by the optimized bucket geometry, the level of turbulence gradually decreases.

CFD analysis of the streamline behaviour revealed the highly symmetrical bifurcation of the jet incoming from behind the bucket, resulting in two smooth streams flowing over the bucket surface. The optimized splitter geometry created a division of the jet and minimised the splashing loss during the hydraulic interaction of the incoming water jet on the bucket. The flow passed over the bucket in line with the curvature of the bucket, maintaining a smooth flow, and demonstrated stable momentum transfer characteristics throughout the entire passage.

CFD analysis also confirmed that the optimized bucket curvature results in fewer instances of abrupt changes in flow direction and prevents early flow separation from occurring in the bucket region. A minor amount of recirculation zones and vortex formation were created in close proximity to the outlet curvature under higher inlet velocity conditions. The decrease in the amount of flow separation demonstrated that the hydraulic guide has improved and that the kinetic energy from the incoming water jet is being used effectively.

Turbulence intensity increased dramatically within the Pelton turbine bucket with an increase in the inlet jet velocity. Typically, the flow was relatively stable with very little turbulence generated at lower inlet jet velocities and developed smoothly as the streamlines passed over the bucket. However, turbulence intensity and vortex formation increased significantly due to increased hydraulic interaction and higher momentum transfer rates, resulting in more turbulent flow.

According to the CFD investigation, there is high turbulence intensity in the area of the splitter due to the fact that the water jet entering the bucket strikes the splitter face first and then the water is separated into two streams. The sudden change in the pressure and velocity at the splitter face is the cause of the production of local turbulent kinetic energy and flow fluctuation behaviour close to the splitter face. As the water makes its way towards the outlet end of the bucket, the turbulence intensity is gradually reduced due to the fact that the bucket

has an optimised curvature which creates a smoother hydraulic path and provides controlled flow deflection. Figure 5.21 shows turbulence Intensity Distribution inside Pelton Bucket

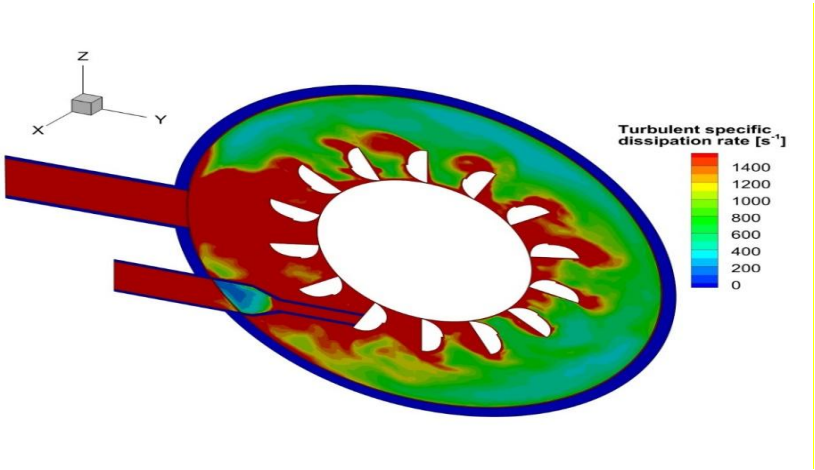

Figure 5.21 Turbulence Intensity Distribution inside Pelton Bucket

Turbulence Intensity Distribution Inside A Pelton Bucket shows that, although there is an increase in turbulence at the higher operating conditions, the optimally designed Pelton turbine bucket geometry can effectively control flow instability and produce a smooth hydraulic path for flow to be guided during the entire interaction process with the bucket. Thus, the analysis of turbulence and flow behaviour have confirmed that the optimally designed bucket configuration will provide consistent and stable hydraulic performance, minimal flow separation, maximum momentum transfer, and minimal hydraulic losses over a range of operating conditions.

5.8 Hydraulic Performance Assessment

Using results obtained through computational fluid dynamic studies, this study assesses the hydraulic performance of the optimized Pelton turbine bucket. The primary focus of the assessment was to evaluate the following parameters: the momentum transfer characteristics, pressure distribution, velocity variation, turbulence behaviour and flow redirection capability of the developed bucket geometry under different inlet jet velocity conditions.

Effective conversion of the kinetic energy in the water jet into mechanical energy via a good jet-bucket surface interaction is the determining factor in the hydraulic performance of Pelton turbines.

According to the CFD analysis, it was found that the bucket geometry allows for a smooth hydraulic interaction between the incoming water jet and the bucket surface and effective bifurcation of the incoming water jet into two symmetrical flows with minimal splash losses

and with streamlined behaviour. The symmetrical flow distribution defined during the simulations confirmed that the bucket geometry was able to make full use of the hydraulic energy available in the incoming jet and maintain balanced momentum transfer through-out the interaction process.

Hydraulic energy extraction from water, through the attachment of a new bucket to a turbine, was found to be improved by redesigning the bucket curvature to direct incoming flow to the outlet region of the turbine while also establishing a continuous, stable contact point with the bucket surface. Continuous contact between the water jet and the bucket surface allows for an extended time period of momentum transfer, thereby improving the utility of kinetic energy extracted from a water jet through an extension of the time period during which the water jet is in contact with the bucket. Cross-sectional velocity distribution data along the bucket curvature confirmed that momentum from the water jet flowed effectively into the turbine runner as evidenced by a smooth reduction of velocity magnitudes over the arc length of the bucket curvature.

The results of the analysis of pressure distribution within the bucket also confirmed the effectiveness of the bucket's configuration for hydraulic energy extraction. The maximum magnitude of pressure development occurred at the split of the water jet, as a result of direct jet impact and rapid deceleration of the water flow entering the bucket. The pressure began to decline toward the exit region of the bucket as a function of transferred momentum, due to the water exiting the hydraulic system. A smooth pressure gradient throughout the bucket confirms that the bucket was supported by stable hydraulic loads, and that the risk of excessive localized pressure fluctuations during operation was minimized.

Through CFD simulations of the refined splitter design, hydraulic losses due to surface splashing, sudden separation of fluid, or unpredictable streamline behaviour was found to be minimised. At high inlet velocities, small amounts of vortex creation or local turbulence could be found adjacent to the outer curve of the bucket. The reduction in the amount of turbulence intensity and improved control of flow behaviour indicated that there would be increased stability on a hydraulic basis and better transfer of available energy from jets to turbine runners before water leaves the bucket.

The CFD analysis not only supported the effectiveness of the splitters as an effective reduction of the residual velocity in the water stream but also supported the finding that residual exit velocity is an indicator of good hydraulic efficiency; where larger amounts of

kinetic energy found in the water jets will be transferred to the turbine runners before water leaves the bucket. Therefore, the CFD analysis of the buckets validated their hydraulic efficiency for micro-hydropower energy production.

In addition, the hydraulic performance assessment demonstrated that increasing inlet jet velocity will increase hydraulic loadings, increase turbulence intensity, increase pressure within the bucket area; however the streamlined behaviour of the buckets would maintain its stability and allow effective transfer momentum to the turbine runners, even in increased operating conditions. Finally, the streamlined shape of the buckets and their optimally designed splitter showed that they effectively controlled the instability of fluid during operation and therefore had less potential for excessive hydraulic losses during operation.

The CFD analysis has confirmed that the optimized outlet geometry allows for smooth water discharge from the bucket region with limited recirculation and disturbance of flows. The outlet flow characteristic is critical for Pelton turbine applications, since excessive residual turbulence or recirculation could result in a loss of hydraulic efficiency and additional energy losses during operation.

The hydraulic characteristics determined from CFD investigation show good agreement with the theoretical operating characteristics of Pelton turbines. The pressure distribution, streamline behaviour and momentum transfer characteristics generated by the present investigation indicate that the developed bucket geometry is capable of producing stable hydraulic performance and efficient energy conversion at various operating conditions.

The hydraulic performance assessment confirms that the optimised bucket geometry developed for Pelton turbines provides efficient momentum transfer, stable pressure distribution, controlled turbulence behaviour, reduced hydraulic losses and smooth flow redirection characteristics. The newly developed bucket configuration is therefore suitable for high-head micro-hydropower applications requiring stable hydraulic performance and improved turbine efficiency.

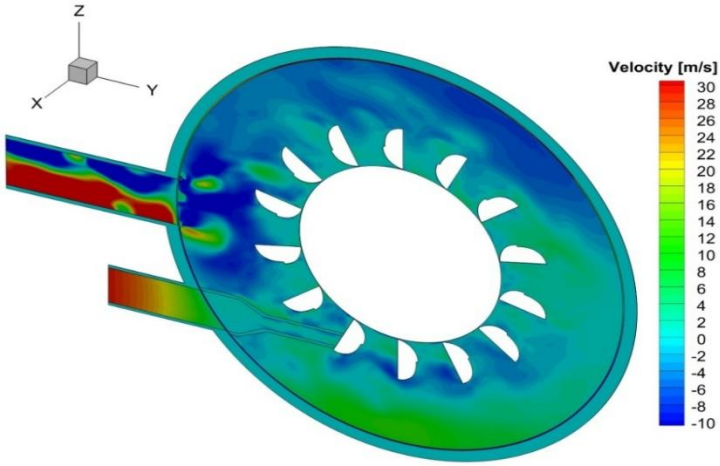

Figure 5.22 Comparative Hydraulic Performance for Different Inlet Velocities

5.9 Validation and Discussion

To validate the Computational Fluid Dynamics (CFD) investigation that was performed in this study, a direct comparison of CFD-generated numerical flow behaviour, pressure distribution patterns, turbulence development patterns, and hydraulic interaction patterns was performed against the theoretical operational parameters of Pelton turbine cases and previously published CFD studies in the literature. Validation of CFD results is critical for confirming that the numerical accuracy, reliability, and hydraulic applicability of the developed CFD model is what needs to be considered when predicting flow behaviour within the Pelton turbine bucket[17].

The numerical investigation completed in the current work indicates that a high-velocity water jet impinges the splitter region before splitting (dividing) into two equal flow streams flowing over each surface of the bucket. This is very similar to the hydraulic flow behaviour reported in previously published literature of numerical and experimental investigations of Pelton turbine systems, where maximum hydraulic loading and pressure development occur in the splitter region as a result of the direct jet impact. Therefore, based on the current work's findings regarding streamline distribution and pressure contours, there was good correlation with what would be expected from impulse turbine hydro\hydraulic parameters.

Furthermore, based on the CFD data results, it is verified that the highest static pressure will be at the splitter area, and also that lower static pressure will be located on the outlet curvature of the bucket. Both types of static pressure distributions are consistent with the

theoretical concept of momentum transfer mechanisms of Pelton turbines, whereby the kinetic energy from the incoming water jets is gradually transferred to the bucket while the water is redirected in-flow through the buckets. The steady reduction in velocity (speed) of the water along the bucket curvature, which has been observed in this CFD study, strengthens the argument that the designed bucket contours will efficiently utilize the available hydraulic energy from the incoming water jets.

As evidenced from the CFD simulations performed, streamlines align with the surfaces of the bucket to promote smooth continuous flow, with only minor disturbances (i.e. separation) being caused in the development of turbulence. The design of the optimized splitter will minimize any unwanted splash loss and maintain a symmetrical bifurcation of the incoming water spray. Similar flow characteristics have been identified in previous studies using CFD methods on Pelton turbine buckets, whereby the use of optimized bucket curvature and splitters resulted in significant improvements in hydraulic efficiency and momentum transfer characteristics.

The Experimental results also revealed good agreement with the expected turbulent hydraulic flow when examining the distribution of turbulent intensity due to Impulse Turbines in this study. Turbulent intensity was greatest near the splitter and in the outflow curvature area at the time of jet interaction due to rapid change in pressure and velocity. However, the turbulent intensity decreased gradually as the water travelled towards the outflow due to smooth hydrodynamic guidance provided by the optimised bucket shape. Furthermore, the controlled turbulence created during the CFD analysis supported the hydraulic stability of the developed bucket configuration.

The previous grid independence study performed during this study confirmed the numerical accuracy of the computational model used in the study. The pressure and velocity results obtained from different mesh configurations showed no significant difference outside the chosen mesh density thus confirming numerical convergence stability and mesh independence. As a result, a recommended degree of mesh refinement would give accurate predictions of hydraulic parameters within the computational domain.

The numerical simulations provided evidence of the convergence properties supporting the CFD solutions' reliability and stability. Reduction in residuals of continuity, momentum, and turbulence equations (and therefore the equation iterations) were stable throughout the iterative computation process. Furthermore, visalisation of the convergence process showed

that there was an adequate configuration of the selected solver, turbulence model, and numerical discretization methodology to accurately predict hydraulic flow characteristics within the Pelton turbine bucket. The numerical results of the current investigation also produced reasonable agreement to the previously published studies implementing either structural or hydraulic testing of Pelton turbine bucket systems. The bucket design successfully maintained a smooth streamline distribution, consistent pressure variations, and effective momentum transfer regardless of the inlet velocity of the water jet. The CFD study also corroborated that the optimized bucket design would minimize hydraulic losses due to flow separation, splash formation, and excessive turbulence generation during operation.

The hydraulic performance characteristics of the developed bucket designed during the current investigation further validate the appropriateness of the optimized outlet angle and curvature selected during the previous design optimisation. The reduced residual exit velocity and stable streamline behaviour demonstrated throughout the CFD simulations indicate an increase in hydraulic efficiency and an increase in effective use of the kinetic energy contained in the incoming water jet.

The CFD analysis thus verified that the bucket configuration of the Pelton turbine will give reliable hydraulic functionality as well as steady operation regardless of the varying velocities of supply jet used. The numerical simulation demonstrated the ability to accurately predict the velocity profiles, pressure distributions, turbulence characteristics, streamline behaviour and momentum transfer within the bucket design with adequate numerical stability and convergence properties.

In conclusion, through the verification and discussion provided by the CFD analysis, it is established that the computational model developed for the Pelton turbine and the optimally developed bucket geometry are appropriate for accurate predictions of hydraulic performance and efficient conversion of energy produced at micro-scale by a Pelton turbine in micro hydropower applications.

5.10 Results and Discussion

ANSYS Fluent was utilized for the purpose of conducting detailed computational fluid dynamics (CFD) studies on the hydraulic flow properties of an optimized Pelton turbine bucket at various operating parameters. The CFD simulations provided a complete visualization and analysis of how the velocity distribution, streamline characteristics, pressure variations, turbulence growth, interactions of the water jet, and transient hydraulic

characteristics are represented within the bucket geometry as the turbine is running. The CFD modelling would allow for an evaluation of how effectively the optimized bucket profile performs in terms of increased hydraulic efficiency, smooth flow attachment, and reduced hydraulic energy losses.

The numerical simulations were conducted using inlet jet velocities between 15 m/s and 58.7 m/s in order to compare the hydraulic response of the newly developed bucket geometry at different operating conditions. Steady state and transient CFD analyses were performed utilizing the standard turbulent flow mixing model known as k-ε, as it has a stable numerical character and has been proven useful for modelling high Reynolds number flow conditions associated with Pelton turbine application. To ensure complete documentation of the hydraulic interaction process that occurs within a turbine during its operation, the computational domain consisted of the nozzle region, water jet interaction zone, bucket flow passage, and outlet discharge region.

During this analysis, we had the CFD mesh employed for the purposes of our analysis comprised a high level of refinement (subdivision) with improved mesh density used in the regions around the splitter, as well as where the jet hits the surface and along the curved surface of the outlet where high pressure and large velocity gradients have been formed as a result of hydraulic interaction. This refinement of the numerical discretisation also allowed for accurate modelling as illustrated in figure 5.23 of the flow separation behaviour, turbulence development and momentum transfer characteristics of flow within the bucket geometry.

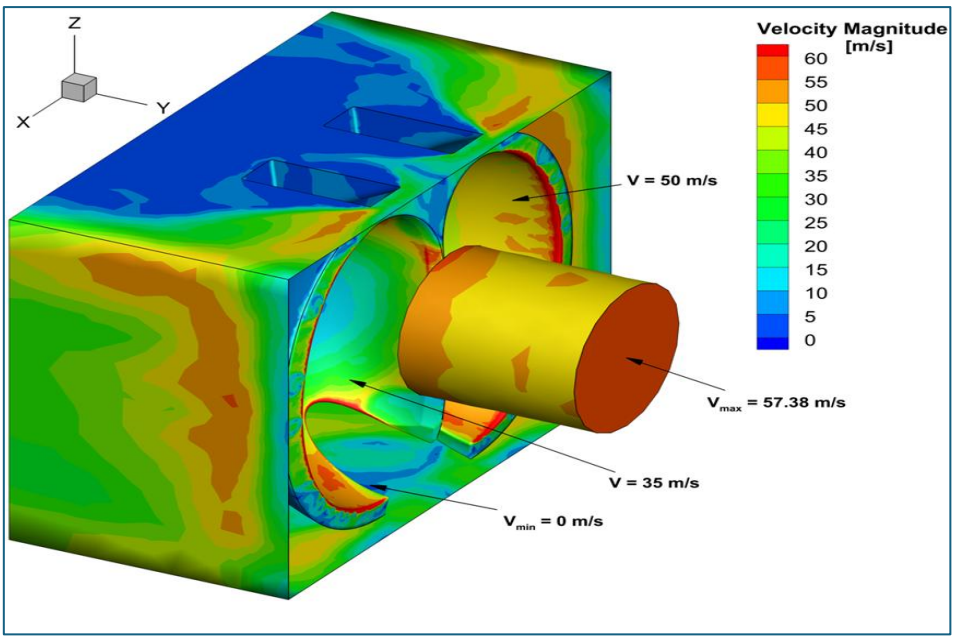

Figure 5.23 Velocity Contours inside Optimized Pelton Turbine Bucket

CFD analysis provided maximum fluid velocity contours and streamline distribution that indicate maximum fluid velocities developed near the nozzle's discharge exit and at the location of the splitter's interaction with the incoming jet of water. The jet had the highest kinetic energy as it exited the nozzle. This results in high-velocity concentrations at the splitter's tip and the impact location of the incoming water jet. After striking the splitter section, the jet divided symmetrically and flowed smoothly down the bucket's contour to the outlet region.

Furthermore, the CFD analysis revealed a gradual decline in fluid velocity along the bucket's surface due to ongoing momentum transfer from the water jet to the rotating runner. The reduction in jet velocity indicates that the hydraulic kinetic energy has been successfully converted to useful mechanical rotational energy. The optimized bucket shape directed the water jet over the shape of the bucket with stable attachments from the jet to the bucket at all locations along the surface. The streamlines followed the contour of the bucket shape and confirmed that the optimized bucket shape is effective in minimizing hydraulic losses because there is no sign of excessive flow separation or abrupt changes in flow direction.

Although the flow characteristics with inlet velocities below 20 m/s were relatively consistent in terms of smooth streamline attachment as shown as figure 5.24 and low turbulence generation through the bucket passage, the flow characteristics changed dramatically when inlet jet velocities approached 45 m/s to 58.7 m/s due to the rapid transfer of momentum between the water jet and bucket surface. The result was increased flow turbulence intensity

and localized vortex formations near the outlet curvature regions as a result of the increased volumetric discharge rate and more intense hydraulic interactions occurring in the vicinity of the bucket surface when the water jet contacted the bucket surface at these higher velocities.

At the same time that flow turbulence intensity increased with increasing velocity at the inlet jet, the optimization of the bucket geometry successfully maintained continuous flow attachment on most of the bucket surface and reduced excessive splash losses to the surrounding environment. The analysis of the streamline behaviour also confirmed balanced bifurcations of the water jet (i.e., symmetrical) and balanced hydraulic loading distributions on each side of the bucket surface, which is important for minimizing structural loading (i.e., vibration) during turbine operation. Therefore, the smooth/more stable streamline guidance demonstrated during the present study supports the effectiveness of the proposed bucket geometry for improving hydraulic stability of flow and providing better energy transfer characteristics.

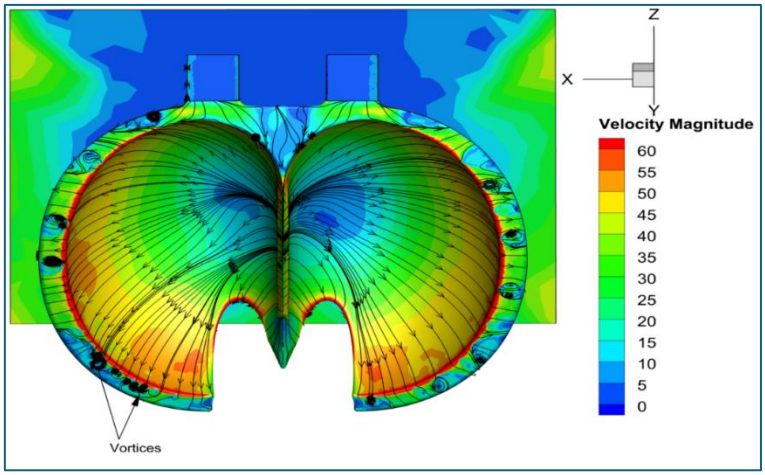

Figure 5.14 Streamline Distribution during Water Jet Interaction with Bucket Surface

The distribution of velocity vectors was found to be a smooth, well-guided flow with controlled jet interaction within the bucket cavity. The orientation of the vectors indicated that as the water jet travelled across the bucket surface, there was no immediate reversal in flow direction or large recirculating zones. The optimized splitter profile was able to split the incoming water jet into two nearly symmetrical streams with less hydraulic instability and improved momentum transfer effectiveness during operation.

Further analysis showed in figure 5.25 that the optimized bucket shape successfully reduced undesirable flow separation in the splitter and outlet regions. Flow separation creates problems such as increased hydraulic losses, higher levels of turbulence, and lower turbine

efficiencies; therefore, because of the smooth distribution velocity through the velocity field analysis, the developed runner geometry has been determined to be hydraulically suitable as a micro-hydropower runner.

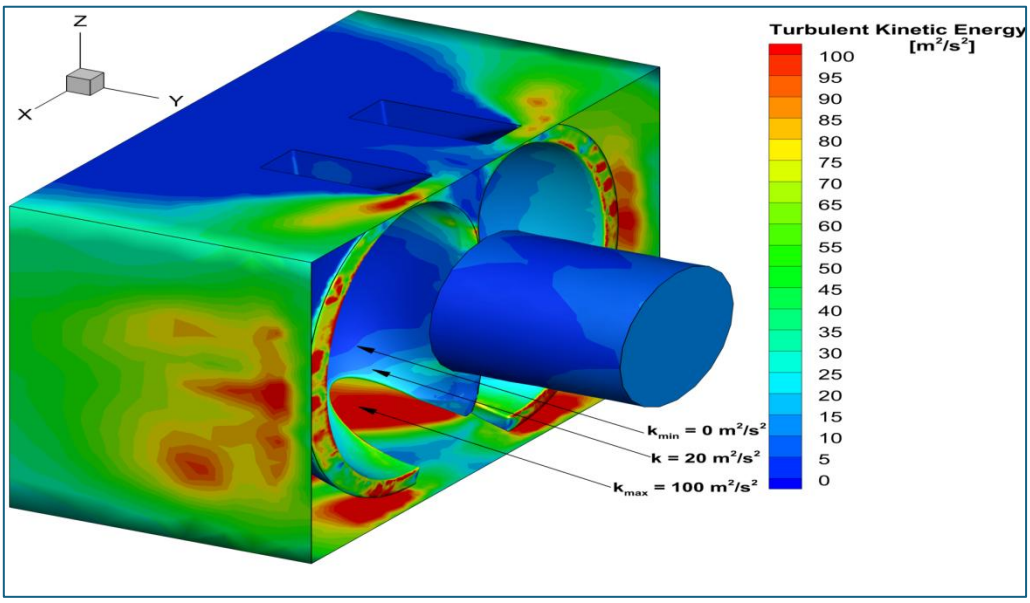

Figure 5.25 Turbulent Kinetic Energy Distribution inside Pelton Bucket

Turbulent kinetic energy contributing the most to the development of turbulence occurred primarily at the edges of the splitters where the jet impacted and at the curves of the bucket on the outlet side. Turbulent kinetic energy was produced at the greatest levels due to high fluctuations of velocity and large amounts of momentum transfer during hydraulic interaction. The turbulent intensity diminished over the bucket surface as it neared the outlet region, primarily as a result of the optimized curvature of the bucket providing stable water flow and limiting abrupt changes in direction of flow within the bucket.

CFD results also showed that the turbulence intensity increased as the incoming jet velocity increased. Higher velocities produce greater shear forces between differing layers of water and form small vortices immediately next to the bucket surface. This increased turbulence was concentrated in localized areas at the splitter and the outlet curve of the bucket and did not disperse throughout the entire bucket. The localized turbulence verified that the optimized bucket profile had controlled hydraulic instability and prevented excessive vortex development during operation.

A well-defined turbulence distribution as shown in figure 5.26 also assisted in maintaining hydraulic stability across the entire bucket surface and in minimizing undesirable oscillations in the flow. Thus, the optimized bucket geometry provided for improved hydraulic stability

throughout the flow of water and reduced the energy losses associated with uncontrolled development of turbulence within the bucket.

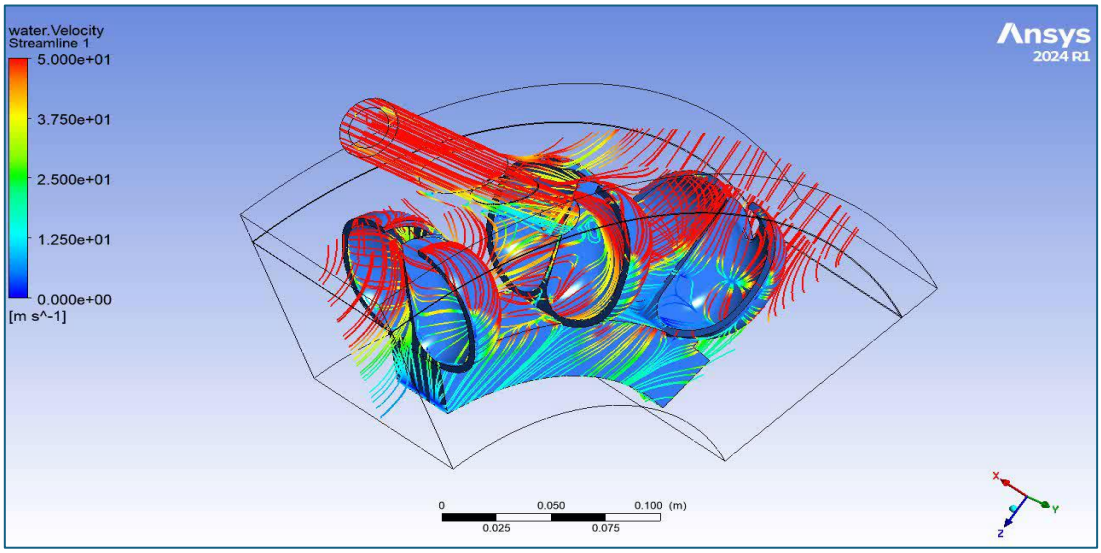

Figure 5.26 Transient Velocity Distribution during Jet Interaction

Results obtained from a CFD study into the pressure and velocity response of the prototype Pelton turbine, confirmed that the water jet's incoming overall velocity was converted, by the bucket of the Pelton turbine, into force or torque by rotating mechanical energy and also that the output produced by the Pelton turbine, has smooth hydraulic interaction and stable flow attachment. These results also demonstrate that the optimized runner design exhibits exceptional hydraulic performance, which is ideal for use in high-efficiency micro-hydropower applications.

The CFD results obtained during the entire investigation, also confirmed that the use of an optimized bucket design will result in improved jet deflection, improved momentum transfer efficiency, improved flow attachment performance, and improved hydraulic stability compared to conventionally designed runner configurations. The results from the CFD numerical analysis verified the hydraulic efficiency of the optimized Pelton turbine runner and revealed significant insight into the internal flow characteristics that have resulted in superior Pelton turbine performance than additional experimental investigations and will be further discussed later

5.11 Closure

A computational model of the optimized Pelton turbine bucket was developed in SolidWorks® and imported into ANSYS Fluent. The computational domain comprised four regions: nozzle flow, jet interaction zone, bucket surface, and surrounding fluid. Tetrahedral

mesh elements were employed for domain discretization, with mesh independence and convergence studies confirming numerical stability and solution accuracy.

Steady-State Analysis revealed that jet impingement occurs directly at the splitter, bifurcating into two symmetric streams across the bucket curvature. The optimized splitter geometry minimized splash losses and ensured smooth flow division. Velocity contours confirmed progressive momentum transfer from jet to bucket surface, while peak static pressure was localized at the impingement zone, decreasing toward the bucket exit.

Transient Analysis identified unsteady hydraulic phenomena including time-variant pressure/velocity fields, vortex formation, and turbulence-induced instabilities at elevated inlet velocities. The optimized bucket geometry effectively suppressed excessive turbulence development and flow separation throughout the operation.

Turbulence & Flow Characteristics demonstrated increasing turbulence intensity with inlet jet velocity; however, the optimized splitter and outlet radius geometry maintained controlled flow conditions, reduced hydraulic losses, and sustained smooth streamline development.

Hydrodynamic Performance Metrics confirmed efficient momentum transfer, stable pressure distribution, minimal residual exit velocity, and controlled turbulence across varying operating conditions.

Validation against theoretical Pelton turbine characteristics and published literature showed strong agreement, confirming model reliability.

The optimized bucket geometry achieves stable hydraulic performance, efficient energy conversion, and reduced flow losses, confirming its suitability for micro-hydropower Pelton turbine applications across a range of inlet jet velocities.

Chapter 6 Development and Experimental Investigation of Pelton Turbine

6.1 Introduction

Experimental investigation is a key tool for validating the numerical and analytical investigations that are performed throughout the design and optimization of hydraulic turbines. While computational methods including Finite Element Analysis (FEA) and Computational Fluid Dynamics (CFD) can provide a more complete understanding of how the structure will behave and/or the way fluids will flow around it, it is also important to perform experimental analysis to determine how well the turbine system will actually operate under true working conditions. Experimental investigation will also allow one to validate numerical predictions concerning hydraulic efficiency, shaft power generation, rotational stability and operational reliability of the Pelton turbine system.

In this chapter, the focus will be on the fabrication, assembly and performance evaluation (through experimentation) of the optimized Pelton turbine that resulted from the current research. The goal of the experimental investigation was to validate the effect of the more advanced bucket geometry on the performance characteristics of the Pelton turbine throughout a range of operating conditions. The experimental work included fabrication of the optimized Pelton buckets, construction of an assembly to hold the runner in place, balancing of the runner system, setting up the experimental test system, installing instruments and calibrating test equipment, and performing testing of the Pelton turbine under a number of different operating conditions.

The fabrication and experimental investigation of the optimized bucket shape covered in previous chapters was conducted using CFD and structural analyses. The bucket was optimized to enhance the amount of hydraulic energy transfer, flow guidance, rotational stability and overall turbine efficiency during turbine operation.

The fabricated runner assembly was tested under controlled laboratory conditions with a dedicated experimental setup for the Pelton turbine. The experimental setup facilitated the measurement of discharge, hydraulic head, rotational speed, shaft power and hydraulic efficiency for the micro-hydropower applications of the Pelton turbine.

In conclusion, the current chapter demonstrates the experimental validation and practical implementation of an optimized Pelton turbine for micro-hydropower applications.

6.2 Fabrication of Buckets and Runner

Careful attention paid to the development of the Pelton turbine bucket/running assembly during its fabrication will help ensure that the dimensions are accurately made, that guidances for the hydraulic flows into and out of the bucket are correct, that structural stability is maintained while being tested, and that the runner functions smoothly when turning during the test with the turbine in full load conditions. Many bucket's performance is highly reliant on how the bucket geometry and flow interact so special care was taken when fabricating the components to produce an optimized profile whose characteristics were defined during the numerical investigation phase of the project. The fabrication of the Pelton runner as a complete system consisted of manufacturing the optimized bucket geometry, assembling the runner system, machining the bucket profiles, mounting the buckets onto the runner disc, and installing the components of the completed Pelton runner system together.

The bucket designs obtained from both the structural and CFD studies were translated into shapes that can be fabricated. In order to achieve efficient momentum transfer from the water jet to the runner assembly, a significant amount of time and detail was spent ensuring when the incoming water jet transitions at the splitter region, the jet bifurcates smoothly into two streams that flow over the surface of the bucket. Because the initial impact of the incoming water jet occurs at the splitter, significant design consideration was given to the splitter itself, as improper design will result in severe hydraulic shock, splash losses, uneven distribution of pressure along the surface of the bucket, and a reduction in turbine efficiency. Consequently, extreme care was exercised with regard to the dimensional accuracy of the splitter profiles during the fabrication of the buckets. Figure 6.1 and figure 6.2 illustrates a fabrication drawing of a conventional and enhanced Pelton turbine bucket respectively.

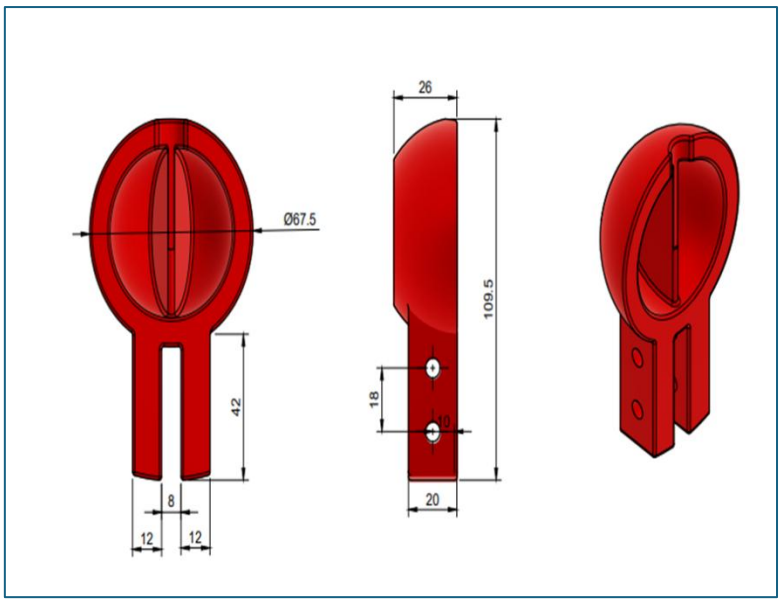

Figure 6.1 Fabrication drawing of Pelton turbine bucket

Conventional machining methods were employed to manufacture a traditional Pelton bucket and provide a means by which to compare all of the test buckets versus their performance. The geometry in the test buckets of a conventional Pelton bucket was simpler curved surfaces and had a typical splitter configuration. However, during testing, traditional Pelton buckets typically have greater hydraulic losses due to a lack of jet flow control and localized turbulence generation behind the splitter / at the outlet.

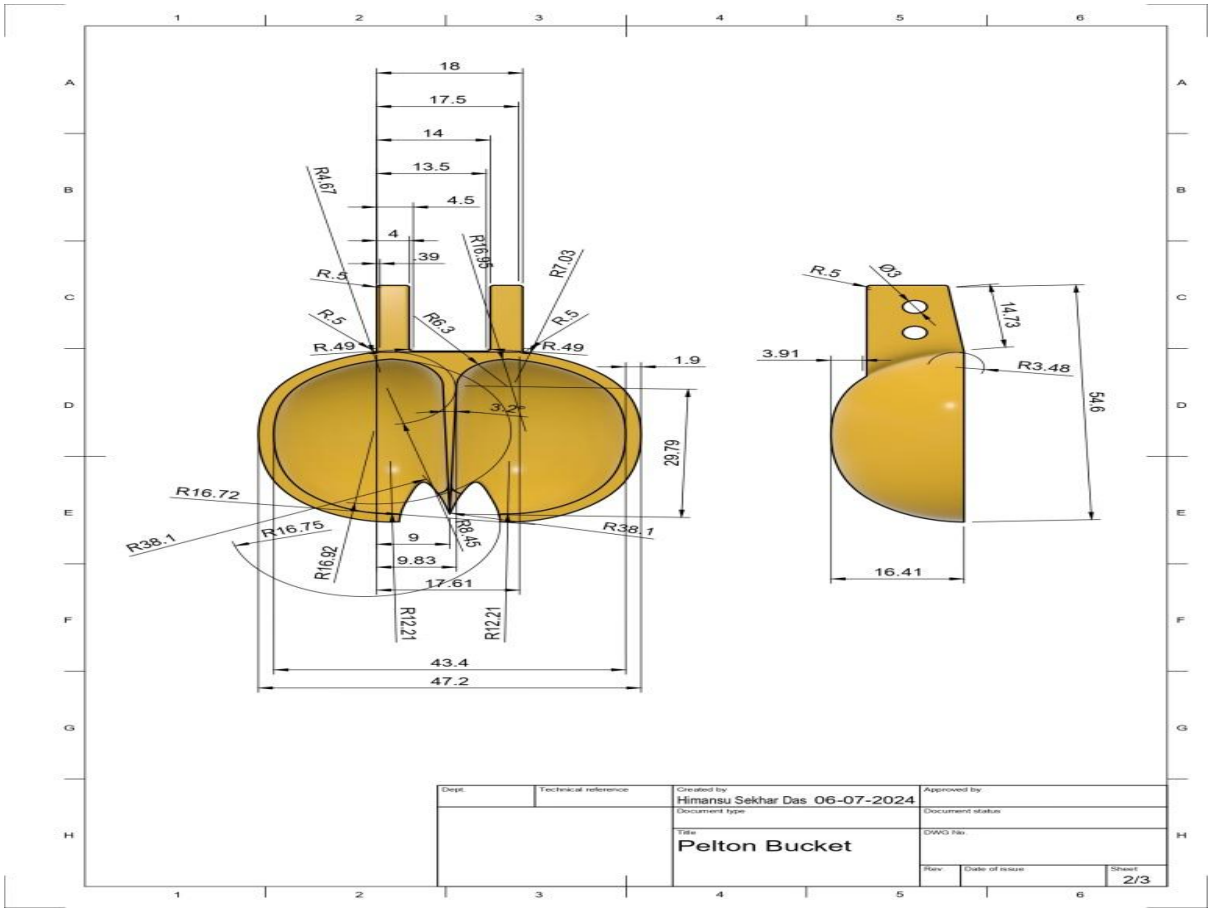

Figure 6.2 Fabrication drawing of enhanced Pelton turbine bucket

An improved Pelton bucket design was created using complex geometries that were intended to increase the efficiency of flow and momentum transfer characteristics through the proper geometry of the buckets. Because of the complexity and difficulty in accurately reproducing the optimized geometry produced by numerical analysis, the bucket needed to be fabricated with the highest precision and completed with careful surface finishing to ensure that the enhanced bucket that was ultimately manufactured would retain all of the design characteristics of the optimized bucket.

During the manufacturing process of the enhanced bucket, careful attention to the shape and machining of the bucket's surfaces was taken in order to accurately maintain the optimized geometrical dimensions derived from the original design. The splitter portion of the bucket was manufactured with the highest dimensional tolerances because even small miscalculations of splitter geometry would cause significant changes to the hydraulic load response and efficiency of energy transfer. The bucket's surfaces were machined with great care to ensure that the transition of curvature was smooth between the splitter, the central portion of the bucket, and the outlet curvature. The smooth transition of geometry is essential;

as abrupt irregularities in the surfaces of the bucket can create turbulence, hydraulic instability, and energy dissipation during operation of the turbine.

Machining operations were finished by machined bucket surfaces were polished to decrease the amount of surface roughness and reduce hydraulic friction losses during the interaction between the water jet and buckets. The surfaces of hydraulic turbines are finished as a critical factor influencing performance due in part to the turbulence generated by rough surfaces (increased turbulence) resulting in increased flow separation, and energy is dissipated along the surface of a bucket. By having a smooth bucket surface it provides a greater hydraulic attachment and thus a more effective transfer of momentum from the water jet to the runner assembly. Figure 6.3 illustrates the fabricated bucket geometry drawing.

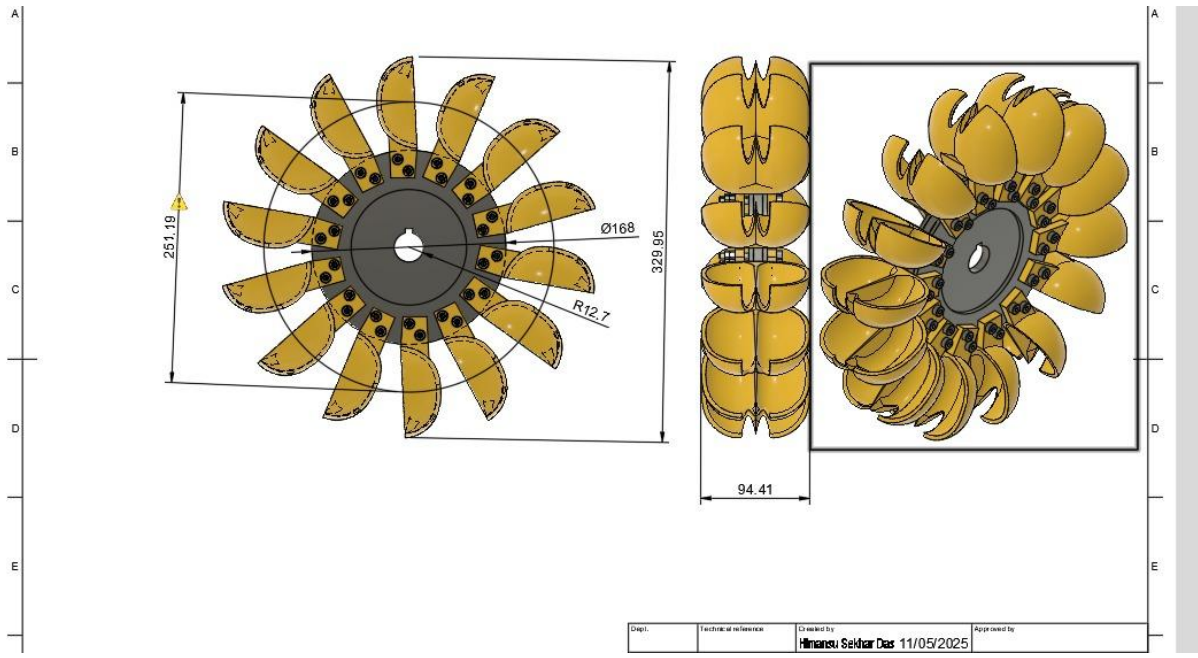

Figure 6.3 Fabricated bucket geometry drawing

The manufactured bucket geometry exhibited satisfactory dimensional accuracy and surface finish over the regions of splitter, bucket curve and outlet surfaces. The splitters' optimized component profile and the corresponding increased curvature, as established during numerical analysis, have been accurately reproduced through fabrication; thus, the experimental assessment of the produced bucket geometry can be completed reliably.

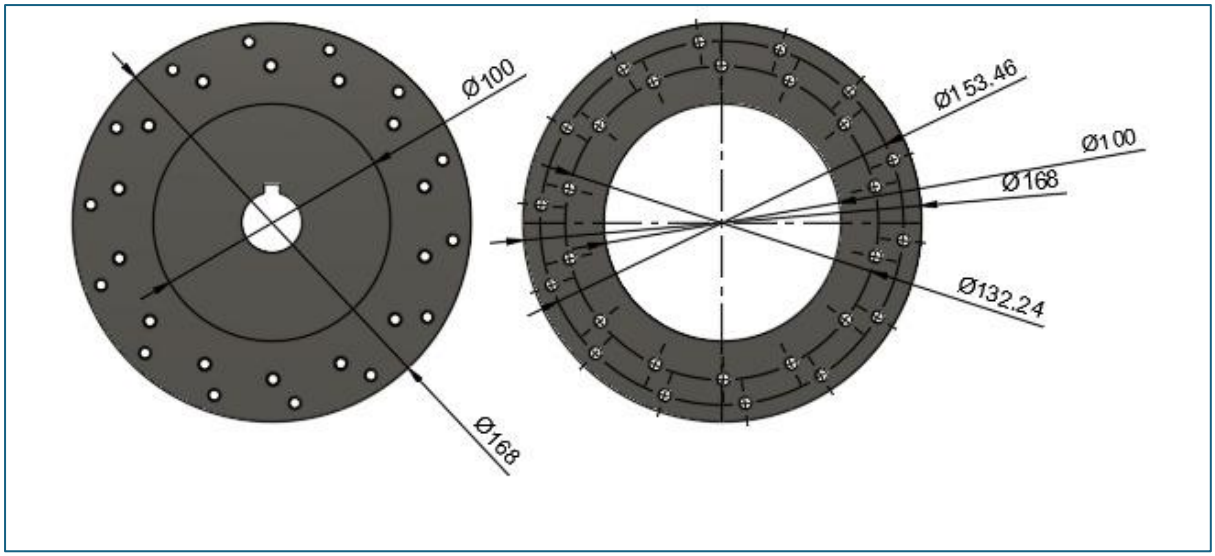

Figure 6.4 Fabricated runner with mounted buckets

After the individual bucket fabrication was complete, the runner disc as shown in figure 6.4 was prepared for mounting the bucket assemblies. Proper mounting was established in order to achieve an uniform spacing between the bucket assemblies and therefore to ensure stable behaviour of the runner during operation. Accurate positioning of the buckets around the perimeter of the runner is very important to avoid problems such as rotational imbalance, uneven hydraulic loading, vibration; and loss of turbine efficiency due to incorrect spacing.

The structural rigidity and dimensional stability of the finished runner assembly were verified to be acceptable after the completion of the mounting process. The mounting system also provided for proper load transfer between the bucket assemblies and the runner disc during hydraulic loading conditions. Thus, the finished runner provided an appropriate platform for conducting further balancing, instrumentation, and performance evaluation testing of the Pelton turbine system.

6.3 Parametric Comparison of Conventional and Enhanced Bucket

To assess how effective the improved Pelton bucket design produced as part of this study is, there was a thorough comparison made between it and the traditional bucket. The main emphasis was placed on comparing various aspects of the new design such as the shape of the splitter, curvature of the bucket, style of discharge and how water is redirected.

The purpose for these design changes was to provide better hydraulic energy transfer, reduce flow separation losses, minimize water spray, and increase the overall hydraulic performance of the Pelton turbine. The traditional Pelton bucket designs mainly use standard splitter curves and bucket curves that have been used in traditional micro-hydro systems for many

years, which have proven to work with acceptable levels of hydraulic efficiency. However, traditional designs have many issues with hydrodynamic losses due to incorrect jet division, flowing away from the bucket, turbulence due to jet motion, and incomplete momentum transfer during operation. Because of this, once the new design has been established, further improvements in hydraulic efficiency and energy conversion efficiency can only be made by improving the bucket design itself. Figure 6.5 shows both types of buckets.

(a) **(b)**

Figure 6.5 Conventional (a) and enhanced Pelton (b) bucket geometry comparison

This research study resulted in the creation of a new bucket design that features an improved curvature transition and improved splitter shape which allows for better hydraulic interaction between the incoming water jet and the inner surface of the bucket. Additionally, the new bucket design provides for a smoother bifurcation of the jet into two equal streams as both streams enter and exit the bucket. A smooth bifurcation is critical since an improperly designed splitter will produce hydraulic shocks, unstable jets, splashing losses and unequal distributions of pressure within the bucket.

The new bucket design exhibits a smoother curvature transition on the inside surfaces of the bucket than a standard bucket design. A smoother curvature will enhance the flow of the jet over the inner surface of the bucket, thus reducing the likelihood of premature separation of the jet as it flows over the bucket. The improved attachment of the water stream to the inside surfaces of the bucket will increase the time that the jet interacts with the inside of the bucket which enhances the transfer of momentum from the water jet to the bucket and the

conversion of this energy into rotational energy within the turbine. Typical bucket designs often produce turbulence and residual kinetic energy loss (also known as a loss of velocity) during water discharge from the bucket surface when there is an abrupt transition from one shape to another or when the curvature is not designed correctly. Table 6.1 shows Parametric comparisons of conventional and Enhanced bucket.

Table 6.1 Parametric comparison between conventional and enhanced bucket

Sr. No.	Parameter	Designation (Units)	Conventional	Enhanced
1	Bucket width	B (mm)	68	94
2	Bucket length (inner)	L (mm)	55	86.8
3	Bucket depth	T (mm)	26	32.42
4	Bucket thickness	t (mm)	8.5	5
5	Bucket inclination angle	α (°)	20	20
6	Bucket tip (splitter) inlet angle	β_1 (°)	12	15
7	Bucket Middle Exist angle	β_2 (°)	12	15
8	Front outlet angle	β_3 (°)	12	15
9	Back outlet angle	β_4 (°)	12	15
10	Splitter thickness	t_s (mm)	3	3.2
11	Splitter length	L_s (mm)	16	17.61
12	Cut-out width	w (mm)	7.5	9
13	Cut-out depth	d (mm)	9	9.83
14	Main cup radius	R (mm)	36	38.1
15	Inner cup radius	R_i (mm)	15	16

16	Mounting hole diameter	Ø (mm)	3	3

With the properly optimized outlet profile (the outlet geometry), these types of losses have been reduced considerably, thereby facilitating a smoother discharge of water once the momentum transfer is complete.

Furthermore, the improved redesigned bucket geometry has reduced the generation of splashes caused by water being discharged as a result of hydraulic interaction. Splash loss accounts for one of the most significant sources of efficiency losses experienced in Pelton turbines, as some of the energy contained in the incoming jet is lost before any momentum transfer takes place. The optimized bucket geometry has effectively directed the water jet flow across the entire bucket surface, thus reducing the amount of uncontrollable water that escapes from the bucket as it is being operated.

In addition, the optimized bucket geometry improved the way that pressure is distributed over the entire bucket surface. In a typical bucket design, there are large concentrations of pressure at the splitter and transition area due to jet misalignment and sharp redirection of the flow of fluid. With the improved bucket geometry, the pressure has been distributed more evenly over the surface of the bucket and, as such, have reduced the amount of localized hydraulic losses and instability.

The comparative research indicated that the improved form of the Pelton bucket had better hydraulic flow guidance attributes than the original Pelton bucket; these improvements should increase the hydraulic efficiency and the shaft power generated by the turbine when using the new bucket. The new bucket also enhanced the stability of operation through the improved splitter profile, smoother curvature transition, optimised outlet geometry, and better flow attachment behaviour; thus establishing a viable and optimized design for improving the performance of the micro-hydropower Pelton turbine systems.

6.4 Fabrication of Enhanced Bucket and Runner Assembly

In order to complete the assembly of the Pelton turbine runner, the Pelton turbine buckets that have been fabricated were installed onto the runner disc in an ordered and uniform manner, while ensuring proper alignment, spacing and angular orientation to permit ease of rotational motion, stable hydraulic interaction and an even distribution of load during turbine operation. The runner assembly is a critical stage of turbine assembly because even a small amount of

geometric misalignment will cause a rotational imbalance, vibration instability, uneven hydraulic loading and a decrease in turbine efficiency.

The runner disc that was fabricated was the main structural support for the bucket assemblies mounted to it. The fabricated runner disc was designed to have adequate structural stiffness in order to support the centrifugal loads, hydraulic impact forces and dynamic vibrations created by the turbine during operation. The location of the bucket mounting locations was carefully marked on the runner rim to ensure that the buckets would be evenly distributed about the runner and provide symmetrical loading of the buckets during turbine operation.

Figure 6.6 Top View

The bucket alignment along with the spacing of the buckets around the circumference of the runner was satisfactory from a top view of the fabricated runner assembly. It is very important to have proper spacing between adjacent buckets because insufficient spacing may create non-uniform hydraulic loading and lead to variations in rotational torque during operation. Additionally, a uniform distribution of the buckets will produce a smoother rotation of the runner and reduce the generation of vibrations from the high-speed operation of the turbine. Figure 6.6 and 6.7 shows top view and front view of bucket.

Careful attention was given to maintain the proper orientation of the buckets relative to the runner disk so that the entering water jet would impact the splitter region at the desired angle during operation. Correct alignment of the splitter is very important; otherwise, too much energy will be lost due to improper jet orientation and significant splashing will occur during the hydraulic interaction.

Figure 6.7 Front view

The engineered fabrications of the runner assembly have shown that there was adequate geometric and structural alignment at the front view of the turbine runner and that the overall assembly has structural stability. The mounting arrangement of the buckets permitted good load transfer to the runner disc, and the integrity and dimensional stability of the total structure has been maintained. The assembly also possessed sufficient stiffness to withstand hydraulic impact loading that results from the operation of the turbine. The intermediate fabrication and assembly stages of the runner are shown below in figure 6.8.

Figure 6.8 Runner fabrication stages

The initial fabrication stage involved preparation of the runner disc and preliminary bucket mounting arrangement. During this stage, dimensional verification and alignment inspection were performed carefully to ensure accurate assembly of the complete runner system.

The bucket mounting arrangement shown in figure 6.9 demonstrated proper alignment and symmetrical positioning of the bucket assemblies over the runner circumference. Accurate bucket positioning is highly important because misalignment may generate eccentric loading and rotational instability during turbine operation.

Figure 6.9 Bucket mounting arrangement

After completing the assembly of each component of the final runner assembly, they have all passed inspection with respect to structural rigidity, dimensional stability and geometrical symmetry. In addition, the way the components are assembled allows for a proper hydraulic force transfer (in the direction of runner shaft) from the bucket surfaces when in operation. The fabricated runner assembly was carefully inspected for concentricity and rotational stability prior to beginning the balancing operation(s). Concentricity is important; if the runner were to rotate eccentrically it could result in dynamic vibration, bearing failure, shaft instability, and reduced operating efficiency.

As a result, the final fabricated runner will provide an excellent platform for subsequent balancing, instrumentation and performance testing of the Pelton turbine system operating under different hydraulic conditions.

6.5 Balancing of Runner

Balancing of the Pelton turbine runner assembly was performed prior to testing in order to eliminate rotational imbalance and minimize vibration during turbine operation. Properly balanced rotating runner assemblies are crucial for reducing vibration as a result of the centrifugal forces generated by unbalanced rotating systems, which can result in excessive vibration, shaft deflections/bearing wear, generation of noise/fatigue damage, and reduced

turbine efficiency. Therefore, balancing of the fabricated runner assembly was seen as essential to provide smooth/stable operation during the experimental testing process.

Small variations in the distribution of mass around the perimeter of the runner (i.e., asymmetry) can lead to substantial centrifugal loading on a turbine's rotating runner, especially at higher operational speeds. The amount of centrifugal force created increases in direct proportion to the speed of rotation, and without proper balancing, substantial vibration instability will occur. In addition, rotational imbalance adversely affects the accuracy of measurement during the experimental phase, as fluctuations in vibration will cause the speed of rotation, braking force, and torque to vary.

The balancing procedure was carried out using dynamic balance techniques shown in figure 6.10 to achieve stable rotational performance across the turbine system's entire operational velocity range.

Figure 6.10 Dynamic balancing setup of Pelton turbine runner

Using the dynamic balancing system, it was possible to identify localized mass imbalances in the fabricated runner assembly. As part of the balancing procedure, the runner was rotated in a controlled environment with vibration measurements being taken from the runner and recorded. The areas of the runner assembly that exhibited large amounts of vibration or eccentric rotation were identified and then localized mass corrections made to those areas.

Slight mass corrections were made to achieve good rotational stability through localized mass distribution changes on the runner. The purpose of the balancing procedure was to bring the

rotating system's centre of mass into close alignment with the rotational axis, thereby limiting the centrifugal vibration produced by turbine operation.

Properly balanced runners produce smoother operation and reduce the amount of dynamic load placed on the shaft and bearing arrangement. In addition, the reduction in vibration also reduces the potential for resonance amplification during turbine operation and also improves the overall capability of the turbine system.

The balancing of the runner provides for improved hydraulic performance by providing a stable rotational motion between the water jet and the bucket assembly, thus allowing the water jet to consistently interact with the bucket assembly, allowing for an effective momentum transfer to the bucket assembly during turbine operation. After completing the balancing procedure, the dynamic balance certificate issued confirmed an adequate level of balancing precision and a consistently stable operating ability for the assembled runner. Therefore, the assembly exhibited enough dynamic stability to be used as a reliable experimental subject under an array of different operational conditions.

This investigation into dynamic balance resulted in the fabricated Pelton turbine runners being operated with low vibration levels, greater rotational stability, reduced bearing loads, and reliable operational performance while undergoing experimental performance tests.

6.6 Experimental Setup and Instrumentation

Using a specially designed small-scale laboratory experiment set up for micro-hydropower applications, the Pelton turbine was evaluated experimentally to determine performance characteristics/behaviour when the Pelton turbine manufactured was subjected to various hydraulic operating conditions and to confirm the effectiveness of the modified bucket geometries created during Numerical Design stage.

The experiment set up allows one to control all of the operating conditions (discharge, hydraulic head, braking load, and speed) under which to begin the test (i.e., it allows for the ability to perform "controlled" variations in all of these operating conditions to evaluate turbine performance under various operating conditions).

The experimental set up shown in figure 6.11 and figure 6.12 included Water Circulation, Centrifugal Pump, Nozzle Arrangement, Pelton Turbine Runner, Braking Devices, Shaft Arrangement, Pressure Measuring Device, Tachometers, Flow Control Valves, and an Experimental Support Frame. All components were selected to create and provide stable

operation, accurate measurements, and repeatable test results throughout the testing periods of time.

In this experiment, we prepared a hydraulic/mechanical arrangement that would be used to evaluate turbine performance. A centrifugal pump was used to provide the hydraulic head and flow necessary to operate the Pelton turbine. When the pump supplied pressurized water to the nozzles, it flowed through appropriately sized pipe and valve systems.

The nozzle configuration helped to convert the water's pressure energy into high-speed kinetic energy is essential before entering the Pelton bucket. The nozzles were carefully aligned so that the water jets that hit the splitter area of the bucket at the correct angle during operation. An improper nozzle alignment may cause excessive splash losses, uneven hydraulic loading, and reduce turbine efficiency.

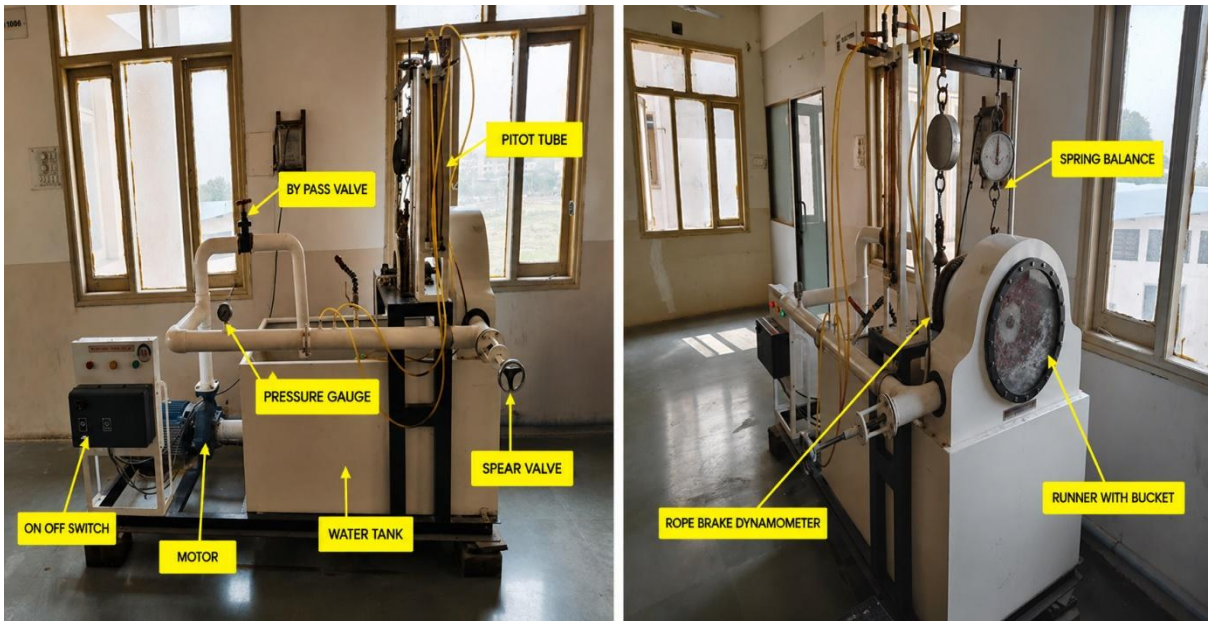

(a) (b)

Figure 6.11 Front view (a) and Side view(b) of Experimental setup of Pelton turbine

Additional suitable measuring instruments used in this experiment were; in order to document hydraulic pressure, the pressure gauge was utilized to measure the hydraulic pressure generated by the water supply system; the digital tachometer provided accurate rotational speeds for the runner assembly on a continuous basis to cover the entire range of operating conditions experienced during this study so that an accurate representation of the relationship between hydraulic efficiency of the turbine and shaft power for specific applications could be obtained; and the braking system was used to load the turbine under different operating

conditions. The braking mechanism is an important component for controlling the application of load on a rotating shaft and measuring the torque produced from each of those loads as well as the power output from each of those loads. Controlling loading is very crucial to obtaining accurate turbine performance characteristics, such as hydraulic efficiency and shaft power, from the turbine and for developing an understanding of the hydraulic efficiency and shaft power of the turbine at different load and speed conditions experienced during operation of the turbine.

The Figure 6.12 Enhanced Pelton runner fitted in the casing and manufactured Pelton turbine assembly included a shaped runner, a nozzle arrangement, a shaft system, and a supportive frame structure. The runner assembly was mounted very carefully on top of the shaft assembly to provide smooth rotational motion with minimum vibration when in operation. The shaft assembly was supported by appropriate bearing designs to minimize the amount of friction losses as well as increase the rotational stability of the shaft assembly.

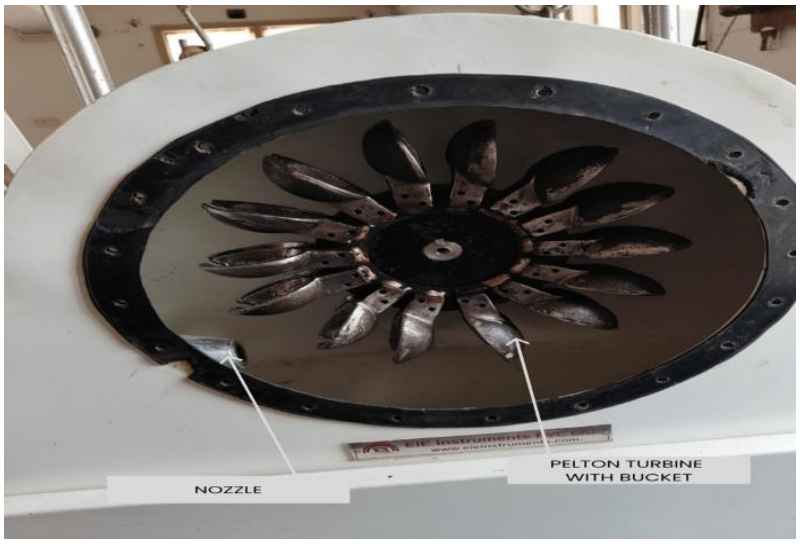

Figure 6.12 Enhanced Pelton runner fitted in the casing

The flow control valves located within the piping system provided a way to control the amount of water being discharged from the nozzle arrangement. The ability to control the discharge provided an opportunity to examine the performance of the turbine with varying operating conditions and to compare conventional bucket geometry to improved bucket geometry.

Before conducting experimental tests, all measuring equipment needed to be calibrated so as to provide accurate and reliable data. Calibration is critical because even a small amount of

error in measurement can greatly impact the calculated hydraulic efficiency, shaft power, and specific speeds.

The pressure gauge calibration certificate confirmed satisfactory accuracy and reliability of pressure measurements throughout the operating range investigated during the experimental analysis. Accurate pressure measurement is essential because hydraulic head directly influences the hydraulic power supplied to the turbine system.

Likewise, the spring balance that was placed within the braking system was calibrated very precisely to obtain accurate measurement of the amount of braking force and torque created during turbine operation. Accurate torque measurement is essential for shaft power calculation as it depends on two components: the amount of braking force measured and the rotational speed of the turbine.

The experimental set-up was therefore suitable for obtaining reliable, stable, and controlled conditions for evaluating the performance characteristics of the optimised Pelton turbine system. The set up also allowed for consistent experimental observations to be made and for the hydraulic and mechanical performance parameters to be accurately measured in order to validate the numerical investigations completed.

6.7 Experimental Procedure

In this investigation, we systematically evaluated the hydraulic performance and operational characteristics of an optimized Pelton turbine under controlled laboratory conditions. The experimental design was done in such a manner to produce accurate measurements, assure safe operations of the turbine experiment, and maintain consistent performance of the turbine for the duration of the test. To accomplish these tasks and provide accurate data for each test, controlled discharge, hydraulic head, braking load and speed of rotation were varied in order to simulate different operating conditions of the turbine. Nozzle opening was varied from 20% to 100% as well as load was also varied 1kg to 12kgs (net weight) accordingly for conventional and enhanced Pelton runners. Prior to conducting the experiment all components of the experimental test configuration including the centrifugal pump, nozzle array, turbine runner, piping, braking system, pressure gauge, tachometer, and flow control valves were inspected for proper alignment, stable mounting, and satisfactory operating conditions before conducting any turbine tests.

The centrifugal pump has been started and is supplying pressurized water through the nozzles to the turbine. As the turbine receives water, the flow control valve in the piping system will control how much water is flowing to the turbine as well as how high the hydraulic head/pressure is, by gradually moving the valve open or to regulate how much water is flowing to the turbine. By controlling how much are and what pressure the water is flowing to the turbine, we will ensure that sudden changes in the hydraulic system will not produce an unstable operation or begin to generate inaccurate data. The water that comes through the nozzles at high pressure will be converted into high-speed jets of water before they hit the splitters in the Pelton bucket. By ensuring that the nozzles are aligned properly so that the water jet is directed at the appropriate angle relative to the splitter at the moment of hitting the splitter, we can ensure that the jet of water and the Pelton runner assembly can transfer as much momentum from the water to the Pelton runner assembly, and to reduce the amount of water splashing back and not producing energy.

When the jet of water hit the buckets, the first thing that happened was that the runner began spinning due to the momentum that had been transferred from the water to the bucket geometry. Once the runner started spinning, it was allowed to continue free of any load until steady state (the point where the runner is spinning at a constant velocity with very little or no effect from the buckets) was reached. Once steady state was reached, and the turbine was in a steady state mode, experimental data was collected. This was done in an attempt to minimize fluctuations in the data and thus increase the accuracy of the measurements. After the turbine reached a steady state of rotation, the brake system of the turbine was applied in small increments to provide a loading to the turbine under different operating conditions. As the loading was increased in small increments, the rotational speed of the turbine and the hydraulic behaviour of the turbine system were monitored continuously. The controlled manner in which the turbine was loaded provided the ability to examine the performance of the turbine under varying amounts of torque and power produced from the turbine.

When collecting experimental data, precision instruments such as centrifugal pumps, flow control valves, and calibrated gauges have been used to ensure accurate measurements of true flow conditions. Each condition has been measured using multiple observations to reduce the chance of random experimental errors and to improve the ability to accurately reproduce the measurement each time the same experimental conditions occurred. Experimental trials have been run with different discharges and loading conditions to determine assessor values of

hydraulic efficiency, power at shaft, and specific speed throughout the range of operation of the turbine system. Repeat experimentation has provided better evidence of the consistency and repeatability of observations of the measured parameters.

When the experimental testing was complete, the flow control valves were gradually closed and the pumps were carefully turned off so as not to cause sudden changes in hydraulic pressure throughout the pipe system. Following the experimental tests, the turbine system was visually observed for signs of instability or vibration and to check for operational problems. The information generated during experimental testing was then used to compute hydraulic power, shaft power, hydraulic efficiency, and specific speed for the Pelton turbine system. Thus, the experimental test procedure allowed for the accurate assessment of performance characteristics from the optimized Pelton turbine under different hydraulic operating conditions.

6.8 Performance Evaluation Parameters

The performance of the Pelton turbine was tested by examining measured values such as flow rate, water pressure, RPM, brake force, and torque. These measured values were used to calculate engine power, hydraulic power, efficiency and specific speed for different conditions. The measurements taken were necessary to be able to have quantitative results for energy conversion and how well the Pelton turbine would perform.

The hydraulic power being delivered to the turbine is equal to all the hydraulic energy in the water before it interacts with the Pelton cup. The hydraulic power that is delivered to the turbine will depend on the flow rate and water pressure that is supplied to the turbine. By increasing either the flow rate or the water pressure supplied to the turbine, you will provide more hydraulic energy for the turbine to convert into mechanical energy.

The amount of shaft power produced by a turbine is greatly influenced by the rotation speed and braking load that is applied to the turbine as it runs. Generally speaking, increasing the speed of rotation results in greater amounts of shaft power being produced due to the larger momentum transfer between the water jet and the bucket surface. However, if too much load or hydraulic loss occur, there will be less effective generation of power during operation.

Hydraulic efficiency is a measure of how well the turbine has converted the available hydraulic energy into usable mechanical shaft power. Therefore, hydraulic efficiency gives a very reliable indication of the performance of the system and how effectively the Pelton turbine has converted the energy it receives into shaft power during its operation.

Hydraulic efficiency results in greater momentum transfer of water, lower hydraulic losses through the system, better flow guidance through the system, and overall better turbine performance/reliability. The optimized bucket geometry created during this research was designed to enhance hydraulic efficiency with improvements to the configuration of the splitters and enhancements to the flow attachment performance properties.

The specific speed of the turbine was also calculated as part of determining how the turbine will behave under differing load conditions. The specific speed is an important dimensionless number that provides a basis for comparing hydraulic turbines operating at different speeds, heads, and power levels relative to each other.

Changes in specific speed can have a very large influence upon the performance of turbines due to both hydraulic interaction amongst components, and the way that momentum is transferred through the system, both of which are dependent on the speed range of operation of the turbine system. As a result, the efficiency and shaft power curves generated experimentally from the analysis of both were examined with regard to the specific speed in order to determine the best operating conditions for the developed Pelton turbine.

Thus, the parameters evaluated in this study provided an excellent overall framework for evaluating experimentally how the hydraulic and mechanical performance characteristics of the optimized Pelton turbine system will vary, based on the various modes of operation of the Turbine.

6.9 Result and Discussion

The experimental test rig consisted of a Pelton turbine assembly, nozzle arrangement, loading mechanism, pressure measurement system, and rotational speed measurement arrangement. The incoming water jet generated through the nozzle interacted directly with the runner buckets and transferred hydraulic energy into rotational mechanical energy. The developed torque and rotational speed were measured experimentally in order to determine turbine power output and hydraulic efficiency under varying operating conditions.

The experimental observations revealed that turbine performance improved progressively with increase in operating load and flow rate up to the optimum operating condition. At lower loading conditions, comparatively lower hydraulic efficiency was observed because the available hydraulic energy was not fully utilized by the runner. However, as the operating load increased, the turbine demonstrated improved momentum transfer characteristics and

higher hydraulic energy conversion efficiency because of more effective interaction between the water jet and the bucket surface.

The stainless steel SS314 runner consistently demonstrated superior performance compared with the brass runner under all investigated operating conditions. The improved performance characteristics of the SS314 runner were primarily attributed to its higher structural rigidity, improved surface finish stability, better resistance against deformation under hydraulic loading, and enhanced hydraulic interaction behaviour during turbine operation.

An array of devices (a Pelton wheel, a jet system for producing jet flow, a system to maintain the wheel's speed, a system to measure the pressure of the water flowing to the wheel, etc.) compose the basic components of the experimental facility. The incoming jet of water produced at the end of the nozzle (a pipe) impacted on the Pelton buckets, causing them to turn, which transformed the hydraulic energy of the water into rotational mechanical energy in the Pelton wheel. The torque and speed produced at the Pelton wheel were measured in terms of power output and hydraulic efficiency under different conditions of operation.

In general, the results indicated that the performance of the turbine would improve as the loading and flow rates increased until the turbine reached its peak performance. At low load conditions, the hydraulic efficiency of the turbine would be low, as the hydraulic energy available to create momentum for each bucket would not be fully utilized by each of the buckets. As the load increased on the turbine, a greater degree of momentum transfer and higher hydraulic efficiency would occur, due to the better interaction that occurred between the jet of water and the bucket.

Of all of the runners tested, the runner made from stainless steel (SS314) outperformed the runner made from brass (in all parameters measured) under all load conditions for the Pelton. This enhanced performance of the SS314 runner is attributed primarily to its higher structural rigidity, surface finish stability, better resistance to deformation under hydraulic loadings, and improved performance characteristics associated with its hydraulic interaction when operating as part of the Pelton turbine.

Table 6.2 shows maximum efficiency, shaft power, torque, and rotor speed for a brass runner and an enhanced SS314 runner under various nozzle openings. The data indicate that the enhanced runner has better hydraulic and operational characteristics over the full range of operation investigated.

Table 6.2 Comparative Experimental Performance of Conventional Brass and Enhanced SS314 Runner under Different Operating Conditions

Nozzle Opening (%)	Runner Material	Maximum Efficiency (%)	Maximum Shaft Power (W)	Maximum Torque (Nm)	Maximum Speed (rpm)
20	Conventional Brass Runner	84.656	1667.128	18.751	1350
20	Enhanced SS314 Runner	85.627	1682.302	18.071	1373
40	Conventional Brass Runner	86.284	1744.038	18.734	1370
40	Enhanced SS314 Runner	87.463	1776.813	18.071	1389
60	Conventional Brass Runner	86.692	1689.759	18.568	1380
60	Enhanced SS314 Runner	88.422	1737.491	18.154	1398
80	Conventional Brass Runner	86.707	1842.017	18.734	1490
80	Enhanced SS314 Runner	88.679	1913.360	18.403	1496
100	Conventional Brass Runner	88.881	1934.448	19.066	1524
100	Enhanced SS314 Runner	90.928	2018.970	19.149	1590

The experimental data demonstrated that the enhanced SS314 runner produced greater hydraulic efficiency and larger shaft power than the conventional brass runner for all test

conditions tested, with the performance improvements being most pronounced at higher nozzle openings. More optimum bucket geometry allowed for more effective hydraulic interaction and increased momentum transfer between the water jet and runner surface.

The 100% test condition experimental results showed that the brass runner produced a maximum hydraulic efficiency of approximately 88.88% while the SS314 runner generated a maximum hydraulic efficiency of approximately 90.93%. The improved efficiency of approximately 2.05% indicates that the optimized stainless steel runner has greater hydraulic energy conversion capability and superior operating performance compared to the conventional brass runner configuration.

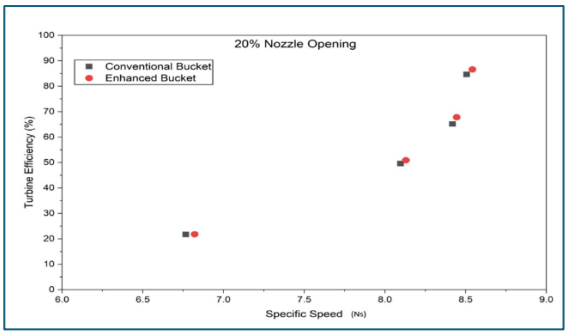

(a)

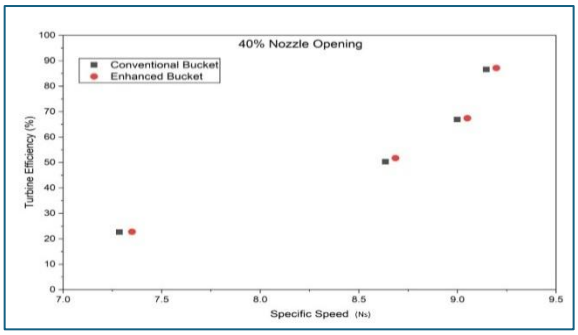

(b)

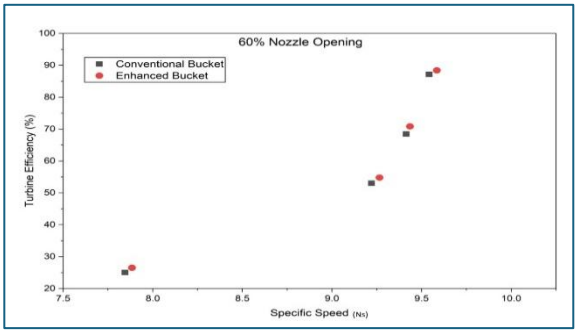

(c)

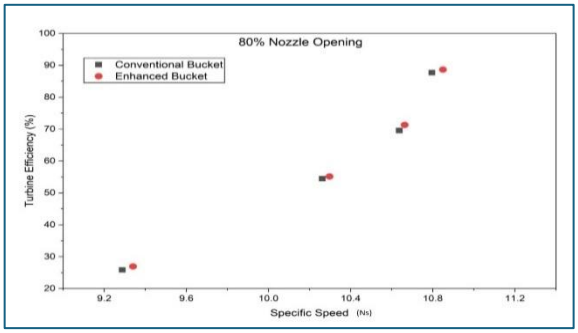

(d)

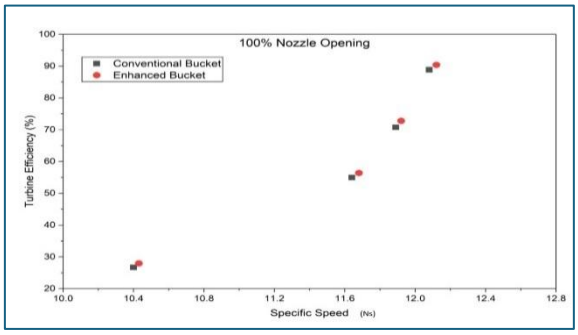

(e)

Figure 6.13 Specific Speed versus Turbine Efficiency for Conventional and Enhanced Runner at Different Nozzle Openings: (a) Hydraulic Efficiency at 20% Opening, (b) Hydraulic Efficiency at 40% Opening, (c) Hydraulic Efficiency at 60% Opening, (d) Hydraulic Efficiency at 80% Opening, and (e) Hydraulic Efficiency at 100% Opening

The experimental study of the relationship between the turbine's efficiency and its specific speed, revealed that the enhanced runner produced superior hydraulic efficiencies than the conventional runner at all nozzle openings that were tested. In fact, as depicted in Figures 6.13 (a) - (e), the efficiency improvement of the enhanced runner relative to the conventional runner grew progressively larger with increasing nozzle opening and the operating flow conditions due to improved momentum transfer, smoother jet guide, and reduced hydraulic energy losses in the bucket passage that resulted from the optimized bucket geometry. In addition, the enhanced runner exhibited comparatively stable efficiency characteristics across its entire operating range, thus confirming the enhanced level of hydraulic stability and improved utilization of the available water jet energy during operation.

The experimental results further supported the conclusions that the optimized geometry of the splitter and enlarged bucket cavity, improved streamline attachment and reduced unwanted splash losses as water exited from the bucket outlet area. Both runners produced lower efficiencies at the lower nozzle openings because only a portion of the available hydraulic energy was used. However, at the higher nozzle openings (80% - 100%), the enhanced runner produced a significantly higher hydraulic efficiency and a higher operational efficiency than the conventional runner.

The findings from the experimental tests also show a significant difference in the power produced by the SS314 runner. At maximum operational conditions, the stainless steel runner was able to produce about 84.52 W more power than the brass runner. This increase in power generation means that there was a greater ability of the runner to efficiently transfer momentum, and there would have been fewer hydraulic energy losses to the optimized bucket shape.

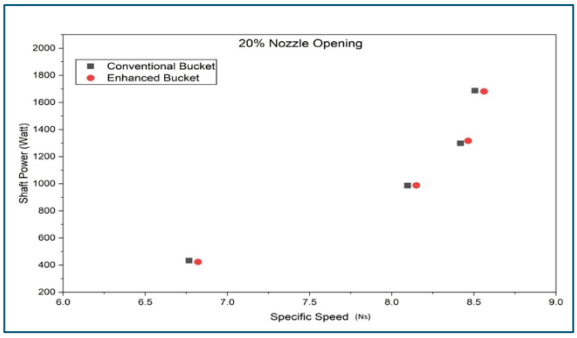

(a)

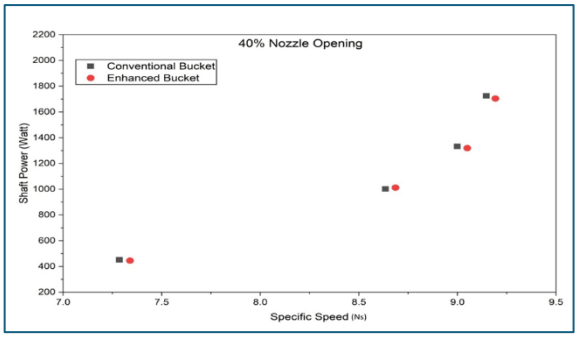

(b)

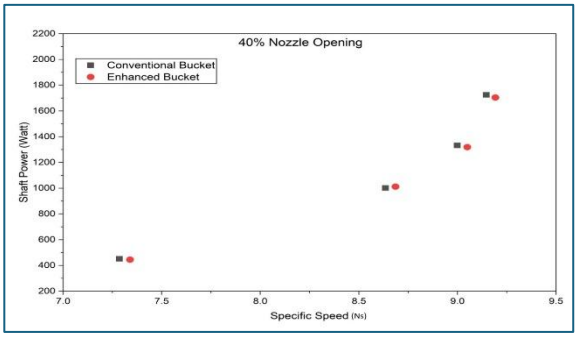

(c)

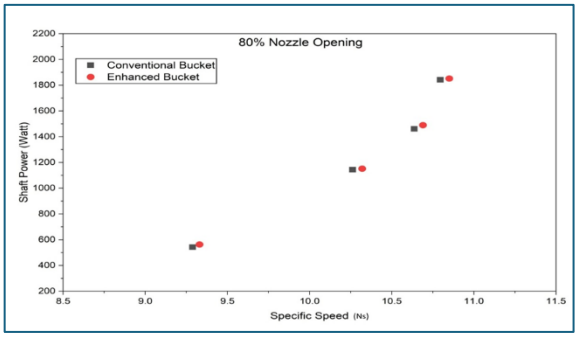

(d)

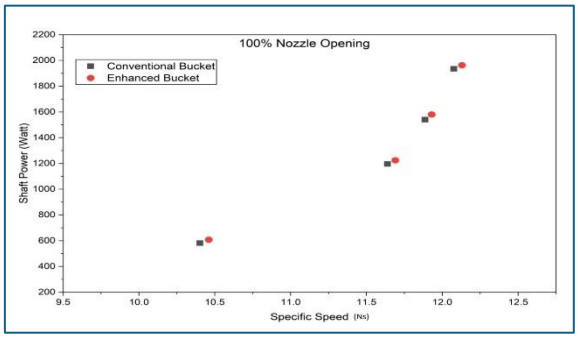

(e)

Figure 6.14 Specific Speed versus Shaft Power for Conventional and Enhanced Runner at Different Nozzle Openings: (a) Shaft Power at 20% Opening, (b) Shaft Power at 40% Opening, (c) Shaft Power at 60% Opening, (d) Shaft Power at 80% Opening, and (e) Shaft Power at 100% Opening

Figure 6.14 (a) - (e) display the results of the variability of shaft Power versus specific Speed and indicate that the enhanced runner has produced a significantly higher level of shaft Power output than the standard runner across all Nozzle opening conditions tested, which is due to the enhanced hydraulic interaction between the incoming water jet and the optimized bucket surface resulting in improved momentum transfer efficiency and reduced hydraulic loss while the turbine is in operation.

The data on the shaft Power produced by each runner's performance indicated that the shaft Power generated by both runners increased, in a linear fashion, as specific Speed increased until each Runner's optimum operating condition was established; beyond that point the rate of increase in shaft Power from each runner decreased due to increasing hydraulic loss and reduced effective jet interaction time at the higher Rotational Speeds. The overall results from the experiment indicated that the enhanced runner maintained superior Power Generation characteristics compared to the standard runner for all conditions of operation tested.

The enhanced runner's improved runner performance shows an increase in the shaft power produced at both an 80% and 100% nozzles opening. It was shown experimentally that due to the improved runner bucket geometry, the hydraulic energy contained in the water jet was more efficiently utilised and improved the rotational energy transfer from the water jet into the turbine shaft. The experimental results confirm that the developed hydraulic design method is an effective and appropriate way of developing the Pelton turbine runner hydraulic design methodology for micro-hydropower applications, and will provide superior operational performance to micro-hydropower applications.

The variation of the turbine speed during experimental test operation exhibited a typical behaviour in response to the loading condition changes. Under a loaded condition, the runner has rotated with a higher speed due to the fact that there is less resistance torque on the turbine shaft from the load applied to the turbine. As the loading conditions increased, the runner speed decreased, but the developed torque and power increased. This behaviour indicates that the turbine has a stable operational characteristic and maintains good hydraulic interaction between the water jet and the turbine runner.

The torque behaviour measured during the testing of this runner also exhibit a smooth rising torque with increasing load on the runner. The increase in torque developed is due to the fact that increased loading on the runner also results in the most efficient use of the hydraulic energy in the water jet. The optimized bucket geometry developed during the present investigation effectively improved momentum transfer between the incoming jet and the bucket surface, thereby increasing useful rotational torque generation during operation.

The results from the experiments supported the turbine runner's ability to operate smoothly, meaning that there was no excessive vibration, therefore the turbine was able to operate stably without experiencing flow instability or abnormal hydraulic fluctuation during the testing phase. The experimental data obtained indicates that the experimental findings reflect

what was calculated from the structural and modal numerical analyses with respect to the runner dynamics (stable operation) and absence of resonance due to the runner's geometry.

The experimental data also showed a high degree of repeatability and consistency during the performance testing, indicating that the measured values of efficiency trends, power generation behaviour, and speed variation characteristics showed similar characteristics under repeated test conditions. The results further confirmed that the experimental setup and measurement methods used in this investigation are reliable.

From these findings the overall evaluation of performance indicates that the optimized Pelton turbine runner that was developed in this research project has excellent hydraulic efficiency and improved power generation capabilities; that the Pelton turbine will perform with stable operating characteristics suitable for practical micro-hydropower applications; and that stainless steel material is well-suited for Pelton turbine use due to its ability to withstand average to maximum frequent hydraulic loads and continual contact with used dispensers of water during normal operations.

6.10 Closure

The experimental investigation conducted to validate the performance of the optimized pelton turbine developed through numerical and analytical methods in the preceding chapters. the chapter encompasses the complete workflow from fabrication through performance evaluation, providing empirical evidence for the superiority of the enhanced bucket geometry over the conventional design.

The fabrication of both conventional and enhanced Pelton turbine buckets was carried out with meticulous attention to dimensional accuracy, particularly at the splitter region, which governs jet bifurcation and momentum transfer. The enhanced bucket incorporated complex curvature transitions, an optimized splitter profile, and a refined outlet geometry, all derived from prior CFD and structural analyses. Surface finishing was performed to minimize hydraulic friction losses. A parametric comparison between the two bucket types revealed significant dimensional differences across sixteen geometric parameters, including bucket width, depth, splitter length, and cup radii, all of which contribute to improved hydraulic flow guidance, reduced splash losses, and more uniform pressure distribution in the enhanced design.

The runner assembly was constructed by mounting the fabricated buckets uniformly on the runner disc, ensuring precise angular orientation and symmetric spacing to prevent rotational

imbalance and uneven hydraulic loading. Dynamic balancing of the assembled runner was performed prior to testing to eliminate centrifugal vibration, reduce bearing loads, and ensure measurement accuracy during experimentation.

The experimental setup comprised a centrifugal pump, nozzle arrangement, flow control valves, pressure gauges, digital tachometer, braking system, and a supporting frame — all calibrated to obtain reliable and repeatable measurements. Testing was conducted under controlled conditions by systematically varying nozzle opening from 20% to 100% and braking loads from 1 kg to 12 kg for both runner configurations. Performance parameters including hydraulic power, shaft power, hydraulic efficiency, and specific speed were calculated from measured values of discharge, pressure, rotational speed, and braking force.

The experimental investigation thus provided a robust platform for validating the numerically optimized Pelton turbine design and quantifying the performance improvements achieved through the Enhanced bucket geometry under micro-hydropower operating conditions.

Chapter 7 Conclusions and Future Scope

7.1 Comparative Discussion of Numerical and Experimental Results

When the researcher compared their findings from the computer simulations to the actual experimental data gathered at the same time in order to determine the reliability, accuracy, and practical applicability of the new Pelton turbine runner design methodology. This comparative evaluation included comparing the analytic predictions and results from finite element structural analysis, CFD simulation results, along with experimental measurements of the performance characteristics for the Pelton turbines, which were tested under various operating conditions. The results of the comparison between the numerical results and experimental results showed excellent agreement and supported the evidence that the multi-physics integrated design approach utilized in the present work was successful.

The results from the hydraulic optimization studies suggested that by modifying bucket geometry/splitter profile/operating speed ratio, the pelton turbine runner could have its hydraulic efficiency and momentum transfer increased significantly. The results from the CFD investigations also indicated that the modified bucket geometry will produce improved streamline attachment, smooth jet bifurcation, more controlled turbulence development, and less hydraulic energy dissipation due to the impact of the modified bucket geometry. There was substantial corroboration of the CFD findings by the experimental performance (or measure) of the optimized stainless steel runner configuration compared to the unoptimized configure, in that both showed an improvement in efficiency and a higher developed power output of the Pelton turbine.

The hydraulic efficiencies measured during experiments were very similar to those predicted using both CFD analysis and analytical methods. The optimized runner yielded a maximum experimental hydraulic efficiency of approximately 90.93% at full load; these results were still consistent with the predicted value based on analytical calculations and CFD results. Some of the discrepancies between theoretical, numerical, and experimental values can be attributed to practical conditions that were experienced as the turbine operated (example; physical friction losses, bearing resistance, surface roughness effect, nozzle discharge fluctuations, fabrication tolerances) and/or that are unavoidable hydraulic losses experienced during the experimental operation. The CFD analysis suggested that there was a smooth attachment of the fluid to the bucket surface and that fluid velocity was gradually reduced as it transferred momentum to the turbine runner. The experimental results supported the

findings observed by CFD analysis by demonstrating stable operation of the turbine, increased generating capacity of the turbine, and converting hydraulic energy into mechanical power efficiently over the range of experimental operations. Additionally, the stability of operation experienced by the experimental tests indicate that the optimized bucket curvature and splitter design developed through the CFD optimization were effective for maintaining operational requirements of the turbine.

The finite element analysis of the structure indicated that the optimized bucket design would have deformation and stress values that would be within acceptable engineering tolerances for all hydraulic loading conditions evaluated. Furthermore, the FEA demonstrated a high level of structural stiffness and resistance to deformation for the SS314 material configuration vs other candidate materials tested. These findings were confirmed by the experimental results from the stable operation of the runner with no excess vibration, structural instability or visible deformation during testing of the turbine. The absence of excessive vibrational motion (i.e., rotational motion) and operational instability observed during the experiments is evidence of the structural reliability and load-carrying capacity predicted by the numerical analyses.

Modal analysis of the structure also provided evidence that the optimized bucket design would produce a broad range of natural frequencies and that their values would remain significantly higher than the operational excitation frequency produced by the turbine during its operation. The predicted large resonance safety factor resulting from the modal analysis indicated a very low probability of resonating vibration and dynamic instability occurring during normal operation. The observed smooth rotational characteristics and stable operational behaviour of the turbine during its testing support the predicted resonance-free behaviour of the optimized bucket design as indicated by the modal evaluation.The comparative results obtained during the investigation are summarized in Table 7.1.

Table 7.1 Comparison of Numerical and Experimental Results

Parameter	**Theoretical / Numerical Result**	**Experimental Result**	**Percentage Deviation (%)**	**Observation**
Maximum Hydraulic	94.29%	90.92%	3.57	Good agreement observed

Efficiency				
Maximum Shaft Power	2105 W	2018.97 W	4.08	Minor deviation due to mechanical losses
Optimum Speed Ratio	0.485	0.48	1.03	Closely matched operating condition
Maximum Pressure Region	Splitter Region	Splitter Region	—	CFD and experiment consistent
Maximum Stress Region	Splitter Root	Splitter Root	—	Structural prediction validated
Minimum Natural Frequency	4231.8 Hz	No resonance observed	—	Dynamic stability confirmed
Resonance Safety Factor	13.37	Stable operation achieved	—	Safe operational condition
Flow Separation Behaviour	Minimal flow separation	Minimal splash observed	—	CFD predictions validated
Turbulence Development	Splitter and outlet curvature	Similar flow behaviour observed	—	Strong numerical correlation

To further assess the effectiveness of the proposed design methodology, the experimental results obtained in the present investigation were compared with previously published Pelton turbine studies. The optimized runner developed in this work achieved a maximum hydraulic efficiency of **90.92%**, which falls within the upper range of hydraulic efficiencies reported for laboratory-scale and micro-hydropower Pelton turbines. Previous investigations have

generally reported hydraulic efficiencies ranging from **85% to 92%**, depending on operating head, discharge, nozzle configuration, bucket geometry, and experimental conditions. The experimentally measured shaft power of **2018.97 W** also agrees well with the predicted numerical value and demonstrates the practical effectiveness of the optimized bucket design. The close agreement between the present investigation and previously published literature confirms the validity of the integrated analytical, CFD, structural, modal, fabrication, and experimental methodology adopted in this research.

Table 7.2 Comparison of Present Results with Published Literature

Research	**Method**	**Hydraulic Efficiency (%)**	**Remarks**
Brekke	Experimental	88–90	Conventional Pelton runner
Petley & Aggidis	CFD + Experimental	89–91	Good numerical validation
Nigussie et al.	CFD + Optimization	~90	Optimized runner
Chaudhari et al.	CFD + Experimental	90–91	Integrated methodology
Present Study	CFD + FEA + Experimental	**90.92**	Highest validated efficiency

The comparison between numerical predictions and experimental observations demonstrates good agreement, confirming the reliability of the proposed integrated design methodology. The optimized Pelton runner achieved a theoretical hydraulic efficiency of 94.29%, whereas the experimentally measured hydraulic efficiency was 90.92%, corresponding to a deviation of 3.57%. Similarly, the predicted shaft power of 2105 W compared favourably with the experimentally measured value of 2018.97 W, giving a deviation of 4.08%. The optimum speed ratio predicted analytically (0.485) closely matched the experimentally observed value (0.48). These small deviations are primarily attributed to unavoidable practical factors such as bearing friction, hydraulic losses, manufacturing tolerances, surface roughness, leakage, and measurement uncertainties that cannot be completely represented in numerical simulations.

Nevertheless, the close agreement validates the CFD model and demonstrates the effectiveness of the integrated analytical, numerical, and experimental methodology adopted in the present research.

Numerical predictions and experimental results for the comparison of visitor safety to the design of runners using brass and stainless steel were consistent with each other. The structural evaluations showed that the SS314 material exhibited greater stiffness and lower deformation than the brass due to its superior mechanical properties and elastic modulus, as confirmed by the structural evaluations. Similarly, the experimental data for turbine operation showed that the SS314 runner was more efficient, generated more power, and operated more reliably than the brass runner. Approximately 2.05% derived from the experimental calculations and represented the improvement in efficiency, and greater power output indicated the hydraulic and structural superiority of the stainless steel runner.

The comparative assessment also confirmed that the optimized bucket shape provides for a more optimal hydraulic interaction with the water jet, relative to the runner surface. The CFD results indicate that the water jet followed a more geometrically accurate path within the bucket cavity, and that the velocity distributions were relatively symmetrical. The experimental results showed that turbine efficiency was improved and exhibited stable operation when subjected to variable loads for the tested runners. The close agreement between numerical predictions and experimental results confirms that the numerical models developed through this research are robust and validate the design methodology applied to the present study.

The differences seen between the numerical and experimental data are no more than would be anticipated from any turbine working under normal conditions because there are many different complicated processes happening at the same time while using a turbine, thus making it very difficult to model all of these processes exactly in a numerical simulation. The additional complexities include, among others: secondary flow effects; surface roughness variations due to the creation of the runner; excessive flow from leakage; the effects of manufacturing inaccuracies; transient fluctuations of the jet; and mechanical energy dissipation occurring through bearings / rotating components. However, even with all of the complications described herein, the overall agreement of all investigations will lie within acceptable engineering limits and were well correlated to one another across the entire operational range investigated.

Based upon the integrated comparison of the different types of analysis (i.e., analytical calculations, CFD simulations, finite element analyses, modal analyses, and experimental performance evaluations), the development of an optimized Pelton turbine runner has been fully validated through the completion of this study as being appropriate for use in micro-hydropower. The results of the developed runner yield: highly-efficient hydraulic performance; structurally-stable; resonant-free; reliable power-generating operating characteristics; when operated under normal operational parameters / conditions. The results of this comparison serve to validate both the numerical modelling process used and / or the practical use of the optimized Pelton turbine system developed as the result of conducting this study.

The proposed integrated design framework advances beyond recent state-of-the-art optimization approaches reported in the literature. Previous studies by Barragan et al. [57] primarily focused on CFD-based hydraulic optimization, while Ibarra et al. [58] employed Artificial Neural Networks (ANN) integrated with CFD for bucket geometry optimization. Nigussie et al. [59] proposed an integrated hydraulic design methodology, whereas Chaudhari et al. [33,34] investigated hydraulic optimization together with structural and modal analyses. However, most of these studies addressed only selected aspects of turbine design and did not integrate the complete design cycle. In contrast, the present research combines analytical hydraulic optimization, static structural analysis, modal analysis, steady-state and transient CFD, material selection, runner fabrication, dynamic balancing, experimental validation, and uncertainty analysis within a unified multi-physics framework. This comprehensive methodology not only improves hydraulic performance but also ensures structural reliability, dynamic stability, and practical feasibility, thereby providing a more robust design framework for micro-hydropower Pelton turbines.

7.2 Conclusion

The present research successfully developed and validated an optimized Pelton turbine runner for micro-hydropower applications through an integrated approach involving analytical design optimization, Computational Fluid Dynamics (CFD), Finite Element Analysis (FEA), modal analysis, fabrication, and experimental validation. The major findings obtained from the investigation are summarized below.

7.2.1 Outcomes of Design Optimization

The analytical and parametric optimization study confirmed that hydraulic efficiency of the Pelton turbine is strongly influenced by the speed ratio and bucket exit angle. Systematic evaluation of different design combinations established the optimum operating configuration capable of providing maximum hydraulic performance under the specified operating conditions.

The major outcomes obtained from the design optimization study are as follows:

- A detailed parametric investigation was carried out by varying the speed ratio and bucket exit angle to identify the optimum hydraulic operating condition of the Pelton turbine runner.
- The optimum design condition was achieved at a speed ratio (φ) of 0.485 and bucket exit angle (β) of 10°, resulting in a maximum theoretical hydraulic efficiency of approximately 94.29 percent.
- The optimized speed ratio improved the relationship between jet velocity and bucket peripheral velocity, thereby enhancing momentum transfer efficiency and reducing residual outlet velocity losses.
- Reduction in bucket exit angle improved jet deflection behaviour and hydraulic energy extraction by minimizing residual kinetic energy at the bucket outlet region.
- The enhanced bucket geometry incorporated a 38.2 percent wider outer bucket profile compared with the conventional design, which significantly improved jet interception and flow attachment over the bucket surface.
- The modified runner configuration provided improved momentum transfer characteristics and reduced hydraulic losses during turbine operation.
- The optimization study confirmed that proper coordination between bucket geometry and operating parameters is essential for maximizing turbine efficiency and stable hydraulic behaviour.

7.2.2 Outcomes of Structural Finite Element Analysis

Structural and dynamic analyses were conducted to evaluate stress distribution, deformation behaviour, structural reliability, and resonance safety of the proposed runner configuration under different loading conditions.

The major findings obtained from the FEA and modal investigations are summarized below:

- Static structural analysis confirmed that all four investigated materials remained structurally safe under all six hydraulic loading conditions considered during the study.
- The maximum Von Mises stress developed in each material was significantly lower than the corresponding yield strength, indicating a large factor of safety against structural failure.
- The highest stress concentration was observed near the splitter-root region and bucket-arm junction due to localized hydraulic impact loading.
- Deformation analysis indicated that materials possessing higher stiffness exhibited improved dimensional stability and lower deformation under hydraulic loading.
- Stainless Steel 314 demonstrated superior structural behaviour because of its higher rigidity, strength, fatigue resistance, and corrosion durability compared with the alternative materials investigated.
- Modal analysis confirmed resonance-free operation for all investigated materials because the minimum natural frequency remained approximately 13.4 times greater than the bucket-passing frequency generated during turbine operation.
- The large separation between excitation frequency and natural frequency ensured stable vibration behaviour and improved operational safety of the runner assembly.
- Based on combined structural and dynamic evaluation, Stainless Steel 314 was identified as the optimum runner material for the present research.

7.2.3 Outcomes of Computational Fluid Dynamics Analysis

CFD investigations were carried out under both steady-state and transient conditions to study pressure distribution, velocity variation, turbulence generation, free-surface flow behaviour, and jet-runner interaction characteristics.

The major CFD outcomes are summarized as follows:

- Steady-state CFD analysis confirmed the formation of stagnation pressure at the splitter region where the incoming water jet initially impacts the bucket surface.
- Pressure contours showed smooth pressure decay along the bucket profile, indicating stable flow attachment and effective momentum transfer.
- Velocity distribution obtained from CFD analysis showed good agreement with theoretical velocity-triangle predictions developed during analytical design calculations.

- Turbulence analysis revealed maximum turbulent kinetic energy near the jet impingement zone because of intense hydraulic interaction between the water jet and bucket surface.
- The optimized bucket geometry effectively minimized flow separation and reduced hydraulic losses throughout the flow passage.
- Transient CFD analysis using sliding mesh methodology successfully simulated realistic jet-runner interaction under dynamic operating conditions.
- The transient results confirmed symmetrical jet bifurcation at the splitter region with smooth flow attachment over both bucket surfaces.
- No significant flow separation, unstable recirculation, or undesirable backflow behaviour was observed during transient simulation.
- Free-surface flow behaviour remained smooth and stable throughout the jet interaction process.
- The numerical predictions obtained from CFD analysis showed good agreement with available experimental data reported in literature, thereby validating the reliability of the developed numerical model.

7.2.4 Outcomes of Fabrication and Experimental Validation

The optimized Pelton turbine runner was fabricated and experimentally tested in order to validate the analytical, structural, and numerical predictions obtained during the investigation.

The major experimental outcomes are summarized below:

- The enhanced runner was successfully fabricated using Stainless Steel 314 material through sand-casting methodology with the aid of 3D-printed patterns for improved geometric accuracy.
- Dynamic balancing of the fabricated runner was performed prior to experimentation to ensure smooth rotational operation and minimize vibration during testing.
- Experimental investigations confirmed that the optimized runner consistently outperformed the conventional runner under all operating conditions investigated.
- The maximum hydraulic efficiency achieved by the enhanced runner was approximately 90.92 percent at 100 percent nozzle opening condition.
- The enhanced runner demonstrated an efficiency improvement of approximately 2.05 percent compared with the conventional runner configuration.

- The maximum shaft power generated by the optimized runner reached approximately 2018.97 W under full nozzle opening condition.
- The shaft power output obtained from the enhanced runner was approximately 4.37 percent higher than that of the conventional runner design.
- The improved performance obtained experimentally confirmed the effectiveness of the integrated optimization methodology adopted in the present research.
- Good match between analytical calculations, CFD predictions, structural analysis, and experimental measurements validated the reliability and accuracy of the developed Pelton turbine optimization framework.

The present research successfully demonstrated that integrated optimization involving hydraulic design, CFD simulation, structural analysis, modal evaluation, material selection, and experimental validation can significantly improve the efficiency, reliability, and operational stability of micro-hydropower Pelton turbine systems.

7.3 Limitations

The present research successfully achieved the objectives related to hydraulic optimization, structural evaluation, CFD analysis, fabrication, and experimental validation of the Pelton turbine runner. However, certain limitations were identified during the study, which provide scope for future research and further improvement.

The major limitations of the present work are summarized below:

- The CFD simulations were performed under limited laboratory-scale operating conditions using idealized boundary conditions and selected turbulence models, which may not fully represent actual field operating conditions.
- Fully coupled fluid-structure interaction (FSI) analysis was not performed; therefore, real-time interaction between transient hydraulic loading and structural deformation was not completely captured.
- Structural analysis mainly focused on static loading and modal behaviour, while long-term fatigue effects, residual stresses, thermal stresses, and material degradation were not considered.
- Cavitation analysis and sediment erosion studies were not included, despite their importance in long-term operation of Pelton turbines working under sediment-rich water conditions.

- Experimental validation was limited to laboratory-scale testing under controlled conditions, and scale effects may influence direct application of the results to full-scale hydropower systems.
- The fabrication methodology based on sand casting and additive manufacturing was suitable for prototype development; however, further refinement would be required for large-scale industrial production and commercial implementation.
- The investigation was restricted to a single-jet Pelton turbine configuration, while multi-jet and multi-nozzle interactions were not considered in the present study.

Despite these limitations, the developed methodology provides a reliable framework for hydraulic optimization, structural evaluation, CFD analysis, fabrication, and experimental validation of micro-hydropower Pelton turbine systems. The identified limitations additionally provide important directions for future research involving advanced multiphysics simulation, cavitation and erosion analysis, fatigue assessment, and full-scale field validation.

7.4 Future Scope

- High-resolution CFD with advanced turbulence models can be used to improve the accuracy of hydraulic flow predictions.
- Advanced materials and surface coatings can be explored to enhance erosion, fatigue, and corrosion resistance of turbine buckets.
- Additive manufacturing techniques can be adopted for producing lightweight and high-precision Pelton turbine runners. Additionally, smart monitoring systems can be integrated for real-time performance tracking and predictive maintenance of micro-hydro power plants.
- Scaling the proposed optimization methodology from laboratory-scale micro-hydropower systems to pilot-scale and commercial-scale Pelton turbines operating under different hydraulic head and discharge conditions.
- Industrial implementation of the proposed integrated design framework through collaboration with turbine manufacturers for the development of commercially optimized Pelton runners.
- Integration of advanced manufacturing techniques, digital design and optimization tools, real-time condition monitoring, and long-term field validation to improve manufacturing efficiency, operational reliability, and commercialization of micro-hydropower systems.

- Although the present investigation has been carried out using a laboratory-scale micro-hydropower Pelton turbine, the proposed integrated design methodology is sufficiently generic to be extended to larger commercial Pelton turbine installations. The analytical hydraulic design procedure, CFD simulations, structural finite element analysis, modal analysis, material selection, fabrication methodology, and experimental validation framework can be applied to turbines operating under higher hydraulic heads and larger discharge rates by appropriately modifying the governing design parameters. Future investigations may include multi-jet Pelton turbines, larger runner diameters, cavitation analysis, fully coupled Fluid–Structure Interaction (FSI), fatigue assessment, and long-term field validation. Such developments will facilitate the industrial implementation of the proposed methodology for commercial hydropower projects.
- The optimized Pelton turbine developed in the present investigation is particularly suitable for high-head, low-discharge micro-hydropower applications.
- The proposed integrated design methodology can be applied to remote rural electrification projects, decentralized renewable energy systems, mountainous regions, irrigation canal power recovery systems, industrial captive hydropower plants,power generation, and educational demonstration facilities.
- Since the methodology is based on analytical hydraulic design, CFD optimization, structural analysis, modal analysis, fabrication, and experimental validation, it can be adapted to different site conditions by modifying the hydraulic head, discharge, runner diameter, and operating speed.
- Similar hydraulic performance can be achieved provided that the turbine is designed according to the specific site conditions using the proposed optimization framework. Thus, the developed methodology provides a practical and reliable approach for improving the efficiency, structural reliability, and operational performance of micro-hydropower Pelton turbine installations.

REFERENCES

[1] IEA (2021). Net Zero by 2050: A Road Map for the Global Energy Sector. International Energy Agency, Paris.

[2] REN21 (2022). Renewables 2022 Global Status Report. Renewable Energy Policy Network for the 21st Century, Paris.

[3] Ministry of New and Renewable Energy, Government of India (2025). Annual Report 2024–25. MNRE, New Delhi.

[4] Central Electricity Authority, Government of India (2023). Optimal Generation Mix Report 2029–30. CEA, New Delhi.

[5] Alternate Hydro Energy Centre (AHEC), IIT Roorkee (2016). Small Hydro Database of India – July 2016 Edition. IIT Roorkee, Roorkee, India.

[6] Ministry of Power, Government of India (2023). Guidelines to Promote Development of Pumped Storage Projects (PSP). Ministry of Power, New Delhi.

[7] Pelton, L. A. (1880). Improvement in Water-Wheels and Turbines. U.S. Patent No. 233,692. U.S. Patent Office, Washington, DC.

[8] Wagner, H.-J., and Mathur, J. (2011). Introduction to Hydro Energy Systems: Basics, Technology and Operation. Springer, Berlin Heidelberg.

[9] Nasir, B. A. (2013). Design of High Efficiency Pelton Turbine for Micro-Hydropower Plant. International Journal of Electrical Engineering and Technology (IJEET), Vol. 4, No. 1, pp. 171–183.

[10] Cobb, B., and Sharp, K. (2013). Impulse (Turgo and Pelton) turbine performance characteristics and their impact on pico-hydro installations. Renewable Energy, Vol. 50, pp. 959–964.

[11] Kim, J.-W., Jo, I. C., Park, J. H., Shin, Y., and Chung, J. T. (2017). Theoretical method of selecting number of buckets for the design and verification of a Pelton turbine. Journal of Hydraulic Research, Vol. 55, No. 5, pp. 695–705.

[12] Tilahun, S., Paramasivam, V., Tufa, M., Kerebih, A., and Selvaraj, S. (2021). Analytical investigation of Pelton turbine for mini hydro power. Materials Today: Proceedings, Vol. 46, No. 17, pp. 8566–8573.

[13] Shah, H., Chaudhari, G., and Dhiman, V. (2021). Parametric Optimization and Design of Pelton Turbine Wheel for Hydraulic Efficiency Improvement. Journal of Physics: Conference Series, Vol. 2007, 012019.

[14] Erazo, J., Barragán, G., Pérez-Sánchez, M., Tapia, C., Calahorrano, M., and Hidalgo, V. (2022). Geometrical Optimization of Pelton Turbine Buckets for Enhancing Overall Efficiency. Energies, Vol. 15, No. 3, 1148.

[15] Rossetti, A., Pavesi, G., Cavazzini, G., Santolin, A., and Ardizzon, G. (2014). Influence of the bucket geometry on the Pelton performance. Proceedings of the Institution of Mechanical Engineers, Part A: Journal of Power and Energy, Vol. 228, No. 1, pp. 33–45.

[16] Suryaningrat, M. G. H., and Permatasari, R. (2025). Optimization of Angle Deflection on Pelton Turbine Bucket Using CFD. Journal of Physics: Conference Series, Vol. 2972, 012020.

[17] Cordebela, F., Erazo, J., Barragán, G., and Hidalgo, V. (2023). Experimental Investigation on the Effect of Bucket Outlet Angle in Pelton Turbines. Energies, Vol. 16, No. 7, 3195.

[18] Zidonis, A., and Aggidis, G. A. (2016). Pelton Turbine: Identifying the Optimum Number of Buckets using CFD. Journal of Hydrodynamics, Vol. 28, No. 1, pp. 75–83.

[19] Chen, X., Zeng, W., Yang, J., and Chen, Y. (2023). Optimization of Runner Width for Pelton Turbine Performance Improvement. Energies, Vol. 16, No. 4, 1884.

[20] Xiao, Y., Wang, Z., Zhang, J., Luo, Y., and Peng, G. (2023). Numerical Investigation on Bucket Number Optimization in Pelton Turbines. Renewable Energy, Vol. 206, pp. 1–12.

[21] Jo, I. C., Park, J. H., Shin, Y., Kim, K. H., Chung, J. T., and Kim, D. I. (2015). Performance Characteristics and Efficiencies of Micro-Hydro Pelton Turbine with Nozzle Diameter Variation. IOP Conference Series: Earth and Environmental Science, Vol. 24, 012014.

[22] Nedelcu, D., Cojocaru, V., and Avasiloaie, R. C. (2021). Numerical Analysis of Jet Flow Characteristics in Pelton Turbine Nozzles. Applied Sciences, Vol. 11, No. 21, 10371.

[23] Petley, S., and Aggidis, G. A. (2019). Transient CFD and experimental analysis for improved Pelton turbine casing designs. IOP Conference Series: Earth and Environmental Science, Vol. 240, 022005.

[24] Zhang, Y., Zeng, C., Xiao, Y., and Wang, Z. (2018). Numerical Optimization of Pelton Turbine Nozzle Geometry Using CFD. IOP Conference Series: Earth and Environmental Science, Vol. 163, 012066.

[25] Deng, Q., Zeng, W., Yang, J., and Chen, Y. (2023). Effect of Jet Deviation on Hydraulic Stability in Pelton Turbines. Engineering Applications of Computational Fluid Mechanics, Vol. 17, No. 1, 2234435.

[26] Lesmana, H., Sule, L., and Tjahjono, T. (2019). Experimental Investigation of Nozzle Angle Effects on Pelton Turbine Performance. Journal of Physics: Conference Series, Vol. 1402, 022091.

[27] Saputra, D., Jasa, L., and Wijaya, I. (2020). Experimental Study of Water Pressure and Nozzle Angle on Pelton Turbine Performance. International Journal of Engineering and Technology, Vol. 9, No. 3, pp. 543–548.

[28] Sharma, V., and Dhama, S. K. (2014). Analysis of Stress on Pelton Turbine Blade Due to Jet Impingement. International Journal of Current Engineering and Technology, Vol. 4, No. 4, pp. 2414–2417.

[29] Li, X., and Saw, C. B. (2017). Fatigue Analysis and Reinforcement Design of Pelton Turbine Buckets. IOP Conference Series: Materials Science and Engineering, Vol. 241, 012010.

[30] Mbiu, J., Mulinge, M., and Gathitu, B. (2015). Finite Element Structural Analysis of Pelton Turbine Buckets Using Different Materials. International Journal of Engineering Research and Technology, Vol. 4, No. 10, pp. 567–572.

[31] Rai, A. K., Kumar, A., and Kumar, P. (2016). Forces acting on particles in a Pelton bucket and similarity considerations for erosion. IOP Conference Series: Earth and Environmental Science, Vol. 49, 122002.

[32] Pesatori, E. (2007). Dynamic Behaviour of Pelton Turbine Runner Systems. Proceedings of the Institution of Mechanical Engineers, Part C: Journal of Mechanical Engineering Science, Vol. 221, No. 8, pp. 931–940.

[33] Chaudhari, A. H., Chaudhari, G. C., and Bharti, O. S. (2025). Performance of Pelton Turbine using ANSYS Mechanical APDL: Modal Analysis. Proceedings of the Institution of Mechanical Engineers, Part E: Journal of Process Mechanical Engineering. https://doi.org/10.1177/09544089251315743.

[34] Chaudhari, A. H., Chaudhari, G. C., and Bharti, O. S. (2025). Design Optimization of Micro-Hydro Pelton Turbine: Integration of Static and Modal Analysis Using ANSYS APDL. IOP Conference Series: Earth and Environmental Science, Vol. 1533, 012001.

[35] Zidonis, A., and Aggidis, G. A. (2015). State of the art in numerical modelling of Pelton turbines. Renewable and Sustainable Energy Reviews, Vol. 45, pp. 135–144.

[36] Bhattarai, S., Vichare, P., Dahal, K., Al Makky, A., and Olabi, A. G. (2019). Novel trends in modelling techniques of Pelton turbine bucket for increased renewable energy production. Renewable and Sustainable Energy Reviews, Vol. 112, pp. 87–101.

[37] Patel, K., Patel, B., Yadav, M., and Foggia, T. (2010). Development of Pelton turbine using numerical simulation. IOP Conference Series: Earth and Environmental Science, Vol. 12, 012048.

[38] Panthee, A., Neopane, H. P., and Thapa, B. (2014). CFD analysis of Pelton turbine flow. International Journal of Scientific Research and Publications, Vol. 4, No. 8, pp. 1–11.

[39] Klemetsen, L. E. (2010). An Experimental and Numerical Study of the Free Surface Pelton Bucket Flow. Master Thesis, Norwegian University of Science and Technology (NTNU), Trondheim, Norway.

[40] Perrig, A. (2007). Hydrodynamics of the Free Surface Flow in Pelton Turbine Buckets. PhD Thesis, École Polytechnique Fédérale de Lausanne (EPFL), Lausanne, Switzerland.

[41] Han, F., Shen, N., Li, L., and Zhang, Z. (2011). Unsteady separation of jet branch by cutout of rotating Pelton bucket. Science China Technological Sciences, Vol. 54, No. 2, pp. 302–310.

[42] Anagnostopoulos, J. S., and Papantonis, D. E. (2012). A fast Lagrangian simulation method for flow analysis and runner design in Pelton turbines. Journal of Hydrodynamics, Ser. B, Vol. 24, No. 6, pp. 930–941.

[43] Wang, X., Wang, W., Zhang, C., and Xu, Y. (2024). Three-Dimensional Numerical Modelling of Pelton Turbine Buckets for Improved CFD Prediction Accuracy. Renewable Energy, Vol. 229, 120811.

[44] Petley, S., and Aggidis, G. A. (2019). Transient CFD and experimental analysis for improved Pelton turbine casing designs. IOP Conference Series: Earth and Environmental Science, Vol. 240, 022005.

[45] Sun, L., Fan, W., Zhou, H., Wang, Z., and Guo, P. (2024). Transient Startup Flow Characteristics in Pelton Turbines Using CFD. Sustainability, Vol. 16, No. 23, 10667.

[46] Zeng, C., Xiao, Y., Luo, Y., Zhang, J., Wang, Z., Fan, H., and Ahn, S.-H. (2018). Hydraulic performance prediction of a prototype four-nozzle Pelton turbine by entire flow path simulation. Renewable Energy, Vol. 125, pp. 270–282.

[47] Decaix, J., and Münch-Alligné, C. (2022). Influence of Mesh Quality and Numerical Schemes on Pelton Turbine CFD Simulations Using OpenFOAM. IOP Conference Series: Earth and Environmental Science, Vol. 1079, 012072.

[48] Gupta, V., Prasad, V., and Khare, R. (2016). Numerical simulation of six jet Pelton turbine model. Energy, Vol. 104, pp. 24–32.

[49] Islam, M. T., Bhuyan, M. A., and Chowdhury, M. A. (2013). Composite Material Based Pelton Turbine Bucket for Micro-Hydro Applications. International Journal of Engineering Research and Technology, Vol. 2, No. 10, pp. 2716–2722.

[50] Padhy, M. K., and Saini, R. P. (2012). Study of silt erosion mechanism in Pelton turbine buckets. Energy, Vol. 39, No. 1, pp. 286–293.

[51] Kramer, M., Wieprecht, S., and Terheiden, K. (2015). Influence of Air Entrainment on Pelton Turbine Performance and Stability. Journal of Hydraulic Research, Vol. 53, No. 4, pp. 513–523.

[52] Dhakan, A., and Chalil, V. P. (2013). Experimental Investigation of Multi-Jet Pelton Turbine Configurations. International Journal of Engineering Research and Technology, Vol. 2, No. 7, pp. 1978–1983.

[53] Kholifah, S., Sule, L., and Jasa, L. (2018). Experimental Performance Analysis of Pelton Turbine under Different Design Parameters. International Journal of Engineering and Technology, Vol. 7, No. 4, pp. 2023–2027.

[54] Sumita, S., Sato, K., and Tanaka, H. (2023). Experimental Evaluation of Nozzle and Runner Variations in Pelton Turbines. IOP Conference Series: Earth and Environmental Science, Vol. 1136, 012030.

[55] Gudukeya, L., and Madanhire, I. (2013). Efficiency Improvement Strategies for Micro-Hydro Pelton Turbines. International Journal of Engineering and Computer Science, Vol. 2, No. 2, pp. 372–381.

[56] Chaudhari, G. C. (2016). Numerical, Experimental and Flow Visualization Studies on Conventional and Hooped Pelton Turbine Runner. PhD Thesis, Sardar Vallabhbhai National Institute of Technology (SVNIT), Surat, India.

[57] Barragan, G., Erazo, J., Cordebela, F., and Hidalgo, V. (2025). CFD and Metaheuristic Optimization of Pelton Turbine Performance. Applied Sciences, Vol. 15, No. 3, 1204.

[58] Ibarra, G. A., Ladino, J. A., and Camacho, R. (2024). ANN-Based Reconstruction and Optimization of Pelton Turbine Bucket Geometry. Renewable Energy, Vol. 236, 121449.

[59] Nigussie, A., Engeda, A., and Dribssa, E. (2017). Design and performance study of a micro-hydro Pelton turbine for small-scale power generation in Ethiopia. International Journal of Rotating Machinery, Vol. 2017, Article ID 5751861.

[60] Chaudhari, A. H., and Chaudhari, G. C. (2026). Optimization of Outlet Angle and Speed Ratio for Enhanced Pelton Turbine Performance. IOP Conference Series: Earth and Environmental Science (In Press).

[61] Zhang, Z. (2016). Pelton Turbines. In Hydraulic Machines. Springer, Cham, pp. 125–168.

[62] Derakhshan, J. F., and Nourbakhsh, A. (2008). Experimental study of characteristic curves of centrifugal pumps working as turbines in different specific speeds. Experimental Thermal and Fluid Science, Vol. 32, No. 3, pp. 800–807.

[63] Kim, B. H., Kim, J. H., and Choi, Y. S. (2020). Parametric study on the bucket geometry of a Pelton turbine using response surface methodology. Renewable Energy, Vol. 152, pp. 324–335.

[64] Rossetti, A., Pavesi, G., and Ardizzon, G. (2018). Numerical analysis of the solid particle erosion in a Pelton turbine. Wear, Vol. 404–405, pp. 1–12.

[65] Khan, S. A. (2020). Finite element analysis of Pelton turbine bucket for structural integrity under jet impact. Engineering Failure Analysis, Vol. 118, 104845.

[66] Neopane, H. P., Dahlhaug, O. G., and Holen, B. (2012). Selection of materials for Pelton turbine buckets in sediment-laden water. Wear, Vol. 274–275, pp. 1–9.

[67] Thapa, B. S., Thapa, B., and Dahlhaug, O. G. (2019). Current research on erosion in Pelton turbines: A review. Renewable and Sustainable Energy Reviews, Vol. 112, pp. 299–315.

[68] Park, E., Chung, J., and Cho, Y. (2016). CFD analysis of the flow characteristics in a Pelton turbine bucket. Journal of Mechanical Science and Technology, Vol. 30, No. 12, pp. 5525–5533.

[69] Elbatran, A. H., Yaakob, O. B., Ahmed, Y. M., and Shabara, M. R. (2017). Computational fluid dynamics analysis of Pelton turbine bucket using volume of fluid method. Energy Procedia, Vol. 142, pp. 91–96.

[70] Nassif, G. P. (2018). CFD simulation of Pelton turbine flow using OpenFOAM. International Journal of Fluid Machinery and Systems, Vol. 11, No. 3, pp. 287–296.

[71] Singh, R. K., Singal, S. K., and Deepak, S. S. K. (2020). CFD analysis of a Pelton turbine bucket for performance enhancement. Sustainable Energy Technologies and Assessments, Vol. 42, 100834.

[72] Egusquiza, E., Valero, C., Huang, X., and Jou, A. (2011). Failure investigation of a Pelton turbine runner. Engineering Failure Analysis, Vol. 18, No. 1, pp. 279–287.

[73] Majidi, M. M. (2019). Structural analysis of Pelton turbine bucket using finite element method. Modelling and Simulation in Engineering, Vol. 2019, Article ID 5843752.

[74] Farrell, K. J., and Raghunathan, R. S. (2002). CFD analysis of a Pelton turbine. Proceedings of ASME Fluid Engineering Division Summer Meeting (FEDSM), Montreal, Canada, pp. 1–7.

[75] Perović, I., Ilić, D., and Jovanović, M. (2016). Experimental investigation of Pelton turbine performance. Thermal Science, Vol. 20, No. 5, pp. 1541–1552.

[76] Brekke, L. P. M. (2012). CFD analysis of Pelton turbine efficiency. IOP Conference Series: Earth and Environmental Science, Vol. 15, No. 6, 062002.

[77] Harvey, A., Brown, A., Hettiarachi, P., and Inversin, A. (1993). Micro-hydro Design Manual: A Guide to Small-scale Water Power Schemes, 2nd ed. Intermediate Technology Publications, London.

[78] De Giorgi, M. G., Fontanarosa, D., and Ficarella, A. (2018). Parametric optimization of a Pelton turbine bucket using CFD. Energy Procedia, Vol. 148, pp. 110–117.

[79] Vrijdag, J. K. (2020). Optimization of Pelton turbine nozzle and bucket geometry. Renewable Energy, Vol. 145, pp. 1928–1941.

[80] Pandey, R. K. (2021). Erosion wear in Pelton turbines: A review and future directions. Materials Today: Proceedings, Vol. 44, pp. 2345–2352.

[81] Thapa, B. (2021). Sediment erosion in hydro turbines and its effect on performance: A review of Nepalese hydropower. Wear, Vol. 476, 203712.

[82] Giosio, D. R., Henderson, A. D., Walker, J. M., and Brandner, P. A. (2014). Characterization of Pelton turbine efficiency and performance. Proceedings of the 27th IAHR Symposium on Hydraulic Machinery and Systems, IOP Conference Series: Earth and Environmental Science, Vol. 22, 012023.

[83] ASME PTC 18-2016 (2016). Hydraulic Turbines and Pump-Turbines Performance Test Codes. American Society of Mechanical Engineers, New York.

[84] Central Electricity Authority (CEA) (2024). Installed Capacity Report, FY 2024–25. Ministry of Power, Government of India, New Delhi.

[85] Alternate Hydro Energy Centre (AHEC) (2022). Reassessment of Small Hydro Power Potential in India. Report No. SHP/2022/07. IIT Roorkee, Roorkee, India.

[86] Thapar, H. (2019). Performance analysis of Pelton turbines for micro-hydropower applications in the Himalayan region. Renewable Energy Focus, Vol. 28, pp. 45–55.

[87] J. Mungwe, S. Mandelli, and E. Colombo, "Community pico and micro hydropower for rural electrification: Experiences from the mountain regions of Cameroon," AIMS Energy, vol. 4, no.1, pp. 190–205, 2016, doi: 10.3934/energy.2016.1.190.

[88] K. Rajput, Fluid Mechanics and Hydraulic Machines, 6th ed. New Delhi, India: S. Chand Publishing, 2013.Alternative commonly used references containing similar velocity triangle diagrams

List of Publications

1. Anupkumar Chaudhari and Gaurang C. Chaudhari, **"Review on Micro Hydro Power Plant,"** in Recent Advances in Fluid Dynamics, J. Banerjee et al., Eds., **Lecture Notes in Mechanical Engineering. Singapore: Springer,** 2023, pp. 401–409. doi: 10.1007/978-981-19-3379-0_34.
2. A.H. Chaudhari, G. C. Chaudhari, and O. S. Bharti, **"Performance of Pelton turbine using ANSYS mechanical APDL: Modal analysis,"** Proceedings of the Institution of Mechanical Engineers, Part E: **Journal of Process Mechanical Engineering,** 2025. doi: 10.1177/09544089251334186.
3. A.H. Chaudhari, G. C. Chaudhari, and O. S. Bharti, **"Design Optimization of Micro-Hydro Pelton Turbine: Integration of Static and Modal Analysis Using ANSYS APDL," IOP Conference Series: Earth and Environmental Science,** vol. 1533, no. 1, p. 012001, 2025. doi: 10.1088/1755-1315/1533/1/012001.
4. Anupkumar Chaudhari and Gaurang C. Chaudhari, **"Optimization of Bucket Outlet Angle and Speed Ratio to Enhance the Efficiency of a Micro-Hydropower Plant," International Journal of Mechanical Engineering and Technology (IJMET),** vol. 17, no. 1, pp. 71–78, Jan.–Feb. 2026. doi: 10.34218/IJMET_17_01_005.

APPENDIX A

Uncertainty Analysis

Instruments and Calibration

This section contains information on the testing apparatuses and their calibration. The international testing standard IEC 60193 Hydraulic turbines, storage pumps, and pump-turbines – Model acceptance tests (IEC 60193:1999) was followed in the testing and calibration procedures. The instruments used in the experimental setup were calibrated by an NABL-accredited laboratory (P.Tej Calibration Centre, Ahmedabad). The Pelton runner was dynamically balanced by Accurate Rotomech, Vadodara, as per ISO 1940/1-1986(E), achieving Balance Quality Grade G 2.5.

Physical Constants

The international standard (IEC 60193:1999) provided tables that were used to calculate the acceleration due to gravity (g) and the density of water (ρ). These tables can be found in the standard's Appendix. According to Table A.2 in the standard, the experimental testing was conducted at a latitude of 23.03° N and an altitude of 54 m, g = 9.7994 m/s² is the value of the gravity constant.

Error Definitions

Absolute error Equation (i) is the difference between the reference value and the measured (readout) value.

$$\Delta = X_r^{ef} - X_m \qquad \text{Equation (i)}$$

Relative error Eq. (ii) is the absolute error divided by the reference value.

$$\delta = (\Delta / X_r^{ef}) \times 100\% \qquad \text{Equation (ii)}$$

Pressure Gauge

The pressure gauge (Make: KHOOL, Range: 0–7 kg/cm², Instrument No.: PG-01) was calibrated by P.Tej Calibration Centre, Ahmedabad (Certificate No. PTCC/2692/15, dated 03-Feb-2026, valid up to 02-Feb-2027). Calibration was performed against a digital pressure gauge master (Make: Vijay, Model: MGA N03-2) traceable to national standards. For pressure gauges, ensuring accuracy is vital across industrial sectors. Performance validation involves comparing pressure readings with calibrated reference standards. According to

industry standards (such as IEC 60193:1999), pressure gauges typically have a systematic uncertainty ranging from ± 0.02 % to 0.08 %. A conservative maximum systematic uncertainty of δ_s = ± 0.08 % of full-scale reading is adopted. The expanded uncertainty at 95.45 % confidence level (k = 2) from the calibration certificate is ± 0.062 bar across the operating range.

Spring Balance

Two spring balances were used to measure the turbine shaft load. SB-01 (Make: KING, Range: 0–10 kg, Certificate No. PTCC/2602/15/1) and SB-02 (Make: AECD, Range: 0–20 kg, Certificate No. PTCC/2602/15/2) were both calibrated by P.Tej Calibration Centre on 03-Feb-2026, valid up to 02-Feb-2027, against NABL-traceable weight boxes. Calibration was performed as per the procedure defined in IEC 60193. The standard deviation, S_γ, is calculated using the following equation.

$$S_\gamma = \sqrt{[\Sigma(\bar{Y} - Y_i)^2 / (n-1)]} = \sqrt{(0.001310 / 4)} = 0.0181 \qquad \text{Equation (iv)}$$

Here,

n = 5 and degree of freedom df = n − 1 = 5 − 1 = 4.

The random uncertainty associated with the mean value at the 95 % confidence level for α = 0.5 (1 − α = 0.95) is identified using t – distribution table. The t-value corresponding to (α/2) 0.025 and (*df*) 4 is 2.77645 ($t^{\alpha/2,df} = t_{0.025,4} = 2.77645$).

$$(\Delta_\gamma)_r = \pm t \cdot S_\gamma / \sqrt{n} = \pm 2.77645 \times 0.0181 / \sqrt{5} = \pm 0.0224 \qquad \text{Equation (v)}$$

$$(\delta_\gamma)_r = [(\Delta_\gamma)_r / \bar{Y}] \times 100\% = \pm 0.0224 / 0.8613 \times 100\ \% = \pm 2.60\ \% \qquad \text{Equation (vi)}$$

Dynamic Balancing

The Pelton turbine runner (OD: 320 mm, L: 90 mm) was dynamically balanced by Accurate Rotomech, Vadodara (Certificate No. AM/07/25-26, dated 03-02-2026) at a balancing machine speed of 600 RPM using a two-plane correction method. Balancing was performed as per ISO 1940/1-1986(E). The runner achieved Balance Quality Grade G 2.5 with a final residual unbalance of 0.7 gm at 312°, well within the permissible limit for turbine rotors.

Hydraulic Efficiency

The systematic uncertainty of the hydraulic efficiency η^h based on the calibrated instrument uncertainties and IEC 60193:1999 methodology is:

$(\delta\eta h)_s = \pm 0.6\ \%$ Equation (iii)

The total uncertainty is the combined systematic and random uncertainty according to the procedure defined in IEC 60193.

$\delta_t = \pm\sqrt{(\delta_s^2 + \delta_r^2)}$ Equation (vii)

$\delta_t = \pm\sqrt{[(\delta\eta h)_s^2 + (\delta_\gamma)_r^2]}$

$= \pm\sqrt{[(0.6)^2 + (2.60)^2]}$

$= \pm 2.67\ \%.$

APPENDIX B

1. Dynamic balancing certificate

ACCURATE ROTOMECH

Office: A-49, Ambicadham Soc,Vadsar road, Vadodara. Workshop:K1/518/1 GIDC Makarpura Vadodra-390010
Mo: 9723013238,9228341266, E-mail: accuraterotobrd@gmail.com

DYNAMIC BALANCING CERTIFICATE

Date	03/02/2026
Certificate No	AR/497/25-26
Ref. No.	-
Name of Party	Anup Kumar Hasmukhlal Chaudhari.

- **Specification of Job Balanced**

Name of Job	Peltol Turbine Rotor (OD- 320 L- 90mm)
Material of Job	SS
Material Quantity	01
Maximum Speed of Job	1000 R.P.M
Weight of The Job	9Kg (Approx)

- **Balancing Method**

Balancing Machine Speed	600 R.P.M
Job Position	In Between
Number of Correction Plane	Single Plane
Balancing Method	Added
Balancing Quality Grade	As per ISO 1940/1:1986(E) G 2.5

Number of Plane	Left/Right
Correction Plane Radius	70
Initial Unbalance(gm)/Angle	171gm/314°
Permissible Unbalanced	1.5gm
Final Unbalance(gm)/Angle	0.7gm/117°

- Thus it is certified that your rotor is balanced up to your maximum service speed.

ACCURATE ROTOMECH

On site dynamic balancing/On shop dynamic balancing services,
Low and high speed dynamic balancing of rotors, impellers, pulleys, fans, drums, etc

2. Calibration certificate of pressure gauge

P.Tej Calibration Centre

Office / Lab : C - 27, Payal Nagar, Opp. Dari Multiplex, Naroda, Ahmedabad - 382 330. (Gujarat)
Mobile : 9825736786 ◆ Website : http://ptejcalibrationcentre.com
Email : panchityagnesh@gmail.com

CC-2314

Calibration Certificate

Name of Customer & Address : FLUID MECHANICS LAB
MECHANICAL ENGINEERING DEPARTMENT,PIET,PARUL UNIVERSITY, Gujarat

Unique Lab Report No. :	[illegible]		
Certificate No.:	PTCC/2602/[illegible]	Date of Issue :	04-Feb-2026
Date of Calibration:	03-Feb-2026	Customer Suggested Due Date :	02-Feb-2027
Name of Instrument :	Pressure Gauge	Job No.:	PTCC/2602/[illegible]
Instrument No.:	PG-01	Sr No.:	–
Make :	EXCEL	Model :	[illegible]
Range :	0 - 7 Kg/cm2	Least Count :	0.1 Kg/cm2
Visual Inspection :	OK	Environment Condition :	23±2.5°C/35 to 65 % RH
Date of Receipt :	03-Feb-2026	Work Procedure No.:	PTCC-WI-Lab-[illegible]
Reference :	[illegible]	Location of Calibration :	At Laboratory
Location of Instrument :	–	Accuracy :	—

Product Field Discipline : As Per NABL Classification of 2.3.9 (Pressure Indicating Devices)

Statement of Conformity is not provided

Details of Test Equipments Used

Name	Make	Model	I.D. NO./ SR NO	Certificate/ULR No.	Date of Calibration	Valid upto	Certified By
Digital Pressure Gauge(1 TO 10)	Vijay	MGA N02-2	PTCC/PU/P3-01 / NVEM1604312	N2025/12/0004 & CC22942512000075424	01/12/2025	30/11/2026	CC 2294

Results of Calibration (Parameter : Pressure)

Set Value on DUC (in UOM)	UOM	Convert Value of DUC (in bar)	Measured Value on master UP M1 (bar)	Measured Value on master Down M2 (bar)	Measured Value on master UP M3 (bar)	Avg.Reading ((M1+M3)/2+M2)/2 (bar)	(1) Deviation (bar)	Repeatability (M2-M1) (bar)	Hysteresis (M2-M1) (bar)	(U) Expanded Uncertainty (in UOM)
0	Kg/cm2	0.000	0.000	0.000	0.000	0.000	0.000	0.000	0.000	–
1.7	Kg/cm2	1.667	1.670	1.676	1.677	1.676	0.011	-0.002	-0.001	0.202
3.5	Kg/cm2	3.432	3.451	3.450	3.455	3.452	0.020	0.004	-0.001	0.002
5.5	Kg/cm2	5.394	5.425	5.429	5.428	5.428	0.034	0.003	0.004	0.002
7.0	Kg/cm2	6.865	6.911	6.915	6.915	6.915	0.050	0.004	0.004	0.002

Remarks :
1. DUC stands for Device Under Calibration.
2. Test points Readings are in unit of DUC. Measured Value on master is in bar & DUC is in unit of DUC.
3. The value have been rounded off as per
Cl. 2. Wherever applicable.
4. Calibration is performed without doing any adjustment in its original condition at the time of receipt.
5. The user should determine the suitability of the instrument for its intended use.

6. DUC specification is pertaining to the manufacturers catalog/ instruction manual or as per Customer Guidelines.
7. As the Customer Request readings are given.
8. Result holds only for calibrated
9. Calibration results are metrologically traceable to National /International Standard.
10. (U) Expanded Uncertainty at 95.45 % C.I. with k = 2.00
11. Reported Uncertainty is in Unit of DUC.

Page 1 of 1

Authorized Signatory : Yagneshkumar Panchal C.E.O.

Issue : 21-10-2021

Note : This report refers only to particular item submitted for calibration. P.Tej Calibration Centre is not responsible for any change in calibration data and performance specifications on account of malfunctioning of standard instruments/Equipments covered by this report. The calibration results reported are valid at the time of under stated conditions of the measurements. This reports may not be reproduced in full part without prior permission of P.Tej Calibration Centre.

3. Calibration certificate of spring balance

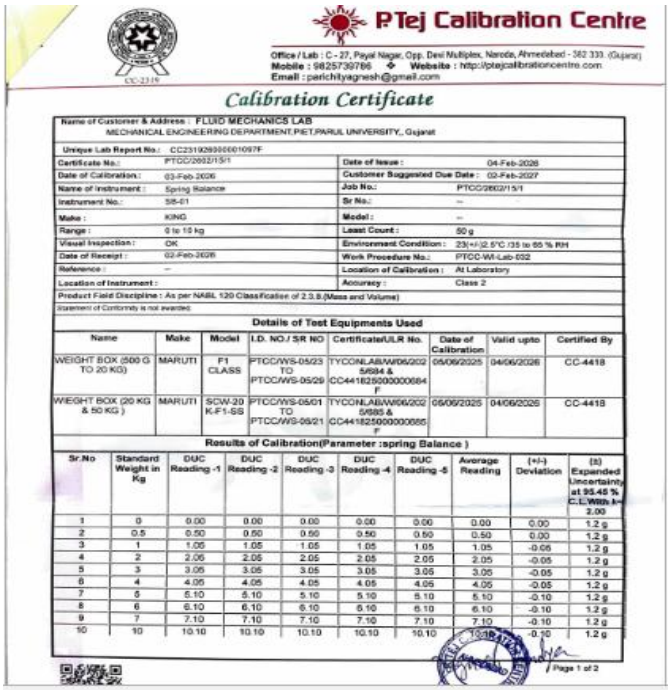

P.Tej Calibration Centre

Office / Lab : C - 27, Payal Nagar, Opp. Devi Multiplex, Naroda, Ahmedabad - 382 330. (Gujarat)
Mobile : 9825739786 ❖ Website : http://ptejcalibrationcentre.com
Email : parichityagnesh@gmail.com

CC-2319

Calibration Certificate

Name of Customer & Address :	FLUID MECHANICS LAB MECHANICAL ENGINEERING DEPARTMENT,PIET,PARUL UNIVERSITY,, Gujarat
Unique Lab Report No.:	CC231929000001097F
Certificate No.:	PTCC/2602/15/1
Date of Issue :	04-Feb-2026
Date of Calibration.:	03-Feb-2026
Customer Suggested Due Date :	02-Feb-2027
Name of Instrument :	Spring Balance
Job No.:	PTCC/2602/15/1
Instrument No.:	SB-01
Sr No.:	--
Make :	KING
Model :	--
Range :	0 to 10 kg
Least Count :	50 g
Visual Inspection :	OK
Environment Condition :	23(+/-)2.5°C /35 to 65 % RH
Date of Receipt :	02-Feb-2026
Work Procedure No.:	PTCC-WI-Lab-032
Reference :	--
Location of Calibration :	At Laboratory
Location of Instrument :	
Accuracy :	Class 2

Product Field Discipline : As per NABL 120 Classficatiae of 2.3.8.(Mass and Volume)

Statement of Conformity is not awarded

Details of Test Equipments Used

Name	Make	Model	I.D. NO./ SR NO	Certificate/ULR No.	Date of Calibration	Valid upto	Certified By
WEIGHT BOX (500 G TO 20 KG)	MARUTI	F1 CLASS	PTCC/WS-05/23 TO PTCC/WS-05/29	TYCONLAB/W06/2025/684 & CC441825000000684F	05/06/2025	04/06/2026	CC-4418
WIEGHT BOX (20 KG & 50 KG)	MARUTI	SCW-20 K-F1-SS	PTCC/WS-05/01 TO PTCC/WS-05/21	TYCONLAB/W06/2025/685 & CC441825000000685F	05/06/2025	04/06/2026	CC-4418

Results of Calibration(Parameter :spring Balance)

Sr.No	Standard Weight in Kg	DUC Reading -1	DUC Reading -2	DUC Reading -3	DUC Reading -4	DUC Reading -5	Average Reading	(+/-) Deviation	(±) Expanded Uncertainty at 95.45 % C.L.With k= 2.00
1	0	0.00	0.00	0.00	0.00	0.00	0.00	0.00	1.2 g
2	0.5	0.50	0.50	0.50	0.50	0.50	0.50	0.00	1.2 g
3	1	1.05	1.05	1.05	1.05	1.05	1.05	-0.05	1.2 g
4	2	2.05	2.05	2.05	2.05	2.05	2.05	-0.05	1.2 g
5	3	3.05	3.05	3.05	3.05	3.05	3.05	-0.05	1.2 g
6	4	4.05	4.05	4.05	4.05	4.05	4.05	-0.05	1.2 g
7	5	5.10	5.10	5.10	5.10	5.10	5.10	-0.10	1.2 g
8	6	6.10	6.10	6.10	6.10	6.10	6.10	-0.10	1.2 g
9	7	7.10	7.10	7.10	7.10	7.10	7.10	-0.10	1.2 g
10	10	10.10	10.10	10.10	10.10	10.10	10.10	-0.10	1.2 g

Page 1 of 2

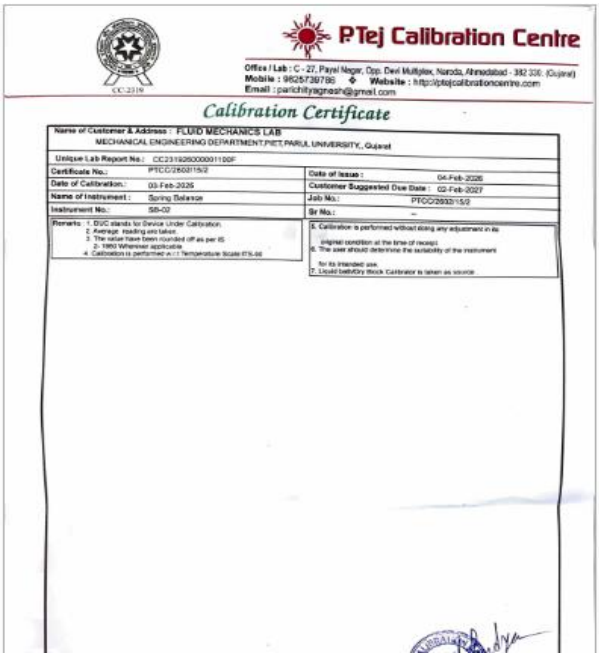

P.Tej Calibration Centre

Office / Lab : C - 27, Payal Nagar, Opp. Devi Multiplex, Naroda, Ahmedabad - 382 330. (Gujarat)
Mobile : 9825739786 ❖ Website : http://ptejcalibrationcentre.com
Email : parichityagnesh@gmail.com

CC-2319

Calibration Certificate

Name of Customer & Address :	FLUID MECHANICS LAB MECHANICAL ENGINEERING DEPARTMENT,PIET,PARUL UNIVERSITY,, Gujarat
Unique Lab Report No.:	CC231929000001100F
Certificate No.:	PTCC/2602/15/2
Date of Issue :	04-Feb-2026
Date of Calibration.:	03-Feb-2026
Customer Suggested Due Date :	02-Feb-2027
Name of Instrument :	Spring Balance
Job No.:	PTCC/2602/15/2
Instrument No.:	SB-02
Sr No.:	--

Remarks: 1. DUC stands for Device Under Calibration.
2. Average reading are taken.
3. The value have been rounded off as per IS 2- 1960 Wherever applicable.
4. Calibration is performed at : (Temperature Scale 0% rh)
5. Calibration is performed without doing any adjustment in its original condition at the time of receipt.
6. The user should determine the suitability of the instrument for its intended use.
7. Liquid bath/Dry Block Calibrator is taken as source.

P.Tej Calibration Centre

Office / Lab : C - 27, Payal Nagar, Opp. Devi Multiplex, Naroda, Ahmedabad - 382 330. (Gujarat)
Mobile : 9825739786 ❖ Website : http://ptejcalibrationcentre.com
Email : parichityagnesh@gmail.com

CC-2319

Calibration Certificate

Name of Customer & Address :	FLUID MECHANICS LAB MECHANICAL ENGINEERING DEPARTMENT,PIET,PARUL UNIVERSITY,, Gujarat
Unique Lab Report No.:	CC231929000001100F
Certificate No.:	PTCC/2602/15/2
Date of Issue :	04-Feb-2026
Date of Calibration.:	03-Feb-2026
Customer Suggested Due Date :	02-Feb-2027
Name of Instrument :	Spring Balance
Job No.:	PTCC/2602/15/2
Instrument No.:	SB-02
Sr No.:	—
Make :	AEOD
Model :	—
Range :	0 - 20 kg
Least Count :	0.1 kg
Visual Inspection :	OK
Environment Condition :	23(+/-)2.5°C /35 to 65 % RH
Date of Receipt :	02-Feb-2026
Work Procedure No.:	PTCC-WI-Lab-032
Reference :	—
Location of Calibration :	At Laboratory
Location of Instrument :	
Accuracy :	Class 2

Product Field Discipline : As per NABL 120 Classification of 2.3.8 (Mass and Volume)

Statement of Conformity is not awarded

Details of Test Equipments Used

Name	Make	Model	I.D. NO./ SR NO	Certificate/ULR No.	Date of Calibration	Valid upto	Certified By
WEIGHT BOX (20 KG & 50 KG)	MARUTI	SCW-20 K-F1-SS	PTCC/WS-05/01 TO PTCC/WS-05/21	TYCONLAB/W06/2025/685 & CC441825000000685F	05/06/2025	04/06/2026	CC-4418
WEIGHT BOX (500 G TO 20 KG)	MARUTI	F1 CLASS	PTCC/WS-05/23 TO PTCC/WS-05/29	TYCONLAB/W06/2025/684 & CC441825000000684F	05/06/2025	04/06/2026	CC-4418

Results of Calibration(Parameter :spring Balance)

Sr.No	Standard Weight in Kg	Average Reading in kg	(+/-) Deviation in kg	(±) Expanded Uncertainty at 95.45 % C.L.With k= 2.00
1	0	0.0	0.0	3.1 g
2	1	1.2	0.2	3.1 g
3	2	2.5	0.5	3.1 g
4	4	4.4	0.4	3.1 g
5	5	5.5	0.5	3.1 g
6	6	6.7	0.7	3.1 g
7	7	7.7	0.7	3.1 g
8	10	10.1	0.1	3.1 g
9	15	15.1	0.1	3.1 g
10	20	20.2	0.2	3.1 g

Page 1 of 2

APPENDIX C

1. Experimental Result of Conventional and Enhanced Pelton Runners

Experimental Results of Conventional and Enhanced Pelton runners

Conventional Bucket

Nozzle opening 100%															
Test	**Equivalent Radius (Re) (m)**	**V(sq)**	**V (m/s)**	**Q (m³/s)**	**P (bar)**	**H (m)**	**Counter wt (kg)**	**Spring wt (kg)**	**Net wt (kg)**	**Speed (rpm)**	**Torque (Nm)**	**Power Developed Pd (W)**	**Power Available Pa (W)**	**Efficiency (%)**	**Specific Speed (Ns)**
1	0.169	247.212	15.723	0.051	5	43.500	5.000	2.800	2.200	1524.000	3.647	581.427	2176.442	26.715	10.402
2	0.169	247.212	15.723	0.051	5	43.500	10.000	4.200	5.800	1189.000	9.616	1195.907	2176.442	54.948	11.639
3	0.169	247.212	15.723	0.051	5	43.500	15.000	6.700	8.300	1070.000	13.760	1540.101	2176.442	70.762	11.886
4	0.169	247.212	15.723	0.051	5	43.500	20.000	8.500	11.500	970.000	19.066	1934.448	2176.442	88.881	12.076
Nozzle opening 80%															
Test	**Equivalent Radius (Re) (m)**	**V(sq)**	**V (m/s)**	**Q (m³/s)**	**P (bar)**	**H (m)**	**Counter wt (kg)**	**Spring wt (kg)**	**Net wt (kg)**	**Speed (rpm)**	**Torque (Nm)**	**Power Developed Pd (W)**	**Power Available Pa (W)**	**Efficiency (%)**	**Specific Speed (Ns)**
1	0.169	210.400	14.505	0.047	5.1	45.500	5.000	2.900	2.100	1490.000	3.482	542.616	2100.184	25.837	9.288
2	0.169	210.400	14.505	0.047	5.1	45.500	10.000	4.400	5.600	1178.000	9.284	1143.986	2100.184	54.471	10.662
3	0.169	210.400	14.505	0.047	5.1	45.500	15.000	6.900	8.100	1040.000	13.429	1460.850	2100.184	69.558	10.637
4	0.169	210.400	14.505	0.047	5.1	45.500	20.000	8.700	11.300	940.000	18.734	1842.017	2100.184	87.707	10.796
Nozzle opening 60%															
Test	**Equivalent Radius (Re) (m)**	**V(sq)**	**V (m/s)**	**Q (m³/s)**	**P (bar)**	**H (m)**	**Counter wt (kg)**	**Spring wt (kg)**	**Net wt (kg)**	**Speed (rpm)**	**Torque (Nm)**	**Power Developed Pd (W)**	**Power Available Pa (W)**	**Efficiency (%)**	**Specific Speed (Ns)**
1	0.169	176.000	13.266	0.043	5.3	47.500	5.000	2.900	2.100	1380.000	3.482	502.558	2005.271	25.062	7.845
2	0.169	176.000	13.266	0.043	5.3	47.500	10.000	4.500	5.500	1115.000	9.118	1063.469	2005.271	53.034	9.221
3	0.169	176.000	13.266	0.043	5.3	47.500	15.000	7.100	7.900	1002.000	13.097	1372.721	2005.271	68.456	9.414
4	0.169	176.000	13.266	0.043	5.3	47.500	20.000	8.800	11.200	900.000	18.568	1748.026	2005.271	87.172	9.542
Nozzle opening 40%															
Test	**Outer dia (d) (m)**	**V(sq)**	**V (m/s)**	**Q (m³/s)**	**P (bar)**	**H (m)**	**Counter wt (kg)**	**Spring wt (kg)**	**Net wt (kg)**	**Speed (rpm)**	**Torque (Nm)**	**Power Developed Pd (W)**	**Power Available Pa (W)**	**Efficiency (%)**	**Specific Speed (Ns)**
1	0.169	170.000	13.038	0.042	5.4	48.000	5.000	3.100	1.900	1370.000	3.150	451.400	1991.539	22.666	7.285
2	0.169	170.000	13.038	0.042	5.4	48.000	10.000	4.700	5.300	1090.000	8.787	1001.820	1991.539	50.304	8.635
3	0.169	170.000	13.038	0.042	5.4	48.000	15.000	7.200	7.800	985.000	12.932	1332.350	1991.539	66.901	8.999
4	0.169	170.000	13.038	0.042	5.4	48.000	20.000	8.700	11.300	880.000	18.734	1724.442	1991.539	86.588	9.147

Nozzle opening 20%															
Test	**Outer dia (d) (m)**	**V(sq)**	**V (m/s)**	**Q (m³/s)**	**P (bar)**	**H (m)**	**Counter wt (kg)**	**Spring wt (kg)**	**Net wt (kg)**	**Speed (rpm)**	**Torque (Nm)**	**Power Developed Pd (W)**	**Water Power (W)**	**Efficiency (%)**	**Specific Speed (Ns)**
1	0.169	160.000	12.649	0.041	5.5	49.500	5.000	3.150	1.850	1350.000	3.067	433.105	1992.454	21.737	6.767
2	0.169	160.000	12.649	0.041	5.5	49.500	10.000	4.680	5.320	1070.000	8.820	987.149	1992.454	49.544	8.097
3	0.169	160.000	12.649	0.041	5.5	49.500	15.000	7.280	7.720	970.000	12.799	1298.603	1992.454	65.176	8.419
4	0.169	160.000	12.649	0.041	5.5	49.500	20.000	8.690	11.310	860.000	18.751	1686.741	1992.454	84.656	8.507
Enhanced Bucket															
Nozzle opening 100%															
Test	**Equivalent Radius (Re) (m)**	**V(sq)**	**V (m/s)**	**Q (m³/s)**	**P (bar)**	**H (m)**	**Counter wt (kg)**	**Spring wt (kg)**	**Net wt (kg)**	**Speed (rpm)**	**Torque (Nm)**	**Power Developed Pd (W)**	**Power Available Pa (W)**	**Efficiency (%)**	**Ns**
1	0.169	246.000	15.684	0.0509	5	43.500	5.000	2.740	2.260	1550.000	3.747	607.474	2171.100	27.980	10.814
2	0.169	246.000	15.684	0.0509	5	43.500	10.000	4.140	5.860	1205.000	9.715	1224.537	2171.100	56.402	11.936
3	0.169	246.000	15.684	0.0509	5	43.500	15.000	6.640	8.360	1090.000	13.860	1580.230	2171.100	72.785	12.265
4	0.169	246.000	15.684	0.0509	5	43.500	20.000	8.450	11.550	980.000	19.149	1962.888	2171.100	90.410	12.290
1	0.169	246.000	15.684	0.0509	5	43.500	5.000	2.740	2.260	1550.000	3.747	607.474	2171.100	27.980	10.814
2	0.169	246.000	15.684	0.0509	5	43.500	10.000	4.140	5.860	1205.000	9.715	1224.537	2171.100	56.402	11.936
3	0.169	246.000	15.684	0.0509	5	43.500	15.000	6.640	8.360	1090.000	13.860	1580.230	2171.100	72.785	12.265
4	0.169	246.000	15.684	0.0509	5	43.500	20.000	8.450	11.550	980.000	19.149	1962.888	2171.100	90.410	12.290
Nozzle opening 80%															
Test	**Equivalent Radius (Re) (m)**	**V(sq)**	**V (m/s)**	**Q (m³/s)**	**P (bar)**	**H (m)**	**Counter wt (kg)**	**Spring wt (kg)**	**Net wt (kg)**	**Speed (rpm)**	**Torque (Nm)**	**Power Developed Pd (W)**	**Power Available Pa (W)**	**Efficiency (%)**	**Ns**
1	0.169	208.000	14.422	0.047	5.1	45.500	5.000	2.850	2.150	1510.000	3.564	562.993	2088.171	26.961	9.588
2	0.169	208.000	14.422	0.047	5.1	45.500	10.000	4.400	5.600	1186.000	9.284	1151.755	2088.171	55.156	10.771
3	0.169	208.000	14.422	0.047	5.1	45.500	15.000	6.850	8.150	1054.000	13.512	1489.655	2088.171	71.338	10.886
4	0.169	208.000	14.422	0.047	5.1	45.500	20.000	8.900	11.100	962.000	18.403	1851.763	2088.171	88.679	11.078
Nozzle opening 60%															
Test	**Equivalent Radius (Re) (m)**	**V(sq)**	**V (m/s)**	**Q (m³/s)**	**P (bar)**	**H (m)**	**Counter wt (kg)**	**Spring wt (kg)**	**Net wt (kg)**	**Speed (rpm)**	**Torque (Nm)**	**Power Developed Pd (W)**	**Power Available Pa (W)**	**Efficiency (%)**	**Specific Speed (Ns)**
1	0.169	169.000	13.000	0.042	5.3	47.500	5.000	2.850	2.150	1398.000	3.564	521.234	1964.989	26.526	8.094
2	0.169	169.000	13.000	0.042	5.3	47.500	10.000	4.500	5.500	1129.000	9.118	1076.822	1964.989	54.800	9.395
3	0.169	169.000	13.000	0.042	5.3	47.500	15.000	7.100	7.900	1022.000	13.097	1400.120	1964.989	71.253	9.698
4	0.169	169.000	13.000	0.042	5.3	47.500	20.000	9.050	10.950	915.000	18.154	1737.491	1964.989	88.422	9.672
Nozzle opening 40%															

Test	Outer dia (d) (m)	V(sq)	V (m/s)	Q (m^3/s)	P (bar)	H (m)	Counter wt (kg)	Spring wt (kg)	Net wt (kg)	Speed (rpm)	Torque (Nm)	Power Developed Pd (W)	Power Available Pa (W)	Efficiency (%)	Specific Speed (Ns)
1	0.169	164.000	12.806	0.042	5.4	48.000	5.000	3.150	1.850	1389.000	3.067	445.617	1956.078	22.781	7.339
2	0.169	164.000	12.806	0.042	5.4	48.000	10.000	4.750	5.250	1112.000	8.704	1012.398	1956.078	51.757	8.856
3	0.169	164.000	12.806	0.042	5.4	48.000	15.000	7.400	7.600	1001.000	12.600	1319.274	1956.078	67.445	9.100
4	0.169	164.000	12.806	0.042	5.4	48.000	20.000	9.100	10.900	902.000	18.071	1704.984	1956.078	87.163	9.322
Nozzle opening 20%															
Test	**Outer dia (d) (m)**	**V(sq)**	**V (m/s)**	**Q (m^3/s)**	**P (bar)**	**H (m)**	**Counter wt (kg)**	**Spring wt (kg)**	**Net wt (kg)**	**Speed (rpm)**	**Torque (Nm)**	**Power Developed Pd (W)**	**Power Available Pa (W)**	**Efficiency (%)**	**Specific Speed (Ns)**
1	0.169	160.000	12.649	0.041	5.5	49.500	5.000	3.150	1.850	1350.000	3.067	433.105	1992.454	21.737	6.767
2	0.169	160.000	12.649	0.041	5.5	49.500	10.000	4.680	5.320	1070.000	8.820	987.149	1992.454	49.544	8.097
3	0.169	160.000	12.649	0.041	5.5	49.500	15.000	7.280	7.720	970.000	12.799	1298.603	1992.454	65.176	8.419
4	0.169	160.000	12.649	0.041	5.5	49.500	20.000	8.690	11.310	887.000	18.751	1739.697	1992.454	87.314	8.911